A Hydromechanically-based Risk Framework for CO_2 Storage Coupled to Underground Coal Gasification

by

Gerardo José González Martínez de Miguel

A thesis submitted for the degree of

Doctor of Philosophy

Sir Joseph Swan Institute for Energy Research

University of Newcastle upon Tyne

July 2014

Abstract

Most of the energy produced in the world comes from fossil fuels: coal, oil and gas. Amongst them, coal is the most abundant and widespread fossil fuel in the world. Underground Coal Gasification (UCG), an *in situ* method to extract the calorific value of the coal, has been known for a century but has had very limited implementation throughout the world, mainly due to the availability of cheap oil over that period. It is now gaining relevance in order to unlock vast resources of coal currently not exploitable by conventional mining.

However, growing concern on increased levels of carbon dioxide concentration in the atmosphere is pointing out the necessity to reduce the use of fossil fuels. Since alternative sources of energy (e.g. nuclear and renewables) are not in a position to meet the constantly increasing demand in a short term, carbon capture and its geological sequestration (CCS) is considered the best remedial option.

An environmental risk assessment framework has been developed for coupling UCG to CCS accounting for benefits and cost from both global and local perspectives. A UCG site presents significant differences from other typical CCS projected scenarios, most notably the injection of CO_2 into a heavily fractured zone. A model which accounts for flow in fractures represented by dual-porosity flow (TOUGH2) is coupled to a geomechanical model (FLAC3D). The impact of this fractured zone in the CO_2 injection pressure buildup and stress field is evaluated. Furthermore the effect of stress-dependent fracture permeability is assessed with the hydro-mechanically

coupled compositional simulator GEM. Simulation results suggest that in such a scenario, CO_2 injectivity and dissolution improve though confinement is compromised and commercial injection rates seem unattainable. The effects of miscibility and relative permeability on pressure buildup implemented in semianalytical solutions are also evaluated. Albeit further research is required, a UCG operation may, therefore, not be able to accommodate the produced CO_2 in the gasified cavity and its surroundings in a safe and economical fashion. Rigorous studies and management practices are needed to establish the requirements for secure long-term confinement of the carbon dioxide in such scenario.

A mis padres

Si el Señor no construye la casa,

en vano se cansan los albañiles

(Salmo 126)

Acknowledgements

I would like to start by thanking my supervisors:

- To Prof. Paul Younger, for giving me the opportunity of undertaking this doctorate. Without him nothing of the following would have happened.

- Very affectionate thanks to my second supervisor Dr. Jaime Amézaga for his continuous support and for giving me the chance to participate in the UK–India knowledge transfer program.

- To Dr. Mohamed Rouainia for encouraging me to seek a research stay at Lawrence Berkeley National Laboratory, which ended being such an amazing experience.

- And very special thanks to the last supervisor in joining the party, Dr. Simon Mathias (Durham University), for his inspiring work and invaluable advice.

My gratitude to my colleagues —researchers, students, lecturers, technical and administrative staff members, visiting researchers— in the Sir Joseph Swan Institute and in the HERO group, for their friendship and the good times we shared in and out the Devonshire Building. To all the good friends in Newcastle University, especially my dear godson Octavio. And to all the good *Geordie* friends.

Thanks to the members of the Ramsay Project —in special Dermot Roddy, Harry Bradbury and Stephen Price— at Newcastle University, with whom I had the privilege to collaborate in that project. Thanks to John Ellis, for sharing with me his

Thanks to the researchers, students and lecturers at the Earth Science Department in Durham University, in special Kate, Francesca, Amy and Ben for our conversations.

Thanks to the Computer Modeling Group for their support during and after the multiple courses that I attended to get familiar with the use of their software.

Thanks to David Wilson and the management of ERC Equipoise Ltd. for their understanding and support while I was trying to cope with a full-time job and my writing-up simultaneously.

To my friends Peter Stanley, for the last proof reading of the manuscript, and to Javier González Yélamos and my best 'old pal' Villi for their comments and support. Thanks to Mel for her encouragement in the final stages of the writing-up. And to Liz for her unceasing kindness, joy, and care.

Last but not least, my deepest gratitude to my family.

I regret I cannot name everyone individually. But to all of you, explicitly or implicitly included in these lines, my most heartfelt gratitude and affection.

Parts of this thesis have been (or are in the process of being) adapted and published in multi-author publications. I declare that the work presented in this thesis has been carried out by me unless otherwise stated. Nevertheless, I do indeed acknowledge the invaluable advice and guidance that the co-authors have provided me with, and without which, neither this thesis nor the publications would have been possible.

Contents

List of Figures

List of Tables

Chapter 1

Introduction

Most of the energy produced in the world comes from fossil fuels: coal, oil and gas. Amongst them, coal is the most abundant and globally widespread fossil fuel. Over 27% of world's primary energy supply was covered by coal in 2010, and this percentage increases to 40% when it refers to electricity generation (IEA, 2012). Renewables and nuclear energy are not in the position at this moment of meeting the energy needs on their own. While currently in UK renewables only account for 11% of the total electricity generation (DECC, 2013), nuclear power supplies 18% and still faces public and also sometimes governmental opposition. Furthermore uranium reserves in the world would be able to sustain energy demand on its own for less than fifty years, probably not even twenty five.

In addition, efficiency in the production and use of energy has not reached levels expected in the 1980s and 1990s.

The rise of oil and gas prices as well as the threat of political instability in main supplier countries is an issue when looking for a safe, economic and reliable source of energy. Consequently, coal is starting again to be regarded as the industry engine as it was in the past and is expected to be an essential part of the energy sources mix in the near future. This allows a time window to develop alternative technologies.

In the UK's Department of Trade and industry (DTI) report under the *Cleaner*

Fossil Fuel Programme on *'Review of the feasibility of underground coal gasification in the UK'*, in-land only UK deep coal resources mineable by means of underground coal gasification (UCG) were estimated at 17 billion tonnes. This is equivalent to 300 years of supply at the current consumption rate (DTI, 2004).

Late growing concern about anthropogenic global warming draws attention to consider the reduction of the use of fossil fuels in order to decrease carbon emissions. However, as explained above, the technology and market are not ready for a change to green energy production technologies in the short time needed. Therefore, in addition to continuing the efforts on developing renewables and improving energy production efficiency, the *International Panel on Climate Change* (IPCC) has suggested carbon sequestration as the only method that would allow meeting the emissions reduction target (Metz et al., 2005).

In accordance with the United Nations Framework Convention on Climate Change (UNFCC) and the recommendation of the IPCC of avoiding CO_2 emissions into the atmosphere, the European Commission published during the course of this research (January 2008) a proposal for a Directive on the geological storage of carbon dioxide. Its aim was to provide a legal framework that allows the development of the carbon capture and storage (CCS) technology. Thus, CCS would be available as a mitigation option to reduce CO_2 emissions by 50% by 2050. In its summary, it states that 'The proposal ensures that CO_2 capture is regulated under Directive 96/61/EC and that both CO_2 capture and pipeline transport are regulated under Directive 85/337/EEC. But its main scope is the regulation of CO_2 storage and the removal of barriers in existing legislation to CO_2 storage.' (EU Parliament, 2009).

A significant legislative imposition with regards to energy related activities has taken place in the last decade in the United Kingdom, with the promulgation of ten UK Public General Acts from year 2000 to 2011 in comparison with the twelve acts released in the previous thirty years (The National Archive, 2013).

The United Kingdom's general energy policy has steadily evolved in the last decade towards CO_2 geological storage since the Utilities Act of 2000, which did not contain any reference to carbon emissions. Its purpose was to regulate the gas and electricity markets. The introduction of the concept of sustainability in an Energy Act occurred in 2003, when the Sustainable Energy Act 2003 was to 'make provision about the development and promotion of sustainable energy policy'. The reports on progress towards achievement of a sustainable energy industry were to pave the way to cutting the United Kingdom's carbon emissions, maintaining the reliability of the country's energy supplies, promoting competition in the energy market and alleviating fuel poverty. These four premises have been developed in subsequent amendments to the Sustainable Energy Act of 2003.

If the Energy Act 2003 demands reports on the afore mentioned four issues and dedicates a section to the residential accommodation energy efficiency, the Climate Change and Sustainable Energy Act 2006 is more specific in its provisions 'about the reduction of emissions of greenhouse gases, the alleviation of fuel poverty, the promotion of microgeneration and the use of heat produced from renewable sources, compliance with building regulations relating to emissions of greenhouse gases and the use of fuel and power, the renewables obligation relating to the generation and supply of electricity and the adjustment of transmission charges for electricity'. It actually states as the principal purpose of the Act to enhance the United Kingdom's contribution to combating climate change.

Gas prices and the pursuit of pushing carbon capture and storage technology led to the promulgation of an Energy Act in 2008 which provided a new licensing regime for importation and offshore storage of natural gas and carbon dioxide within the territorial sea and continental shelf. Part I is dedicated to gas importation and storage, and it includes one chapter (Chapter 3) dedicated to the storage of carbon dioxide. This chapter reviews licensing, abandonment of offshore installations and

safety zones and Enhanced Oil Recovery (EOR) issues. The Energy Act 2008 was one of the vehicles for transposition of EU legislation such as the Directive 2009/31/EC of the European Parliament and of the Council on the geological storage of carbon dioxide, Directive 85/337/EEC on the assessment of the effects of certain public and private projects on the environment, Directive 92/43/EEC on the conservation of natural habitats and of wild fauna and flora, Directive 2009/174/EC of the European Parliament and of the Council on the conservation of wild birds, Directive 2008/1/EC of the European Parliament and of the Council of 15 January 2008 concerning integrated pollution prevention and control, Directive 2003/87/EC of the European Parliament and of the Council establishing a scheme for greenhouse gas emission allowance trading within the Community, Regulation (EC) No 1907/2006 of the European Parliament and of the Council concerning the Registration, Evaluation, Authorization and Restriction of Chemicals and Regulation (EC) No 842/2006 of the European Parliament and of the Council on certain fluorinated greenhouse gases.

The culmination of this legislation with regards to CCS arrives with the Energy Act 2010 provision for demonstrating, assessing and using CCS technology. Consultation and tender for construction of a CCS demonstration project was announced in 2007. However, a financial agreement between the parts could not be reached for what was meant to be the first UK CCS demonstration project, located in Longannet power plant (Scotland). In 2010 the government committed £1 billion for four full scale demonstration plants.

Another aspect of the UK CCS policy framework is the requirement since 2009 for all new power plants over 300 MWe net generating capacity to be built *carbon capture ready*. This is a transposition of the EU CCS Directive and means that it will be feasible to retrofit carbon capture, transport and storage technologies to the plant in its life cycle.

The Energy Act 2011 advances in the legislation of further aspects related to CCS, the offshore transmission and distribution of electricity, the abandonment of infrastructure converted for CCS demonstration projects, including submarine pipelines. Interestingly, the Coal Authority is granted additional powers relating subsidence and water discharge in a broader context than coal mining.

Climate Change Acts 2006 and 2008 contribute to the picture by setting emission reduction targets and establishing carbon trading schemes among other measures. The new target for 2050 in the Climate Change Act 2008 was set as at least 80% lower than the 1990 baseline.

The main drivers for incentivizing CCS technology in the UK are the policies related to climate change and energy security and the commercial opportunity presented by the upcoming depletion of hydrocarbon fields in the North Sea and oil and gas offshore industry expertise. The North Sea and continental shelf would provide the new industry with infrastructures and storage capacity saving costs of exploration and decommissioning. It has been suggested that CCS technology development would benefit energy security by allowing the exploitation of local fossil fuels. However, this can be argued, as CCS technology does not provide any additional resources -unless used in EOR-, but an energy penalty on actual reserves.

It is also noteworthy that all policy and regulations constructed so far in the UK consider only offshore CO_2 storage.

In this scenario, it seems plausible to expect that future deployment of Underground Coal Gasification (UCG) in the UK will be heavily linked to CCS.

1.1 History and current state of Underground Coal Gasification

In his very interesting account of the history of UCG, Olness (1977) traces back the first documented idea of UCG to Sir William Siemens in his speech to the Chemical Society of London in May 7, 1868. Other scientists, such as Dmitriy Mendeleyev and Sir William Ramsay took great interest in UCG. Ramsay designed an experiment to be carried out in Co. Durham, in the North East of England, but his premature death and the outbreak of the World War I stopped any further development in the UK. However, his enthusiasm was decisive in the development of UCG in the former Soviet Union, thanks to the influence that Ramsays lectures had on Lenin. Since then, most of the world's underground coal gasification in terms of quantity and ranges of coal has occurred in the former Soviet Union. Though many of the plants constructed in the 1950s were closed due to the availability of natural gas, two of them remain operational: Yuzhno-Abinsk (Siberia) and Angren (Uzbekistan), the latter with more than 40 years of activity.

In the UK the UCG research programme was resumed after the World War II, leading to a successful trial at Newman Spinney in Derbyshire (1950s). However, low oil prices led to a second abandonment of the investigation until a new unfruitful review in the 1960s-1970s. Later on, the UK became one of the parties in the *European Trial*, together with Belgium and Spain. After Thulin (Belgium) in the 1980s and El Tremedal (Spain) in the 1990s experiments, the UK was to perform another one in its territory. Once again, the UK was undertaking a new feasibility study in the late 1990s. The Firth of the Forth was selected as a potential pilot project location. Current public opinion in the UK is however very reluctant to this type of trials, as has been seen in the strong opposition to fracturing (e.g. `www.frack-off.org.uk`).

Meanwhile, the US ran an intensive UCG research program in the 1970s and 1980s. Though some of the trials (i.e. Rocky Mountain, Rawlins) complied with the environmental requirements, the serious groundwater contamination encountered in Hoe Creek caused the cancellation of the program. More recently, and coinciding with the beginning of this work, significant research in UCG environmental risk assessment was undertaken by the US government (Burton et al., 2006). Burton et al. (2006) refers to the possibility of coupling UCG–CCS, but their study is focused in UCG. In this brief period, the coupling of UCG and CCS has become a paramount issue in the development of the UCG technology to a commercial scale, due to increasingly restrictive emission legislations.

Another remarkable experience is that of Australia from late 1990s onwards. A UCG plant has been in operation for several years at Chinchilla with considerable success and there are new developments planned. However, another trial in Queensland —Kingaroy—, eventually faced the intervention of the Australian government under suspicion of environmental contamination (ABC, 2013).

The increasing concern about energy supply, which highly affects developing countries, has led China and India to make a strong investment in UCG development. China is now the country with most projects, 30 since 1995 (World Coal Association, 2013), and abundant research in the underground coal gasification process (e.g Li et al., 2013; Liu et al., 2009; Yang et al., 2010).

The previous examples, although not exhaustive, show the momentum created in UCG around the world in the last decade and the opportunity of this research.

1.2 The UCG scenario for UCG–CCS

UCG involves gasifying coal in situ by means of directionally drilled wells. The process of underground coal gasification and subsequent injection of CO_2 commences

with the drilling and completion of two boreholes: the injection well and the production well. There are different alternatives in the drilling pattern layout, which will differ from pilot projects to commercial scale operations. After completion of boreholes, ignition takes place and coal is partially oxidized. In the case of coal, about 80% of the original calorific value of the solid coal will be present in the resultant gas. Gasification is achieved by an exothermic reaction, which is initiated by reaction with hot steam and oxygen introduced via the injection borehole. As the operator controls the availability of oxygen, so the degree of oxidation is under the operators control. The resultant hot gas mixture —known as synthesis gas or *syngas*— contains hydrogen, methane and carbon monoxide, all of which have significant calorific value. Depending on precise gasification conditions, varying proportions of CO_2 and hydrogen sulphide may also be present in the syngas, although hydrogen sulphide is mobilized to a far lesser degree than in conventional coal combustion (National Coal Council, 2008). The precise proportions of the various component gases in any particular syngas mixture is a function of depth (since gasification is more efficient at high pressure), oxygen injection rate and coal seam quality. Examples of typical UCG syngas compositions from a variety of coals are reported by Galli et al. (1983); Pirard et al. (2000); Perkins and Sahajwalla (2006); Khadse et al. (2007) and Yang (2008). These sources reveal component gas fractions in the ranges shown in Table 1.1:

Table 1.1: Syngas composition range.

H_2	11-35%
CO	2-16%
CH_4	1-8%
CO_2	12-28%
H_2S	0.03-3.5%

The syngas is drawn to the surface via neighbouring production boreholes, whence

it can be transported by pipeline for use in a wide range of applications, such as driving turbines to generate electricity or for manufacturing products ranging from plastics to gas and liquid transport fuels. Pre- and/or post-combustion cleanup to minimize emissions of SO_x and NO_x is typically not required for UCG applications, due to the paucity of H_2S and NH_3 in the raw syngas (NH_3 is usually entirely absent because of the strongly exothermic nature of the nitrogen oxidation reaction, which at high temperatures and pressures favours the persistence of nitrogen gas). Gaseous emissions of toxic metals are also generally negligible, as the ash present in the coal remains below ground, and largely avoids fusion (National Coal Council, 2008). Given that most UCG processes are oxygen fuelled, CO_2 and water vapour are the only gaseous exhaust streams produced after gasification, thus making separation and capture of the CO_2 relatively simple and cheap. The process is, therefore, particularly compatible with CCS.

The UCG process creates voids deep underground following gasification of the coal. These voids will inevitably collapse, just as voids produced by longwall coal mining do, leaving high permeability zones of artificial breccias. Where UCG has taken place at depths in excess of about 700 – 800 m, storage of CO_2 in these artificial high-permeability zones is a very attractive proposition. Figure 1.1 shows schematically the underground processes described above. A combined UCG–CCS project could achieve a reduction in CO_2 emissions of as much as 85% compared with conventional coal-fired power generation. Such a project therefore offers a very appealing solution and is the only process yet devised that offers integrated energy recovery from coal and storage of CO_2 at the same site. In principle, UCG–CCS can also sit happily alongside some other CCS approaches: where CO_2 collection and transmission pipelines can be linked together, new degrees of freedom for carbon management emerge (Roddy, 2008).

Subsurface injection of gases is being successfully accomplished worldwide for
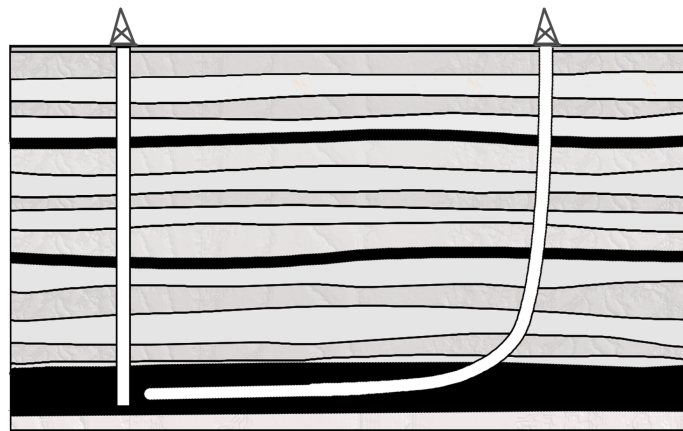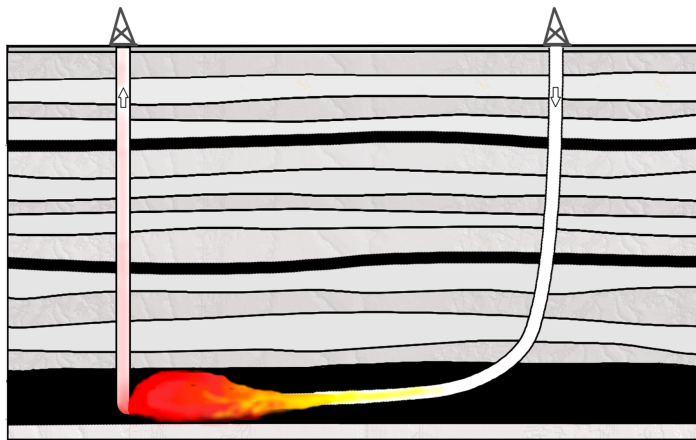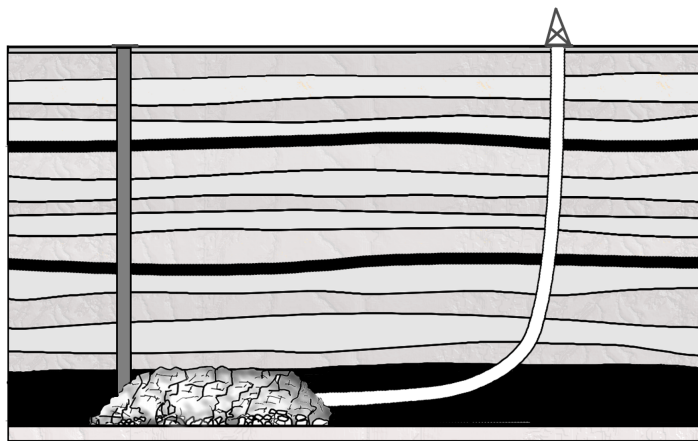
Figure 1.1: UCG–CCS schematic process: *a)* Drilling of the two boreholes, injector on the right and producer on the left; *b)* Coal gasification and cavity creation; *c)* Subsequent cavity collapse, and sealing of the producer well. Ready to commence CO_2 injection through the injection borehole into the 'goaf'

different purposes and in different scenarios. This includes oil and gas operations, temporary storage and permanent disposal. As some examples of this, since the 1970s, the oil industry has been practising enhanced oil recovery (EOR), which involves the injection of CO_2 into the oil reservoir, and more recently enhanced gas recovery (EGR) for gas reservoirs and coal bed methane. For almost one hundred years natural gas storage in salt caverns has been practised to allow supply flexibility against a fluctuating demand, and acid gas has been injected underground since the 1990s as waste in Canada.

With regard to CO_2 geological sequestration, the Intergovernmental Panel on Climate Change (Metz et al., 2005) proposed the following main scenarios for underground storage of CO_2: active and depleted oil and gas fields, deep saline aquifers, deep 'unmineable' coal seams and —marginally— caverns or basalts. Based on the expected storage capacity and current experience, most of the efforts in research and all of the commercial–scale operations have been directed to storage in oil and gas operations, depleted hydrocarbon fields and associated deep saline aquifers. That is the case with Sleipner, Weyburn, In-Salah and more recently, Snohvit. Their individual annual injection rates are in a range of $0.7 - 2 \times 10^6$ tonnes of CO_2 and their total storage will amount to $17 - 20 \times 10^6$ tonnes of CO_2 each. Injection into deep unmineable coal seams has been tested in laboratory and field, with disparate results. The *Recopol* project in Poland found major problems in the injection of the CO_2 due to the plasticization and swelling of coal when the CO_2 is adsorbed in the coal matrix and displaces the methane. However, one option that has not been widely considered yet and could be of great interest due to a combination of economic and technical aspects is the storage of the CO_2 in the voids created by UCG.

The prospects for carbon sequestration in a UCG operation arise from a serendipitous association of a source of CO_2 and a viable long-term storage site. As with the other major CCS options, UCG–CCS takes place in a sedimentary basin with

11

specific geological features that are particularly appropriate for geological storage. The general requirements of a site for carbon geological storage are (Metz et al., 2005):

- proximity to a source of CO_2 — to guarantee the supply of CO_2 and improve the economics of the operation by avoiding long transportation routes —;

- injectivity — the formation needs a high enough permeability to allow the injection of the fluid —;

- storage capacity — sufficient to store the CO_2 produced during the plant lifetime —;

- containment — some trapping mechanism has to guarantee the permanence of the CO_2 store for a considerable amount of time, c. 1,000 years —.

This research will be concerned with the three last requirements, with special focus in the injectivity and containment aspects.

1.3   Motivation and objectives

As discussed in the previous sections, coal is expected to continue to be one of the major players in the energy portfolio all over the world. At the same time, with the current political and legislative framework, it is hard to envisage that development of UCG in the UK can progress without a strong link to CCS. There are currently efforts in developing both technologies separately, but there is a gap in research in the potential storage of CO_2 in UCG sites. This scenario was not even considered among the variety of scenarios proposed by the IPCC (Metz et al., 2005). Despite the long held concerns on groundwater contamination and subsidence issues caused by UCG (e.g. Humenick and Mattox, 1978; Laquer and Manahan, 1987; Ganow et al., 1978), it was only in 2006 that an effort was made to establish the basis for a best practice

12

in the technology with special emphasis in the environmental risks (Burton et al., 2006). Similarly, geological storage of CO_2 had commenced in mid 90s in Norway (Sleipner), but research, regulations and risk assessment frameworks (e.g. OSPAR, 2007) had not been initiated or were still under development in 2007. Therefore, at the beginning of this research there was a gap in studies which comprised a UCG–CCS combined operation. It is therefore the objective of this study to establish the interactions between both processes and propose an Environmental Risk Assessment Framework which can guide the deployment of UCG–CCS in a responsible way.

One of the points addressed by an Environmental Risk Assessment is the evaluation of pathways between the source of contamination and the receptor. Abundant modelling work is in progress with regards to the injection and storage of CO_2 in deep saline aquifers (e.g. Goerke et al., 2011; Goodarzi et al., 2011), hydrocarbon depleted fields (e.g. Trivedi and Babadagli, 2009; Hawkes et al., 2004; Ferronato et al., 2010) and 'unmineable' coal seams (e.g. Dutta and Zoback, 2012) (the latter heavily linked to Enhanced Coal Bed Methane). However, the majority of this research does not consider injection in heavily altered and fractured porous media. In addition, the previous thermal, mechanical, hydrological and chemical processes taking place during gasification will introduce severe differences in the modelling and data requirements compared to conventional scenarios. A second major objective of this research is to produce an account of these requirements that can guide future model development. To achieve this objective, a number of sub-objectives are set:

- analyze how other analogies, particularly coal mining, and current model capabilities can help in the understanding of the UCG–CCS modelling issues and analyze their limitations;

- examine CO_2 injection in a fractured zone using double-porosity models in comparison with injection in single porous medium and

- evaluate analytical and semi-analytical solutions that can help in faster calculations and in model validation.

1.4 Thesis outline

To achieve the aforementioned objectives, Chapter 2 reviews the fundamental principles and concepts in Environmental Risk Assessment and analyses the current environmental guidelines for UCG and CCS and their applicability to a combined UCG–CCS.

Chapter 3 analyses how analogies in coal mining can be incorporated in absence of further UCG field tests data as a first approach and which are their limitations. Conjointly, the Chapter contrasts the available simulation models for flow in fractured porous media with the requirements that will emerge in UCG-CCS.

In Chapter 4, a hydromechanical coupling allowing dual-porosity models is implemented in the coupling of TOUGH2 and FLAC3D codes. Two cases of injection in a fractured area or below a fractured area are studied.

Chapter 5 aims to include a factor which can be expected in coupled UCG–CCS; that is the opening of existing fractures around the injection zone and subsequent changes in fracture permeability. The Barton–Bandis criterion is applied to gain understanding of the response of the flow and stress when fracture permeability is variable. This allows comparison with cases when there are no fractures or their permeability is constant. Subsequent evaluation of the impact of this circumstance on caprock integrity is undertaken. Computer Modelling Group (CMG) compositional simulator, GEM, is used for this purpose.

Though not directly applicable for UCG–CCS, Chapter 6 evaluates the semi-analytical solutions for pressure buildup estimation under CO_2 constant injection rate developed by (Mathias et al., 2011a,b, 2013). Acknowledging that this is an

over-simplified scenario compared to UCG–CCS, these solutions account for relevant problems such as miscibility and relative permeability in closed and open formations which will be of interest in UCG–CCS.

Finally, Chapter 7 presents the summary and conclusion of the thesis.

Chapter 2

Environmental Risk Assessment Framework for Underground Coal Gasification coupled to Carbon Capture and Storage

2.1 Introduction

Energy is a basic requirement for social and economic growth; inevitably, its production implies certain impacts —positive and negative— on the environment, and has traditionally made extensive use of limited natural resources. While good practices are always aiming to reduce any negative effects, these will exist and therefore have to be foreseen and remedial measures planned.

The objective of this chapter is to analyze the current environmental guidelines and their applicability to a combined UCG–CCS operation which would aim to sequester the CO_2 produced by the gasification in the reactor zone. First, we will review the fundamental concepts and principles applied nowadays in environmental risk assessment (ERA); then, we will review and analyze the issues and advances in environmental risk assessment in both fields —UCG and CCS— separately; and finally, we will evaluate the particularities arisen from coupling UCG to CCS and propose a framework for the Environmental Risk Assessment.

2.2 Fundamental principles and concepts for an Environmental Risk Assessment Framework

Historically, the risk assessment process emerged to respond either to the requirements of food and drug legislation (US) or to health and safety requirements in industrial activities (Europe) (Pollard et al., 2002). Due to its origin, in the first case, the focus was on dose-response effects, while the latter emphasized the consequences of 'component failure' (i.e. valves in a pipe network). Risk assessment subsequently evolved and was extended to other spheres of activity, including public welfare, ecological and financial. As a result, risk assessment terminology came to be used in a variety of situations and disciplines. In addition, the iterative nature of the risk assessment process has often led to a lack of consistency in terminology. For instance, 'risk management' is variously used to refer to the entire process of decision making, or just to measures for monitoring and mitigating risks. It is therefore important that such terms are always explained in the specific application context.

2.2.1 Principles

When attempting to perform an environmental risk assessment, some key principles must be considered. First amongst these is 'justification of intention': As pointed out by DEFRA (2008), there must be a justifiable need to undertake certain activity *'which by its nature may pose a risk to the environment (natural or built) and the life it sustains'*. Secondly, uncertainty is often inherent in risk estimation. Strict application of the precautionary principle would preclude any action subject to uncertainty (European Environmental Agency, 1998). However, precautionary inactivity must itself be assessed objectively in terms of its costs and benefits. Nevertheless, four basic principles of risk evaluation should preserve the objectivity implicit in the precautionary principle: transparency, clarity, consistency and reasonableness.

Another key factor derived from these considerations and principles, is the comparative nature of the risk assessment. Risks have to be set against other alternatives, as it is relative risk which most profoundly affects decisions (Jenkins et al., 2010).

In summary, an approach to risk assessment has to be justified and reasonable in comparison to other risks and has to be conducted with transparency, clarity and consistency. While risk evaluation for underground coal gasification seems more tractable under these principles, their application is proving quite problematic in the case of CO_2 sequestration. Comparison and quantification of local and global effects and cost and benefits of action are tremendously difficult to assess. It could be argued that the intention is not sufficiently justified; for instance, it has been disputed that the evidence base is circumstantial (Akasofu, 2009), that the precautionary principle lacks the desired objectivity (Lomborg, 2001) and that principles of transparency, clarity, consistency and reasonableness have not been satisfactorily met (Webster, 2010). Therefore, the author considers that mechanisms for guaranteeing the implementation of these principles in UCG–CCS should be included in an environmental risk assessment framework.

2.2.2 Concepts

Division of risk-based decision making into 'risk assessment', 'risk characterization and 'risk management' is helpful in clarifying the range of necessary tasks. Risk assessment identifies the hazards, evaluates their consequences for certain receptors and identifies the pathways between the two, and thus also possible degrees of exposure. Risk characterization should define the endpoints, and estimate qualitatively or quantitatively the probability of risk. Risk management involves the initial problem formulation and justification of intention, the risk analysis (including all the typologies of risk assessment), formulation of acceptability criteria and identification of mitigation measures.

2.2.3 Development of ERA frameworks

Frameworks for ERA have been developed by various regulatory bodies since the first attempt by the US Environmental Protection Agency (EPA) to understand and manage food and drug risks to human health. Problem formulation and risk estimation issues were added to the strict source-pathway-receptor scheme. A comparison (Figure 2.1) of National Research Council (NRC), Water Environment Research Foundation (WERF) and US EPA frameworks (Kolluru, 1996) shows that the NRC

	US EPA	NRC	WERF
I. Problem formulation and justification of intention	Problem formulation	Policy	Tier 1: Screening assessment Problem definition
II. Risk Assessment		Hazard identification	Source characterization
	Characterization of exposure	Exposure assessment	Exposure assessment
	Characterization of effects	Exposure-response assessment	Receptor and endpoint characterization Effects characterization
III. Risk characterization	Risk characterization	Risk characterization	Risk characterization
IV. Risk Management		Risk management	Risk management Stop or Tier 2: Risk estimation with existing data Stop or Tier 3: Risk estimation with new data

Figure 2.1: Comparison of NRC, WERF and US EPA Environmental Risk Assessment Frameworks (modified from Kolluru (1996)) showing the emphasis and level of detail of each framework in the four stages of the Risk Assessment (I-IV at the left of the figure)

emphasizes a policy-driven assessment, while the US EPA integrates the risk management and risk analysis in the problem formulation phase to separate them again during the assessment process and WERF focuses on the sequential approach.

Subsequent European guidelines for ERA (European Environmental Agency, 1998) comprehensively combined these prior approaches to develop an assessment framework which includes consideration of political, social, economic and legal factors in problem formulation; then hazard identification, release assessment, exposure assessment and consequence analysis to quantitatively or qualitatively estimate the risk; finally, the result is evaluated in light of the political, social, economic and legal factors to arrive at a final risk characterization. Risk management is then implemented, making decisions, developing alternatives and mitigation options, and taking actions. DEFRA (2008) stresses the importance of problem formulation, the need to screen and prioritize all risk before quantification (tiered approach), the need of to consider all risks in the options appraisal stage and (risk management) the iterative nature of the process.

It can be concluded that a comprehensive framework for environmental risk assessment of UCG–CCS has to be approached firstly in an integral way that truly accounts for benefits and costs from both global and local perspectives. Due to the uniqueness of ecological systems, site-specific characterization is crucial to problem formulation. A tiered approach allows resources to be spent in accordance with the current stage of knowledge. Iteration is needed to ensure new information is incorporated as it arises.

2.3   Environmental issues and best practice in UCG

One of the main attractions of underground coal gasification is that is has numerous environmental advantages compared to other fossil fuel extraction processes, in-

cluding: elimination of major land disturbance; minimization of rehabilitation work after completion of operations; the absence of any need for people to work in perilous underground conditions; a higher percentage recovery compared with coal bed methane recovery, and no need to dispose of ash and other solid waste products, as these remain underground. Nevertheless, UCG has the potential to give rise to some unfavourable environmental impacts too, as has been revealed in various US and European field tests from the 1970s through the 1990s (Sury et al., 2004; DTI, 2004). As in other deep drilling industries, the generic impacts of drilling operations and waste streams in the surface environment must be carefully considered. More specific to UCG are risks relating to depletion of groundwater resources, contamination of groundwater or surface water, gas leakage and subsidence.

Depletion of groundwater resources can result from inter-connection of UCG zones with major aquifers, because the creation of the gasified seam void can induce high rates of inflow, with water being lost into the exhaust stream as steam. If laterally extensive high transmissivity aquifers occur in the overburden (Iglesias, 2008), or can become connected to it by fissures or fractures, there is potential for large volumes of water to be consumed. This is also detrimental to the gasification process.

Water pollutants produced as by-products of gasification include both organics (mainly sourced from condensation of gas) and inorganics (primarily produced in ash leachate). Among the organic pollutants, the predominant species are phenols, aromatic carboxylic acids, aromatic hydrocarbons, ketones, aldehydes, pyridines, quinolines, isoquinolines, aromatic amines, naphtalene, o-xylene, 2-methyl pyridine and o-cresol, benzene. Inorganic contaminants can include calcium, sodium, sulphate, bicarbonate, ammonia, aluminium, arsenic, boron, iron, zinc, selenium, hydroxide and uranium (Humenick and Mattox, 1978; Stuermer et al., 1982; Liu et al., 2007). In general, higher temperatures of gasification result in less contaminant release (Burton et al., 2006).

Episodes of groundwater contamination have occurred during UCG tests in Russia (Gregg et al., 1976) and the USA (Stuermer et al., 1982), albeit levels of phenols had returned to background concentrations within about two years. Adsorption of organics by clay and lignite is an effective removal mechanism, however some total organic carbon (TOC) may be non-adsorbable (Humenick and Mattox, 1978). A shutdown strategy to quench the reactor as quickly as possible will minimize the post gasification formation of organic pollutants, decreasing the risk of contaminant migration. Where groundwater inflow does not quench the UCG zone quickly enough, water can be injected using wells . In case of water injection, the counter-effect is the addition of contaminated water to the waste-stream. Depressurization by venting to avoid a rapid cavity pressure increase might normally take more than one week in commercial operations. Failure to do this operation could result in spread of contaminants out of the cavity (DTI, 2004) and fracture propagation.

Subsidence can be an important issue in shallow UCG operations, as experienced at Hoe Creek (USA) (Thorsness and Creighton, 1983).The extent of the subsidence depends on seam depth, thickness of the overburden, effective rock stiffness and yield strength, fracture density and orientation, structural disposition of the seam and in situ stress tensor (Burton et al., 2006), width and number of reactors (DTI, 2004). The failure can follow four different patterns, known as stoping, chimney formation, bending subsidence and plug failure. Bending is the most common in longwall mining and it is well quantified and understood (Burton et al., 2006) and the most probable to occur in case of gasification of deep narrow coal seams.

So far, UCG has been mainly carried out in shallow sites. Increasing depths beyond 800 m (the minimum depth needed for subsequent use of UCG voids for CCS) would impact the operation and products. Factors varying with increasing depth include coal rank (which increases with depth to the range of bituminous-anthracite); cost of gasifying agents (as at great depth steam could be replaced by water) and

synthesis gas quality: at increased depth there will be more methane in the gas mix, and the calorific value will be higher. Increasing depth also reduces geotechnical and environmental risks, as compaction of the reactor zone will be greater and strata permeability and the proportion of long-chain and cyclic hydrocarbons produced will be lower (DTI, 2004). Increasing depth will, however, increase capital and operational costs, due to greater difficulties of in-seam drilling and well linkage, and it can also be expected to result in wells encountering more saline groundwater, with subsequent increase in chloride corrosion risks (Burton and Ezzedine, 2010).

It can be concluded that rational site selection and characterization is critical to the success of every UCG operation.

2.4 Environmental risk assessment in CO_2 storage

In order to comply with objectives of atmospheric CO_2 concentration reduction, subsurface injection of 3.6 Gtonnes/year of carbon dioxide worldwide would have to be achieved. To put this in perspective, this corresponds to 900 times the current CO_2 injection rate taking place in Sleipner, In-Salah, Snohvit and Weyburn put together. Once injected, the CO_2 must remain in place: it is generally recommended that the fraction of CO_2 retained over 1,000 years should be more than 99% (Metz et al., 2005). This means that, for a constant global injection of 3.6 Gtonnes/year during a period of 30 years, a leakage of 1 Gt would be considered admissible. For this to be accepted globally, the risk which this 1 Gt poses to local communities and ecosystems will have to be adjudged to be proportional to the expected benefit.

Although this study focuses on the risks of underground storage, it cannot be disconnected from other environmental impacts posed by CCS and conclusions on storage safety cannot be regarded in isolation. Impacts associated with capture might include the process efficiency penalty, the production of waste streams (especially

the solvent slurry from the capture process) and potential escape of CO_2 during capture and transport. Main risks of CO_2 underground storage include CO_2 leakage into atmosphere, soils, groundwater and surface waters, directly affecting local life or changing chemical composition of water and geological formations; displacement of brine to potable aquifers; mobilization of heavy metals and other substances; hindrance of the use of other natural resources; or increasing the global atmospheric concentration (reduction of which was the initial objective for implementation of CCS).

Assessment of risks posed by geological sequestration of CO_2 has been addressed under a number of headings (Stenhouse et al., 2009b), mainly risk assessment frameworks, site ranking and screening, and associated methodologies, modelling, monitoring, uncertainty and effects on endpoints. However, the majority of assessments of storage projects have focused more on the containment of the storage sites rather than determining the potential impacts of leakage of CO_2 (and any additional impurities or mobilized elements) on specific endpoints (Stenhouse et al., 2009a). Given that most of the existing knowledge applicable to CO_2 storage is qualitative in nature and has been obtained by analogy to other activities, risk characterization remains the most difficult challenge yet to be overcome. Yet the drive for quantified risk assessments is essential. Therefore, in the first instance, the local risks to health and safety, environment and equity need to be properly assessed and managed (Bachu, 2008), although ultimately global risks and effects of storage have to be quantitatively compared on the same terms with global warming and use of resources.

With regard to risk assessment frameworks, a series of workshops gave rise to the OSPAR Guidelines for Risk Assessment of CO_2 sequestration in geological formations (OSPAR, 2007) and in sub-seabed formations by the London Convention (London Convention, 2006). This framework follows consistently the steps of risk assessment expressed in European countries legislation guidelines (DEFRA, 2008) while placing

the necessary emphasis on site specific assessment. Figure 2.2 shows the different headlines and workflow used by the OSPAR guidelines and the Energy International Agency (EIA–GHG).
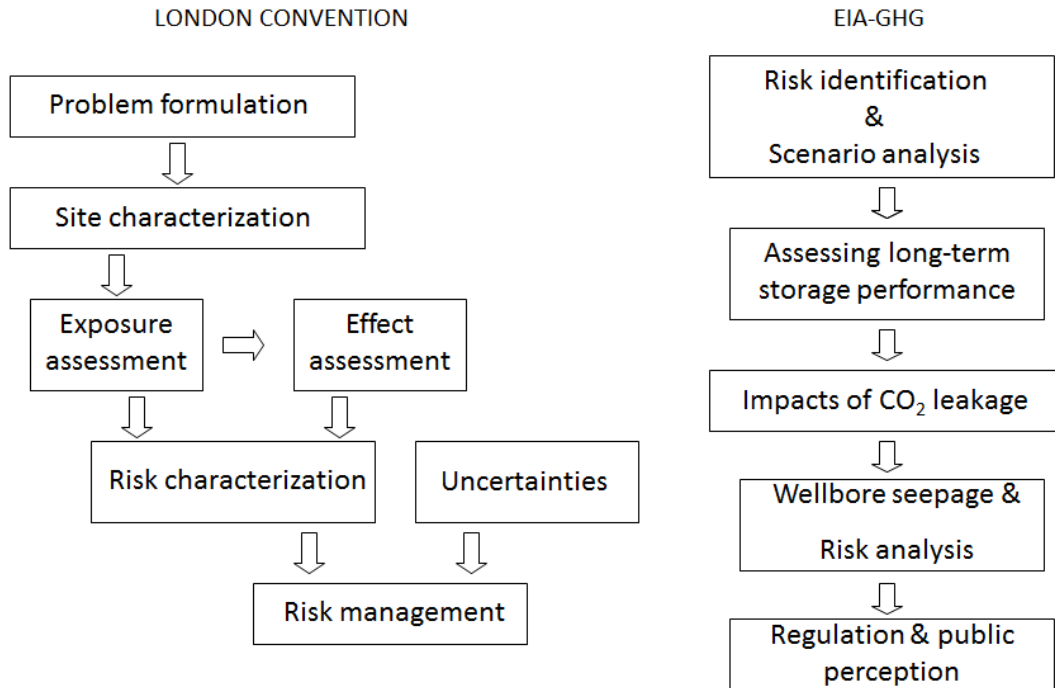
Figure 2.2: Workflow for the risk assessment of CO_2 sequestration in geological formations according to the OSPAR and the EIA–GHG guidelines: while OSPAR guidelines follow more closely the general ERA framework scheme, the EIA–GHG focus on particular issues with a view to develop the regulations and manage public perception. This second approach poses the risk of losing consistency and fail to include all aspects that have to be considered in the ERA framework.

In the context of a tiered approach, screening and ranking methods have been developed for a first quick assessment among several sites. These methods, such as the Screening and Ranking Framework (Oldenburg, 2008) or VEF (Vulnerability Evaluation Framework) (EPA, 2008), are mostly qualitative and either based to some extent in expert judgement or they can be based on simplified semi-analytical methods (Mathias et al., 2009c,b; Gasda et al., 2009; Saripalli et al., 2003). In all cases, the objective is to determine a reduced number of parameters which can give

a quick qualitative or semi-quantitative evaluation of a site.

With regard to methodologies, the most extended methodology for hazard identification and evaluation of exposure scenarios has been the 'Features, Events and Processes (FEP)' approach, in which an attempt is made to formalize the construction of scenarios (e.g. Quintessa and TNO databases). FEPs are identified from natural and industrial analogues such as natural CO_2 accumulations, injection of waste fluids, storage of natural gas (Lewicki et al., 2007), enhanced oil recovery operations (Duncan et al., 2009), and nuclear waste repositories (Maul et al., 2007). Other approaches used to build scenarios (Wildenborg et al., 2005) are based on experts lists of events and vulnerable elements (Bouc et al., 2009), SWIFT (Structured What If Technique) and Fault and Event Tree analysis. The main hindrance they all face is difficulty of guaranteeing that all possible events have been covered.

More detailed Probabilistic Risk Assessment (PRA) can be made using Monte Carlo simulations. However, the probability distribution functions of certain parameters and events are unknown, and such simulations demand great computing and human resources. To overcome these issues, Vivalda presented two approaches to risk calculation to obtain a Storage Risk Profile (Vivalda et al., 2009), pointing out that ultimately, the interest lies in the function which gives the leakage as a function of space and time.

Regarding specific and system modelling, deterministic models are used to assess the pathways and exposure and study the physico-chemical processes and support probabilistic models. Though more generalist numerical models have been tested (Pruess et al., 2002) most of the approaches rely on dedicated models for CO_2 fate and transport, such as GEM (Computer Modeling Group), Eclipse (Schlumberger) and TOUGH2 (LBNL). Complementary to numerical models, analytical and semi-analytical models (Gasda et al., 2009; Saripalli et al., 2003; Mathias et al., 2009a) have been developed to obtain quick estimates and gain understanding of the processes.

26

Validation of models is accomplished by monitoring and performance assessment (PA) of field operations (Maul et al., 2007). Several programs have been ongoing to monitor and assess performance of Sleipner (SACS, SACS2 and CO_2STORE) (Chadwick et al., 2008), Weyburn (IEA-GHG) and In-Salah (GeoSeq).

System models make use of compartments and estimate the possibility that they are affected (Oldenburg et al., 2009) and can account not only for physical aspects but also for financial and organizational systems using a flexible probabilistic platform (GoldSim) for visualization and dynamic simulation (Zhang et al., 2007).

Regarding the consequences of exposure, though the effects of CO_2 on humans are well understood, the effects on other endpoints are not so well known (London Convention, 2006). There is limited information about effects in terrestrial soils and plants (Beaubien et al., 2008) and in marine environments (Blackford et al., 2009), especially at low doses. Research is ongoing to determine the baseline sediment quality (Reguera et al., 2009) and the effects on ecosystems (Stenhouse et al., 2009a). Quantification of consequences can also be assessed by means of near-Field/GIS models (Bogen et al., 2006) to rank relative lethality using wind-speed and terrain-specific lethal-range information (meteorological and topographic conditions).

Uncertainty is an important area of research in risk assessment. Uncertainty arises from epistemic and stochastic sources. Uncertainty about geological and compositional parameters can be addressed using sensitivity analyses with deterministic models, or by using fully probabilistic models. In contrast, uncertainty in arising from definitions of events and scenarios, from conceptual models and numerical efficiency requires further research in the physics and chemistry of processes and mathematical modelling (Stenhouse et al., 2009b), usually by means of benchmarking exercises (Pruess et al., 2002). The particular event of well failure has been more thoroughly studied thanks to the experience on oil industry and extensive statistics can support the calculation of probabilities (Celia et al., 2005, 2009). As probabilistic assessments

do not always properly represent correlations between parameters, complementary approaches are required: Metcalfe et al. (2009) combine the output from numerical models and expert judgments within a decision-support framework while Bouc (Bouc et al., 2009) proposed the IRS (independent random set) method to combine both aleatory and epistemic uncertainties, 'in a way that a strong component of subjectivity is only introduced at a decision-making stage, instead of in the analysis stage', as in the Bayesian approach (Bellenfant et al., 2009; Rohmer and Bouc, 2009).

In conclusion, the variety of approaches confirms that a leakage/no leakage assessment does not seem a sufficient response for decision making and regulations. There will be a requirement for:

- Deterministic methods for a variety of applications, including detailed study of complex physical, chemical, and thermal processes,

- Expert judgment,

- Analytical and semi-analytical methods for ranking and screening,

- Advances in uncertainty calculations and

- Understanding consequences and ultimately system level analysis.

2.5 Environmental risk assessment framework for UCG–CCS

The environmental risk assessment framework for UCG–CCS requires a multi-objective optimization study with key variables to understand trade-offs between environmental benefits, human health and safety risks, costs and social impacts. Though risks include the operational risks of drilling, gas production and handling, CO_2 capture, compression, transport and injection, this framework focuses on underground activities. Furthermore, it has to be remembered that the introduction of CO_2 storage is

undertaken as a mitigation option itself intending to make a change in global temperature evolution. Comparison of cost/benefit analysis of incurred risks with its desired effects is therefore essential and should always be included in the risk assessment of any CO_2 storage operation. The comparison should also be made in equivalent terms of quantification and uncertainty, following the fundamental principles of clarity, consistency and transparency and necessary justification for application of the precautionary principle. For the purpose of comparison of disparate risk issues, the concept of 'environmental harm' was developed (Pollard et al., 2004). The fundamental challenge of the 'environmental harm' is to understand, define and quantify the attributes scores. The importance of this concept is underlined by considering that some authors (Bachu, 2008) acknowledge that the increase in global average temperatures has been produced in the last 150 years, not only since the 1940s; that the detailed response of the climate system to increasing atmospheric CO_2 concentrations is uncertain because of its inherent complexity and natural variability, and that a direct causal link between the rise in greenhouse gas concentrations in the atmosphere and global warming has not been definitively demonstrated and the evidence for it remains circumstantial. Other authors (Akasofu, 2009; Lomborg, 2001) point out that trends in global warming could be more powerfully driven by factors other than atmospheric CO_2 concentration. Since 1998, the maximum temperature reached has not been exceeded (Douglass and Christy, 2009). Additionally, climate model outputs do not reproduce tropospheric temperature measurements (Douglass et al., 2008), so the level of uncertainty on how CO_2 affects temperature in a global scale is far more unknown than local effects of leakage. Another factor is the energy penalty for coal fired power plants — over 43% —, which together with the uncertainties in the geological CO_2 storage, would make questionable the investment in CCS (Page et al., 2009).

Separate experience in UCG and CO_2 storage has shown that site selection and

characterization is critical to the success of an operation of this kind. In addition, the varied possibilities in the engineering design of the gasification will directly affect the response of the site. Therefore, it is necessary to include UCG operational design in the environmental risk assessment process.

Following the guidelines and considerations outlined in the previous sections, a framework for UCG–CCS is proposed and the issues it presents are examined qualitatively. Figure 2.3 shows a recommended workflow for the assessment.

2.5.1 Problem formulation, justification of intention and scope definition

Definition of intention

UCG–CCS aims to provide an energy or chemicals source which otherwise would not be economic using other extraction methods, complying with potential future environmental and regulation requirements and sequestering permanently the CO_2 produced in the process in the reactor zone.

Justification of intention

The necessity for continued energy supply while economic and efficient renewable energies are developed and adaption to CO_2 emissions reduction requirements.

Scope

UCG–CCS is aimed at coal seams at depths unexploitable by conventional mining methods. At the same time, where injected CO_2 would be in supercritical state (with sufficient density to optimize storage capacity). This means targeting formations at a minimum depth of approximately 800 m (depending on local hydrostatic pressure and geothermal gradient). Injected CO_2 will initially be that arising from the operation, whether UCG is undertaken for chemicals production or energy generation, and whether the capture method is pre-combustion, oxy-fuel or post-combustion. Stream
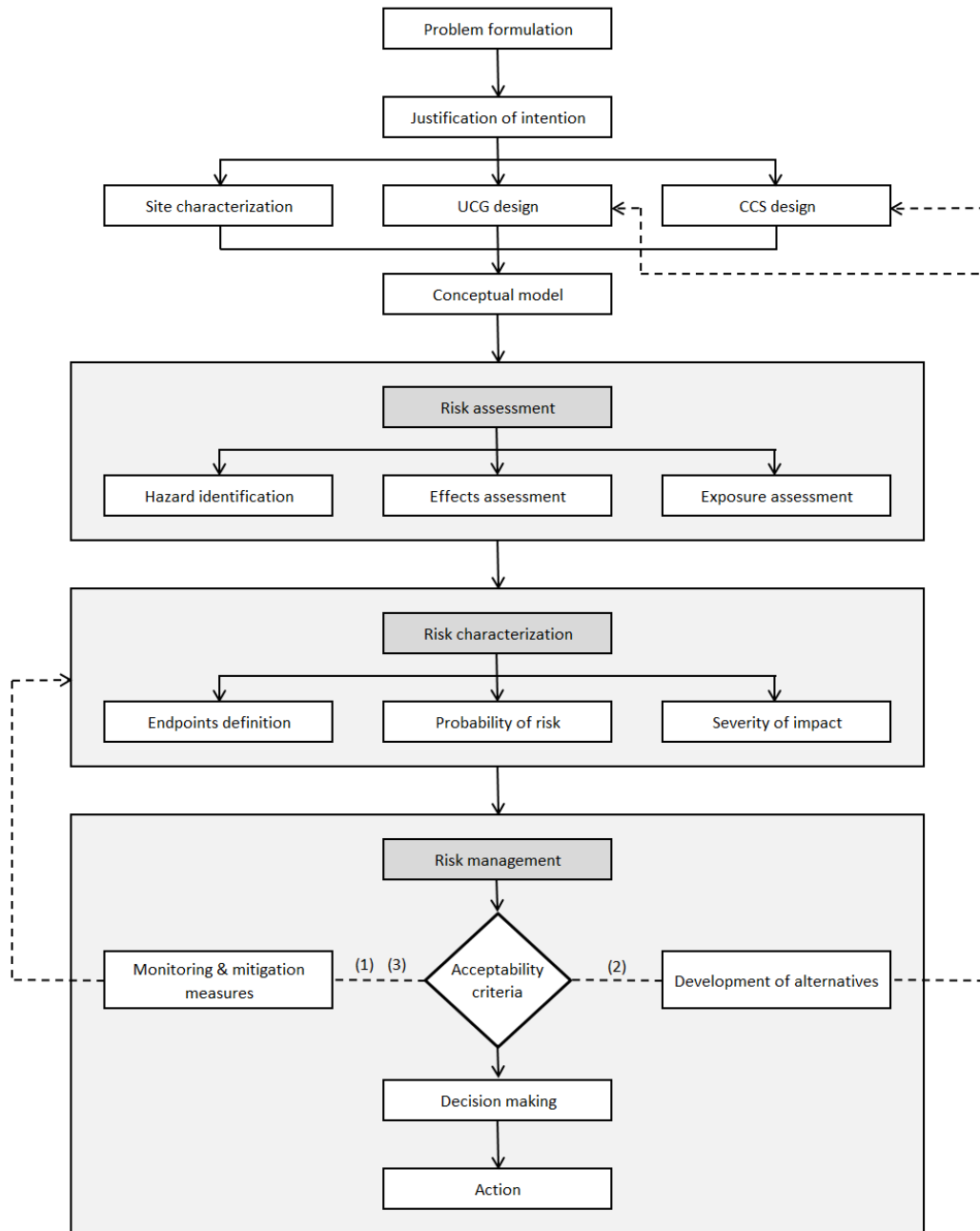
Figure 2.3: Workflow for the UCG-CCS Environmental Risk Assessment. (1), (2) and (3) represent successive iterations in the process. The first iteration step (1) should evaluate if *monitoring and mitigation measures* on the current *conceptual model* are enough to meet the *acceptability criteria*. In case the answer is negative, the second step (2) is the *development of alternatives*. The new *conceptual model* and (3) *monitoring and mitigation measures* will be assessed until the *acceptability criteria* are met.

gas characteristics will have to be taken into account. The UCG–CCS can be applied on-shore or off-shore. In the second case, it is most probable that the depths of water will be relatively shallow (in the continental shelf), so this framework would not deal with pelagic depths where CO_2 might not be buoyant.

Major issues to be addressed are operational suitability of coal seams, water or soil contamination with UCG pollutants, CO_2 storage capacity, injectivity and short and long-term containment.

2.5.2 Site characterization

The goals of the site characterization are to evaluate the coal reserves and their suitability for UCG exploitation, and capacity, injectivity and containment for subsequent CO_2 injection (Gibson-Poole et al., 2008; Lucier and Zoback, 2008).

Site characterization improves as a project goes from the initial exploration to appraisal and development stages. Therefore, it will be subjected to iterative review as more information becomes available. In the absence of detailed quality data, and bearing in mind the complexity and time-consuming nature of desk studies, evaluation of a potential site can initially be based on coarse screening using criteria based on proxies (Oldenburg, 2008). The basic information required for preliminary evaluation of a site include (Johnson, 2009):

- coal, strata and seal mineralogy characteristics, in situ fluids, wellbore cement, mud and casing, variations in composition of the CO_2 stream,

- rates of coal burning and CO_2 injection,

- porosity and permeability (including heterogeneity),

- residual fluid phase saturations,

- lateral continuity and topography of the cap rock, and

- depth, pressure and local geothermal gradient.

Site characterization involves data collection to support the construction of models of geology, hydrogeology, geochemistry and geomechanics. Techniques for characterization include geological mapping, geophysical imaging, well logging, core and water analysis, and hydraulic well testing (Johnson, 2009; Doughty et al., 2007). Thus, the site is defined by its depositional environment (Grimstad et al., 2009), stratigraphy and lithology, coal properties (rank, seam thickness, and content of ash, sulphur, chlorine and humidity), its seal structure, heterogeneities, temperature, pressure, permeability, porosity, faults and fractures structure, density, aperture and orientation, in situ stress field, rock strength, mineralogical composition, hydrodynamics and geochemistry of the in situ fluids. All of these influence the behaviour of subsurface under the gasification process and subsequent injection of CO_2.

It must be taken into account that cavity creation during gasification will significantly alter initial conditions. Prediction and monitoring of field conditions after gasification are essential prior to any CO_2 injection. Additionally, further progress of gasification in the area would affect strata conditions of previously injected cavities. Enough information has to be collected to define baseline conditions for later monitoring.

Assessment of suitable exploitable coal reserves

Tonnage and percentage of recovery, number of seams, seam depth, inclination and thickness, coal composition and rank will affect the economics and the potential design of the exploitation. Excessive thickness (20 m) can create problems in the progression of gasification, while too thin seams (<2m) make in-seam drilling more challenging and accentuate the calorific loss of the syngas; preferred coal ranks are 700–900 according to UK National Coal Board (NCB) classification due to their chemical reactivity, chemical analysis, swelling characteristics and thermal decom-

position characteristics (volatiles content); shallow seam dipping is preferred, not only for the gasification but also for future CO_2 storage; the degree of disturbance requires the absence of major faulting in the vicinity (<45 m); adjacent strata (immediate roof) should cave readily and no overlying aquifers within a distance of 25 times the seam height should be present (DTI, 2004).

Assessment of storage capacity

At pressures and temperatures corresponding to underground conditions at 800 m, super-critical CO_2 is expected to occupy four to five times more volume than the space occupied by the equivalent coal (Roddy and González, 2010). This can vary depending on coal carbon content, pressure and temperature conditions, efficiency of the capture process and impurities of the CO_2 stream. In the cavity, in addition to the roof collapses, two processes take place: the redistribution of tensions around the void which tend to close it and the effect of rubble rock expansion, which can have a factor of 1.5 (DTI, 2004). As a result, the void will be filled by rubble (termed goaf) with a much higher porosity and permeability than the intact rock. Increases in permeability in the overlying fractured strata can also provide access to further porosity. Taken together, these represent a higher storage capacity than that corresponding to the extracted coal volume alone. However, the main factor for total storage capacity will remain related to maximum injection pressure, as most of the CO_2 will have to be injected to achieve over-pressuring of a system already filled with brine. A more precise estimation of the storage capacity requires a detailed knowledge of the physical and chemical behaviour of the CO_2/brine/UCG by-products, maximum injection pressure and porosity (LBNL, 2004). These factors are controlled by multiphase flow and transport process, buoyancy forces and local and regional geologic variability.

Given the conditions, storage capacity in the area could include not only the

reactor zone and its surroundings, but also ECBM in other coal layers and/or deeper formations in the same location.

Injectivity of the formation

Permeability being one of the key parameters for feasibility and economics of injection (in terms of number of drilled wells and injection pressure), a UCG scenario provides a good advantage over current deep saline aquifer prospects for CCS. CCS in a former UCG zone would not need additional drilling, and separation of boreholes would be such that high overpressures in a single well would not be required. Regarding injection energy requirements, the existence of a 'sweet' injection zone (Law and Bachu, 1996) represented by goaf would significantly decrease the consumed energy in comparison to deep saline aquifers.This aspect is non-negligible, as Pruess (Pruess, 2008) estimates the compression power required to inject in a deep saline aquifer the CO_2 produced during 30 years in a power plant at a rate of 10 Mt/year, is 4.74×10^{15} J.

Containment

Level of containment depends on site sealing capacity and active trapping mechanisms. Sealing capacity depends on capillary entry pressure and presence of discontinuities. Capillary entry pressure at which other gases (N_2 or Ar) will leak into a seal has been determined by (Bildstein et al., 2009) in lab experimental work in a range of 2 to 5 MPa. According to their simulations, these pressures can easily be reached. Additionally, in case of UCG, the presence of fractures and fault reactivation due to roof collapse and high temperatures diminishes the required injection pressure for fracture propagation in comparison with intact rock. However, the number of wells available for injection would diminish the maximum local pressures. Regarding trapping mechanisms, four main ones have been described (Bachu, 2008). A strati-

graphic or structural trapping that slows vertical migration and increases pathway length, augments the other two hydrodynamic trapping mechanisms (i.e. residual and dissolution) (Gibson-Poole et al., 2008). In UCG the collapse and subsequent subsidence effects with fracturing and bending of strata extend over a large area, so it has to be proved that 'secondary' boundaries offer enough confidence for sealing. Depositional environment will have an impact on structural trapping capacity. For instance, turbidite flows in shallow parts of prograding delta systems may leave high-permeable channels and lobes through the otherwise low-permeable shale layers (Grimstad et al., 2009). Connections among lobes and channels may create potential weak points in the cap-rock.

Residual trapping depends on multiphase fluid processes immobilizing free-phase CO_2. This phenomenon is history-dependent and can be modelled using hysteric capillary pressure and relative permeability curves, determined through field experiments. Dissolution trapping relies on the higher density of CO_2 saturated brine. When it sinks, a circulation pattern with the native brine is created, allowing more CO_2 dissolution in non-saturated brine. However, Lu et al. (2009b) points out the existence of an 'equal density temperature' beyond which CO_2 saturated brine has a lower density, counteracting the described effect. Thus, residual high temperature in a former UCG zone might lead not only to potential phase change and decreased density of CO_2 (and thus of subsequent storage capacity) but also to diminution of the dissolution trapping mechanism. In addition, the dispersion of a high temperature field would be more acute in the case of a connected fracture network via convective flow.

In the case of UCG, adsorption of CO_2 into coal can also act as a trapping mechanism; though adsorption would imply the release of a certain amount of methane, and swelling of the coal could close cleats in the coal, conferring sealing properties to the coal layers. Reciprocally, the presence of methane in the plume will alter

physico-chemical properties.

Lastly, the mineral trapping mechanism in the long term would depend on the geochemistry of the rocks, but also on the geochemistry of the fluid. No studies including the type of impurities expected in the CO_2 stream plus the contaminants released during and after gasification or additional methane have been carried out to evaluate the chemical reactivity of such a plume with host rock.

It is worth noting that, though the first attempt is to store CO_2 in the gasification void, it could be the case that other alternatives have to be evaluated for economic or technical reasons.

2.5.3 UCG engineering design

Response of the surrounding rock to cavity creation depends on the geometry of the void, depth and thickness of the coal seam, rate of extraction and rock parameters of the adjacent strata. High temperatures will also modify rock characteristics. As the gasification operational design affects so strongly the response of the subsurface, site characterization and design of exploitation should inform each other iteratively.

Drilling pattern

Different designs have been proposed and tested in UCG pilots (Gregg et al., 1976; Olness, 1977; Yang et al., 2003; Mallet and Davis, 2010). The simplest model would consist of two vertical wells (one for injection and one for production) spaced 30 m to 40 m apart, producing a cavity separated from the next one by a pillar. This model has variants with different distances between wells and well inclination and relies on controlled retraction and injection point (CRIP) technology for ignition and development of the gasification chamber. Recently, in Australia (Bloodwood Creek) two parallel wells were driven along the coal seam to intersect a vertical one where ignition is produced (Mallet and Davis, 2010). These two wells, separated 30 m,

can run for 600 m and produce a gasification panel of 600 m x 30 m analogous to 'shortwall' mining panels. Other proposed designs (Siemaszko, 2010) are based on oil drilling technology, with a daisy drilling well and circular sections of gasification chambers which are backfilled as the gasification progresses. The design, either if it resembles stope and pillar, longwall mining method or a new pattern, will have a significant impact in the subsequent mechanical and hydrogeological behaviour of the site, the extraction ratio and the number of wells.

Cavity geometry and size

The geometry and size of cavities can be inferred by means of thermocouple measurements and mass balance. Cavity growth responds mainly to operating temperature, water influx, gas pressure and coal characteristics (thermomechanical spalling, ash and fixed carbon content) (Perkins and Sahajwalla, 2006). The number of cavities, distance between wells and pillars width will affect the geomechanical behaviour of the immediate roof.

Cavity flushing/cooling time

If cavities are flushed and contaminants removed to an extent, it is necessary to provide water treatment plants for the contaminated water. The decision of whether or not to flush the cavity will also affect the cooling time of the surrounding rock mass and consequently the fluid properties (brine and injected CO_2). Density of supercritical CO_2 varies greatly within a few degrees change, so storage capacity will also be altered. Quick cooling reduces the pyrolysis and the resulting undesired compounds. The geomechanical response of the rocks can also be altered by the sudden cooling of rocks subjected to high temperatures, with increased thermal fractures development.

Rate of extraction

Multi-seam extraction sequence and ratio play a critical role in stability of the formation. Number of seams where extraction will occur, sequence of extraction (bottom upwards would be recommended) and extraction ratio, that is, the size of pillars between stopes or panels to be left, will also determine the hydro-geomechanical behaviour.

Rate, sequence and amount of CO_2 to inject

Depending on the planned production and velocity of deployment, expected rate and amount of CO_2 to inject will require a determined sequence of the production.

Surrounding rock parameters

Coal seams overlain by strong, dry roof rocks are preferred, to minimize heat losses and escape of gas to the overburden (Burton et al., 2006). There should not be any major aquifer over the coal seam at least within 60 to 105 m depending on the width of the excavation (National Coal Board, 1969) or 25 times the seam thickness (Sury et al., 2004).

2.5.4   Conceptual model

Site characterization and UCG engineering design will allow the development of a particular and site specific conceptual model which accounts for potential pathways and consequences of release of CO_2, organic and heavy metal contaminants, groundwater depletion, subsidence or seismic activity.

2.5.5   Hazard identification

As described in CO_2 risk assessment, several hazard evaluation techniques have been used to identify potential hazards. The most relevant has been Features, Events and

Processes (FEP). However, a UCG scenario has not been considered to date. That would require integrating new features, processes and events not currently considered in the Quintessa database (`http://www.quintessa-online.com/co2.php`).

Hazards inherent to UCG–CCS include gas accumulations; water resource depletion; gas escapes; mobilization of organic contaminants and heavy metals; displacement of brine; change of hydrogeological regime; leakage of CO_2 (into soils, seabed, groundwater, surface waters or the atmosphere); ground subsidence; seismic activity and fault reactivation. Waste streams from syngas treatment and water flushing may contain sulphur compounds, mercury and other volatiles.

2.5.6 Effects assessment

The effects assessment should evaluate the sensitivity of species, communities, habitats and processes (Bouc et al., 2009) to different grades of exposition to contaminants, leakage of CO_2, ground subsidence or seismic activation. Some of these effects are well known and there are specific regulations to control them, like acceptable limits for subsidence (National Coal Board, 1969) or content of organic compounds and metals in water (EU Parliament, 2000). Also CO_2 effects on individuals are well understood and quantified. However, how sustained low dose exposure can affect ecosystems and their resilience is poorly understood (London Convention, 2006). Even if the threshold of risk acceptability is zero, should failure occur then potential impacts have to be foreseen in relation to human health, the marine or terrestrial environment and other legitimate uses of the sea or land. Not only the amount of released CO_2 or contaminants has to be assessed, but also it is necessary to quantify to what extent it comes in contact with the ecosystem. In a UCG-CCS operation, effects can be due to gasification, storage or a combination of both.

Due to the gasification operation

Subsidence or ground movement can affect both the built environment (buildings, bridges, roads, sewages, water, gas and electricity supply lines) and soils and surface drainage. Subsidence at surface induced by deep UCG is expected to be small (at most a few millimetres), and by analogy to long- and shortwall mining activities, it may well be immeasurably small where depths are great (>500m) and void widths modest (<50m). Full prediction must take into account the number and thicknesses of seams thickness, void width, rate of exploitation and local hydrogeology and rock mass properties.

Depletion of groundwater resources could affect natural wetland ecosystems and human activities such as irrigation.

Water and soil contamination might arise from migration of pollutants from the gasification zone or from process waste-streams (e.g. water used in cavity flushing or syngas clean-up). Possible impacts on sensitive receptors would occur as in other polluted environments.

Potential gas escape from the cavity will affect the economics of the project and can transport contaminants away from the reactor zone.

Variability in syngas flow and composition has a direct effect on turbine performance and overall benefit.

Due to CO_2 injection

The effects of leakage of CO_2 depend on whether it occurs to water, to the open atmosphere or into confined spaces; in the latter it can have acute toxic effects. The effects of increasing concentrations of CO_2 in aerobic living organisms are acidosis, hypercapnia and asphyxiation (Metz et al., 2005). There is no current knowledge of which benthic invertebrates, plants or or soil microbes are most susceptible to different levels of exposure. CO_2 could well affect microbes which bio-degrade organic

contaminants, nitrates and ammonia. In aerobic groundwaters, ammonia would tend not to persist but convert to nitrate, whereas in anaerobic conditions, nitrate converts to nitrogen gas (Burton et al., 2006). Though the Water Framework Directive has clear stipulations for organic and metal contaminants, CO_2 is not directly regulated. CO_2 dissolution can cause changes in pH in sediments, soils and water, affecting aquatic organisms. Clearly, BTEX (benzene, toluene, ethylbenzene, and xylenes) compounds transported from gasification zones in the CO_2 stream could have toxic impacts if they enter the biosphere in high concentrations. Finally, brine displacement could lead to saline intrusion in fresh water aquifers, making them unsuitable for further exploitation.

Additionally, other effects resulting from combination of UCG–CCS could be the migration and accumulation of methane in closed spaces with subsequent risk of explosion and the corrosion and failure of structures due to carbonic, sulphuric and hydrochloric acids.

Severity of impacts depends as much on the physical and geochemical dynamics of the recipient medium as it does on the magnitude and rate of pollutant release. If implemented below shallow coal resources amenable to conventional mining, UCG–CCS might sterilize them (i.e. put them off-limits for mining). In most cases this is an unlikely scenario as UCG will only proceed after shallower deposits have been mined conventionally. Consequences of UCG–CCS are as highly site specific as geology , topography, meteorology and distribution of vulnerable receptors (Bouc and Fabriol, 2006). However, it is likely that enforcement of the EU Water Framework Directive will mean that UCG–CCS operations would only ever take place in permanently unusable (PU) waterbodies, either off-shore or in deep, saline onshore strata. For instance, provisional licenses for UCG in the UK have all been granted for offshore sites where there are no freshwater aquifers.

2.5.7 Exposure assessment

Exposure assessment involves the characterization of potentially vulnerable populations or individuals, identifying processes and pathways, and determining the possible extent of exposure in quantity and time. It should also evaluate pollutant attenuation processes and examine the resilience of ecosystems.

Upper and lower-bound estimates for how the ecosystem might be affected must be defined and monitored, to establish a baseline and check the impact. Quantitative exposure assessment measures the average daily intake, which combined with the toxicity of the substance (studied in dose-response assays) produces a quantified value of the risk.

Chemical and physical characterization of the syngas and the CO_2 stream is therefore necessary, not only to understand the processes that influence the migration and leakage of the plume, but also to determine with which substances and in what ways ecosystems might be impacted.

As a preliminary guide, injected CO_2 streams will have between 1% and 10% of impurities: in oxyfuel combustion, impurities can be up to 10%; in pre-combustion capture less than 5%, and in post-combustion capture less than 1% (Seevam et al., 2008). Components in the gas stream which are critical for the storage process are H_2O, SO_2, NO, H_2S, O_2, CH_4, HCN, Ar, N_2, H_2 and particulates (Anheden et al., 2005). Tars and ashes deposited in the gasification void can impact the composition of the stream and contribute to clogging of the pore space. Reactivity of these components can add to the acidification caused by CO_2, formation of hydrate compounds or alter redox conditions and force precipitation (Anheden et al., 2005). Characterization of the coal and gasification products is also necessary to predict the gas composition and the pollutants. Content of Cl and S in the coal can be critical. In addition, the salinity of the brine has to be established in order to evaluate first,

the amount of Cl that incoming water into the cavity could contribute, and secondly, the solubility of CO_2 in it.

Processes

Physical, chemical and biological processes and their close interdependency have to be understood and represented in the models. Thermo-hydro-mechanical-chemical reactions in gasification occur at different speeds and with different durations in time and space. They start with high temperatures and changes in pressure and local hydrogeology due to the injection and production of gases, accompanied by mechanical and chemical changes. That will cause brine displacement and changes in regional hydrogeological conditions both by the depletion of water during gasification and by subsequent CO_2 injection. In the first case, a cone of depression can be formed due to the flow of water into the cavity, which is below the hydrostatic pressure. In the second case, the over pressurization of the water in the formation can lead to brine displacement and intrusion into freshwater aquifers.

Flow and transport processes will depend primarily on viscosity ratio, injection rate, relative permeability, reservoir heterogeneity and structural configuration (Gibson-Poole et al., 2008). In addition, hydrothermal effects combined with phase transition between supercritical and gaseous CO_2 can lead to very complex multiphase flow/multicomponent transport processes. During the gasification phase, complexity of flow is increased with turbulent flow of gases from injection and combustion and water inrush and changes of phase. In the case of UCG–CCS, flow in fractures can dominate due to the rock failure and the low permeability of intact rock.

Once high temperatures from gasification have dissipated and the temperature field has stabilized, during subsequent injection of CO_2 and its migration along any potential leakage pathway, there will be three phases: liquid water, liquid or super-

critical CO_2 and gaseous CO_2. Three-phase relative permeability functions which govern the interference among the phases can be expected to vary depending on whether the fluid is retreating (draining) or advancing (imbibing), and depending on the initial saturation level of the fluid (Tsang et al., 2008). Gas transport can be by diffusion through water, advection dissolved in water, transport of free gas as discrete bubbles within water-filled media, and movement of free gas phase by displacement of water from media. When considering longer term migration of aqueous phase contaminants, the mechanisms to be considered are diffusion and advection. In a low permeability environment such as the Coal Measures, flow via fissures, vertical and horizontal fractures created with cavity collapse, faults and bedding planes interface will be far more significant than the permeability of the rock matrix itself (DTI, 2004).

Leakage of CO_2 into surface may well be governed by phase change, dissolution, multiphase interference (Pruess, 2008) and the Joule-Thomson effect, which results in cyclic behaviour (Tsang et al., 2008; DTI, 2004). In contrast to mechanisms which would enhance leakage once begun, such as the lower density of CO_2 compared to water and buoyancy force that would increase as water is replaced by CO_2. the cooling effect of adiabatic expansion acts as a self-limiting mechanism through the interference of gas, liquid or even solid (dry ice) phases. The Joule-Thomson effect depends on the source of CO_2 and the depth at which secondary accumulations may have an important role in this process. The temperature change due to isenthalpic expansion can make CO_2 temperature drop to -15 ^{o}C (if the secondary accumulation is at 300 m depth) or -47 ^{o}C (if the accumulation is at -540 m) (Pruess, 2008).

Transport of contaminants which could be present in the CO_2 plume e.g. phenols or heavy metals- proceeding from gasification or reaction of the CO_2 with the host rock would be subject to the processes of diffusion into the larger groundwater volume or carbon dioxide plume, sorption onto coal, mineral grains and organic

carbon, abiotic and bio-degradation and removal via oxidation/reduction reactions (DTI, 2004). The effect of retardation of organic and metal on spread pollution in the concentration levels expected with UCG has not been studied with CO_2 acting as solvent. Its presence would interfere in the chemical and biological reactions responsible for the retardation. In addition, in some subsurface environments, microbially mediated conversion of CO_2 to methane may be possible (Pruess, 2008).

In case of leakage to surface, the transport, mixing processes and rates of leakage to the seabed sediments, water column, soils and atmosphere should be assessed. Once in the atmosphere, surface and meteorological conditions act on the exposure pattern. It is well known that one of the dangers of CO_2 is accumulation in valleys or low topographic areas. In addition, meteorological effects (wind, atmospheric pressure, precipitation, temperature) play a key role in the dispersion and time and rate of exposure.

Mechanical processes of spalling, caving and changes in the stress field have been estimated by empirical and numerical methods used in the mining industry (National Coal Board Mining Department, 1975). The development of fractures and bending planes and reactivation of faults are of major importance as future potential pathways for migration of CO_2 and contaminants. They are governed by two mechanical failure mechanisms: tensile fracturing and shear slip reactivation. Rock failure and modifications in the in situ stress field can trigger micro-seismic events as encountered in longwall coal mining (Goulty and Kragh, 1989). Though areas with natural seismicity are not targets for carbon geological storage, induced seismicity effects on potential structures and faults have to be considered.

Thermal processes, with temperatures up to 1000 ^{o}C, will affect chemical reactions in the rock and its mechanical and hydrogeological properties. Shale layers in the immediate roof subjected to such thermal stress could not maintain their required mechanical properties and sealing conditions (Burton et al., 2006). Fluids —

brine, gases or supercritical CO_2 — subjected to high temperatures can have sudden phase and density changes, increasing pressures in the rock, and modify their solvent capacity and reactivity.

Hydro-geochemical processes are expected to take place due to the high reactivity of O_2 and acids coming from the gasification and CO_2 injection and high temperatures and pressures. Carbonic, sulphuric and hydrochloric acids can leach metals and alter the local chemistry by dissolution, alteration and precipitation and corrosion of wells cement and casing.

Pathways

Pathways include a source and mechanism of chemical release to the environment, an environmental transport medium, a point of contact with the receptors (exposure point) and a route of intake (ingestion, inhalation, dermal absorption) at the exposure point. Leakage of CO_2 and contaminants can occur through joints, cleats and slips in coal, permeable rock matrices (high permeability consolidated or unconsolidated sands and gravels), joints, fissures, fractures and bed separation, faulting (though faults can act as barriers or pathways), igneous dykes and sills, karsts/solution features (either ancient or induced by dissolution in injected CO_2), mining/caving induced features and abandoned boreholes (DTI, 2004).

Faults and fractures may not only exist in the rock prior to UCG–CCS: they may be induced by UCG through subsidence, or else develop later as a consequence of increased pressure due to CO_2 injection. Experience in coal mining under waterbodies including the sea - has shown that it is possible to mine coal without inducing a connection between the void and the water body (Bicer, 1987). Gale (Gale, 2006) summarizes the results of a study in longwall panels up to 400 m depth where it was concluded that panels with a width to depth ratio greater than one typically resulted in connection to surface waters; panels with a width:depth ratio of less than 0.4 did

not develop any connection.

Permeability to gas (specifically methane) has been extensively studied around coal cavities (Esterhuizen and Karacan, 2005). Increased depths decrease the risk of connection. However, in a different time scale (from the 30-40 years lifespan of a mine to hundreds of years), these connections might appear if increased pressure contributes to existing fracture propagation or fault shear slip. Additionally, the buoyancy and different physico-chemical characteristics of CO_2, can impact the flow through fractures, having a lower viscosity and reacting with rock minerals, which could be dissolved creating a pathway for migration.

Leakage through cap rock can occur where: capillary entry pressure for CO_2 is surpassed; cap rock is locally absent; or due to the presence of faults or fractures in the cap rock. Hydromechanics of the cap rock and calculation of the maximum injection pressure are therefore essential.

Pore space (rock matrix) is the least probable pathway for leakage in a Coal Measures scenario due to the low permeability of the rock. Permeability in other CO_2 storage scenarios ranges between 0.01-10 Darcies in Kingfish Formation, Gippsland Basin, Australia (Gibson-Poole et al., 2008) or the 2.264 D in Frio Basin (Doughty et al., 2007), while in Coal Measures, permeabilities have been estimated in the order of 10^{-5} D (Sury et al., 2004). However, alteration of in situ stresses and chemical reactions will affect porosity and permeability. Petrological information can help in assessing the likelihood of potential host rock mineral reactions with CO_2, whether by dissolution, alteration or precipitation (Gibson-Poole et al., 2008). In carbonate lithologies CO_2 saturated water has a high reactivity that can seriously affect the reservoir structure. Though long term reactions would be more related to effectiveness of mineral trapping, dissolution can increase the risk of leakage while precipitation can close pore space helping to enhance confinement, though at the same time complicating injection and requiring increases in pressure to accomplish

it. In addition, increased acidity of CO_2 bearing water may enhance the solubility of heavy metals present in minerals or adsorbed on mineral surfaces, adding them to the undesired contaminants carried by the plume (Tsang et al., 2008). On the other hand, supercritical CO_2 is weakly reactive with the host rock but a very good solvent of organic substances present in the gasification chamber. However, the hydraulic processes of drainage and imbibition induced by supercritical CO_2, can lead to the precipitation of salts and other secondary minerals, modifying porosity and injectivity (André et al., 2007), adding its effect to the pore blockage of tars and ashes.

Additional potential pathways and processes for migration are pockmarks and paleo gas chimneys. Many of the underlying processes of seepage through the seabed are still unknown (Judd, 2004) and pockmarks and vents are not always related (Schroot et al., 2005), but it is recognized that hydrocarbon seepage is present throughout the world (Kvenvolden and Cooper, 2003) and some estimates ranks as high as 47% the proportion of crude oil entering the marine environment through these natural pathways versus the 53% due to man-made structures and spills. Thus, the structure of the basin has a great importance regarding heterogeneity and preferential paths or channelling flow for migration of CO_2 and contaminants. Fluvial deposits are characterized by reservoir heterogeneity (Doughty et al., 2007). Depositional settings such as barrier bars (with continuous high-permeability sands), distributary channels (with intermingled sands and shales with a large high-permeability sand component) and inter-distributary bayfills (predominantly formed by low-permeability discontinuous shale lenses, interspersed with moderate-permeability sand) confer a degree of heterogeneity which combined with buoyancy flow is critical in determining the effectiveness of structural and stratigraphic trapping (Tsang et al., 2008).

Due to the extension of a CO_2 plume, is it not expected that a single cap rock can cover it with no fault, fracture, or discontinuity. Therefore, multilayer cap rock

is preferred. The lithology of Coal Measures where UCG would take place is principally formed by alternation of mudstones, shales, coal and sandstones, providing a convenient scenario in relation to multi cap rocks. Mudstones and shales could be expected to act as cap rocks, but in the case of CO_2 injection, there is a particularity of its interaction with coal that could make coal act as a sealing cap rock to a certain extent. As CO_2 replaces the methane molecule in the coal structure, a swelling of coal takes place, closing cleats and small fractures. As most permeability in coal is due to fractures and cleats, a certain amount of CO_2 reaching the coal could make it act as a sealing layer.

Wells are the most critical pathways for leakage. Leakage through wells in enhanced oil recovery operations or in other fluids injection has been long studied and methods for estimating probabilities of failure are available (Carey et al., 2007; Jordan and Benson, 2009). Based on this experience, Celia et al. (2005) used a stochastic approach to estimate leakage through wells for CO_2 storage.

Wells perforated in UCG are subject to much harsher conditions than CO_2 injection wells in saline aquifers, mainly due to thermal stresses (due to the high temperatures of several hundreds of degrees Celsius reached during gasification), but also due to tensional stress (due to expansion and compression) and the action of acids produced by gasification: HCl and H_2S acids are formed from S and Cl in coal or Cl in brine. Though a CO_2 stream could have some traces of these acids as impurities, the amounts formed in the gasification process are much more significant and could create serious concern for the corrosion of well casings. Another very inconvenient process for well cementation durability is the variation in the stress field in the surrounding rock. Subsidence produces zones of tension and compression. These tension zones are likely to intersect the wells after they have been drilled, with the subsequent risk of tensional failure of the cement and creation of a pathway along the annulus. In the event of annulus or section open-hole failure, an additional consideration of

turbulence in the modelling of wellbore flow, normally conceptualized as Darcian, should be taken (Pruess, 2008). Additionally, distinctively from the case of direct injection through one well in deep saline aquifers, each injection point could have at least two boreholes that connect it to a main borehole (in case of ramification) and to surface, increasing the probability of leakage through wells. In cases where a third well is used for ignition, the situation would be worsened. Also, attempts to converge both wells at such depth and with in-seam drilling, is likely to be subject to error and re-drilling. This potentially adds new uncompleted boreholes to the net of leakage pathways and strata disturbance.

Once site characterization has been carried out, a conceptual model has been developed and receptors and pathways have been identified, fate and transport modelling is used to calculate flux rates. Processes and spatial and time scales are so varied that, due to inherent limitations of numerical models, it does not seem reasonable to expect that a single numerical model can address all the exposure processes and pathways occurring in time with sufficient resolution, so dedicated models should be used.

Simulation of these phenomena require the coupling of multiphase flow and multicomponent transport processes, kinetically-controlled geochemical processes, high-temperature thermal processes and geomechanical deformation processes. In particular, multiphase advection, molecular diffusion, and mechanical dispersion, fluid-fluid and fluid-mineral mass transfer, stress-strain evolution, and the relative permeability, capillary pressure, thermodynamics, phase changes, kinetic and fracture stiffness play a role in the interaction of the fluid and the geological medium (Johnson, 2009). In situ pressure, temperature and water salinity and macro/meso/micro pore size distribution of the rock affect capillary pressure, interfacial tension and relative permeability, which affect CO_2 displacement and therefore CO_2 injectivity, migration and trapping mechanisms. Neglecting these effects will lead to errors in modelling

and decision making (Bachu and Bennion, 2008)

Likelihood of exposure:

Numerical models and simulation tools can assess the amount of CO_2 and additional contaminants proceeding from UCG or mobilized by the plume and their flux in time and space. Modelling of processes and pathways is done generally in a deterministic way (Pruess et al., 2002) and yet most of the functions of distribution of probabilities of input parameters are unknown. Stochastic representation of selected geological parameters allows uncertainty to be accounted for to some extent. However, methods such as Monte Carlo simulations demand such computational effort that these methods become impractical. Nevertheless, total uncertainty and its propagation have to be quantified in order to be able to produce an adequate risk characterization.

2.5.8   Risk characterization

Risk characterization determines the likelihood and severity of impacts. According to the information available, it can be qualitative, semi-quantitative or quantitative. In initial stages when data are scarce, risk characterization will be qualitative, though ultimately a UCG–CCS risk characterization has to aim to be quantitative. As explained above, it is necessary to demonstrate that local and global risks of UCG with CO_2 storage are quantitatively lower than the local and global quantified risks of other alternatives. Currently, quantification of probability of exposure and quantification of effects in relation to that exposure are both pending issues to be satisfactorily solved. The absence of field data and statistics hinder the acquisition of reliable values for the probability distribution functions and therefore the leakage rate is usually calculated with deterministic models using a range of scenarios.

Risk characterization requires a thorough and adequate site characterization and definition of temporal and spatial scales. Ultimately, the value of interest is the

leakage rate as a function of space and time (Vivalda et al., 2009). Uncertainties have to be identified and quantified. Some of the epistemic uncertainties and knowledge gaps have been listed for UCG (Burton et al., 2006) and CCS (Johnson, 2009). In lieu of other approaches, methods such as expert judgment must be used to account for uncertainty. Some uncertainties can be addressed using experience from natural or industrial analogues, such as wells from EOR and hazardous waste injection and long-term isolation assurance in the nuclear industry. Well failures have been sufficiently well documented to yield statistical data for understanding uncertainty in failure rates. However, it cannot be directly applied to UCG–CCS due to the different stresses that wells in UCG–CCS will be subjected to. Similarly, rock types and engineering of a nuclear waste repository differ from a UCG–CCS site. Another analogy that can be useful is underground coal mining, in which geomechanical behaviour is well known and changes in permeability and porosity and development of fractures are better understood. However, there are also some differences present in this analogy, mainly the high temperatures reached in UCG and the long term sealing expectation. A certain connection to a water bearing strata that causes a limited inflow of water into a mine void, as long as it can be economically pumped, could be acceptable in the lifespan of a mine (e.g. 20 to 40 years), while it would not be acceptable in the case of CO_2 storage as the leakage target is zero and the timeframe is of hundreds of years.

A critical issue is how to address uncertainty. By their very nature, geological systems possess a combination of aleatory uncertainty due to their heterogeneity and epistemic uncertainty due to the impossibility of a complete sampling and testing of the whole system. UCG–CCS processes add a large epistemic uncertainty. Representation and propagation of this type of uncertainty is still a subject of research (Oberkampf et al., 2004). The conclusion is that an increase in knowledge is essential before a comprehensive risk characterization can take place.

2.5.9 Monitoring and mitigation options in risk management

Objectives for monitoring are to provide baseline data and verify and validate modelling predictions. As such, monitoring has to occur during every stage of the process. During gasification, monitoring will elucidate changing hydrological and geomechanical conditions that can hinder subsequent CO_2 injection. Essential elements of process control and monitoring during UCG are the injection rates of steam, air or oxygen, product gas flow, composition of the syngas, continuous pressure and temperature conditions, cavity formation and failure progression, subsidence and mechanical integrity and corrosion of wells.

After gasification and during CO_2 injection, CO_2 injection rates, pressure and hydraulic gradients in the area, micro-seismic activity, ground subsidence or uplift, composition and properties of the injected fluid and mechanical integrity and corrosion of wells should be monitored, so any pressure builds-up, confinement problems and mechanical complications (corrosion, erosion, failures of wellhead, etc.) can be detected.

Monitoring after the injection period has to assure proper performance of the containment and warn of any leakage. Post-injection migration of the CO_2 through strata, seafloor and water column must be monitored, as well as potential receptors, such as benthic communities if storage is located under the sea. A local high rate of CO_2 leakage is far easier to monitor than modest leakage spread over a wide area. Monitoring equipment exists for use on land and off-shore, but monitoring of CO_2 leakage in the seabed and water column is an issue, especially if leakage is not continuous in time. Experience in monitoring natural gas seepage in the seabed (Judd, 2004) shows the difficulty in differentiating gas from a shoal of fish with seismic systems or measuring flux rates over a vent.

Different techniques are suggested for monitoring the migration of CO_2 under-

ground and entering surface water or atmosphere (Chadwick et al., 2009b; Pearce et al., 2005). It can be done with indirect methods, such as vertical seismic profiles to monitor the plume or CO_2 (saturation) sensitive well logs or directly by sampling fluid at an observation well (Doughty et al., 2007). However, current technologies are insufficient for measuring fluxes or concentrations and establishing mass balances. For instance, seismic methods can detect concentrations of CO_2 dissolved in brine over 5% but cannot discriminate between this value and maximum values of 60–70% (Johnson, 2009). Similarly, remote sensing, e.g. hyperspectral imaging, can detect plant stress associated with gas leakage but not the amount of CO_2 released into the soil or the atmosphere.

Other techniques applicable to the operational phase of UCG are microseismic analysis to detect cavity failure and electrical resistance tomography or electromagnetic induction tomography to monitor cavity evolution, groundwater transport and potential loss of product gas (Burton et al., 2006).

In any case, methods chosen for monitoring should not compromise the integrity of the cap rocks which seal the formation. Area and frequency of monitoring will depend on time since injection and acting trapping mechanisms.

Mitigation measures have to be planned for gasification, CO_2 injection and post-injection operations. During gasification, control of pressure and combustion agents can stop gas escape and burning. Following recommended procedures to shut down will avoid pyrolysis with subsequent increase in contaminant formation. Other modifications that can take place to minimize the risk of pollution of UCG contaminants can be the flushing of gasification chambers and treatment of waste water. Soils and ground waters contaminated with UCG by-products can be treated with physical and chemical processes for removal of contaminants (e.g. carbon adsorption for phenols, other organics and metals, steam stripping for ammonia and H_2S) (Covell, 1986). In addition, in some environments, natural biodegradation can also attenuate

the contaminant levels. Should gasification operations compromise the possibility of CO_2 injection in the reactor zone, alternatives can be studied, such as use of CO_2 for ECBM in other coal layers, injection into deeper formations far away from the gasification zone, transport to other storage site or venting. Confinement issues during CO_2 injection can be addressed similarly.

Well failures can be dealt with by recapping wells or filling fissures in the annulus between cement and casing, drilling intersecting wells, controlling the release with heavy mud and recapping. Cement types resisting acid conditions (HCl, H_2S, CO_2) and high temperatures would be needed. In case of leakage through fractures and faults, suggested mitigation measures (London Convention, 2006) are oriented to lower the injection pressure (by pumping fluids, halting the injection or transferring CO_2 to another reservoir) and plugging the pathway by injecting sealing material.

At depths where UCG–CCS would take place and with the high temperatures involved, no bio-remediation activity in the organic contaminants will occur. Chemical and biological degradation of the contaminants will be related to shallower environments, near surface vadose zones or aquifers (DTI, 2004).

The qualitative assessment of UCG particularities discussed in this Chapter gives evidence of counteracting processes which will impact the storage capacity, injectivity and containment of CO_2. Table 2.1 summarizes these issues in comparison with the two main foreseen scenarios for CO_2 geological storage –depleted hydrocarbon fields and deep saline aquifers–, underlying the need for further research to quantify these opposed effects.

Table 2.1: Comparison of differentiating factors between UCG-CCS and CO$_2$ storage in depleted hydrocarbon fields and deep saline aquifers and their impact on capacity, injectivity and containment

Factor	Comparison	Impacts		Effects		
		Positive	Negative	On storage capacity	On injectivity	On containment
Depth	Reduced depth (~800 m) in comparison with depleted hydrocarbon fields (average well depth ~ 1,800 m*) and deep saline aquifers (Sleipner ~1,000 m, Weyburn ~1,500 mln-Salah ~2,000 m)	Lower temperature due to the geothermal gradient	Being close to its critical conditions, phase changes in CO$_2$; Reduced overburden results in reduced migration pathway distance	Dependent on balance of counteracting effects of pressure and temperature in CO$_2$ density	Potenitially improved due to generally lower hydrostatic pressures and higher permeabilities (lower compaction) at shallower depths	Compromised due to the reduced overburden
Number of wells	High number of wells (low to medium in oil and gas fields, very low in deep saline aquifers)	Better knowledge of the local geology and features; Reduced overpressure due to CO$_2$ injection in each individual well; Reduced energy consumption for the compression	Increased number of potential leakage pathways	Improved due to the reduced local overpressure during injection and alternatives for managing injection	Improved due to the lower injection pressure requirement	Compromised by the increased number of potential leakage pathways
High temperatures during coal gasification	Temperatures over 1,000 º C in UCG operations. No alteration of geothermal conditions in deep saline aquifers; smaller alteration (one or two orders of magnitude lower) of geothermal conditions in thermal recovery (steam injection) and water injection operations in oil and gas fields	Remaining elevated field temperatures decrease potential hydrate formation during CO$_2$ injection due to the Joule-Thomson effect	Decrease mechanical resistance of the rocks; Mineralogical changes in the rock which affect its sealing capacity; Change of phase and density in fluids subjected to rapid changes in temperature, leading to increased pressure in the rock; Changes in reactivity and solubility between fluids and rock; Decreaed CO$_2$ density; Thermal stress and failure in well cementing and casing	Reduced due to the increased CO$_2$ density by temperature and potentially by the loss of permeability and porosity in the surrounding rocks	Dependent on the effects of temperature and fluids in the mineralogical composition of the rocks (increased or reduced permeability)	Compromised due the the higher buoyancy of lower density CO$_2$, the thermal stress and failure of the surrounding rock and wells cementing and casing, diminished dissolution trapping mechanism
Presence of overlying and lateral coal layers	Presence of coal seams over and around the CO$_2$ injection zone in UCG. Not necessarily present in other hydrocarbon scenarios or deep saline aquifers	CO$_2$ adsorption into coal produces swelling of the coal and closes cleats which are the main hydraulic conductivity pathways in coal, providing sealing properties	Methane liberation as it is substituted by CO$_2$	Compromised if coal limits access to more permeable and porous formations	Compromised if local pressure builds up quickly due to surrounding coal	Improved due to the addition of layers which acquire sealing properties when in contact with CO$_2$

*Source: http://www.eia.gov/dnav/pet/pet_crd_welldep_s1_a.htm

Factor	Comparison	Impacts		Effects		
		Positive	Negative	On storage capacity	On injectivity	On containment
Cavity formation, cavity roof collapse and fracturing of the rock	UCG produces a very high degree of disturbance in the rock and stress field. Except for hydraulic fracture operations in hydrocarbon fields, -by nature no good candidates for CO_2 storage anyway-, no such disturbance occurs in prospective depleted hydrocarbon fields and deep saline aquifers	Creation of a high porosity and high permeability zone around the future injection well	Development of fractures, joints opening and fault reactivation; ground subsidence and heaving; stress field and displacement variations causing mechanical stress on wells	Improved thanks to the created voids and increased porosity as a result of lower stresses	Improved due to the high permeability or "sweet" zone around the injection point	Potentially compromised if CO_2 migration pathways extend beyond the sealing formations and well integrity is affected
Cavity flushing	Water can be injected in hydrocarbon fields for the purpose of sustaining the reservoir pressure or water flooding recovery. However, the contrast in reservoir and temperatures will not be so significant	Cools down the area, reducing pyrolysis and therefore the production of contaminants, washes existing contaminants and solid particles	Thermal stress. Production of waste water streams which require treatment	Improved by the lower reservoir temperature when CO_2 is injected	Improved due to the removal of particles which may clog the pore throats, reducing permeability	Potentially compromised by additional fracture development due to thermal stress
Presence of by-products of the coal gasification (tars, ashes, organic compounds and metals)	These products are not present in deep saline aquifers. Depleted hydrocarbon fields will have residual oil and gas	Heavy organic compounds highly soluble in the CO_2 stream will increase its density and reduced buoyancy	Metals, chlorides and sulphides may form acids and corrode wells. Tars and ashes may clog pore throats. Potential presence of organic and metal contaminants in leaking CO_2. Increased acidification of CO_2 in conjunction with chlorine and sulphur. Formation of hydrates and precipitation. Alteration of the rock mineralogy. Uncertain effects on residual saturation and relative permeability in the fluids	Dependent on the effects of geochemical reactions on porosity	Potentially compromised by tars and ashes and precipitates affecting permeability	Potentially compromised by well corrosion and improved by CO_2 stream density

2.6 Conclusions

An environmental risk assessment framework for UCG–CCS has to comply with fundamental criteria of transparency, clarity, consistency and reasonableness, in order to be able to take decisions at a risk management stage that can truly compare the risks of different alternatives for energy production. Ultimately, any CO_2 storage environmental assessment should quantify and compare the risks of undertaking the sequestration to the benefits that are expected to be obtained, notwithstanding that the storage is only one of the cumulative risks of capture, transport and sequestration.

Though hazards present in UCG and CCS are well known, important gaps exist in knowledge of exposure and effects quantification, and therefore in risk characterization. The combination of both technologies presents environmental advantages and disadvantages which need further research. A conclusion which can never be over-stated is the necessity for a thorough site characterization to ensure success of the operation, as well as the proper design of the UCG layout. Some of the uncertainties arise from antagonistic effects that occur with UCG–CCS: regarding CO_2 storage capacity in a UCG–CCS operation, if the creation of a zone with higher porosity and permeability yields an initial higher capacity than e.g. in a deep saline aquifer or an intact coal seam, the presence of fractures and low permeability of the rock will compromise the maximum injection pressure, when capacity is ultimately based in overpressurization of the reservoir. In addition, time for dissipation of high temperatures will compromise the CO_2 storage capacity for obvious reasons of density and injection sequence. For the same reason, injectivity is favoured by the creation of a high permeability zone around the injection point, and the elevated number of injection wells, but maximum pressures will be more limited due to the presence of fractures. Containment is disfavoured by the disturbance of the rock and an increased number of wells, and also by the degree to which these are subjected to

elevated thermal and mechanical stresses, chemical attack and corrosion. However, upper layers of coal can add sealing properties once cleats have closed due to the swelling of coal after contact with CO_2. Major leakage pathways are likely to be wells, fractures, faults, dykes and other structural elements which give rise to discontinuities in the cap rock. Wells — the weakest link — will be especially stressed in UCG–CCS applications. Therefore, an understanding of flow and transport processes in porous and fractured media, coupled with thermo-mechanical and chemical effects, is necessary to predict the behaviour of CO_2 and contaminants in UCG–CCS and ground movement. Other critical issues for exposure assessment, such as characterization of coal, gas and CO_2 streams, are essential to achieve quantitative estimates of exposure risk. Effects of subsidence, organic contaminants, metals and CO_2 are well known in structures and individuals. However, effects of low releases extended in time on communities and their resilience is not so well understood. As in the case of the exposure assessment, more research is needed in order to be able to quantify the consequences. It follows that, since risk characterization is the product of the probability of exposure and the severity of the consequence, current risk characterization can only be done in a qualitative or semi-quantitative form. However, the risk assessment of UCG–CCS demands a quantitative assessment, so more research has to be done in both fields of climatology and CCS to be able to make a comparative analysis. Monitoring technologies face several difficulties, and probably the main one is to obtain the mass balance between injected fluids and produced gas or migrating CO_2. Accurate measurement of leakage fluxes is a requirement in order to implement the mechanisms for CCS and current monitoring technologies cannot guarantee providing that information, except in very specific cases.

It can be concluded that a comprehensive framework for environmental risk assessment of UCG–CCS has to be approached in an holistic way that truly accounts for benefits and costs from both global and local perspectives. Due to the uniqueness

of ecological systems, site-specific characterization is a key factor in problem formulation. On the other hand, it is advisable to clearly differentiate the steps and parts of the risk management process so a systematic approach can be applied without losing clarity, especially when different methods and techniques for hazard identification, exposure assessment or uncertainty treatment will have to be combined to obtain a satisfactory answer.

Chapter 3

Modelling UCG-CCS

3.1 Introduction

Early development of UCG modelling in the 1970s and 1980s in the USA and in the 1990s in Australia, focused on the assessment of the hydro-mechanical response with a special attention to surface subsidence (e.g. Trent and Langland, 1981). Cavity growth in the gasification process is also being addressed (e.g. Park and Edgar, 1987; Perkins and Sahajwalla, 2006). However, probably the main concern about UCG has been related to groundwater contamination of shallow aquifers (e.g. Humenick and Mattox, 1978; Blinderman, 2002; Burton et al., 2006). The concerns for subsidence and shallow groundwater contamination are obviously stronger at shallower depths, e.g. in the range of 40 m in Angren (Uzbekistan) to 300 m (Queensland). Only a few deeper pilot projects beyond 500 m (in Spain, Belgium and South Africa) have been carried out to date.

Consideration of coupled thermo-hydro-mechanical-chemical effects in fractured and porous rocks will be essential for the understanding and evaluation of potential CO_2 storage in the vicinity of an underground coal gasification void. The majority of research related to geological sequestration of carbon dioxide so far has focused on depleted oil and gas fields (e.g. Trivedi and Babadagli, 2009; Hawkes et al., 2004; Ferronato et al., 2010) and deep saline aquifers (e.g. Goerke et al., 2011; Goodarzi et al.,

2011), and to a lesser extent, in unexploitable coal seams (e.g. Dutta and Zoback, 2012). In addition, the limited experience in large scale sequestration projects (Sleipner, Weyburn, In-Salah and recently Snohvit) has not dealt with the highly fractured environment expected in a UCG operation. Moreover, initial storage safety criteria tend to consider sites with a low level of natural fracturing. Only recently, research in injection of CO_2 in fractured porous media is starting to be developed (Talebian et al., 2013; Liu and Rutqvist, 2013), mainly as a result of leakage issues and observed heaving occurred in In-Salah. These problems have been attributed to the existing faults and fractures network (Morris et al., 2011a; Smith et al., 2011; Iding and Ringrose, 2009, 2010). The general approach for the engineering design has been to consider that injection overpressure should not exceed the fracture pressure. In some cases and following legislation related to underground waste fluid injection, this suggested pressure is limited to 90% of the fracturing pressure (EPA, 2008). On the other hand, exceeding such thresholds can lead to the vertical propagation of fractures. Distances travelled vertically by hydraulic fractures can be up to several hundreds of metres (Davies et al., 2012).

Most of the simulation research in coupled geomechanical systems applied to CO_2 sequestration has therefore considered a single porous medium and the Mohr-Coulomb failure criteria to determine the tensile or shear fault slip potential. With regards to CO_2 injection in fractures, research has focused more in fault reactivation and fault conductivity of discrete faults and caprock failure potential rather than in fracture development since, as mentioned, it is foreseen that injection pressure should be below the fracturing limit.

The inclusion of UCG scenarios in the list of potential CO_2 storage sites is highly likely to request at least a similar — if not more demanding — standard for CO_2 plume evolution prediction as those being used for depleted hydrocarbon fields and deep saline aquifers. Modified rock geomechanical parameters, rock failure and sub-

sequent fracture development and alteration of in situ stress field represent major issues in estimating the caprock failure potential. It is well known that the initial in situ stress regime is critical for evaluation of maximum sustainable CO_2 injection rate (Rutqvist et al., 2008).

If simplified conceptual models and analytical calculations, or experimental and analogue approaches may be acceptable at initial stages, ultimately, a detailed modelling exercise is foreseen to be necessary for final approval of a storage site. Predictive tools to guarantee with an acceptable level of uncertainty the short and long term containment of CO_2 cannot rely only on limited analogies which otherwise might be very useful for the design of the UCG operations (e.g. Younger, 2011). Indeed, the stress field of a formation subjected to spalling, fracturing, strata bending and chemical and thermal effects, will have to be well understood before commencing CO_2 injection. In this context, it is necessary to incorporate models which approach the problem by including the flow in fractures and geomechanical coupling, thermal and chemical reactions.

There are different possible approaches to represent geomechanical processes in fractured rock relevant to UCG–CCS (Jing, 2003). Continuum methods have been extensively used in studying various problems (Detournay and Hart, 1999), including coal longwall mining (Esterhuizen and Karacan, 2005). Discrete methods containing rigid or deformable blocks, and fractures explicitly modeled provide higher accuracy in the description of the flow. However, for large scale problems and uncertain fracture distributions, their application is impractical. Due to the nature of the UCG–CCS, little or no information about the fractures would presumably be obtained by core drilling and dual-porosity or hybrid models appear as the preferential choice.

The general purpose of coupled systems is to account for reciprocal interactions between different physical and chemical processes. Though initially the main concern

in research groups and coding was to establish the flow of CO_2 in the subsurface by means of flow and transport simulation (Pruess et al., 2002; Class et al., 2009), it soon appeared that it was necessary to understand the effect of pressure in the stress field and subsequent changes in permeability and porosity to obtain a more accurate prediction (Rutqvist et al., 2002). Numerous geomechanical and coupled hydro-mechanical studies have been carried out since (e.g. Rutqvist et al., 2008; Morris et al., 2011a; Preisig and Prvost, 2011; Ouellet et al., 2011; Chiaramonte et al., 2008, 2011). Indeed, the elastic deformation of the rock and changes in permeability is only one aspect of the issues to be addressed. Rock plastic deformation (e.g. Ranjith et al., 2012), fracture creation and propagation, fault stability and reactivation (e.g. Streit and Hillis, 2004; Rutqvist et al., 2007; Soltanzadeh and Hawkes, 2009), caprock failure (e.g. Rutqvist et al., 2008; Rohmer and Bouc, 2010; Vilarrasa et al., 2011), surface heaving (e.g. Morris et al., 2011a; Selvadurai, 2009) and seismicity have to be well understood in order to assess the risks and operational parameters of a storage site. Geochemistry can also play a role in the long term fate of the CO_2: depending on the lithology and formation fluids, it can help fixing the CO_2 in place through mineralization or it can alter the properties of host formation rock and caprock and produce new leakage pathways through dissolution (Andreani et al., 2008). Thermal effects may also be decisive (Gor et al., 2013; Ranjith et al., 2012) due to their impact in geochemistry processes and thermal stress fracturing.

The objective of this Chapter is therefore to evaluate the requirements for the simulation of CO_2 injection in the fractured zone as expected in a UCG operation. The chapter is structured as follows: first, the analogue of underground coal mining's short and longwall mining extractive methods for an initial estimation of rock and hydrological parameters is discussed. Physico-chemical processes occurring during and after gasification are examined, as well as other potential effects during subsequent CO_2 injection. Section 3.4 proposes a methodology for modelling UCG–CCS.

Section 3.5 reviews the hydro-mechanical coupling, coupled models used in CO_2 storage and their application to fluid flow in fractured formations. The Chapter finishes with a summary and conclusions.

3.2 An analogue for formation damage after coal gasification: coal mining under water bodies

Though coal mining in the United Kingdom dates from ancient times, deep shaft mining began to develop extensively in the 18th century. Through two centuries, until the last underground coal mine in the North East — Ellington Colliery — was closed in 2004, a considerable experience in coal mining in the UK coal measures has been acquired. Historically, records of catastrophic water in-rushes, e.g. those compiled by Orchard (1969), created an awareness of the necessity of understanding the hydrogeological and geomechanical changes produced by the mine workings, specially when mines progressed under the sea. The interest for us here is to extrapolate that experience, together with the gas emission control around mining panels, to provide an empirical base for initial assessment of of CO_2 sequestration in the Coal Measures of North East England. The parameters involved in the evaluation of water inrush hazard are hydrogeological, geological, geomechanical and operational (Bicer, 1987) (e.g. depth of mining, thickness of extraction, hydrogeological properties, dip and lithology of the strata between the source of water and working horizon, primary and secondary permeability related to flow, aquifer thickness and geometry, permeability and transmissivity of the aquifer and piezometric surface of each aquifer). However, it is the interrelationship between these individual parameters which ultimately defines the sealing capacity of the strata (Orchard, 1969). Changes in permeability in the rock are due to stress redistribution as excavation advances. It can cause fractures in formerly intact rock by tensile or shear stress, opening or closing of

existing fractures and bedding separation by reduced confining stress. The lack of available measurements and the complexity of the interrelationships between stress and permeability often led to difficulties in finding stress-permeability relationships. Historically, coal mining engineers have made use of empirical laws valid for each basin to overcome this obstacle. The development of these empirical formulae to define the cover required between the mine workings and an aquifer or bodies of surface water by the coal mining industry has led to the elaboration of certain codes of practice. These codes vary from one country to another as coalfield conditions vary as well and also the safety factors applied in each case. British regulations for mining under the seabed are collected in the *National Coal Board Mining Department Instruction PI1968/8 (revised 1971)* and *The Mines (Precautions against inrushes) Regulations (1979)*. They prohibit working within 45 m of any potentially existing water body and 105 m from the seabed, 60 m of which must be carboniferous. In addition, the tensile strain created at the seabed cannot exceed 10 mm/m. These values are applicable to longwall working faces. In the case of room and pillar, these distances are reduced to 60 m and 45 m of cover to seabed and cover of carboniferous respectively.

According to Chen (2008), six factors influence the water flowing fractured zone height: mining thickness, base rock thickness, dip angle, uniaxial compressive strength of roof, mudstone proportion in overlying rock and structure of overlying rock. Codes of practice collected by Bai (1986) for mining under the sea take into account the extension of the failure zone. The estimated height of the fractured zone in different countries is shown in Table 3.1.

For a seam thickness of 2 m, the UK National Coal Board gives a height of 122 m, and the most conservative approach, the Canadian, results in 200 m. For workings below 700 m depth, Bai (1986) estimated that the fracture zone is concentrated within about 150 m above the seam. More recently, results from Whittles et al.

Table 3.1: Height of the fractured zone over longwall panels by countries. h is the height of the fractured zone, M is the thickness of the seam, x is a constant dependent on a safety factor

Country	Formula
UK	h=$58.7 \times M + 5$
USA	h=$30 \times M + x$
Canada	$h = 100 \times M$
Australia	$h = 60 \times M$
Former USSR	$h = 40 \times M$

(2006) simulating permeability changes over a longwall face 700 m deep corroborate this value. An area of increased permeability ($10^{-8} - 10^{-9}$ m^2) extends to 150 m over the extracted seam and 25 m below in his simulation. The same author considers that the fracture zone can extend 30 to 60 times the extraction thickness. It is also important to note that there is a critical width of the exploitation panel from which any additional increase on this distance does not cause further vertical extension of the failure zone. In the UK, this critical value is estimated at 80 m (Bai, 1986).

Comprehensive studies carried out by Bicer (1987) and Garrity (1980) on water incidents in subsea collieries in the North East revealed that water at the wet faces came from the Permian and Coal Measures, only with one or two exceptions coming from the sea. In the panels studied in the Low Main seam at Blackhall Colliery, the face length varied from 50 to 200 m, seam thickness was between 127 cm and 180 cm, the cover to base of Permian was 87 m to 158 m and the tensile strain was in a range of 2 mm/m to 8.3 mm/m. Similarly, at Horder Colliery, the High Main seam face width was between 40 m and 70 m, its length was 278 m to 700 m, cover to base of Permian was 75 m – 101 m and cover to seabed varied from 233 m to 248 m. As the mines moved in the north eastern direction, the incidence of wet faces decreased. In Ellington Colliery, partial extraction with effective pillar design was adopted as a mean to prevent water inflow.

Bicer (1987) did not attempt a comprehensive analysis of initial permeability and post-mining permeability. Later on, effects of longwall mining in the Coal Measures have been quantitatively studied by Dumpleton (2002). The change in the aquifer properties were investigated from measurements taken during two years using piezometers installed in the Sherwood Sandstone in the Selby Coalfield (York). Wistow Mine had extracted one panel and was prepared to initiate the extraction of a second one at a depth of 550–600 m, 170 m wide and 2.5 m thick. Results showed that post-mining hydraulic values increased between 138–234% in the case of transmissivity and 79–126% for storativity in the Sherwood Sandstone aquifer. The Selby study showed that mining at greater depths than 400 m could have a more significant impact on shallow aquifers hydrogeological properties than had previously been recognized. However, it was acknowledged that when the panel went deeper, the water inflow problems ceased. The increased transmissivity and storativity in the upper zone has implications for increased contaminant transport and potential CO_2 leakage rates.

The fact that mining under the seabed at depths of less than 300 m has progressed without water inflows coming from the sea, gives reasons to believe that the Coal Measures could potentially provide a sealing caprock for CO_2 sequestration in a UCG site, as long as the depth of injection is sufficient, properties and layout of the strata are adequate (e.g. sufficient thickness of mudstones and shaly formations) and no fractures develop to the Permian formations.

3.3   Conceptual model

With additional considerations, the empirical knowledge on cavity collapse and changes in stress and hydraulic parameters in the coal mining industry can be applied to UCG, specially in the gasification phase. These results can be extrapolated to

estimate the initial state for subsequent CO_2 injection. However, three fundamental differences with regards to leakage risk have to be taken into account when assessing CO_2 injection:

- The redistribution of stresses during CO_2 injection;

- the difference in mobility of CO_2 and water, and

- the different time and spatial scales involved.

3.3.1 Redistribution of stresses

The production stage of underground coal gasification commences with the drilling and completion of two boreholes: the injection well and the production well. After boreholes completion, ignition takes place. Air or oxygen are provided as comburent and occasionally steam can be added if formation water is insufficient to optimize the partial combustion reactions. The process of gasification is controlled by the flow and pressure of injected air or oxygen. Good practice indicates that this pressure has to be slightly lower than the hydrostatic pressure Burton et al. (2006), so the loss of syngas in the formation and spread of contaminants is minimized. Depending on the hydrogeological conditions and geomechanical response of the surrounding rock, a variable amount of water will inflow into the cavity, reducing the process temperature and reacting in the gasification. Temperatures during gasification can reach 900–1200 ^{o}C and a cavity is created as coal is consumed. As the unsupported roof span increases, the roof will eventually collapse. A compression stress arch will develop over the collapsed area while tensile stresses will appear from the edge of the collapsed area towards the surface according to a certain angle of draw (National Coal Board Mining Department, 1975). The three dimensional in situ stress regime will be notably altered. As a result, the following differentiated areas (Figure 3.1) from bottom to top will be formed (Esterhuizen and Karacan, 2005):
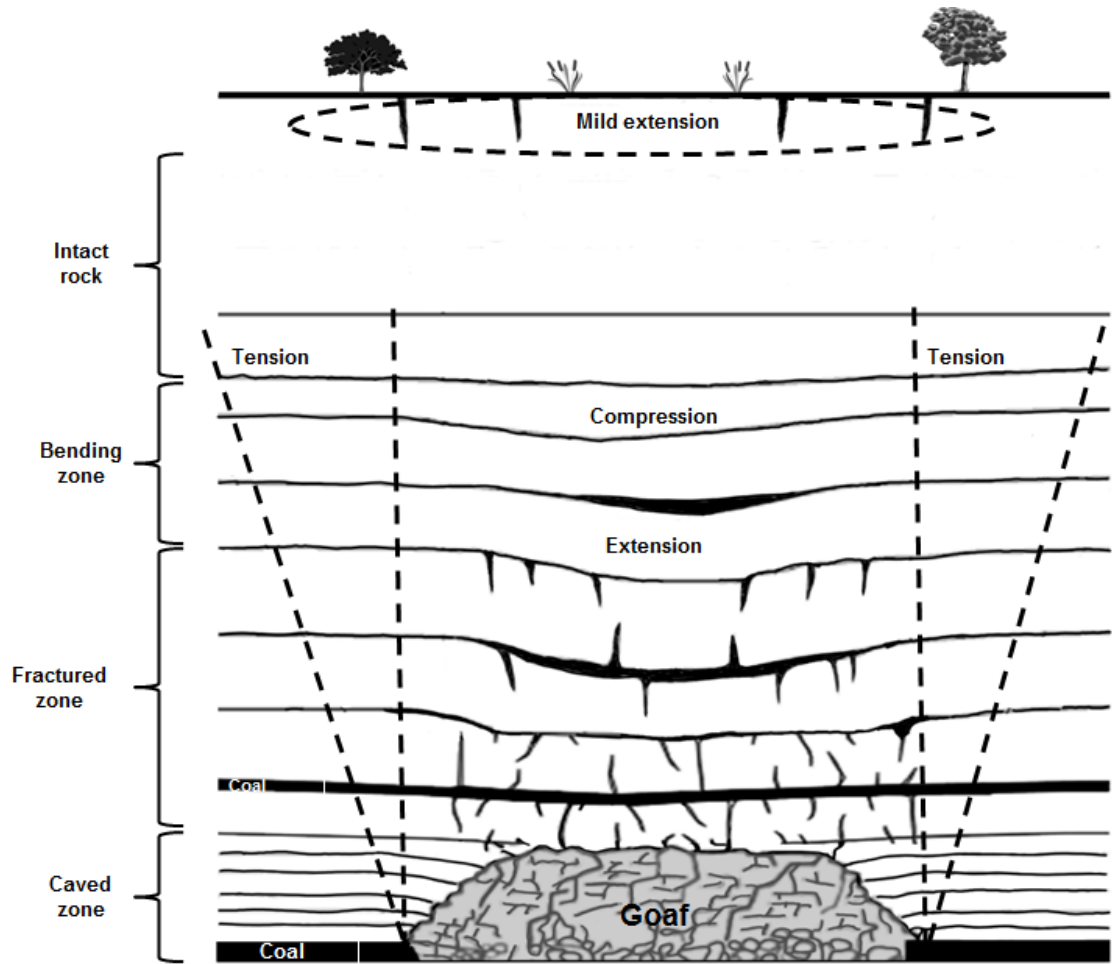
Figure 3.1: Fracture and stress zonation after seam coal extraction and cavity collapse.

1. A caved zone, with broken blocks that have come off the roof — this is the broken material referred to as 'goaf' (UK) or 'gob' (USA). The zone extends vertically to between three and six times the coal seam thickness. The final permeability of this zone will depend on the grade of re-compaction of the goaf. The void ratio in the collapsed cavity is high (up to a 30–45%). Longitudinal pillars along the cavity would help to decrease the compaction, resulting in a higher permeability of the goaf. Direct measurements of saturated goaf are rather rare, but reported values are in the range of 1–20 Darcies (Younger et al.,

2002), while values inferred from the hydrological behaviour of large systems of flooded panels range up to several hundred Darcies.

2. A fractured zone with continuous fractures, joint opening and low stress, presenting mainly vertical or sub-vertical fractures and bedding plane shearing and possibly separation. It may reach 30 to 60 times the extraction height. Water and gas can drain directly to the void, as permeability in this zone can be more than one order of magnitude higher than the original permeability.

3. A bending zone where horizontal bed separation and joint opening takes place, increasing horizontal hydraulic conductivity.

4. A zone of intact rock, often subject to compression beneath a final carapace of mildly extensionally disturbed rock, at or below the ground surface.

These empirical estimations do not account for the higher temperatures occurring in UCG. Changes in rock mechanical properties which would affect the rock failure and crack propagation have to be considered for further modelling of UCG operations. The cumulative effects of multi-seam extraction have to be included.

Data of the effects of high temperatures in the physical properties of rock formations are rare in literature. Applications concerned with high temperatures underground are fundamentally nuclear repositories, geothermal energy and underground coal gasification. The rocks of interest for UCG are sedimentary rocks: sandstones, siltstones, mudstones and shales. Ranjith et al. (2012) subjected sandstones samples up to 950 ^{o}C, finding that compressive strength and elastic modulus in the specimens tested decrease as temperature exceeds 500 ^{o}C. Luo and Wang (2011) investigated mudstones up to 750 ^{o}C, observing a maximum value of the modulus of elasticity at the mentioned temperature, which seems to indicate that the rock did not reach its expansion limit at that temperature yet. Malkowski et al. (2013) increased the

temperature limit to 1200 ºC to find that, macroscopically, the claystones (shales) were the most affected by temperature. They presented stratification and heavy cracking. Siltstones cracked in planes parallel to the bed surface and mineralogical changes were seeing in the sandstones, though no fractures appeared visible to the naked eye.

Changes in physical properties are due to changes in mineralogical composition. Exact mineral composition is site specific, so conclusions extracted from a single test cannot be generalized. However, as the number of these tests increases, it should be possible to statistically establish ranges of variation for the parameters of interest.

UCG operations are expected to be undertaken with a relative negative pressure in the gasification chamber, so no hydraulic fracturing will occur. However, the alteration in mechanical properties of the rock during gasification will increase their vulnerability to thermal stress when a cold fluid is injected afterwards, be it water for quenching the gasification chamber or CO_2. The cooling effect of the CO_2 can be due to injected CO_2 having a lower temperature than the reservoirs or also to the Joule-Thomson effect if the gas pressure drop entering the formation is too high (Oldenburg, 2007; Mathias et al., 2010). If it is clear in general regulations and industry practice that CO_2 injection pressures will have to be maintained below the fracture tension threshold of unaltered rock, it is not so obvious how to obtain an accurate value for this parameter after rock deformation, mineralogical change and field stress readjustment subsequent to UCG.

3.3.2 Fluid mobility

By-products of the gasification comprise tars, ashes, and organic compounds — mainly phenols — (Humenick and Mattox, 1978). These organic contaminants present a high solubility in carbon dioxide in supercritical state. In addition coal pockets may have remained unburnt in the cavity. Impurities in CO_2 affect the ther-

modynamics (density, viscosity, critical point) compared with pure CO_2 (Li et al., 2009). In general, the presence of impurities decreases the critical temperature (31.1 ${}^oC$ for pure CO_2) and increases the critical pressure (73.9 bar for pure CO_2) at which CO_2 enters its supercritical state (Seevam et al., 2008). A stream emanating from a post-combustion process shows the smallest difference compared with pure CO_2, but in the case of pre-combustion or oxyfuel processes, the supercritical pressure can reach 83 or 93 bar while the critical temperature decreases to 29 or 27 ${}^oC$ respectively (Seevam et al., 2008). A fluid sampling and characterization will be needed to estimate the thermodynamic properties of the injected CO_2 in a UCG cavity. An additional factor for fluid mobility will be its chemical reactivity with the host formation. The higher affinity of coal for CO_2 molecules rather than methane results in the substitution of the latter by the former in the coal structure. Fluid composition and its properties are therefore altered, notwithstanding the swelling and plasticization that occurs in the coal with this molecule substitution. Since the matrix permeability of the coal is extremely low (primary porosity), most of the fluid flow through the coal takes place through fractures, joints and cleats (secondary porosity). As a consequence, coal swelling will contribute to the sealing effect of coal seams, but also with a counteractive effect of increasing pressure buildup.

3.3.3 Time and spatial scales

Though there are examples like Tower Colliery (UK) of underground coal mines which were worked uninterruptedly for 200 years, generally exploitation plans are devised for several decades (e.g. 10 to 40 years). Collieries have to manage water and gas (methane) influx in the mine for safety of personnel and operations, as well as surface subsidence for environmental and safety precautions. They are therefore mostly concerned with the ground behaviour proximal to the moving working face and the permanent mine infrastructures. In contrast, a UCG–CCS operation has to

be able to model processes extending from a few hours (gasification) to hundreds of years (geochemical reactions) and is concerned with a wider area (the 'storage complex') as defined by legislation to cover the potential CO_2 migration pathways.

3.4 Modelling methodology

UCG–CCS involves a significant number of thermal, mechanical, chemical and hydrological problems at different spatial and time scales. It cannot be expected that a single model can incorporate all of them in a practical way. However, these problems are strongly linked to one another, so a minimum degree of coupling needs to be achieved.

Concurring processes strongly interlinked relevant to CO_2 storage performance include: cavity growth and geometry during gasification, effect of temperature on surrounding rock mechanics parameters (plastification, vitrification) thermal stress fracture during *i)* gasification, *ii)* subsequent cavity quenching, *iii)* CO_2 injection, cavity collapse and stress field redistribution, changes in hydrological parameters (porosity and permeability), coal adsorption of CO_2 and coal swelling, miscibility of CO_2 with gasification byproducts, tars and ashes, relative permeabilities of CO_2/gasifications byproducts mixtures and brine, pressure buildup due to CO_2 injection in the fractured area, fracture permeability relationship to stress and fracture opening and fracture propagation.

Figure 3.2 shows the modelling workflow, the input data for the design and development of the conceptual model, the results obtained from each modelling exercise and the links existing between them.
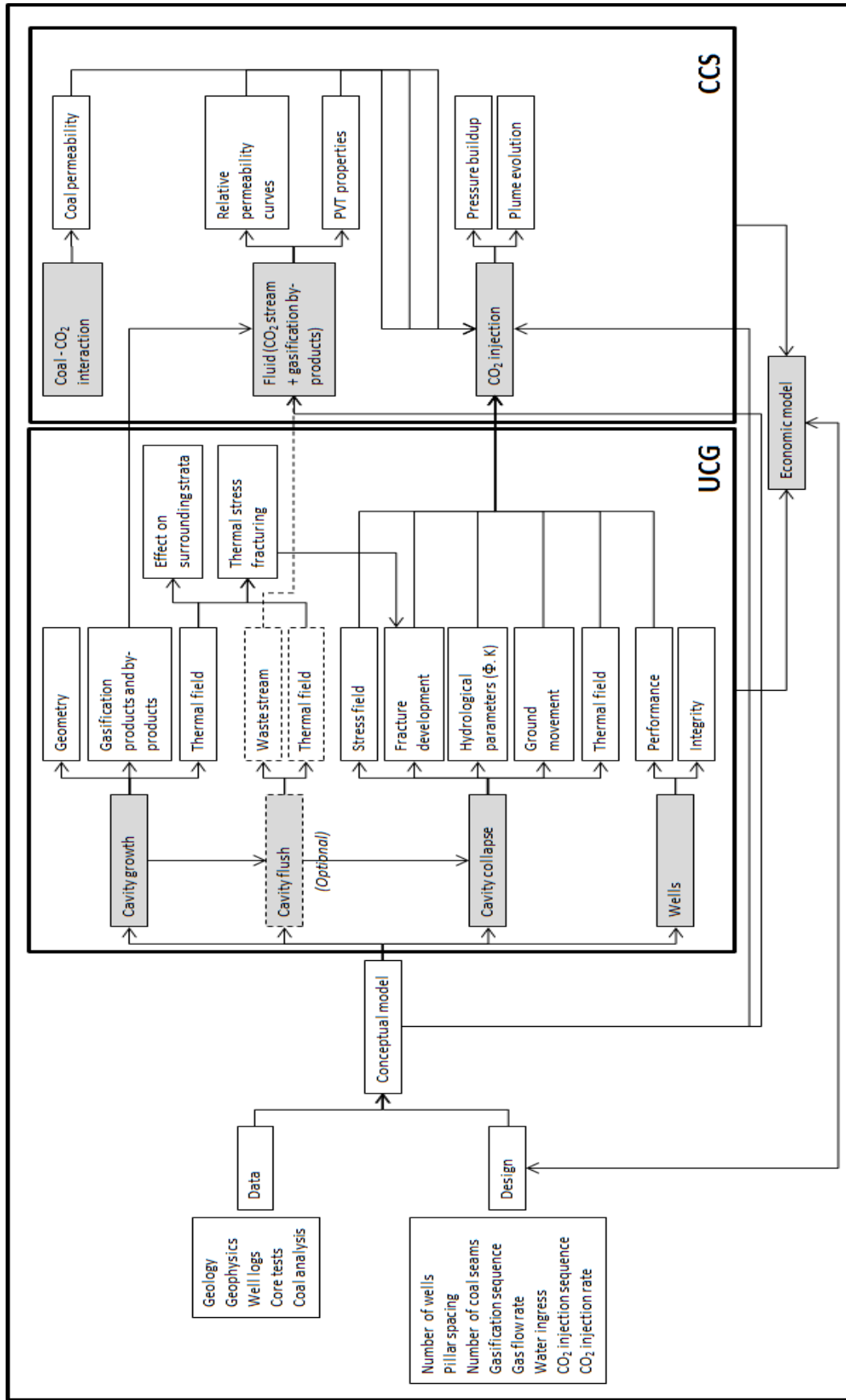
Figure 3.2: Modelling workflow for a UCG–CCS operation.

76

Further research to establish the contribution of each process into the general picture is needed to optimize the coupling and modelling methodology. Research on CO_2 storage is continuously advancing and will be extremely meaningful to the UCG–CCS, as well as the research on UCG alone. However, one critical aspect in the coupling of UCG–CCS which seems rather unattended is the fluid characterization of the CO_2 mixture with tars, ashes and other gasification by-products. Dissolution, diffusion, thermodynamical properties, relative permeability, chemical reactivity, are all dependent on this neglected area.

3.5 Hydro-mechanical coupling

Many subsurface industrial applications involve simultaneous processes of multiphase flow, heat transfer and stress-strain induction. Examples of these are nuclear or fluid waste disposal in deep deposits, underground gas storage, remediation of near surface hydrocarbon contamination, hydraulic fracturing and techniques for enhanced oil and gas recovery, such as cyclic steam flooding, and more recently, geological storage of CO_2 (Settari and Mourits, 1998; Rutqvist et al., 2002). When the coupling between processes is not very strong, the problems can be addressed separately with the use of geomechanical models for calculating stress and strain, flow and transport models to solve multiphase flow and heat transfer in porous and fractured media or fracture mechanics to study crack development and propagation. However, the requirements presented by the enunciated problems and others has led to coupling thermo-hydro-mechanical-chemical models which can account for the interactions among them.

3.5.1 Types of coupling

There are three main approaches for coupling the solution of flow and geomechanics equations: one-way coupling, two-way coupling and full coupling. The first and simplest one consists on using the pressure values obtained in the flow simulation

as an input for a subsequent geomechanical simulation. In this case, no information from the geomechanical module is passed on to the flow simulator, and it can be considered as a geomechanical post-processing. An example of this is form of coupling is Eclipse-Visage from Schlumberger. The second one is the two-way or iterative coupling. During calculation, the coupling parameters are fed to the other module in each iteration. Though it depends on how the coupling relationships have been defined, normally pressure and temperature output from the flow module are passed on to the geomechanical module. Once the stress and the strain are calculated, porosity, permeability and capillary pressure are updated according to their relation to the new mean stress. The iterative coupling can be explicit, if porosity and permeability are calculated only at the beginning of each time step, or implicit, if they are calculated with every Newton iteration. The third approach, the fully coupled method, solves simultaneously all the differential equations for the flow and the stress problems. Most of the coupling codes (e.g. GEM, TOUGH2-FLAC3D, NUFT-SYNEF) use the iterative approach, since it presents the advantage of being able to use well established and proved flow and geomechanics codes and it is generally less computationally demanding in comparison with the fully coupled method. However, Preisig and Prvost (2011) discusses the advantages of the use of the full over the iterative coupling since the number of iterations needed to achieve the desired accuracy may counteract the benefit of lighter computational workload. This argument had previously been discussed by Tran et al. (2004), who sustained that the development of coupling relationships can help improving the accuracy of the iterative coupling and therefore reduce the number of iterations needed. Dean et al. (2006) compared the iterative coupling method with its explicit and implicit variations and the fully coupled method, concluding that the performance of each is heavily dependent on the particular problem to be solved but those differences can be overcome with adequate tolerances. Since there is not an absolute advantage of

iterative coupling over full coupling or viceversa, it can be concluded that the use of both methods is justified.

3.5.2   Flow through fractured porous media

The approaches more commonly used to model fluid flow in fractured formations at field-scale are dual-porosity, dual-permeability and discrete fractures. The dual porosity concept was developed by Warren and Root (1963) to model flow in a fractured porous media. The dual-porosity and dual-permeability models consist of an idealization of the system, in which individual heterogeneous fractures of diverse length, aperture and direction are grouped by their aggregate effective properties in an equivalent regional homogeneous fracture network. Usually, this equivalent system is formed by orthogonal fractures equally spaced (Fig. 3.3) known as the 'sugar-cube model'. The way this is achieved is by superimposing two meshes (dual-continuum approach), one for the fracture and one for the matrix grid blocks.
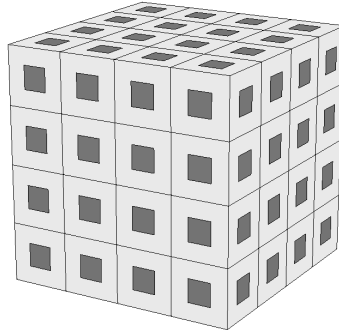
Figure 3.3: 'Sugar–cube' model representing the matrix blocks surrounded by the orthogonal fractures.

In the dual-porosity model, global flow occurs only through fractures. Rock matrix and fractures are interconnected locally through the 'interporosity' flow, which depends on the differential pressure between matrix and fractures, but matrix acts only as fluid and heat storage. The MINC (multiple interacting continua) (Pruess

and Narasimhan, 1985) appeared as a refinement of the dual porosity model to account for non-quasi-steady interporosity flow as assumed by Warren and Root (1963). In the MINC, the pressure, temperature and mass fraction gradients are solved by means of nesting additional blocks in the matrix, allowing its application to multiphase non-isothermal flow (Pruess, 1999). In the dual-permeability model the matrix blocks also communicate with each other and there is matrix-to-matrix flow in addition to fracture and matrix-to-fracture flow. The third approach, the most recent one, is the discrete fracture network method. It relies on a credible reservoir description that includes three dimensional spatial mapping of fractures. Fractures should also be defined in terms of aperture size, length, height, connectivity, conductivity, and frequency distribution. Matrix blocks are delimited by the fracture planes that form the interconnected network of fractures. Mixed methods have also been applied where small fractures are represented in a continuum while large fluid conductive fractures are explicitly represented (e.g Dershowitz et al., 2000; Hui Deng and Li, 2011).

Explicit representation of fractures is problematic using continuum methods. However, they have been extensively used in studying various problems (Detournay and Hart, 1999), including coal longwall mining (Esterhuizen and Karacan, 2005). On the contrary, discrete methods contain rigid or deformable blocks, and the contact patterns between blocks change with the deformation process. Their main drawback is the necessity of knowing the fracture geometry. In the case of UCG–CCS, little or no information about the fractures would presumably be obtained by core drilling.

3.5.3 Coupled hydro-mechanical numerical simulators applied to CO_2

Numerous numerical models have been adapted for application to geological CO_2 storage in the last decade. The majority of them consist of multiphase multicompo-

nent fluid and heat flow and transport equations which now include CO_2 and brine properties. Commercial reservoir simulators in the oil industry have dealt with CO_2 for the purpose of Enhanced Oil Recovery since earlier times and therefore offer the capabilities for the inclusion of hydrocarbons or coal in the system (e.g. CMG GEM, ECLIPSE–VISAGE). Some of the issues that needed to be addressed in the numerical simulation of CO_2 geological sequestration were fluid characterization, miscibility of the gas in the aqueous phase and viceversa, calculation of density and viscosity, CO_2 phase changes, relative permeabilities, water vaporization and salt precipitation and mineralization reactions. Geomechanical models coupled for the purpose commonly use poroelastic consitutive models, though viscoelastoplastic models have also been implemented (Vilarrasa et al., 2010a). In general, flow simulators are based in the finite difference method while geomechanical models are based in finite elements (e.g. TOUGH2, VISAGE). Unification of multi-field problems under partial differential equations has also been explored (Wang and Kolditz, 2007). The presence of fractures and simulation of fractured porous media was contemplated over a decade ago for the analysis of groundwater behavior within a geothermal reservoir by Bower and Zyvoloski (1997) and is being currently applied to CO_2 injection studies (e.g. Tran et al., 2009).

Examples of applications of these codes to CO_2 injection problems are: the study of maximum overpressure sustainable by single (Rutqvist et al., 2002) and multiple (Rutqvist et al., 2008) caprocks (*code: TOUGH-FLAC*); the potential occurrence and location of caprock failure and fault reactivation and ground surface elevation changes (Ouellet et al., 2011) (*code: ECLIPSE-VISAGE*) ; the opening and leakege through an existing fracture in the caprock over the injection point (Tran et al., 2010) (*code: CMG GEM, CMG STARS*); fault conductive or sealing characteristics and surface displacement (Morris et al., 2011a,b) (*code: NUFT/SYNTEF, NUFT/Livermore Distinct Element Code, NUFT/GEODYNE*); viscoplastic caprock failure mech-

81

anisms (Vilarrasa et al., 2010a) (*code: CODE–BRIGHT*); and ground uplift (Preisig and Prvost, 2011) (*code: DYNAFLOW*).

3.6 Summary and conclusions

In the case of combined UCG–CCS, strongly coupled thermal–hydraulic–mechanical–chemical (THMC) processes are expected to occur in the various stages of operation and over the longer term after closure. However, at this point there is a lack of empirical UCG–CCS data and therefore, the use and comparison of different methods, models and scenarios seems the best way to narrow the uncertainty range. An analogue found in the coal mining industry can lay the basis for modelling stress field redistribution and its relation to hydrological parameters. General research on CO_2 and more recent laboratory research in sedimentary rock properties subjected to high temperature and coal gasification will help to populate the simulation models with adequate parameters and validate them.

Due to the complexity and scales of processes, it cannot be foreseen that a single model can solve all the governing equations in a reasonable time and computational framework. When developing modelling tools, it will be necessary to achieve a minimum degree of coupling between the models, so the physics of the problem may be more accurately represented. In addition, upscaling of the problems from one model to another has to be possible.

When dealing with the thermo-hydro-mechanical modelling aspect of UCG–CCS, the system can be conceptualized as a fractured porous rock (in the caved and fractured area) and a porous rock in the rest of the model (Fig. 3.1). Thus, the former is treated as a multicontinuum and the latter as a single continuum. In the case of a typical sedimentary basin where a UCG–CCS operation would be carried out, the system consists of several horizontal or sub-horizontal layers of sandstone, shale,

coal, mudstone and siltstone. Simplified models can group several of these layers and use average parameters to decrease the numerical calculation load.

The following Chapters will be concerned with the relevance of including double-porosity flow models in coupled hydro-mechanical models and the effect of variation of fracture permeability in the safety of the storage.

Chapter 4

Implementation of a hydro-mechanical coupling for dual-porosity models in TOUGH2-FLAC3D

4.1 Introduction

Following the rationale presented in Chapter 3, in this Chapter we apply and adapt a pragmatic approach to coupled THM modeling developed by Rutqvist et al. (2002) using two well- proved models: TOUGH2 and FLAC3D. TOUGH2 is a multiphase, multi-component flow and transport model. It was released in the 1980s by the Lawrence Berkeley National Laboratory (Pruess and Wang, 1984) and has been in constant improvement and application since then (e.g. Pruess and Narasimhan, 1985; O'Sullivan et al., 1985; Tsang and Pruess, 1987; Pruess and Tsang, 1990; Persoff and Pruess, 1995; Pruess and Garcia, 2002; Xu et al., 2004; Pan et al., 2009). FLAC3D is a globally recognized numerical modelling application for advanced geotechnical analysis in three dimensions. In this study we adapt this modeling approach to UCG–CCS, including further development and implementation of the dual continuum approach using the so-called multiple interacting continua option in TOUGH2.

The objective of this Chapter is then to extend the capabilities of the hydro-

mechanically coupled model TOUGH2–FLAC3D to a dual-porosity model that can reproduce the highly fractured zone adjacent to an UCG void. This model is based in the 'multiple interacting continua' (MINC) and could eventually be extended to a 'dual-permeability' model, rather than the overlapping of two different meshes as it occurs in the dual-porosity model. The effective stress is corrected according to the pore pressure in the fractures and the matrix and hydraulic properties of the fractured rocks are adjusted with correction factors related to fracture aperture.

The Chapter is structured as follows: firstly, TOUGH2 and FLAC3D capabilities are reviewed; the governing equations and numerical procedures in the coupling of the two codes developed by Rutqvist et al. (2002) are explained. The code implementation and workflow are described (detailed development is presented in the Appendix). Section 4.5 describes the model setup for the two study cases. Section 4.6 presents the simulation results and the summary and conclusions close the Chapter.

4.2   TOUGH2 overview

TOUGH2 is a numerical simulator for fluid and heat flow and transport in porous and fractured media. It is capable of simulating non-isothermal flow of multiphase fluid mixtures with several components and phases as well as the transition between phases.

The mobile fluid is conceptualized as a mixture of CO_2, water and NaCl. In each phase several components may be present. The system is considered to have voids filled partially with liquid and partially with gas. Generally, fluids consist of one or two phases: a water-rich aqueous phase (liquid) and a CO_2-rich phase (gas). In addition, fluid phases may appear or disappear during the simulation, as solid salt may also dissolve or precipitate (Pruess, 2005). The two-phase flow of CO_2 and water is subject to relative permeability and capillary effects. Relative permeability

of gas and liquid phases and capillary pressure are obtained from Coreys and van Genutchen functions respectively (Rutqvist et al., 2008).

TOUGH2 architecture is built upon functional blocks. ECO2N is the fluid property module developed for geological sequestration of CO_2 in saline aquifers. It contains the equations of state which describe the thermodynamical and thermophysical properties of CO_2, H_2O and NaCl. The ranges for which these equations comply accurately with experimental values are shown in Table 4.1.

Table 4.1: ECO2N conditions range (Pruess, 2005)).

Property	Range
Temperature	10 ^{o}C <T <110 ^{o}C
Pressure	<600 bar
Salinity	Full halite saturation

There are seven possible combinations of phases for a system of water, liquid CO_2 and gaseous CO_2 (see p. 3–4 Pruess (2005)). ECO2N cannot distinguish if a CO_2-rich phase is liquid or gas, and therefore, it can neither represent a two-phase mixture of liquid and gaseous CO_2 nor three-phase mixtures. Thus, ECO2N can be applied in subcritical conditions only if no mixtures of liquid and gas CO_2 exist and no change of phase between them occurs. The only reactive chemistry considered is the dissolution of CO_2 in the aqueous phase (Pruess et al., 2002). It includes equilibrium phase partitioning of water and carbon dioxide between the liquid and gaseous phases and precipitation and dissolution of solid salt (Pruess, 2005). Interdiffusion and mixing of CO_2 and CH_4 arising from coal or from the gasification process is neglected.

4.3 FLAC3D overview

FLAC3D (Fast Lagrangian Analysis of Continua in 3 Dimensions) is a three-dimensional explicit finite- difference program for simulation of mechanical behaviour of materials under stress (ITASCA, 2006). FLAC3D was developed for solution of geotechnical engineering problems and can represent the elasto-plastic deformation. Linear or non-linear stress-strain laws dictate the response of each element of the grid to applied stress and boundary restraints. The grid is built with polyhedral cells within a three-dimensional mesh which adapts to the shape of the model.

Boundary conditions can be specified as velocity, or displacement and stress or force in any direction. Initial stress conditions such as gravitational load and water table can be defined for effective stress calculation. Both boundary and initial conditions can be defined cell by cell or as a gradient.

Finite elements and finite differences methods convert differential equations into matrix equations for each element. These matrices relate the force and displacement at the nodes of the elements. In the case of an elastic material and constant-strain tetrahedra, the element matrices from both methods are identical. However, FLAC3D finite differences methods present advantages and disadvantages compared to the finite elements methods: explicit solutions schemes can compute non-linear stress-strain laws in a very similar CPU time as linear laws and storage of matrices is not necessary. This decreases the computer memory requirements and time to solve problems with a larger number of elements and large strains. In addition, FLAC3D needs no adjustment of the solution algorithm for different constitutive models. However, two of the drawbacks of the explicit formulation in FLAC3D are *i)* the requirement of mechanical damping to provide non-inertial solutions and *ii)* the limitation in the size of the timestep.

The program contains thirteen built-in constitutive models divided into three

groups (null, elastic and plastic) plus the capability of programming new ones. The 'null' mode sets a zero stress and is used to represent voids. The elastic group comprises an isotropic, an orthotropic and a transversely isotropic model. Plastic models include Mohr-Coulomb, Hoek-Brown and Drucker-Prager among others.

FLAC3D capabilities include hydro-mechanical coupled for single-phase fluid flow and one-way coupled thermo-mechanical analyses.

4.4   Governing equations and numerical procedures

A multicomponent multiphase deformable system such as the one in this problem requires solving conservation equations for mass, energy and momentum.

TOUGH2 (Pruess, 1999) solves the equations for mass and energy conversion. As each component can be present in different phases (it is a three phase system), its total mass balance has to be calculated as the sum of its mass in each phase. The mass flux of each component is formed by an advective term (representing the Darcy flow) and a diffusive term (calculated using Ficks law). The energy conservation equation includes the contributions to the heat storage and flux of all phases. The heat flux is divided in an advective component and a conductive (or diffusive) one governed by Fouriers law (see Eq. (1) to (7) in Rutqvist et al. (2002)).

Space discretization in TOUGH2 is done using an integral finite-difference method, while time is discretized as a first order-finite difference with a fully implicit scheme. The resultant non-linear algebraic equations (Eq. (8) in Rutqvist et al. (2002)) are solved with a Newton-Raphson iteration.

FLAC3D solves the equation of motion with a stress-strain law. Stress and strain increments in time follow constitutive laws which relate the new effective stress with previous effective stress, strain and time increment. The effective stress can be calculated as a function of stress and pore pressure applying Biot's coefficient. A

first order difference technique is used in FLAC3D to do the spatial discretization. Additionally, a special mixed approach using tetrahedral elements is required to allow modes of deformation during plastic flow. Time is discretized with an explicit finite differences method.

The coupling of both codes is accomplished through nonlinear empirical expressions which relate effective stress and hydraulic parameters. Once these values are updated in each step by the coupling modules, both codes solve sequentially their own governing equations described above. The linking module from the thermo-hydrological model to the mechanical model calculates a pore pressure and temperature to be used as input in FLAC3D from the pressure, saturation and temperature in each phase in TOUGH2. Similarly, TOUGH2 requires for its equations the updated value of porosity, permeability and capillary pressure, which are derived in this linking module from the stress and deformation obtained in FLAC3D (Rutqvist et al., 2002).

The use of the multiple interacting continua method (Pruess, 1999) implies that, though temperature, pressure and effective stress may be different in the matrix and the fracture, total stress is the same. This is a requirement for maintaining the continuity of stress (Rutqvist et al., 2002).

The mechanical response of the porous and fractured media is a function of temperature, effective stress and strain. Changes in those three parameters result in new porosity and permeability values. It is also assumed that fluid and solid components are in local thermal equilibrium (Rutqvist et al., 2002). The basic coupled reservoir-geomechanical analysis is conducted with the Mohr-Coulomb constitutive model, though other models can be applied.
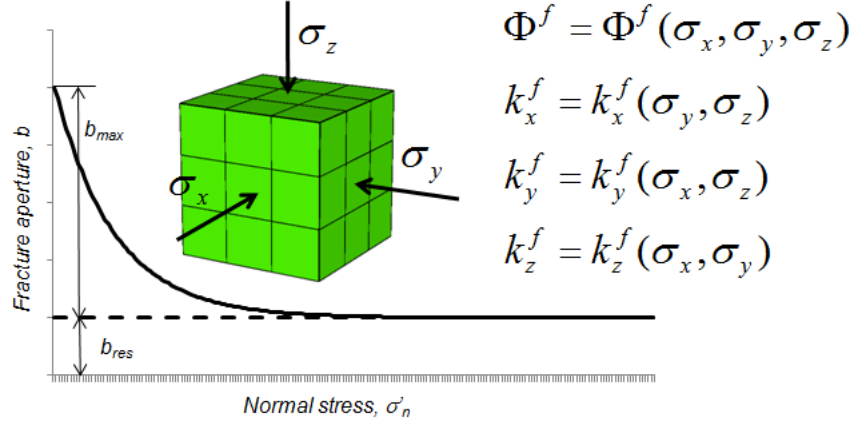
Figure 4.1: Conceptual model of a porous block with orthogonal fractures (from *Rutqvist, 2002*)

4.4.1 Effective stress functions for porous in highly fractured sedimentary rocks and hydraulic corrections

Effective stress functions used for the coupling modules are based on the conceptual model of a porous block and a porous block with orthogonal fractures (Fig. 4.1).

In the case of a porous continuum, an average pressure can be calculated as a function of pressure and saturation in the liquid and gas phases.

$$P = S_l P_l + (1 - S_l)P_g \tag{4.1}$$

where P is the pore pressure, S_l is the saturation in the liquid phase and P_l and P_g are the pressures in the liquid and gas phases respectively.

In a fractured porous medium, while pressure in the matrix can still be approximated by the equation (4.1), the pore pressure in the equivalent medium is a combination of the pressure in the fracture and in the matrix, affected by a correction coefficient.

$$\alpha P = \alpha^f P_f + \alpha^m P_m \tag{4.2}$$

where P_f and P_m are the pore pressures in the matrix and in the fracture calculated according to (4.1) and f and m are effective stress constants for fractures and matrix.

90

$\alpha = 1 - K/K_s$, where K and K_s are the solid matrix and solid phase bulk moduli respectively. For saturated rocks, K/K_s is usually in the range of 0.1-0.5. In soils, the ratio K/K_s is very small and therefore, α is considered 1. In fractures, Walsh (1981) proposed a value of $\alpha = 0.56$ after experimental research. More recently, Alam et al. (2010) has calculated a Biot's coefficient value of 0.89 for chalk at a depth of 625 mbsl.

Linking modules have to provide values of effective stress, temperature, pressure, porosity, permeability and capillary pressure and the way these variables are related depend on the conceptual model selected: an isotropic porous media or an anisotropic fractured block.

In the hydraulic corrections for a sedimentary rock, porosity, permeability and capillary pressure can be related to the mean effective stress (e.g., with Eq. (19) to (21) in Rutqvist et al. (2002)). However, in a fractured continuum, the hydro-geological parameters are related to the effective normal stress and aperture of the fractures. A higher compressive stress causes a reduced cross sectional area for the fluid to flow and a longer and more tortuous path to follow. The corrections for porosity, permeability and capillary pressure in this case are given by Rutqvist et al. (2002)'s equations (22) to (31). For a more detailed explanation of the governing equations and coupling of the two codes, and hydraulic corrections, the reading of Rutqvist et al. (2002) is recommended.

4.4.2 Code implementation

The coupling of the effective stress functions for fractured rocks and hydraulic corrections summarized in Section 4.4.1 and fully described in Rutqvist et al. (2002) has been implemented by means of modifications in the TOUGH2 source code and in the coupling module between TOUGH2 and FLAC developed by Rutqvist et al. (2002). The former is written in FORTRAN programming language and the latter

in FISH, a programming language existing in FLAC3D. Previously, the coupling did not allow for dual-porosity models. The current modifications calculate the parameters for the equivalent medium (fracture and matrix) in the output of flow model so one equivalent parameter from the two superimposed meshes (fractures and matirx) can be passed onto the geomechanical module. The ratio of fractured volume to total volume and Biot's coefficient can be specified in the coupling.

A number of pre and post processing tools were tested for compatibility with the modified code: *Petrasim* (RockWare, Inc.), *ParaView 3.10* (Kitware Open Source), *T2B* (beta version) (BRGM). However, different limitations in all of them at the time, the main of which was their lack of capability to create or integrate results of a dual porosity system made them unsuitable for the task. Therefore, several scripts have been written in FORTRAN and MATLAB to prepare the input data for the simulation and to display results graphically.

TOUGH2 is set up with a modular architecture (Pruess, 1999), in which a main module contains the executive routine. Other subroutines contain the functions for problem initialization (INPUT, RFILE), time stepping (CYCIT), thermophysical properties (EOS), assembly of mass and energy balance equations (MULTI), sink and source terms (QU), solution of linear equations (LINEQ), conclusion of converged time steps, updating of thermodynamic variables and iteration counters (CONVER) and output results (WRIFI, OUT, BALLA). The coupling between FLAC3D and TOUGH2 is contained in a subroutine called HMPROP. Thanks to this modular architecture, in order to implement the required changes to include dual porosity models in the coupling capabilities, the coding had only to be modified in HMPROP. Then, a TOUGH2 executable is created by compiling the executive routine and subroutines with Microsoft Visual Studio compiler.

The modifications needed in the subroutine correspond to the correction factors for hydraulic properties of a highly fractured rock (Rutqvist et al., 2002) in the

fractured continuum,

$$\phi = F_\phi \phi_i, \tag{4.3}$$

$$k_x = F_{kx} k_{xi}, k_y = F_{ky} k_{yi}, k_z = F_{kz} k_{zi}, \tag{4.4}$$

$$P_c = F_{Pc} P_{ci}, \tag{4.5}$$

where ϕ is porosity, k is permeability, P_c is capillary pressure, F are the correction factors, subscript i denotes initial conditions and subscripts x, y, z denote the three orthogonal directions. The porosity and permeability correction factors are a function of fracture aperture and normal effective stress in x, y, z directions and the capillary pressure is corrected according to the Leverette function.

In FLAC3D, the correction for fractured continuum consists on updating the pore pressure as a function of the pore pressure in the fractured continuum and the porous continuum through the expression

$$\alpha P = \alpha^f P_f + \alpha^m P_m, \tag{4.6}$$

where α are effective stress constants, P is pressure and sub/superscripts denote fractured continuum or matrix. Table 4.2 shows the scripts written or modified with the programming language used and the objective of the code. The *Appendix A1* contains the details of the code implementation and workflow.

Table 4.2: Scripts modified and coded and objectives.

Script	Programming language	Objective
Executables		
TOUGH2 subroutine	FORTRAN	Calculate correction factors for ϕ, k, P_c as per Rutqvist et al. (2002)
TOUGH–FLAC coupling subroutine	FISH	Calculate pore pressure for FLAC as a function of pressure in matrix and pressure in fractures; produce effective stress components for both matrix and fractures in TOUGH2
Pre-processing		
AssignROCK	FORTRAN	Assign ROCK type to horizontal layers in TOUGH2 input
AssignFRAC		Assign ROCK type to fracture elements in TOUGH2 input
AssignVOL		Assign volume to a ROCK type cell in TOUGH2 input
Post-processing		
FRACTURE MATRIX COMBINED	FORTRAN	Read TOUGH2 output and produce a format readable by MATLAB for plotting each simulation written output time for matrix, fracture elements and the combination of both
FOFT-graphs	MATLAB	Automate creation of plots from FOFT (property value in a cell in time) TOUGH2 output
SPATIAL		Create contour plots from FRACTURE/MATRIX/COMBINED

A coupled TOUGH2 and FLAC3D analysis for a particular problem is typically developed according to the steps shown in Figure 4.2.
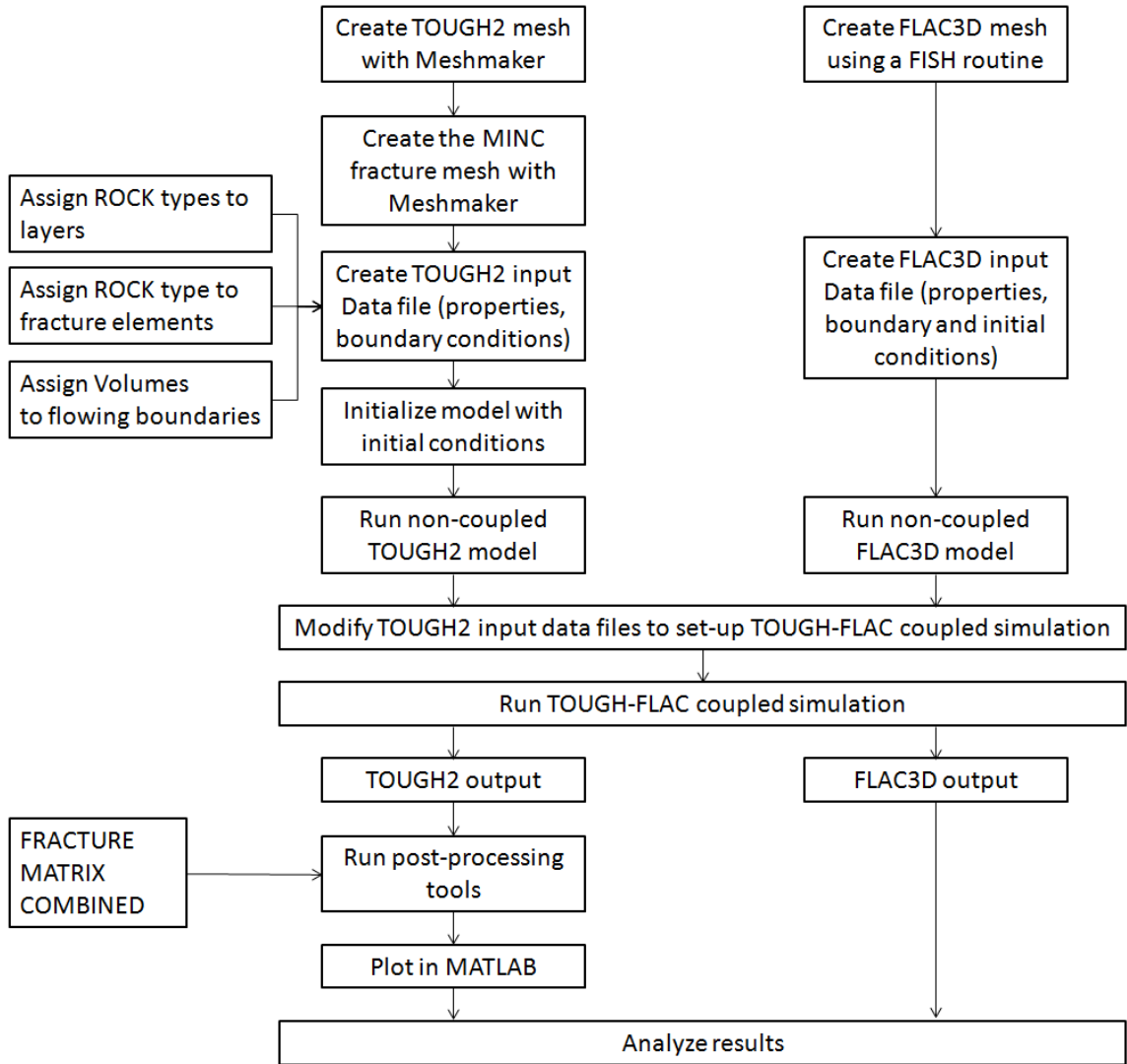
Figure 4.2: Steps for the construction of a coupled TOUGH2-FLAC model with dual-permeability option.

The geometry and element numbering should be consistent in TOUGH2 and FLAC3D. This can be achieved by generating the meshes using the MESHMAKER with the TOUGH2 code and by a special FISH routine in FLAC3D that is programmed such that it produces the same mesh consistent with the MESHMAKER.

Once input data for TOUGH2 and FLAC3D have been created, steady state simulations should be run to establish initial conditions, such as pressure, thermal and stress profiles. Then simulations should be run separately before coupling to assure the correction of input data files and that the problem converges to a solution. Once the result is satisfactory, the TOUGH2 file has to be modified to allow for the coupling (adding a line in the ROCK type). With the newly compiled TOUGH2 executable and the FLAC3D initial file, the coupled simulation can be run. TOUGH2 calls FLAC3D to perform a quasi-static mechanical analysis. When FLAC3D is activated, it looks for a FLAC3D.ini file and conducts the commands in it. The first command restores the current geomechanical conditions stored in a file called FLAC3D.sav. Subsequent commands read the data from the external file TOU-FLA that contains pressure, temperature and phase saturation and imports those in the FLAC3D grid. Then the mechanical analysis is performed and a new command exports the stresses and strains to the external file FLA-TOU, which is read by TOUGH2.

Two cases were run to test the code. The model setup, simulations and results are as follows.

4.5   Model setup

Three potential options have been suggested for coupling CO_2 storage with UCG: the first one consists in injecting the captured CO_2 in the gasified area; the second one would store it in deep aquifers below the UCG area; lastly, a third option would make use of storage areas away from the gasification zone, either depleted hydrocarbon fields or saline aquifers. In this work, we study the two first options. In the *Case A*, it will be assumed that the carbon dioxide is injected in deep aquifer layers below the UCG zone and that a rich CO_2 fluid migrates vertically in the vicinity of a

gasified zone. The objective is to study how the presence of a fractured area close to a migration path will affect the evolution of the CO_2 plume and pressure. *Case B* will deal with CO_2 injection in the fractured area.

The model consists of a 1 m thick transverse section of a two-layered formation (Fig. 4.3).
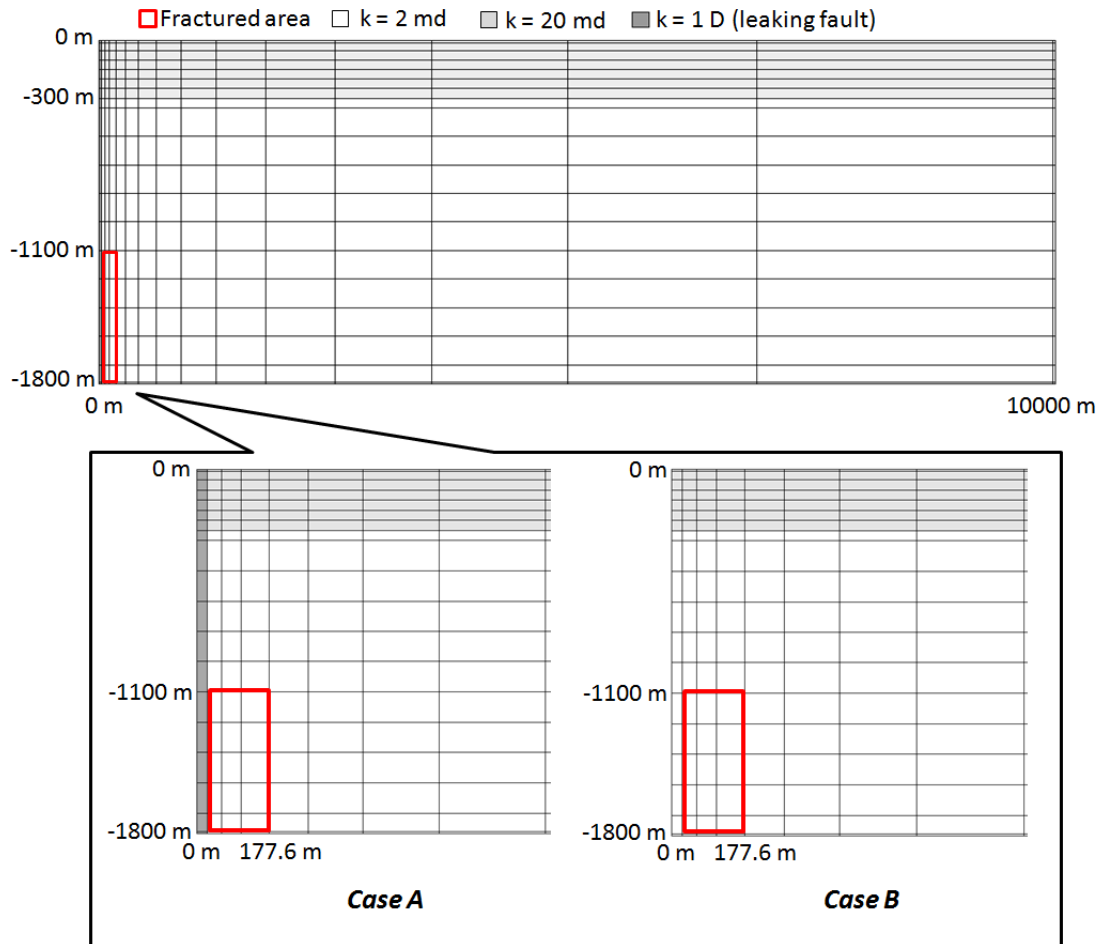
Figure 4.3: Model mesh dimensions, location of the leaking fault and fractured area and permeability distribution. The detail shows the differences between *Case A* (with leaking fault) and *Case B* (without leaking fault).

The longitudinal and vertical dimensions are 10,000 m and 1,800 m respectively. The domain is discretized horizontally in sixteen nodes. The first element is 25 m

long and distance between nodes increases continuously until 3092.5 m in the last element prior to the model boundary. Vertically, the domain is divided into nineteen horizontal layers. Excluding the two layers at the top and bottom of the model, which are 10 and 40 m and 90 and 10 m respectively, the rest of the layers are either 50 m thick or 150 m thick. The upper 300 m zone presents higher permeability (2×10^{-14} m^2 or 20 md) than the lower layers (2×10^{-15} m^2 or 2 md). The rock density is constant in the model with a value of 2,260 kg/m^3, while porosity remains 10% throughout all the domain. The heat conductivity is 1.8 W/m ^{o}C and the specific heat is 1,500 J/kg ^{o}C.

In *Case A*, a vertical fault in the left boundary of the model has an increased permeability of 1×10^{-12} m^2 (or 1 D). A mixture of circa 95% brine and 5% CO_2 is injected at the bottom of the model (1,800 m depth) to simulate the flow of such fluid migrating vertically through the fault. In *Case B* model, the injected fluid in the gasified zone, at a depth of 1,700 m, is pure CO_2. In both cases, the injection rate is 100 t of CO_2 per year.

The fractured zone is located at a depth of 1,100 m. Horizontally, it extends 152.6 m, and vertically, 690 m. The fracture mesh was created using TOUGH2 Multiple Interacting Continua (MINC) with three orthogonal sets of plane parallel fractures. Global flow in the fractured zone occurs through the fracture continuum, whereas local interaction between rock matrix and fractures takes place through interporosity flow (known as 'double-porosity' model) (Pruess, 1999). The volume fraction of the fractures is 0.02 and the spacing between fractures is 0.5 m. Arguably, these parameters are site specific and will vary in each Underground Coal Gasification operation and will depend on technical and economic factors.

The model is initialized with hydrostatic pressure equilibrium. At the top of the model, which is located at surface, the pressure load is 0.15 MPa, while at the bottom of the model it reaches 40 MPa approximately. Fluid flow is allowed through the

top layer (leakage into the atmosphere) but restricted in the bottom and all lateral boundaries. Due to the distance to the lateral boundary opposite to the injection point, the model acts as an open system, in the sense that the pressure wave is not reflected from the lateral boundary. The vertical to horizontal stress ratio is σ_h/σ_v=1. Initial stress in the model is calculated by applying a gradient to the stress at surface (surface considered to have null stress). The gradient value is zero in both horizontal directions, while in the vertical direction it increases at a rate of 22.17 MPa/km.

TOUGH2 allows the use of a number of specified functions for calculation of the relative permeability and capillary pressure, as well as user defined ones (Pruess, 1999). Relative permeability curves are calculated with Corey's curves (1954) (Eq. (4.7) and (4.8)).

$$k_{rl} = \hat{S}^4 \tag{4.7}$$

$$k_{rg} = (1 - \hat{S})^2(1 - \hat{S}^2) \tag{4.8}$$

where

$$\hat{S} = \frac{(S_l - S_{lr})}{(1 - S_{lr} - S_{gr})} \tag{4.9}$$

k_{rl} is the liquid phase relative permeability, k_{rg} is the gas phase relative permeability, S_l[-] is the liquid saturation, S_{lr}[-] is the residual liquid saturation (0.3 in this model) and S_{gr}[-] is the residual gas saturation (0.5 in this model).

Capillary pressure is obtained through the Van Genuchten function (1980) (Eq. (4.10)).

$$P_{cap} = -P_0 \left([S^*]^{-1/\lambda} - 1 \right)^{1-\lambda} \tag{4.10}$$

with the restriction of

$$-P_{max} \leqslant P_{cap} \leqslant 0, \tag{4.11}$$

where

$$S^* = \frac{(S_l - S_{lr})}{(1 - S_{gc} - S_{lr})}, \tag{4.12}$$

$$\lambda = 1 - 1/\beta, \tag{4.13}$$

$$1/P_0 = \alpha/\rho_w g, \tag{4.14}$$

P_{cap} [FL^{-2}] is the capillary pressure, S_l[-] is the liquid saturation, S_{lr}[-] is the residual liquid saturation and S_{gc}[-] is the critical gas saturation , α and β are Van Genuchten parameters, ρ_w [ML^{-3}] is the density of the liquid phase and g [LT^{-2}] is the acceleration constant.

The parameters used for the capillary pressure function in this model are presented in Table 4.3.

Table 4.3: Parameters for Van Genuchten calculation of capillary pressure (from Rutqvist (2009)).

Van Genuchten parameter	$\lambda = 0.457$
Van Genuchten parameter	$P_0 = 19881 Pa (matrix)$
Van Genuchten parameter	$P_0 = 909 Pa (fracture)$
Residual liquid saturation	$S_{lr} = 0$
Maximum pressure	$P_{max} = 50$ MPa
Critical gas saturation	$S_g c = 0.01$

4.6 Simulations and results

4.6.1 *Case A*: CO_2 leakage along a fault in the vicinity of the fractured area

CO_2 plume evolution

Figures 4.4 and 4.5 show the CO_2 free phase saturation and dissolved CO_2 in the *Case A* model without a fractured zone (*Case A-1*) and with a fractured zone (*Case A-2*) (both in matrix and fractures). CO_2 migrates vertically along the fault, which has a permeability three orders of magnitude higher than the adjacent formation. When fractures are present, a certain amount of CO_2 diverts into the fracture network, which has the same high permeability as the fault, though a much smaller pore volume. Remind that fractures only account for a 2% of the volume in the block. Free phase (supercritical) CO_2 migrates quickly vertically due to the buoyancy force until it reaches the top of the fractured zone, where it accumulates and extends laterally to continue migrating vertically along the fault. Dissolved CO_2 sinks into the bottom of the fractured zone due to the higher density of CO_2 saturated brine. The same effect can be appreciated in the top layer due to the discontinuity in permeability, with the obvious difference that free-phase CO_2 does not accumulate laterally at the top because it escapes to the atmosphere.

Both free-phase and dissolved CO_2 plots show that the concentrations of CO_2 in the matrix in the fractured area are negligible in comparison with the concentration in the fractures. This is in part due to the assumption that pressure changes in the fractures are transmitted quickly to the inner of the matrix blocks. The subdivision of the matrix into concentric blocks (MINC) allows a more accurate resolution of the gradients at the matrix-fracture interface. Therefore, a more general approach of fracture-matrix and matrix-matrix flow ('dual-permeability model') when the time spans of interest are in the order of tenths of years could be preferred.
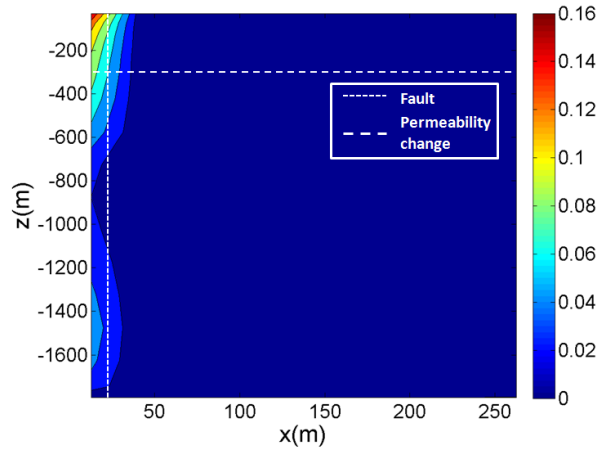
(a) Without a fractured zone
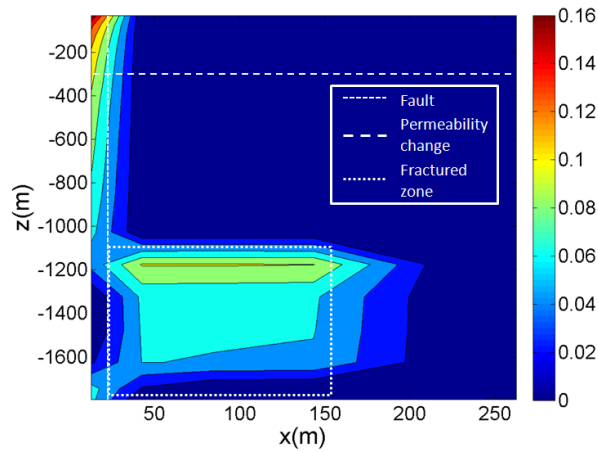
(b) With fractured zone (in the fractures)
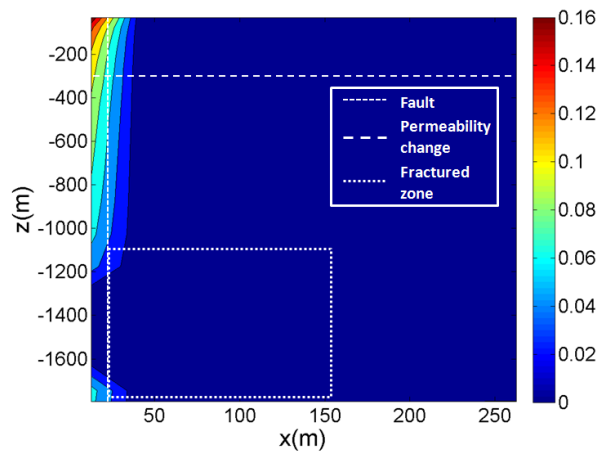
(c) With fractured zone (in the matrix)

Figure 4.4: Free phase CO_2 saturation in *Case A* model after 1460 days of injection. Colour bar shows the saturation as a fraction of 1.
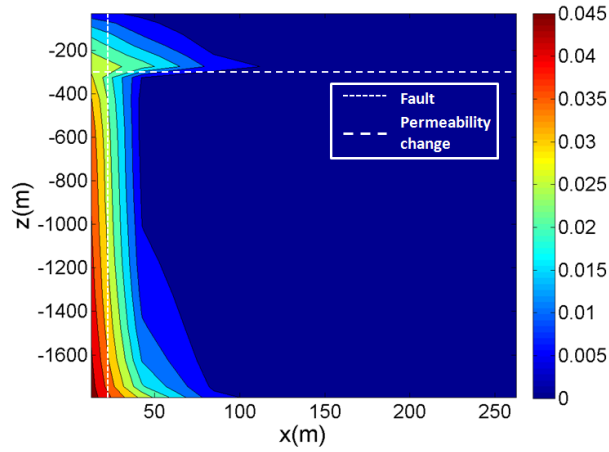
(a) Without a fractured zone
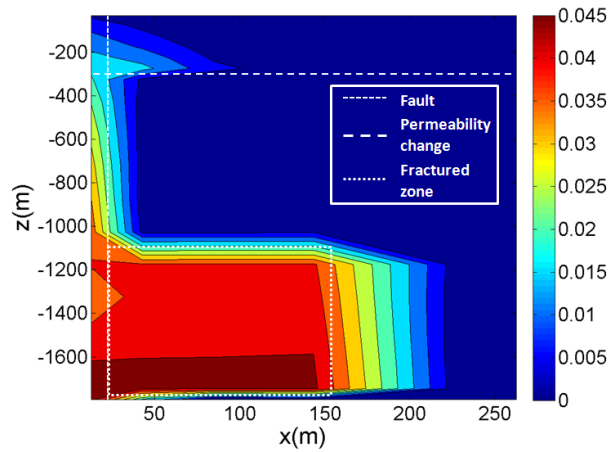
(b) With fractured zone (in the fractures)
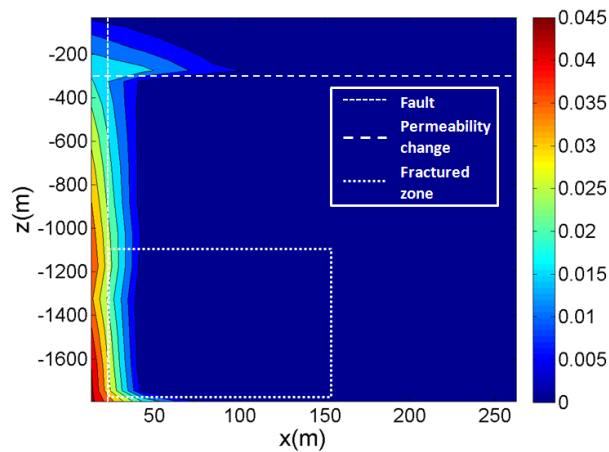
(c) With fractured zone (in the matrix)

Figure 4.5: Dissolved CO_2 in *Case A* model after 1460 days of injection. Colour bar shows mass fraction

It should also be noticed that the plotting of properties in 'fractures' or 'matrix' only affects the dual-porosity area marked as 'Fractured zone', where two meshes coexist. Outside that area, in all plots the only existing single porous medium is represented. One of the current limitations of the contour plots in MATLAB at the time of this study is the impossibility to use colour logarithmic scales, which would be useful in having a single view of total free-phase and dissolved CO_2 of the combined fracture and matrix grids. To overcome this problem, the variation of CO_2 in time in the system was plotted in Figure 4.6.

(a) Without a fractured zone (*Case A-1*)   (b) With fractured zone (*Case A-2*)
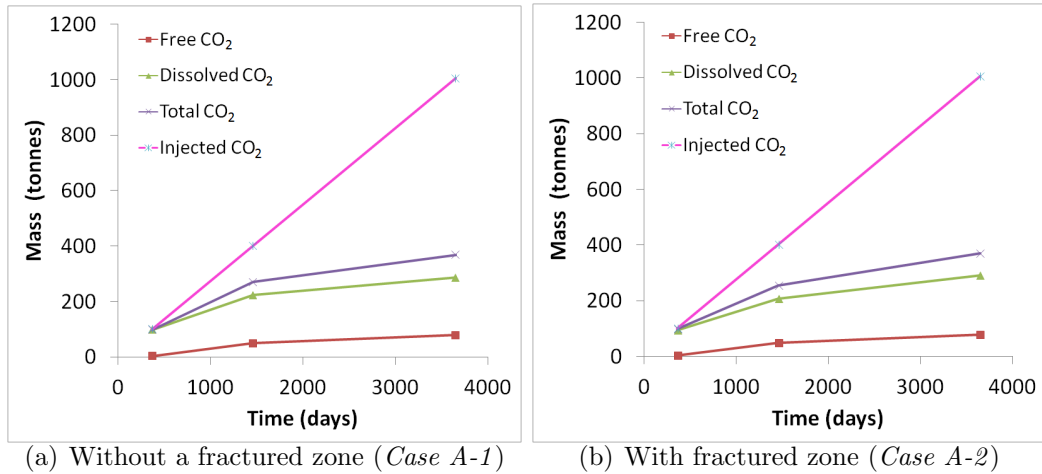
Figure 4.6: Evolution in time of free, dissolved and total CO_2 in the system and CO_2 injected in the model for the *Case A*.

Figure 4.6 shows that there is virtually no difference in the amount of free-phase and dissolved gas in both *Case A-1* and *Case A-2*, with and without the fractured zone. It also shows the amount of CO_2 that has escaped into the atmosphere via the leaking fault. Table 4.4 provides a more detailed idea of the difference in CO_2 distribution in *Case A-1* and *Case A-2*.

Table 4.4: Comparison of total CO_2 in the system, dissolved and free phase CO_2 in the model without a fractured zone and the model with a fractured zone after 3650 days. Total CO_2 sourced into the model is 1005.37 tonnes. (*Case A*)

	Without fractures	With fractures
Total (t)	368.84	369.14
Dissolved (t)	286.53	290.26
Free phase (t)	82.31	78.88

Geomechanical response

Rock failure normally occurs due to tension or shear stress. Consequently, effective normal stress and shear stress should be analyzed to assure the stability of the rock massif. Comparison of the normal effective stresses (Fig. 4.7) in the two models shows that stress induced by CO_2 injection is slightly higher in the case without
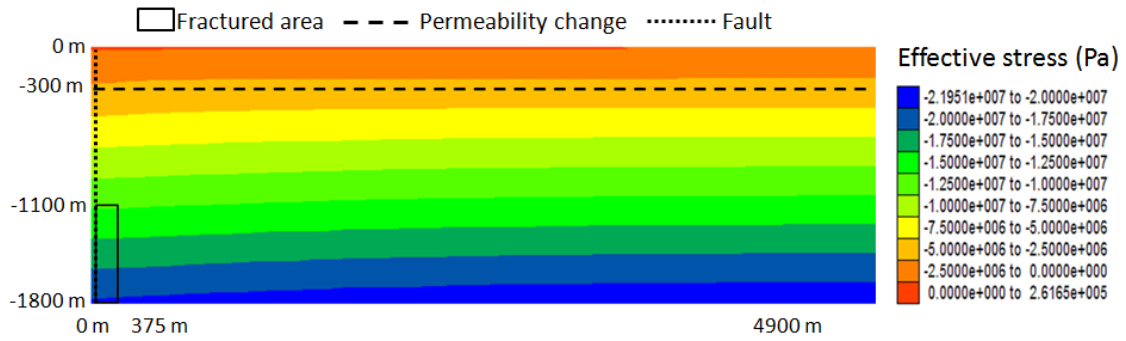
(a) Without fractures (*Case A-1*)
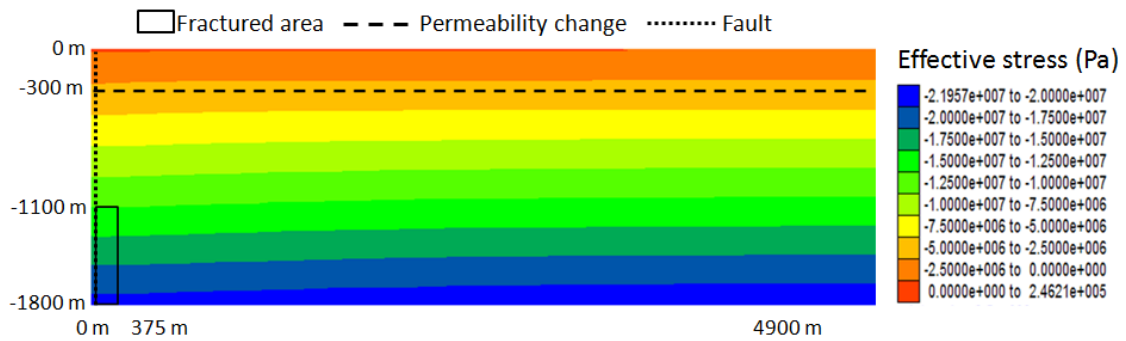
(b) With fractures (*Case A-2*)

Figure 4.7: Effective Stress in *Case A* model after 1460 days of injection

a fractured zone (*Case A-1*). It can also be observed that the stress propagation reaches the top layers, even if it is damped. More importantly, the effective stress at surface reaches a tensional rather than compressional stress. Remind that, as opposed to other models in literature which extend only to a caprock constrained by a loaded overburden, the model in this study extends to surface. The boundary condition at surface allows flow of CO_2 and free vertical movement.

Consequently to what is observed in the effective stress, Figure 4.8 shows that the maximum displacements are found at surface. As it corresponds to the higher tensional stress at surface found in the case of non-fractured model (*Case A-1*) – 0.26165 MPa – compared to the 0.24621 MPa found in the fractured model (*Case A-2*), the non-fractured model suffers a higher surface heaving.

(a) Without fractures

(b) With fractures
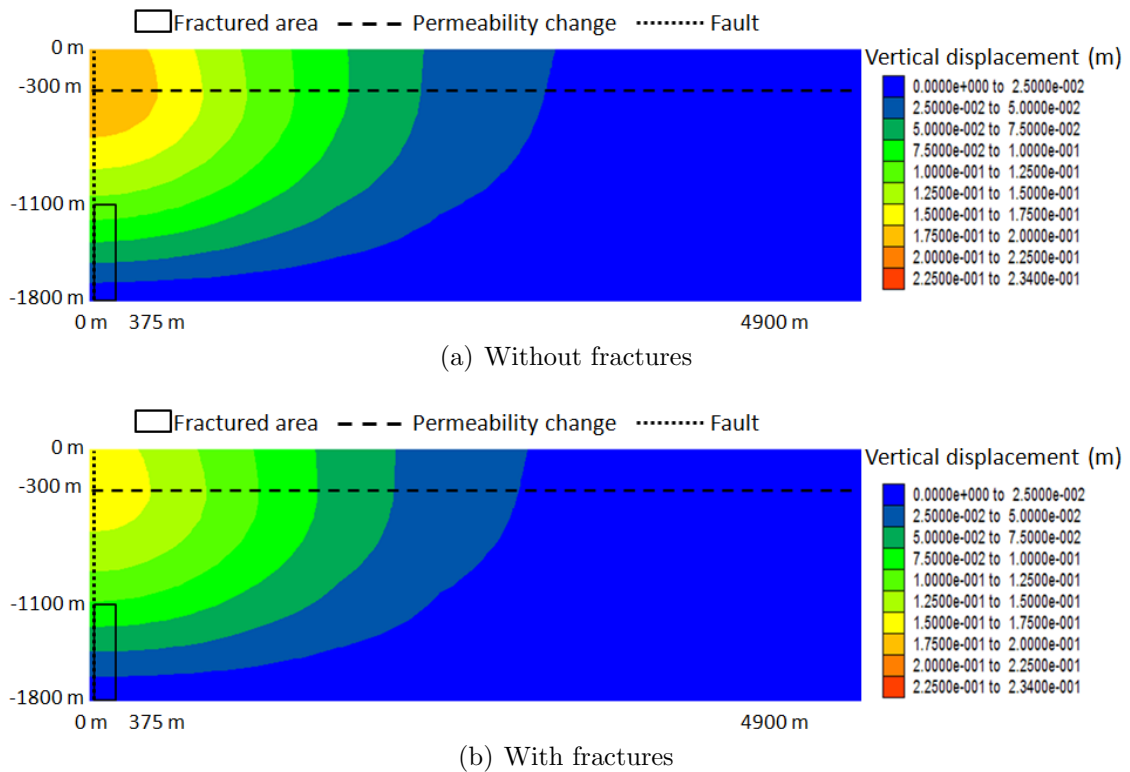
Figure 4.8: Vertical displacement in *Case A* model after 1460 days of injection

In view of this, when analyzing the shear stress, it reflects that the tensions created in the model are primarily due to the displacement at surface. Figure 4.9 shows that the shear stress in the XZ plane is also governed by what occurs at the near surface, with effective stresses and displacements higher than at depth. In agreement with observation in effective stress and displacement, maximum shear stresses takes place in the non-fractured model.

(a) Without fractures

(b) With fractures
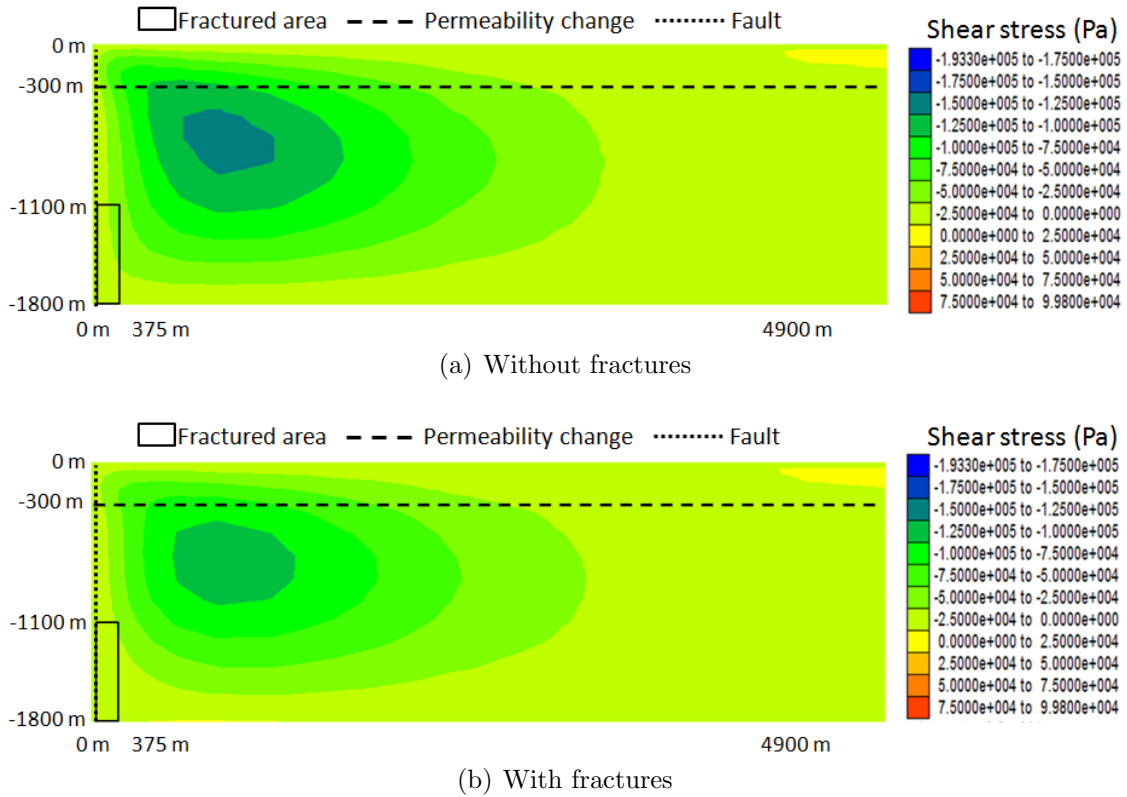
Figure 4.9: Stress in the XZ plane in *Case A* model after 1460 days of injection

It can be concluded that the presence of a fractured zone helps in diverting and dissolving the CO_2 on its way to surface along a leaking fault, and that it also reduces the stresses to which the rock is subjected. However, the whole system is dominated by the leaking fault and the surface displacement produced by it, which renders the effect of the fractured zone almost negligible for the parameters of this study.

107

Biot's coefficient

It is a common simplification to use a Biot's coefficient of 1.0 in hydro-mechanical models (e.g. Hawkes et al., 2005). This value is more characteristic of unconsolidated grainy sediments where Terzaghi's effective stress concept is applied. However, at depths over 600 m, consolidated chalk (Alam et al., 2010) or sandstone can present Biot's coefficient values lower than one. Furthermore, Biot's coefficient in fractured continua may be even lower (Walsh, 1981). In addition to the existing cementation of the lithology, the high temperatures during gasification can induce geochemical changes in the surrounding rock, including vitrification (Ranjith et al., 2012), from which resulting Biot's coefficient is uncertain.

Albeit empirical studies have not yet provided a probable range for alteration of Biot's coefficients values in a UCG environment and their distribution in the domain, the author has applied values from literature to gain some understanding on the effect of Biot's coefficients lower than 1.0 in the simulation model. In particular, to capture the widest range, the lowest value (0.56) matched by Walsh (1981) in data from experiments on a tension fracture was applied.

Results show a significant change in effective (Fig. 4.10) and shear (Fig. 4.11) stresses.
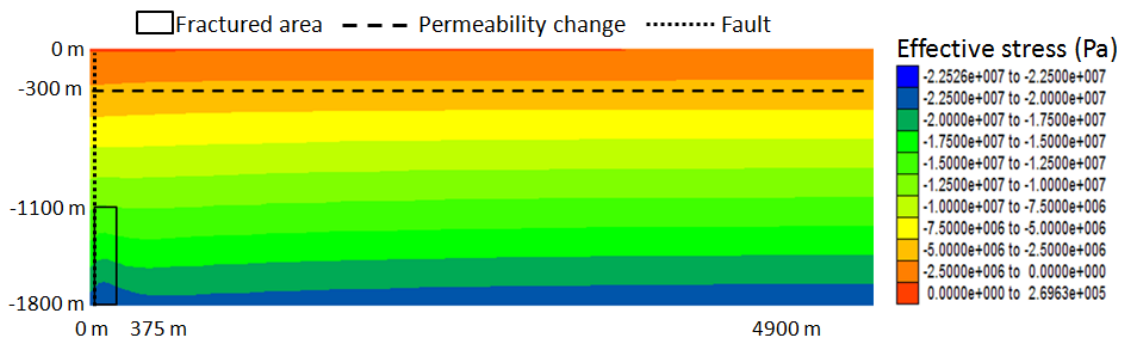
Figure 4.10: Effective stress after 1460 days of injection (Biot's coefficient is 1 in the porous continuum and 0.56 in the fractured continuum (after Walsh (1981))
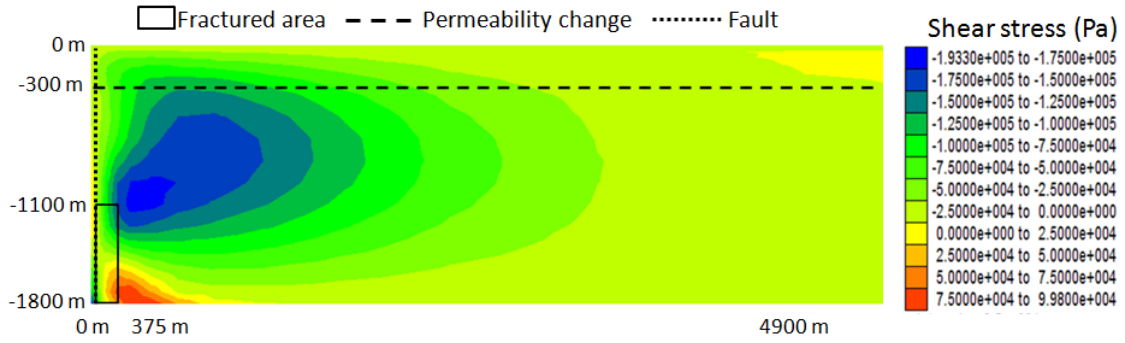
Figure 4.11: Plane shear stress in the XZ plane after 1460 days of injection (Biot's coefficient is 1 in the porous continuum and 0.56 in the fractured continuum (after Walsh (1981))
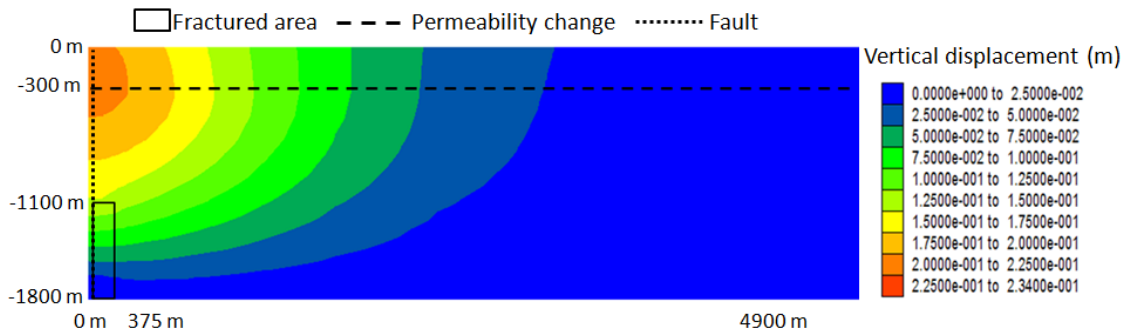
Figure 4.12: Vertical displacement after 1460 days of injection (Biot's coefficient is 1 in the porous continuum and 0.56 in the fractured continuum (after Walsh (1981))

The changes in pore pressure are much more effectively transmitted to the fractured area and tensional and compressional stresses appear at the corners of the fractured area as a response to increased pressure in one of the opposite corners, where injection takes place. Effective stresses are also transmitted vertically more effectively and tensional effective stress at surface reaches a peak of 0.26963 MPa, inducing the highest displacements (Fig. 4.12).

4.6.2 *Case B*: CO$_2$ injection in the fractured area

A second option for coupling CCS with UCG is injecting the captured CO$_2$ in the gasified area.

Pressure buildup at the injection point

The pressure buildup during injection is one of the criteria to consider in the risk assessment. Lower injection pressure means lower energy consumption for storage and higher safety, since lower pore pressures in the system would induce lower tensional effective stresses. Results of the simulation show that the presence of a fractured zone represented by the dual-porosity model close to the injection point results in a lower pressure increase at that injection point (Fig. 4.13).
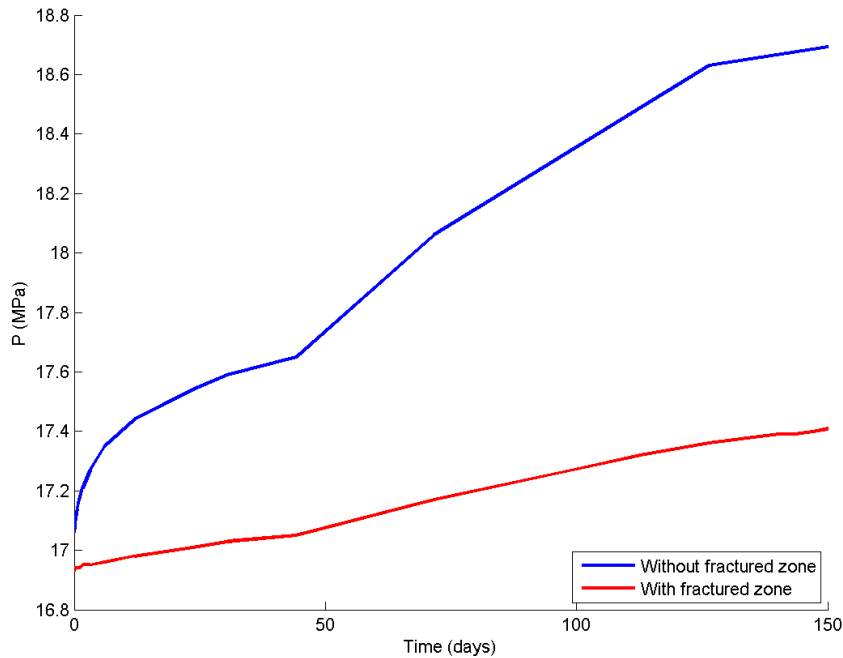
Figure 4.13: Pressure build-up at the injection point after one year of injection in *Cae B* model

CO$_2$ plume evolution

In the absence of a clear preferential pathway such as a fault, it can be observed that free-phase CO$_2$ saturation (Fig. 4.14) and dissolved CO$_2$ (Fig. 4.15) progress vertically very quickly when the formation is fractured, compared to the same low permeability single porous medium. Horizontal fractures, however, play a secondary role in the evolution of the plume, acting as main pathways only when the difference with vertical permeability is very high. This is illustrated in Fig. 4.6.2: though vertical and horizontal permeabilities in the fractures are the same, the CO$_2$ clearly raises from the injection point at the bottom left corner of the fractured area to the top of the fractured area, where it accumulates and starts spreading laterally. This accumulations of CO$_2$ in free phase where its migration velocity is reduced help in the dissolution of CO$_2$ in the brine. As seen previously in *Case A-2*, the dissolved CO$_2$ sinks into the bottom of the fractured area. It can be noted as well that, contrary to *Case A-2* where CO$_2$ moved quickly to escape along the fault and had no time to percolate into the matrix in the fractured area, in *Case B-2* (injection in a fractured zone), with no route to escape and increased resident time, it can be observed that the free-phase and dissolved CO$_2$ concentrations in the matrix elements in the fractured zone are significantly higher than in *Case A-2*.

(a) Without a fractured zone

(b) With a fractured zone (in the matrix)

(c) With a fractured zone (in the fractures)
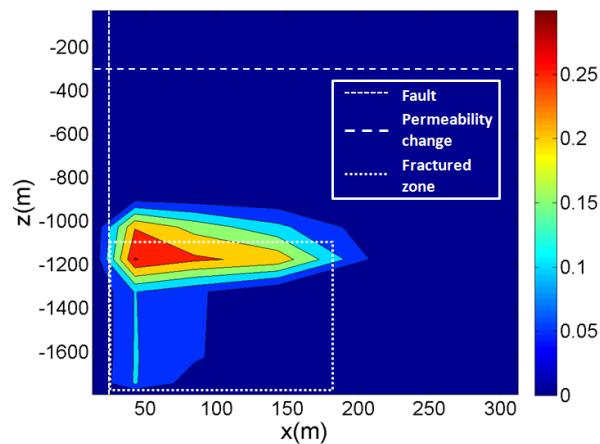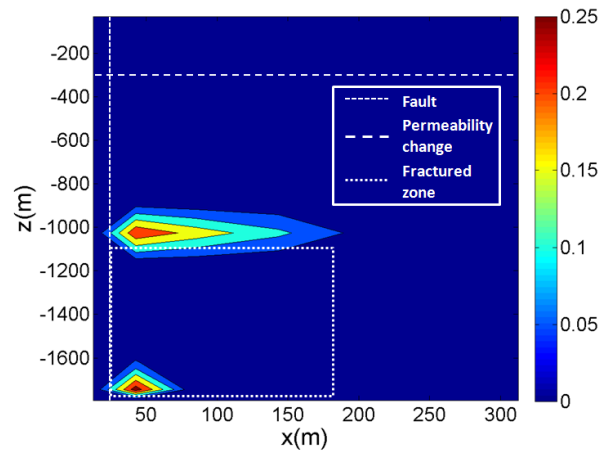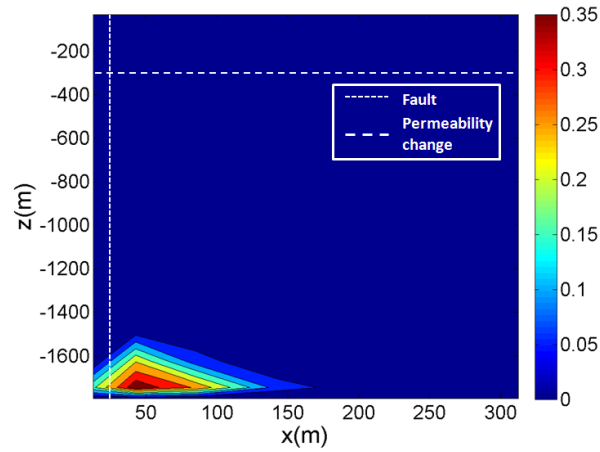
Figure 4.14: Free-phase CO_2 saturation in *Case B* model after 1460 days of injection
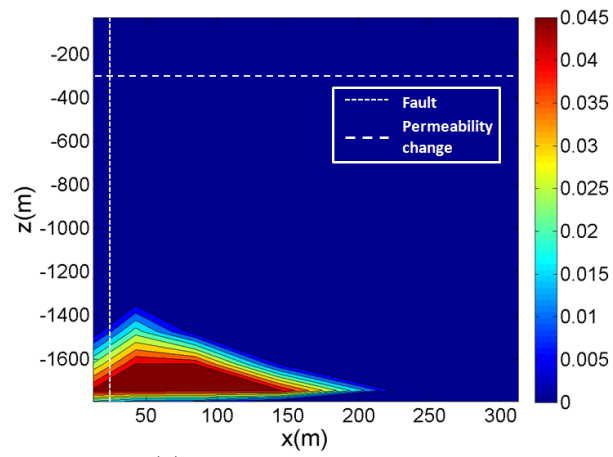
(a) Without a fractured zone
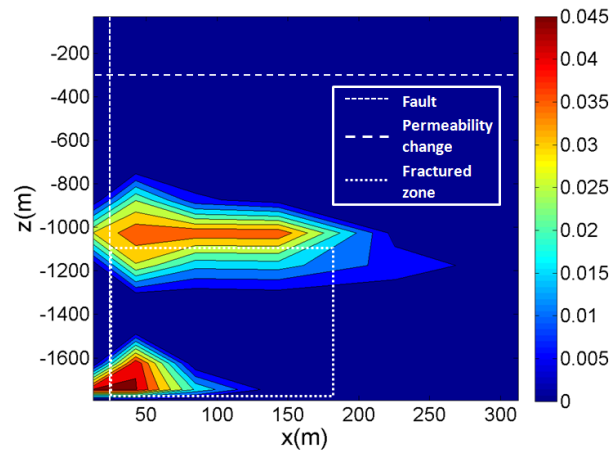
(b) With a fractured zone (in the matrix)
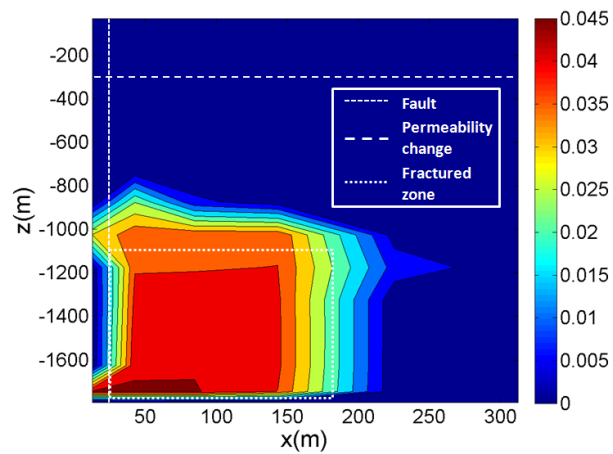
(c) With a fractured zone (in the fractures)

Figure 4.15: Dissolved CO_2 in *Case B* model after 1460 days of injection. Colour bar shows mass fraction

113

Figure 4.16 and Table 4.5 show the evolution of the injected CO_2 in the system. As opposed to *Case A*, there is a clear difference in the dissolved and free-phase CO_2 in *Case B-1* and *Case B-2*. The injection into a fractured area improves the dissolution mechanisms, increasing the storage security. In *Case B*, hardly any CO_2 escapes through surface.

(a) Without a fractured zone (*Case B-1*) (b) With fractured zone (*Case B-2*)
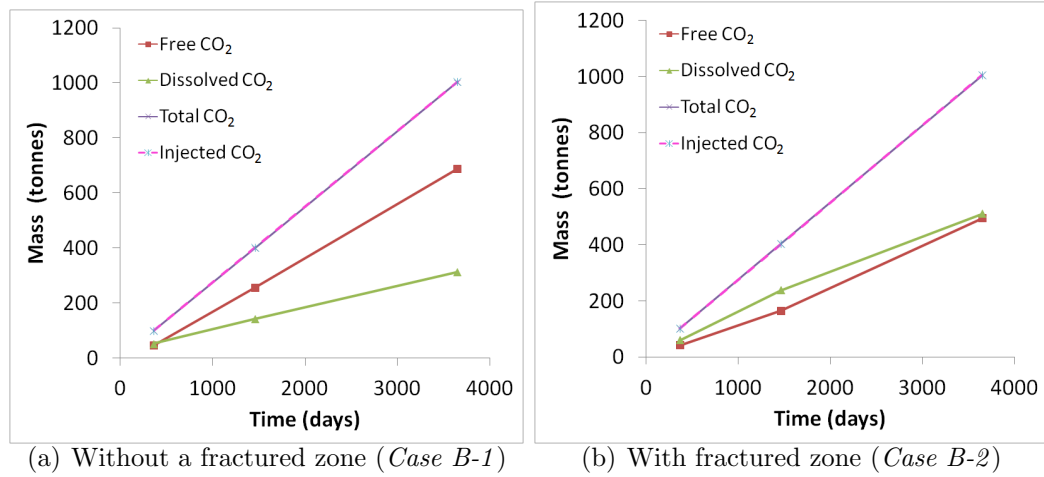
Figure 4.16: Evolution in time of free-phase, dissolved and total CO_2 in the system and CO_2 injected in the model for the *Case B*.

Table 4.5: Comparison of total CO_2 in the system, dissolved and free phase CO_2 in the model without a fractured zone and the model with a fractured zone after 3650 days. Total CO_2 sourced in the model is 1005.37 tonnes. (*Case B*)

	Without fractures	With fractures
Total	1002.21	1005.08
Dissolved	313.29	510.48
Free phase	688.92	494.60

Geomechanical response

Observation of the effective stress (Fig. 4.17) show that induced stresses in the case of injection in a non-fractured formation (*Case B-1*) are higher at the point of injection but are more contained in the deeper layer. Effective stress at surface in the case of injection into a fractured zone (*Case B-2*) is slightly higher (0.20465 MPa against 0.20124 MPa).

(a) Without a fractured zone (*Case B-1*)

(b) With a fractured zone (*Case B-2*)
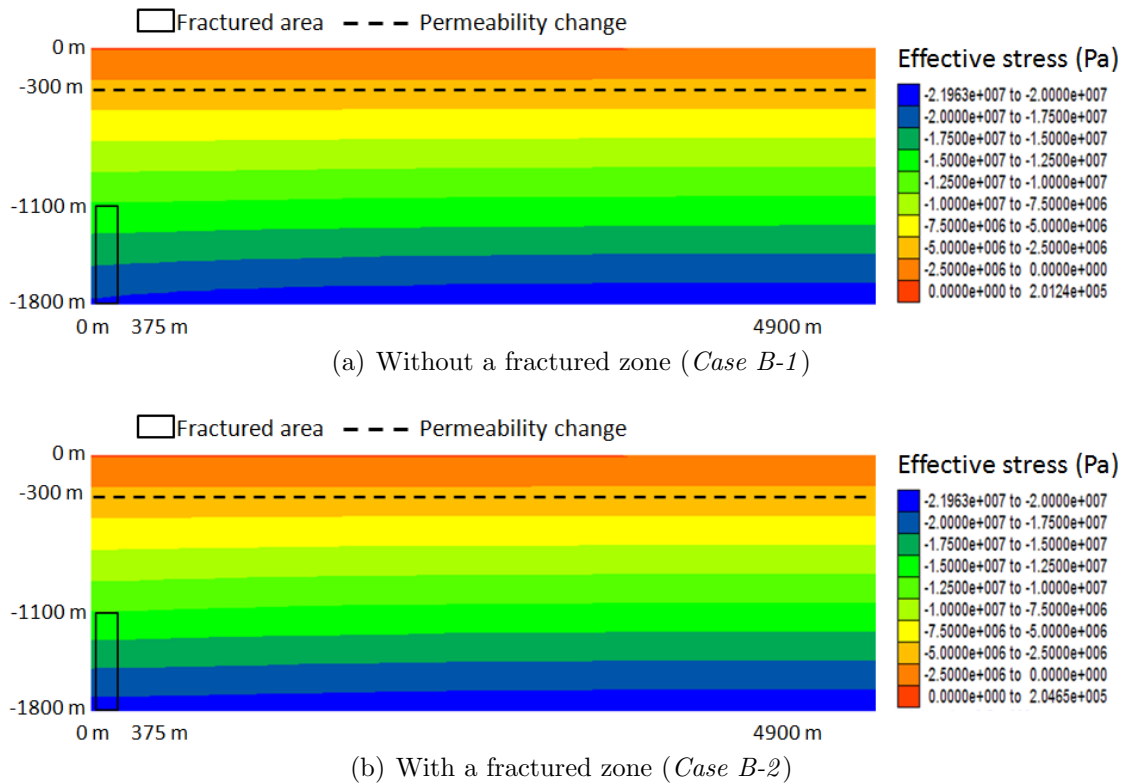
Figure 4.17: Stress in the XZ plane after 1460 days of injection

This results in very similar displacement profiles (Fig. 4.18) and slightly different shear stresses distributions (Fig. 4.19). Interestingly, Figure 4.19(a) shows a different profile of the shear stress, where it can be seen that the effect of near surface displacement does not completely overweight the induced stress at the bottom in the injection point.
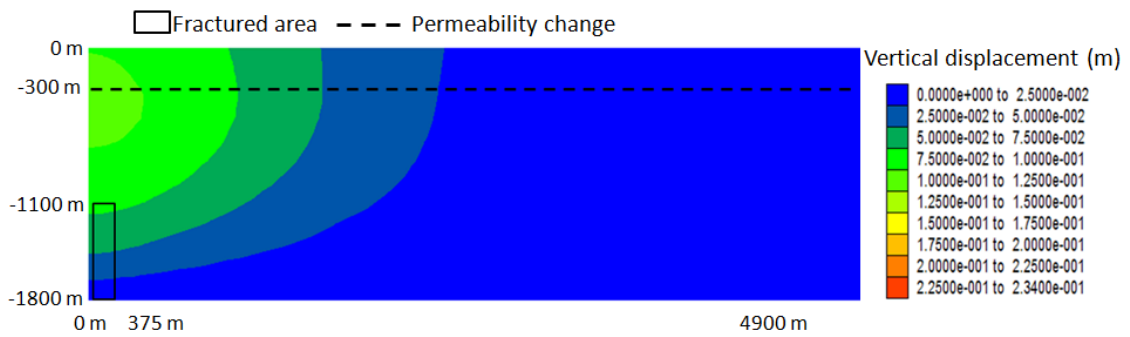
(a) Without a fractured zone (*Case B-1*)
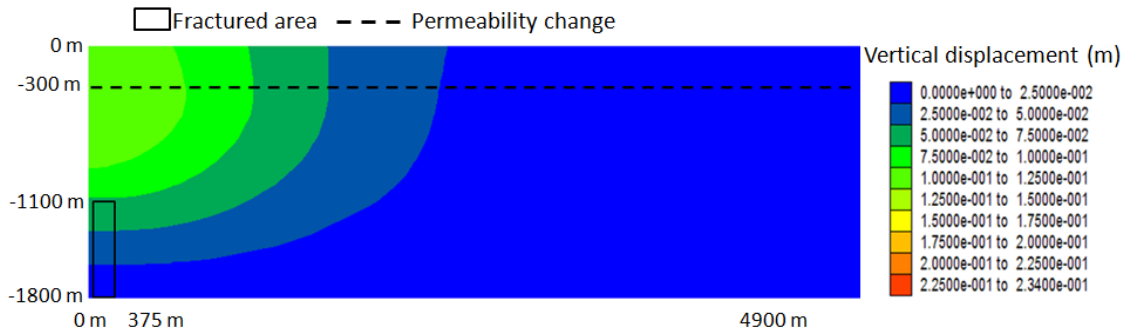
(b) With fractures (*Case B-2*)

Figure 4.18: Vertical displacement after 1460 days of injection
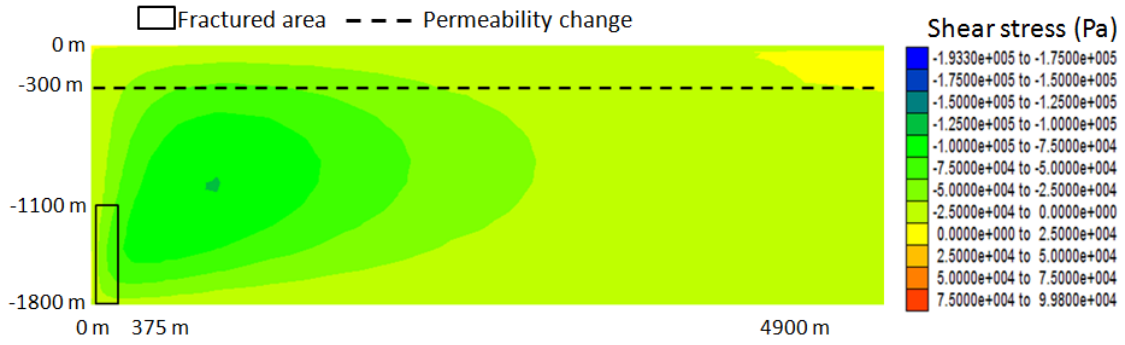
(a) Without a fractured zone (*Case B-1*)
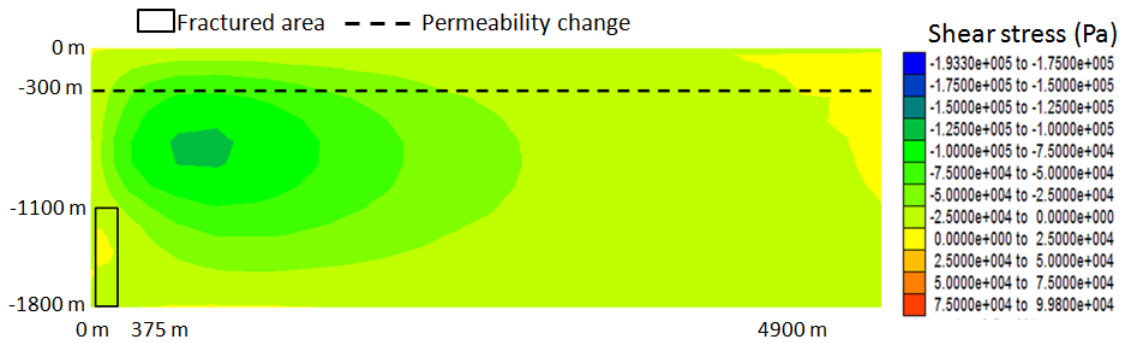
(b) With a fractured zone (*Case B-2*)

Figure 4.19: Stress in the XZ plane after 1460 days of injection

4.7 Summary and Conclusions

The necessity of hydro-mechanically coupled simulation models which can account for dual-porosity to represent the fractured area in UCG–CCS has been established. This Chapter implements this concept between two well-known models, TOUGH2 and FLAC3D. TOUGH2 is a multiphase, multi-component flow and transport model. FLAC3D is a numerical code for advanced geotechnical analysis in three dimensions. Rutqvist et al. (2002) developed a two-way iterative coupling module to link both codes. Here, this coupling module is extended to account for dual-porosity flow models.

One of the main advantages of using a research open source code such as TOUGH2 is the possibility to implement changes as required by the developer. FLAC3D also

facilitates certain development potential by means of its built-in code FISH. However, ultimately, access to a commercial FLAC3D source code is not available. This may limit more drastic incursions and eventually an open source geomechanical code for TOUGH2 might be developed (Liu and Rutqvist, 2013).

Two cases have been setup and simulated: injection of CO_2 below the fractured area and migration along a vertical fault in the vicinity of that fractured zone and injection in the fracture area itself.

Results show that the simulator seems to adequately capture the flow and geomechanical processes. Benchmarking exercises to further test the implementation of the code are the next necessary step in the development of a code.

Two cases were simulated: a fractured area in the vicinity of a leaking fault and injection into a fractured zone. The presence of the fault dominates the behaviour of the system due to the significant difference in permeability and the reduced volume of fractures. Special attention has to be paid to effective stresses, which can induce surface heaving and development of shear stress in a large area distant from the injection point and therefore potentially less monitored. Though improvement in CO_2 dissolution and therefore storage security was observed when a fractured area is present, the flow rates along the leaking fault preferential path rendered it negligible.

A very significant outcome is the impact of avoiding the common simplification of using a Biot's coefficient of 1 and use a lower value for the fractured continuum. The subsequent calculation of pore pressure and its impact on effective stress, displacement and shear stress is paramount. It will be a key parameter to consider in hydromechanical simulation of UCG–CCS.

The second case, injection into a fractured zone, proved the advantage in terms of injectivity and dissolution of CO_2 as a trapping mechanism. However, it is also patent in this model that the buoyancy of CO_2 drives it to migrate vertically to the top of the fractured area. Horizontal fractures have a secondary role in CO_2 migration,

to become important when vertical permeability differs greatly from permeability in the horizontal plane, as in the top of the fractured zone. Geomechanical response in this case yielded slightly harsher conditions in the case of injection in the fractured zone, but ultimately, this is dependent of the in-situ stress regime.

Though successfully tested in two scenarios, the current development of this dual-porosity, hydromechanically coupled TOUGH-FLAC3D model has a number of simplifications and limitations which may hinder its use:

One of the limitations is the temperature range (up to 110 ^{o}C) of the ECO2N equation of state module. In UCG-CCS applications it will be desirable to investigate the effect of higher temperatures. Even if it is foreseen that sufficient cooling might take place in the gasification chamber before injection, a commercial operation with several gasification chambers operating simultaneously in the proximity may alter the temperature field over this value.

Mathematical convergence difficulties were found during the simulation and further attempts of a thorough sensitivity analysis and case variations. In particular, the injection rate in the *Case B* (injection into a fractured area) could not be increased to levels of commercial exploitation (e.g. the equivalent of 1–2 Mt/y for the model section considered). Linear equation failure to converge was repeatedly present despite the tuning of other parameters in TOUGH2. This can be due to the small fracture volume, especially in elements close to major flow paths, of fracture elements in comparison with the matrix block.

Simultaneously, several pre and post processing softwares were evaluated to integrate a dual-porosity model (e.g. *PetraSim, Paraview, T2B*). However, at the time of this research, none of them could provide the necessary capabilities, so pre and post processing tools have been developed during this work using FORTRAN and MATLAB. As a result of both the convergence difficulties and the laborious process of model preparation and analysis, only a limited number of simulations could be

successfully run.

Therefore, in addition to the general framework issues for developing UCG–CCS modelling presented in Chapter 3, and also applicable to TOUGH2–FLAC3D, it is recommend that further work on the TOUGH2–FLAC3D model should initially concentrate on:

- generalization of the model to account for dual-permeability systems (that is, with several nested blocks in the matrix which allow matrix-matrix flow)

- further development and generalization of pre and post processing tools which help in speeding up the model setup process and results analysis

- extensive model validation and comparison with other simulators and semi-analytical solutions

- implementation of additional capabilities in the ECO2N module to extend the temperature range

- research in Biot's coefficients expected in a UCG–CCS environment

- improvement of graphical output, e.g. inclusion of contour logarithmic colour plots

The next chapter will study an alternative hydro-mechanically coupled simulator, GEM from Computer Modeling Group (CMG) Ltd.

Chapter 5

Modelling CO_2 injection into fractured zones with Barton-Bandis fracture stress-dependent permeability

5.1 Introduction

Assessment of caprock integrity is one of the key issues in evaluating the suitability of a CO_2 storage site. In preliminary studies of reservoir scale pressure variation, geomechanical coupling with a single phase fluid flow model can provide a first approximated estimate (Chiaramonte et al., 2011). Similarly, analytical and semi-analytical solutions have been developed for that purpose. For instance, Streit and Hillis (2004) analyzes fault stability with the shear fault-failure envelope of the Mohr–Coulomb criterion and the slip tendency, which is the ratio between shear and normal stresses. Hawkes et al. (2005) sets up a Mohr–Coulomb uniaxial compression scenario to predict the direction of faults susceptible of failure using two variables: the horizontal stress and the pore pressure. Soltanzadeh and Hawkes (2009) calculate the induced stress with Eshelby's theory of inclusions and applies the Mohr–Coulomb criterion to observe the predominant areas of the reservoir where reactivation occurs. Ultimately, since the in-situ stress tensor does not remain constant in time, and the failure po-

tential is strongly dependent on it, it is necessary to have coupled numerical models which can account for these changes and provide more accurate predictions. Numerical models which include more sophisticated permeability changes in faults already exist (e.g. Tran et al., 2008; Bower and Zyvoloski, 1997) or are being developed (e.g. Chiaramonte et al., 2011; Ji et al., 2009).

As the pore pressure increases due to the injection of CO_2, the effective stress decreases (see Figure 5.1) and tensile and shear failure of both existing and new fractures may occur.
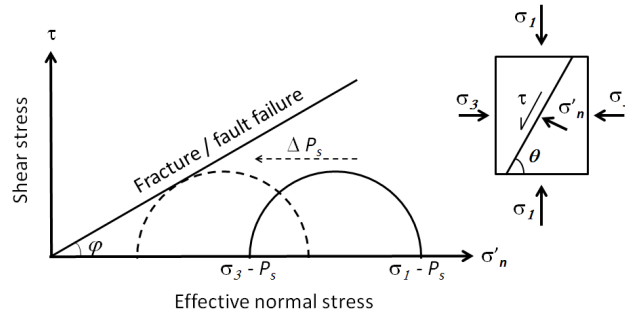
Figure 5.1: Effect of increasing pore pressure P_s in the stability of fractures and faults. The *Fracture/fault failure* line shows the failure envelope of a fracture or fault with null cohesion. As the effective stress normal (σ'_n) to the plane of the discontinuity decreases, the Mohr-Coulomb circle is displaced towards the failure envelope, increasing the possibility of shear failure.

The order in which the shearing and tensile failure appear depends on the in-situ stress tensor, the ratio of principal stresses, the fault orientation and the pore pressure (Olson et al., 2009; Mathias et al., 2009c; Streit and Hillis, 2004).

The fracture permeability is often modelled through the cubic law for flow between parallel plates, in which the flow is a function of the length and aperture of the fracture, the pressure and the viscosity of the fluid.

Therefore, to model the conductivity changes in fractured zones, it is necessary to know the changes in aperture caused by joint closure, shear dilatancy or tensile

opening. Barton et al. (1985) studied the relationship between the fracture conductivity, the aperture, and the normal fracture effective stress (e.g. the component of the effective stress normal to the plane of the fracture, see σ'_n in Figure 5.1). The threshold value of the normal fracture effective stress will be zero or negative in the case of tensile failure and positive in the case of shear failure paralell to the fracture plane, where the Mohr-Coulomb criteria would apply (Tran et al., 2009).

Figure 5.2 shows the mechanisms of fracture shear dilatancy and tensile opening. While the tensile opening is a function of the stress normal to the surface (e.g. between blocks A and B), the shear dilatancy displacement (e.g. between blocks B and C) depends not only on the stress normal to the surface (F_N), but also on the shear stress F_T, the roughness of the surfaces and the strength of the peaks at the surface.
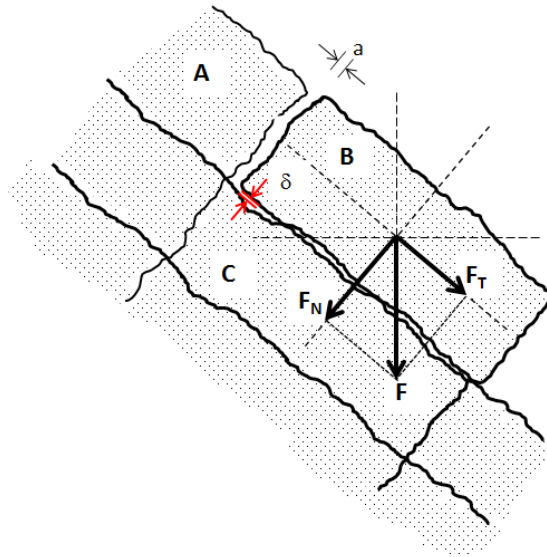
Figure 5.2: The force F applied on the block B produces a tensile opening between blocks A and B, a. The aperture between blocks A and C, δ, is due to shear dilatancy. (Modified from Barton and Bandis (1982))

Cohesion in uncemented fractures is null or very small, and their tensile strength is null. Since cohesion and tensile strength in the fractures are lower than in the

intact rock, it is assumed that opening of existing fractures will take place before new fractures are developed in that same direction. Other assumptions are that development of new fractures in other directions and propagation of existing ones do not occur.

Based on these assumptions, a model which relates the fracture normal effective stress with the fracture opening, and subsequently with its permeability, can be implemented. This approach of combining a dual permeability model with a fracture stress dependent permeability has also been implemented and verified by Bower and Zyvoloski (1997) in the FEHM code for geothermal, petroleum production and nuclear waste repository applications.

The aim of this chapter is to compare the differences observed in pressure evolution and the caprock response when injecting CO_2 in a fractured zone underneath the caprock and when doing so in a single porous medium. The effect of fracture opening on the sealing caprock is studied by applying the dual-permeability hydromechanical coupling. This has been accomplished with the use of the Barton–Bandis model, which allows for accounting of permeability changes in the fracture due to variations in normal fracture tensional stress. The chapter is structured as follows: first, the reservoir compositional simulator GEM from Computer Modeling Group, Ltd. (CMG) is described, along with the Barton–Bandis model for fracture permeability variation as a function of stress. Then the model setup for the numerical simulation is described. Section 5.5 develops the comparative study of four selected scenarios modelled with GEM, which include different combinations of porous and fractured zones and hydromechanical coupling. A sensitivity analysis on a variety of parameters in one of the scenarios studied in the previous section is carried out and results discussed. Finally, conclusions are summarized.

5.2 CMG GEM overview

The numerical simulator selected to carry out this work has been the compositional simulator GEM from Computer Modeling Group Ltd. (CMG). GEM is an advanced multiphase muticomponent flow, transport and heat simulator which incorporates among other options, equations of state to calculate the fluid properties, dual porosity and permeability, miscibility of gases including CO_2 and numerous features commonly used in the simulation of hydrocarbons reservoirs. GEM can also be coupled with a finite- element geomechanical module with plastic and nonlinear elastic deformation model or a single-well boundary unloading model. The relationships between stresses and strains are taken from the theory of poroelasticity and plasticity. GEM can also be coupled with a geochemistry model, which allows the modelling of mineral and fluid chemical reactions (CMG Ltd., 2012). Therefore, GEM has the capacity of integrating a thermo–hydro–mechanical–chemical (THMC) approach for the simulation of CO_2 and UCG.

GEM incorporates the following theory and physics of CO_2 sequestration:

- Modelling gas solubility in aqueous phase

- Phase behaviour and chemical equilibrium

- Fluid flow and convection

- Residual gas trapping

- Mineral trapping

- Geochemistry

5.3 Fracture permeability stress dependency: the Barton–Bandis model

In a coupled hydromechanical model, the flow simulator evaluates the changes in temperature, pressure and saturation, while the geomechanics module calculates deformation and stress to return an updated permeability and porosity. In this study, in conjunction with this approach for the porous rock matrix, the modified Barton–Bandis empirical model (Barton, 1973) has been used in the fractured continuum. (see Barton et al. (1987) and Her-Yuan Chen (2000)). The Barton–Bandis model calculates the permeability of a fracture as a function of the normal effective stress σ'_n and its history. Figure 5.3 (after CMG Ltd. (2012)) shows the path that permeability in the fracture follows. For values of the normal effective stress greater than the opening fracture stress frs, the permeability remains low along the path AB. If σ'_n falls below that threshold value of frs, permeability increases instantaneously to its maximum value khf (path BC) and will remain there (path DCE) until the σ'_n becomes positive. At that moment, the permeability is reduced instantly to the fracture closure permeability $kccf$ (path EF) and as the σ'_n increases, the permeability tends asymptotically to the residual value of fracture closure $krcf$ according to equation 5.1 (path FG). It has to be noted that only paths AB and EFG are reversible. Therefore, the fracture permeability depends not only on the value of the normal effective stress, which is equivalent to the minimum principle effective stress, but also on its history.
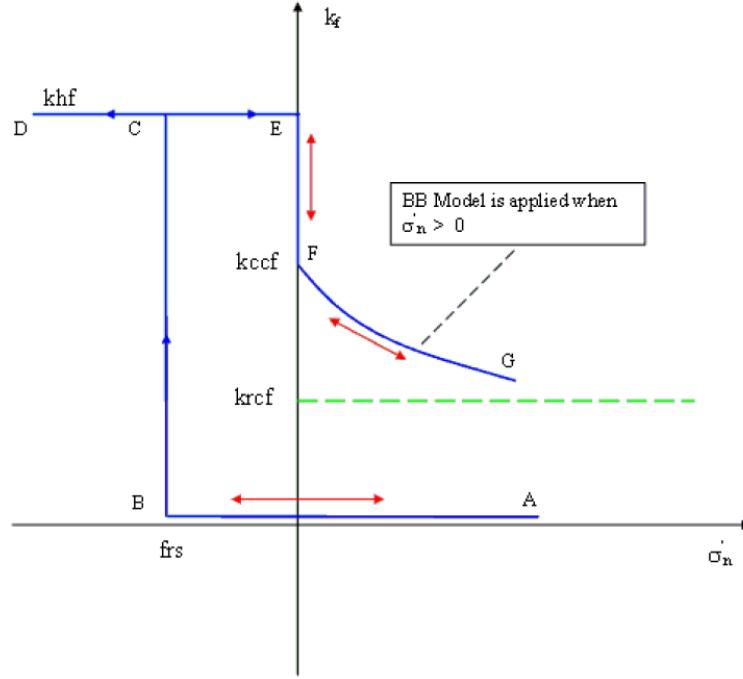
Figure 5.3: Fracture permeability evolution in the Barton–Bandis model

The fracture closure permeability is calculated (CMG Ltd., 2012) as:

$$k_f = kccf \left(\frac{e}{e_0}\right)^4 \geqslant krcf \qquad (5.1)$$

where:

kf is the fracture closure permeability [L]

$kccf$ is the fracture closure permeability [md]

$e = e_0 - V_j$

e_0 is the initial fracture aperture [L]

$V_j = \frac{\sigma'_n}{kni + \sigma'_n/V_m}$ is the joint closure under a normal fracture effective stress σ'_n

$V_m = e_0 \left[1 - \left(\frac{krcf}{kccf}\right)^{\frac{1}{4}}\right]$ is the maximum fracture closure [L]

$krcf$ is the residual value of fracture closure permeability [md]

5.4 Model setup

A two-dimensional model based on Tran et al. (2009, 2010) is built with a cartesian grid of 29 blocks in the horizontal direction and 33 blocks in the vertical direction, which extends 4621 m horizontally and 321.1 m vertically, being the other orthogonal horizontal dimension 100 m. The model contains two caprocks with their respective overburdens, and the storage formation below which the injection takes place. The caprocks consist of one layer 4.5 m thick, while the overburdens are comprised of five 15.25 m thick layers each. The storage area underneath is formed by 21 layers 7.6 m thick each. Horizontally, the grid blocks are 100 m long, except towards the lateral boundaries where their size increases to 500 m in increments of 100 m. The horizontal dimension is also reduced in the proximity of the well. The cell containing the well is 1 m long and the adjacent blocks are 10 m long. The base model considers a dual permeability system only active in the two caprocks and their immediate adjacent layers in order to account for the fracture permeability variation according to the modified Barton–Bandis model (Tran et al., 2009). The injection is carried out in the 30 m at the bottom of the formation by means of a vertical well. The hydraulic parameters are shown in Table 5.1.

Table 5.1: Hydraulic parameters used in the five horizontal layers of the model (from Tran et al. (2009)).

Layer (from top to bottom)	Permeability k_h (md)	k_v/k_h [-]	Porosity ϕ (fraction)
Top overburden	25	0.25	0.13
Top caprock	1.0E-07	0.25	0.13
Intermediate overburden	20	0.25	0.13
Bottom caprock	1.0E-07	0.25	0.13
Storage formation	15	0.25	0.13

The system considered is closed, with no flow through boundaries. Displacement is allowed in the horizontal direction along the model –except in the lateral boundaries– but not in the horizontal direction normal to the model plane. Vertical displacement is permitted with the only exception of the bottom boundary. The model is isothermal, with a reservoir temperature of 38 ^{o}C.

The injection rate is constant through the injection period and in all scenarios and it is set to 100,000 m^3/day at surface conditions (pressure 1 atm, temperature 15.5 ^{o}C). This is equivalent to ca. 0.07 MMt/y. Nakaten et al. (2014) estimate that the coal that needs to be gasified to feed a 308 MW combined cycle gas turbine (CCGT) plant is approximately 3100 t/d and the CO_2 captured after all efficiencies are accounted is roughly 2.4 times the coal burnt, that is, 7405 t/d. However, since that amount of CO_2 occupies four to five times the space that the coal occupied before gasification (Roddy and González, 2010), Nakaten et al. (2014) assume that 20% of the CO_2 (0.54 MMt/y) would be injected back into the cavity. The drawback of Nakaten et al. (2014) assumption is that it does not evaluate the overpressure achievable in the system before caprock seal failure.

A secondary constraint on the well bottom-hole pressure of 51,710 kPa is also set, though it is never reached during the simulations. CO_2 injection is stopped after 2,891 days and total time simulation is ten years (3,650 days), allowing time to observe the system pressure decrement after ceasing injection.

The injected fluid is 99.9% pure CO_2 and its PVT properties are calculated with the Peng-Robinson equation of state. A trace of methane is incorporated to facilitate the numerical solvers work. Water salinity is not considered and the CO_2 solubility in water is modeled with the Henry Law, Henry's coefficients being calculated at a reservoir temperature of 38 ^{o}C and a reference pressure of 10,662.4 kPa at 1,000 m depth. Aqueous molar density and viscosity are calculated using Rowe-Chou and Kestin correlations respectively.

The gas-water relative permeability curves are shown in Figure 5.4. A hysteresis curve for drainage and imbibition in the gas phase can be observed.
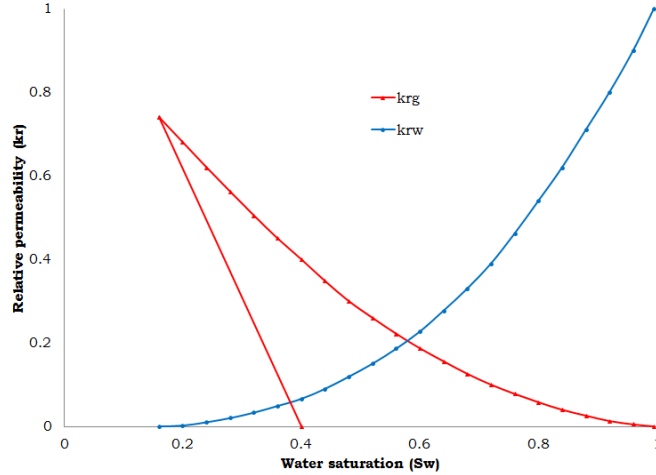
Figure 5.4: Gas-water relative permeability curves (from Tran et al. (2009))

Stress is referenced to the left top block cell and initial stress is calculated as the sum of the reference stress and the stress gradient. The top of the reservoir is located at 800 m depth and initial stress at the reference block is 1,218.7 kPa in the horizontal direction and 2,437.4 kPa in the vertical direction. The stress gradient is -10.4688 kPa/m and -20.9346 kPa/m respectively. Cohesion is constant in all layers (10 MPa). Other geomechanical parameters are shown in Table 5.2.

Table 5.2: Geomechanical parameters used in the base case (from Tran et al. (2009)).

Rock type	Young's modulus (kPa)	Poisson's ratio	Rock compressibility (1/kPa)
Top overburden	4.9987E+06	0.25	1.28213e-06
Top caprock	4.9987E+06	0.25	1.28213e-05
Intermediate overburden	8.6185E+05	0.3	1.28213e-06
Bottom caprock	4.9987E+06	0.25	1.28213e-05
Storage formation	4.9987E+06	0.25	1.28213e-06

The base model is modified (see Section 5.5) with the implementation of a fractured zone around the well which simulates the goaf and propagated strata bending and fracturing subsequent to gasification. This area has dimensions of 53 m of height and 1821 m of length. Dual permeability blocks are therefore active in this dominion as well as in the caprocks. Hydraulic and geomechanical parameters in this fractured zone are equal to the ones in the fractured caprocks. The dual permeability model represents orthogonal fractures with a fracture spacing of 10 m in all three directions.

The Barton–Bandis parameters used to calculate the stress dependent fracture permeability in the caprock and fractured lower zone are shown in Table 5.3. Note that, for simplification, only one model for the stress and fracture permeability is used, regardless the cause of fracture reactivation (if it is shear or tensile failure).

Table 5.3: Fracture parameters in the Barton–Bandis model (modified from Tran et al. (2009)).

Initial fracture aperture (m)	1.981E-05
Initial normal fracture stiffness (kPa/m)	6.786E+05
Fracture opening stress (kPa)	1600
Hydraulic fracture permeability (md)	233
Fracture closure permeability (md)	233
Residual value for fracture closure permeability (md)	33

5.5   Scenarios studied

A number of scenarios have been developed from a base case corresponding to Tran et al. (2009, 2010). The intention is to compare this typical scenario for CO_2 sequestration in saline aquifers with another where the injection takes place in a fractured area, as it would be the UCG– CCS. In addition, the fractured area is modelled with and without fracture permeability stress dependency and without hydromechanical

coupling to reflect the impact of different simplifications. Therefore, a region around the injection area in which the dual permeability model is active has been added to Tran et al. (2009).

The grids of the base case (*Case 1*) and modified models (*Cases 2, 3* and *4*), are illustrated in Fig. 5.5.
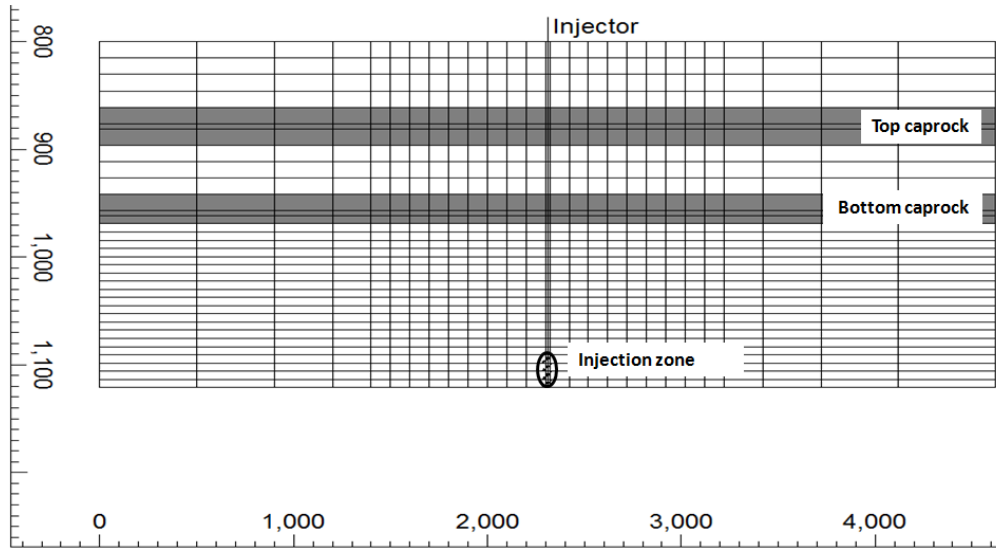
(a) Base case (*Case 1*)
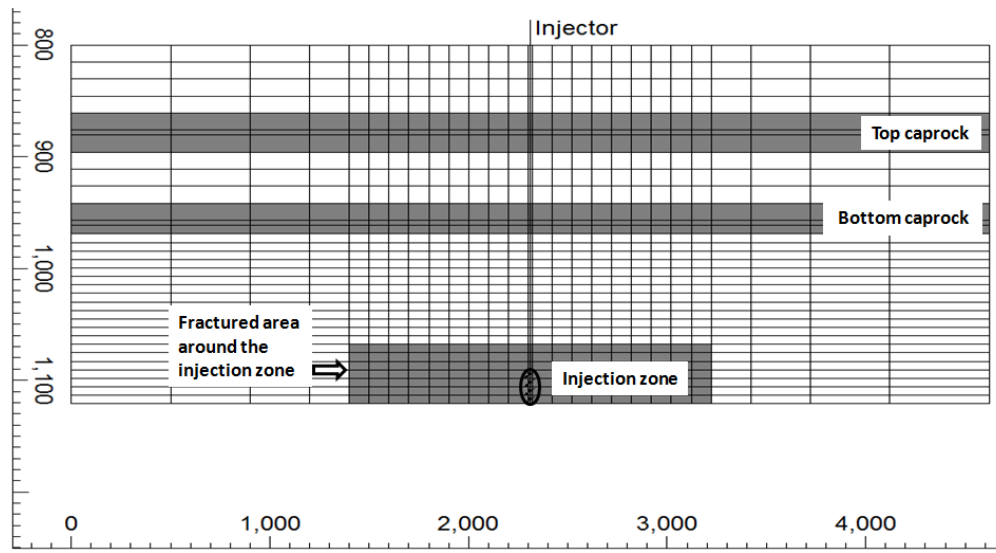
(b) Modified cases (Case 2, Case 3 and Case 4)

Figure 5.5: Model set up based in Tran et al. (2009) (a) and modified (b). Grey blocks show the areas with active dual permeability. Axes units are in metres.

The three hydromechanically coupled scenarios and the non-coupled scenario studied are then:

1. *Case 1:* A base case scenario with the two fractured caprocks with fracture stress dependent permeability and injection in a single porous medium (see Tran et al. (2009, 2010)).

2. *Case 2:* A modified scenario with the same two caprocks with fracture stress dependent permeability but with and added fractured area around the injection point represented by a dual permeability flow model. In the new dual permeability zone where Mohr–Coulomb criterion applies, the fracture permeability is set up as the maximum permeability achievable when the fracture is open and is fixed to that value during the whole simulation.

3. *Case 3:* A similar scenario to *Case 2* but with fracture stress dependent permeability in the fractured area around the injection well and the caprock modelled with Barton–Bandis model. The constitutive law for the rest of the reservoir is Mohr–Coulomb.

4. *Case 4: Case 4* corresponds to the same flow and transport model of *Case 2* but without geomechanical coupling and fixed fracture permeabilities both in the fractured area around the injection point and in the caprocks.

The differences between the four study cases are summarized in Table 5.4.

Table 5.4: Summary of the four study cases

	Case 1	Case 2	Case 3	Case 4
Caprocks fracture permeability	Stress dependent	Stress dependent	Stress dependent	$2.5e^{-08}$ md
Bottom fractures around the well	No	Yes	Yes	Yes
Bottom fracture vertical permeability	N/A	233 md	Stress dependent	233 md
Geomechanical coupling	Yes	Yes	Yes	No

5.5.1 Pressure buildup and fracture normal effective stress

Pressure buildup and fracture normal effective stress provide a measurement on the injectivity of the system and the safety of maintaining a certain injection rate without reactivating faults and opening fractures. Comparison of the four selected scenarios show the impact of coupling geomechanics and the models used to simulate the fracture behaviour. Figure 5.6 shows well bottom-hole pressure evolution.
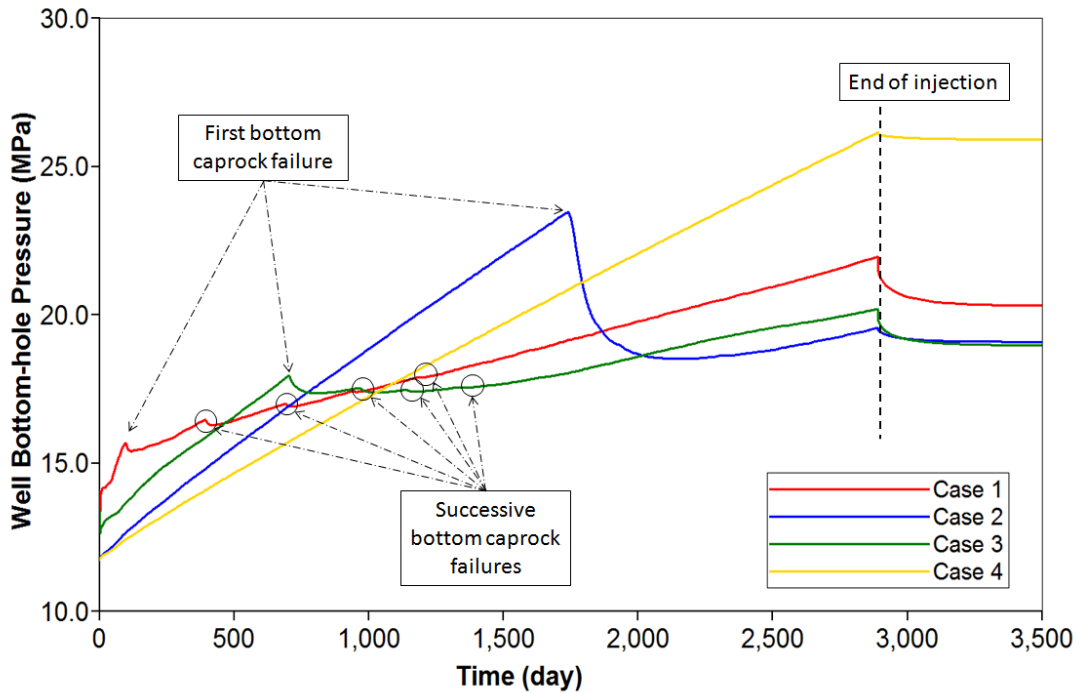
Figure 5.6: Evolution of the well bottom-hole pressure for the four modelling scenarios. The first pressure reduction corresponds to the opening of the bottom caprock. As the caprock failure progresses laterally, successive smaller reductions can be observed in the well bottom-hole pressure. After that, pressures continues to increase monotonically until injection is stopped.

It can be observed that *Case 1* presents the highest initial pressure buildup. As a consequence, normal fracture effective stress in the bottom caprock decreases at a faster rate (Fig. 5.7) and the fracture in the caprock opens up earlier.

The opening of the fracture has an effect on releasing the pressure in the formation, and from that moment, the well bottom-hole pressure increases at a slower pace. *Cases 2* to *4* differ from the base case in the fractured area added around the injection well. All of them present an initial well bottom-hole pressure lower than the case of injection in a single porous formation. This can be explained by the increased permeability and porosity of the fractures. Similarly, these three cases attain a longer injection time compared to the base case before caprock failure. However, there are

135
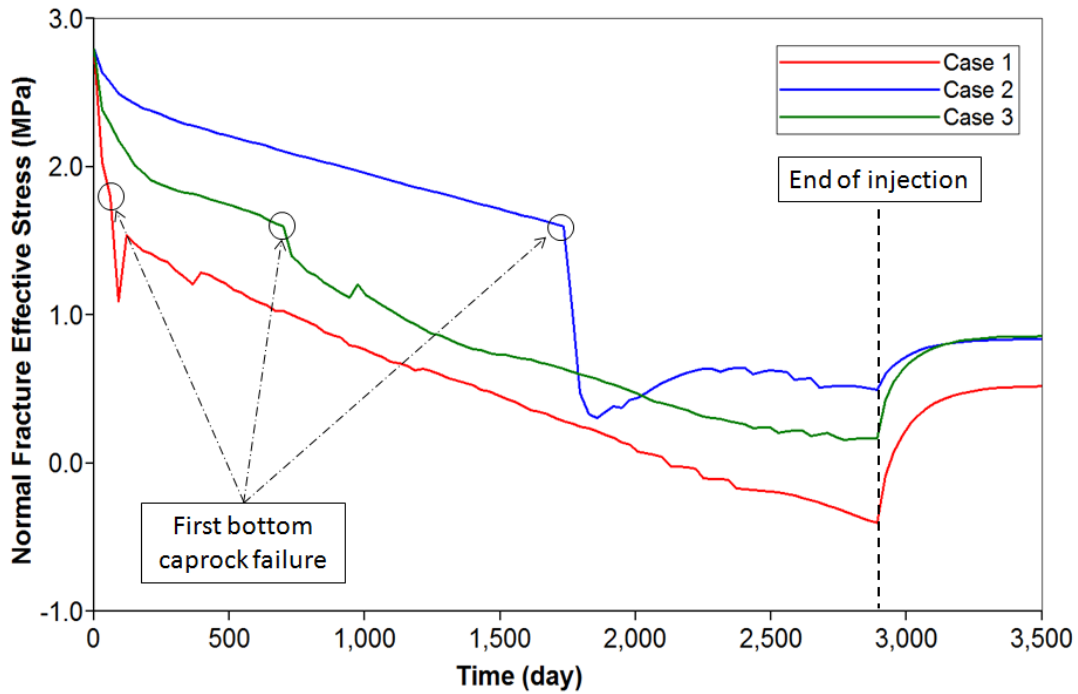
Figure 5.7: Evolution of the normal fracture effective stress at the bottom caprock for the three hydromechanically coupled modelling scenarios.

differences among them. In the absence of geomechanical coupling (*Case 4*), the well bottom-hole pressure increases continuously until injection stops. Since there is no consideration of fracture permeability variation, but it is set to its maximum from the beginning of the injection, the well bottom-hole pressure evolution starts at a lower point and is lower than in the other cases before caprock failure affects their pressure profile. The addition of a geomechanical coupling using a Mohr–Coulomb constitutive model in the fractured area around the well (*Case 2*) results in a faster increase of the well bottom-hole pressure compared to Case 4. When the normal fracture opening stress threshold is reached (at about 1,700 days of injection), the caprock fracture opens and injection pressure decreases drastically. Lastly, if a fracture permeability stress dependent model is used in the fractured area around the well (*Case 3*), the pressure increases faster initially until the caprock fails. As the

136
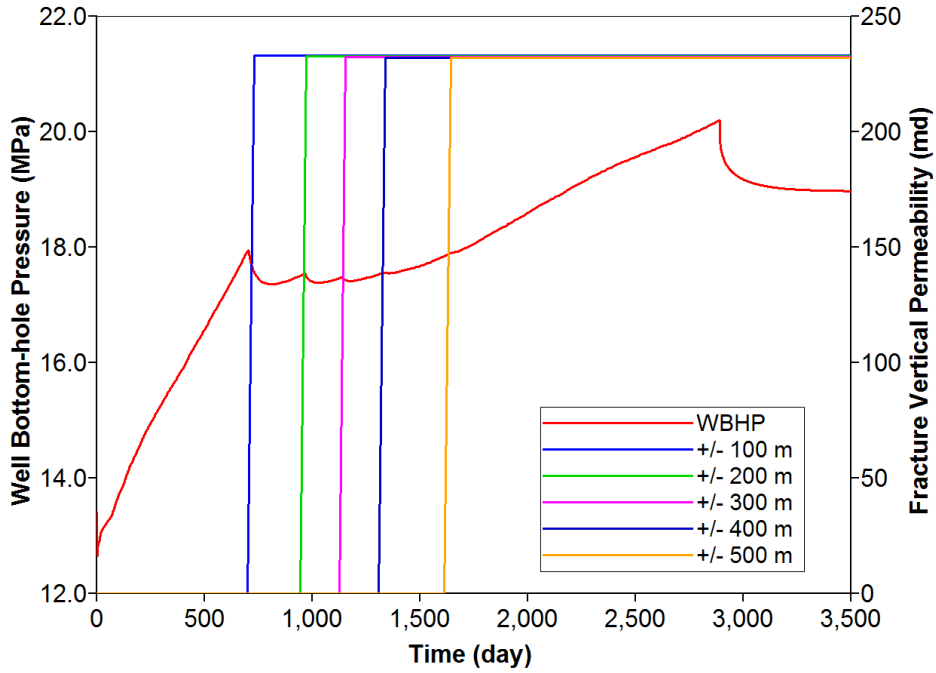
Figure 5.8: Successive down steps in bottom-hole pressure and fracture permeability in the caprock at increasing horizontal distances from the injection point.

shear of the fractures extends laterally in the caprock, successive down steps in the well bottom-hole pressure coinciding with the increased permeability are observed (Figure 5.8).

5.5.2   Fracture permeability

Fracture permeability in the Barton–Bandis model is a function of normal fracture effective stress as seen in Section 5.3. Once the normal fracture effective stress has surpassed a determined threshold, the fractures open and permeability increases. Fig. 5.9 shows how in *Case 1*, fracture permeability increases 60 days after commencement of injection, while *Case 3* caprock fracture opens up at day 700 and fracture permeability in *Case 2* changes at 1,704 days.
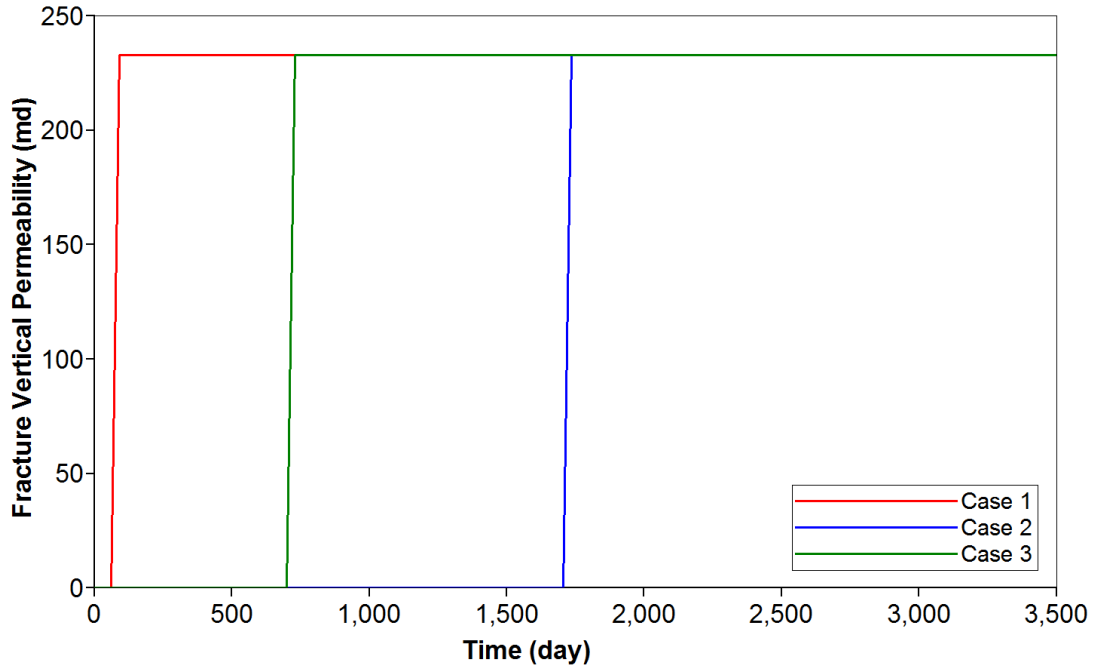
Figure 5.9: Evolution of the fracture permeability in the vertical direction for Cases 1, 2 and 3

5.5.3 Vertical displacement

Displacement at the top of the reservoir is calculated by the geomechanical module. After one year of injection, the base case shows a maximum displacement over the injection point of 0.21 m while for *Cases 2* and *3* this maximum displacement is limited to 0.07 m and 0.08 m respectively. At the end of injection, maximum displacement in *Case 3* (0.798 m) remains lower than in *Case 1* (0.95 m). *Case 2* shows a maximum displacement slightly inferior (0.79 m) to *Case 3* over the injection point, though the profile of the displacement is slightly wider as well (see Figure 5.10).
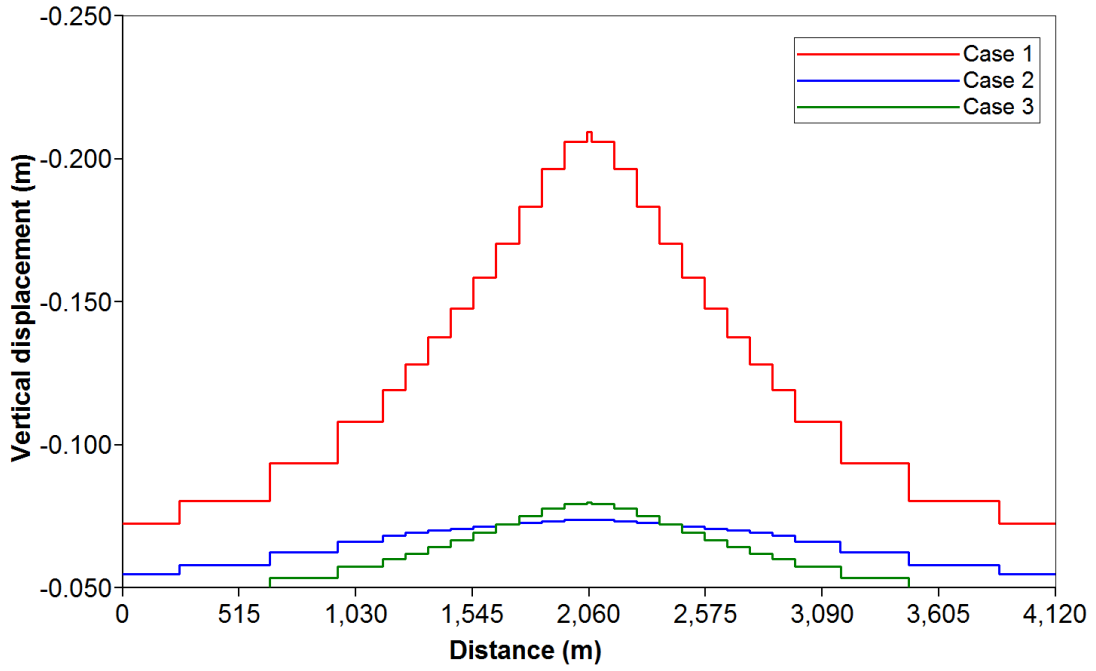
(a) After one year of injection
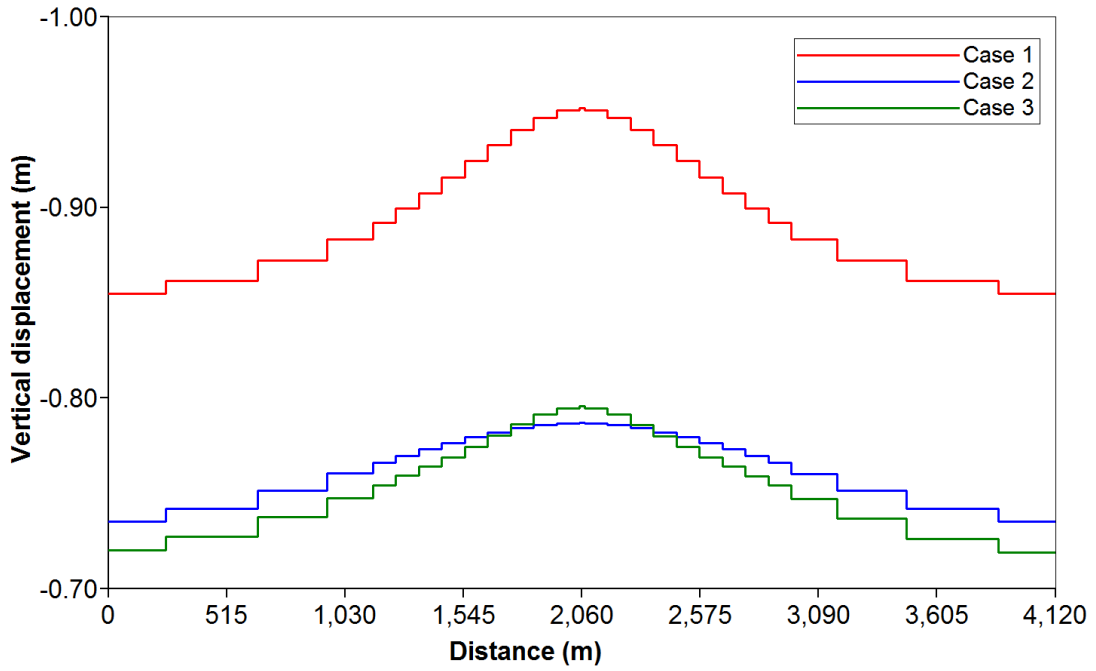
(b) At the end of injection

Figure 5.10: Vertical displacement for Cases 1, 2 and 3

139

5.5.4 CO$_2$ plume evolution

Visualization of the gas saturation shows the differences in the CO$_2$ plume speed and shape in the selected scenarios. Figures 5.11, 5.12 and 5.13 show respectively the gas saturation *i)* when the plume reaches the bottom caprock, *ii)* when the CO$_2$ gas phase appears over the bottom caprock and *iii)* at the end of injection. It can be observed that in *Cases 2* and *4*, where initial permeability in the fractures is higher, the CO$_2$ plume tends to migrate faster towards the top of the fractured area and extends horizontally there before progressing again vertically.
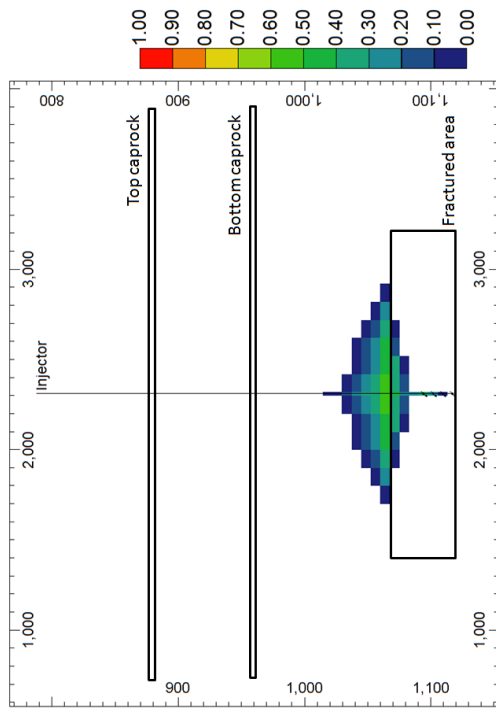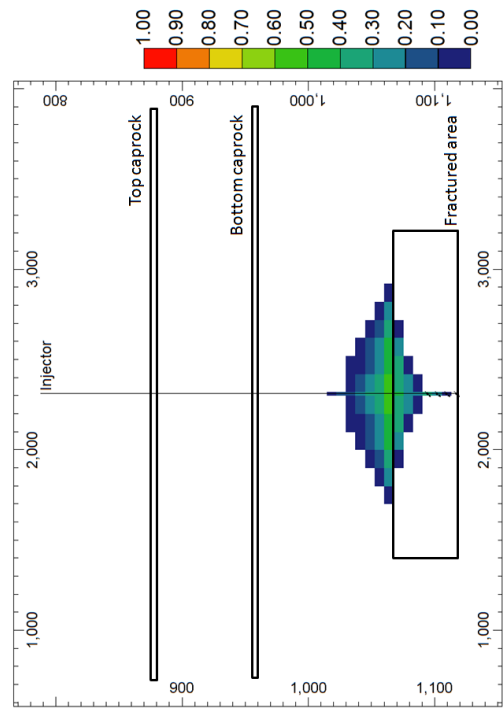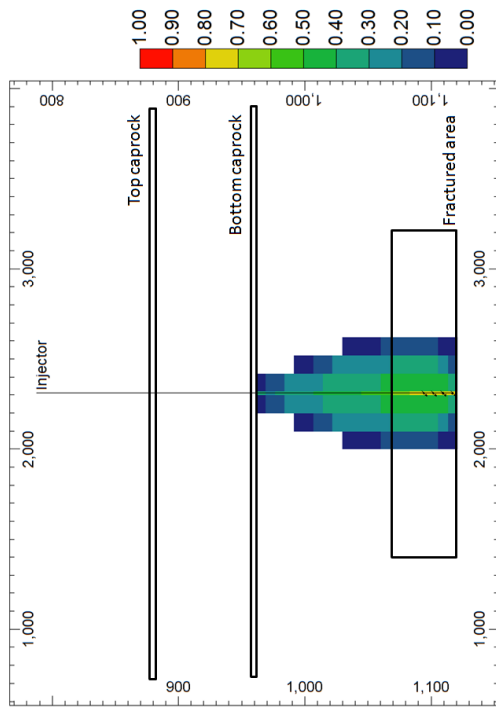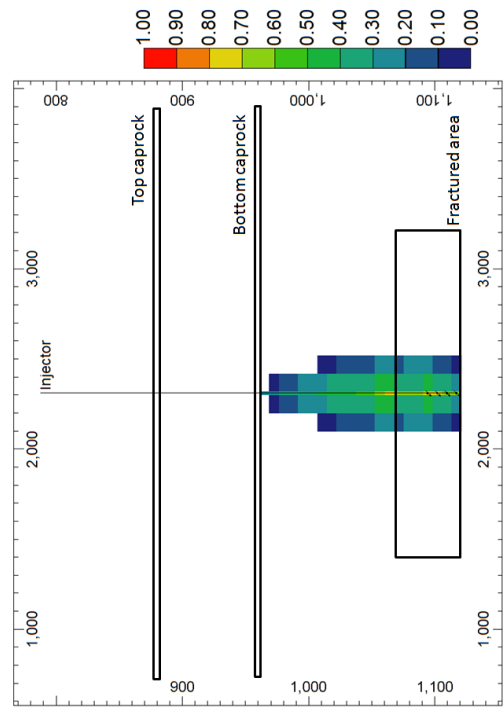
Figure 5.11: Free-phase CO$_2$ saturation 1461 days after commencement of injection for the four study cases. Saturation is expressed as fraction according to the color bar. Distances are in metres.
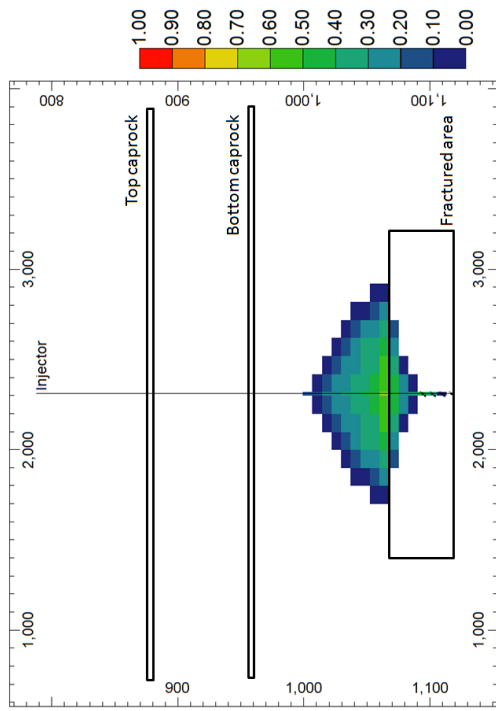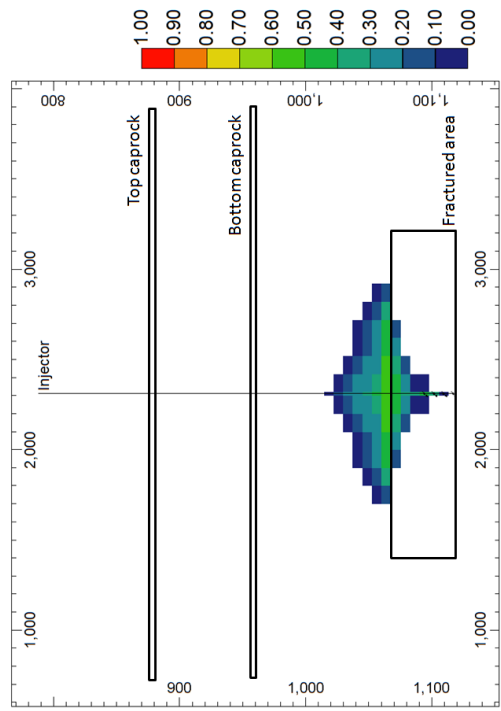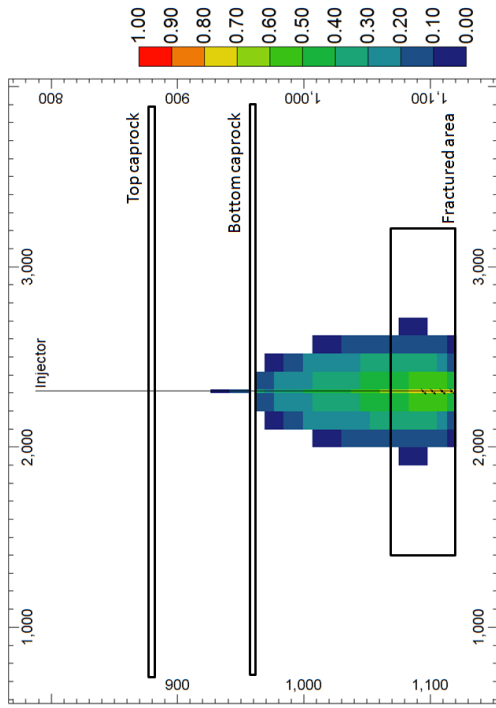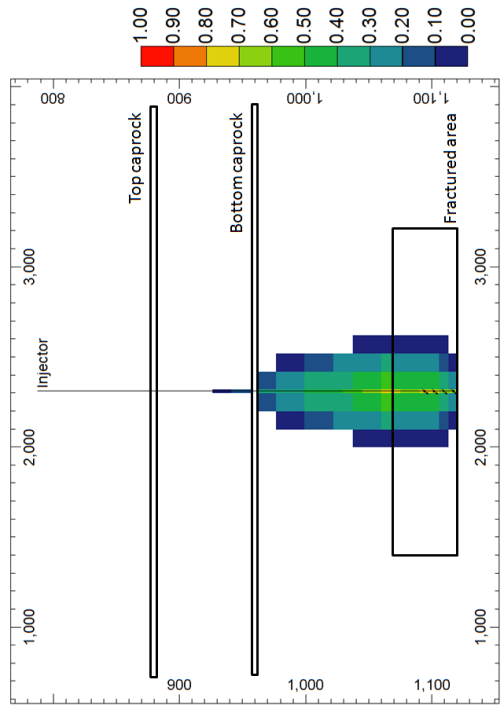
Figure 5.12: Free-phase CO_2 saturation 1826 days after commencement of injection for the four study cases. Saturation is expressed as fraction according to the color bar. Distances are in metres.
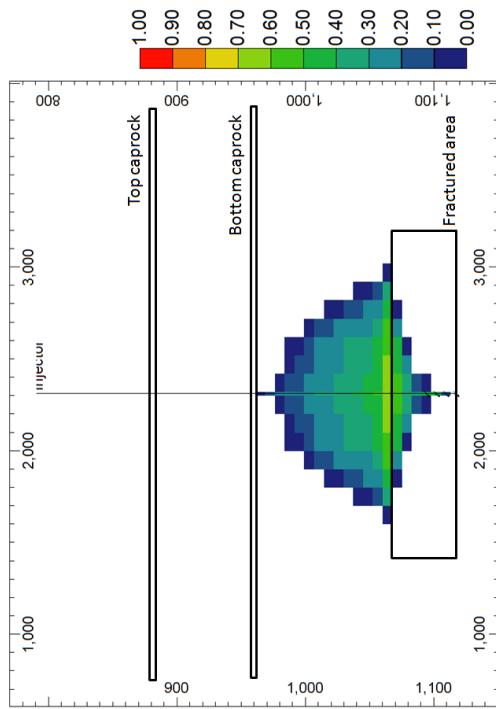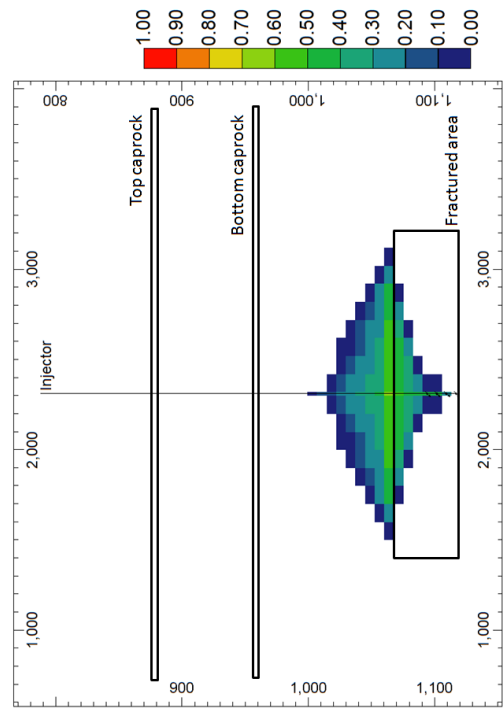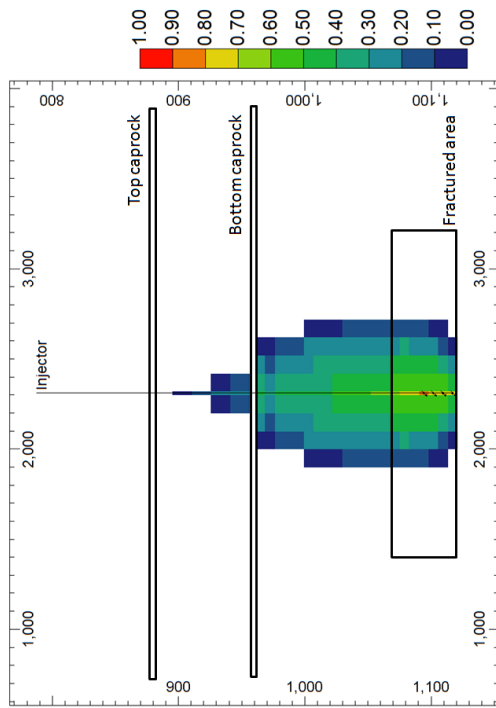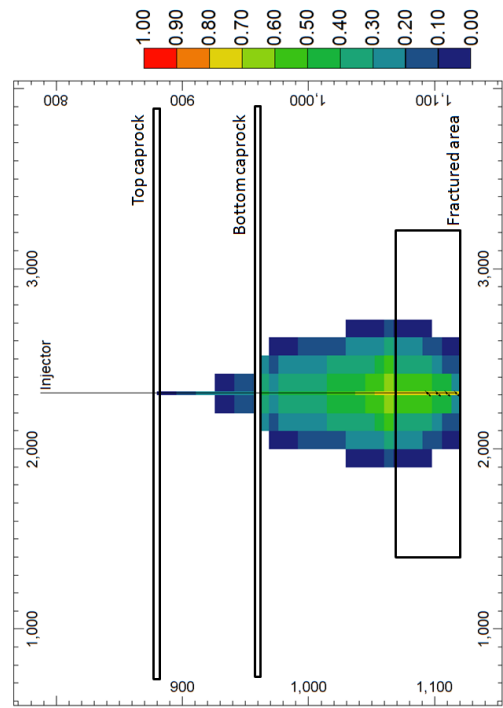
Figure 5.13: Free-phase CO$_2$ saturation at the end of injection (2891 days) for the four study cases. Saturation is expressed as fraction according to the color bar. Distances are in metres.

143

5.5.5 Discussion of results

The production of the previous four scenarios aims to quantify the differences in approaching the model of CO_2 in a fractured zone with a variety of simplifications. One would intuitively expect that fractures around the injection point will enhance injectivity and decrease pressure buildup and consequently caprock failure. This is confirmed by the numerical model. However, other considerations are important to notice:

It is common practice in reservoir modelling to estimate the pressure buildup with non-coupled models. That built-up pressure is then related to the maximum stress of rock before failure and a limit is set –usually 90% of that maximum stress– to estimate the storage capacity. However, results comparing *Case 2* and *Case 4* show that the pressure buildup at the point of caprock failure can be underestimated by more than 10%. This leads to an overestimation of the storage capacity of more than 31% in this particular scenario if the procedure of the 90% of the maximum stress as limit is followed. More importantly, the slope of the pressure buildup is also different in coupled and non-coupled models, so the difference between estimation with the two methods would not be constant but dependent on the rock maximum stress. In addition, the CO_2 plume when the model is not hydromechanically coupled tends to travel further horizontally and less vertically compared with the coupled scenario. The reason behind is that non-coupled models do not account as accurately for stress dependent porosity and permeability changes and changes in effective stress.

When hydromechanically coupled models are compared, the results show that the presence of fractures around the injection point can increase the amount of injected CO_2 by orders of magnitude (e.g. from 60 days of injection up to 1700 days). However, it greatly depends on the history of the permeability of the fractures around the injection point. Two effects here are noteworthy: one is the significant differ-

ence in storage capacity between *Case 2* –with a high constant permeability fracture permeability around the well perforations– and *Case 3* –with a stress dependent permeability–; another is the CO_2 plume evolution in both cases. Horizontal permeabilities four times higher than vertical ones are not enough for a significant horizontal spread of the plume on top of the fractured area, which however occurs when horizontal permeabilities in the fractures are 40 times higher than vertical permeabilities in the non-fractured rock above.

At this point it is worth noting the main limitations of the model. A significant simplification in the hydrological and geomechanical parameters has been undertaken for the following reasons: first, the lack of experimental data on final permeability and porosity distribution around the gasified area at the time of this research. Secondly, as it can be inferred from the analogues used in estimating the aforementioned values, these can change quite drastically through a limited distance. In order to keep a reduced number of cells in the model and avoid numerical convergence problems caused by extreme differences in values in neighbouring cells (e.g. several orders of magnitude in permeability), average values at a bigger scale zonation have been adopted. Finally, probably the more critical simplification is that the field stress redistribution after cavity collapse has not been taken into account in this model. Future work should therefore include refined sensitivity analysis for UCG–CCS parameters as discussed above and in Chapter 3.

Despite the current limitations, the comparison between the four scenarios shows that the wide range of results within the studied simplifications requires to incorporate hydromechanical coupling and stress dependent fracture permeability in order to accurately estimate the storage capacity.

5.6 Sensitivity analysis

Current model validation and calibration with laboratory or field data is not possible due to the absence of such experiments. It has also been proved the significance of using a model which includes hydro-mechanical coupling and fracture permeability stress dependency. Thus, a sensitivity analysis on *Case 3* has been carried out to assess the influence of several parameters, such as the injection rate, the fracture opening stress, the hydraulic fracture permeability, and the temperature of the reservoir (see Table 5.5 for a complete list). The aim of the sensitivity analysis is to gain understanding on the range of uncertainty due to some common and controlled parameters and to some others of which their accurate determination presents a high difficulty. The injection rate or the reservoir temperature are among the former ones, while Barton–Bandis model parameters are among the latter ones.

Table 5.5: List of parameters analyzed during the sensitivity study of *Case 3* scenario. The parameters are grouped under *Design*, *Fracture* and *Formation* if they can be engineeringly designed, are specific of the fractures or correspond to the porous formation. (*Dependent on CO_2–brine miscibility)

Design parameters	Fracture parameters	Formation parameters
Injection rate	Fracture opening stress	Rock compressibility
Well horizontal leg	Maximum fracture permeability	Young's modulus
Cavity cooling	Fracture spacing	Poisson's coefficient
	Fracture porosity	Matrix porosity
	Initial fracture permeability	Permeability
		k_h/k_v ratio
		Water vaporization (*)

The following sections present the results of the sensitivity analysis of the design parameters, for being these of major importance since they can be acted upon, the sensitivity analysis of the fracture Barton–Bandis model, since the application of

this model is the main objective of this study and the effect of water vaporization, in order to evaluate a potential simplification in the numerical simulation. The rest of the parameters are not individually presented in the following sections but they are included in the discussion of results.

5.6.1 Design parameters

Effect of injection rate

The parameter which is more easily known and controlled in the engineering design when planning a CO_2 sequestration project is the injection rate. Figure 5.14 illustrates the effect of the injection rate in the well bottom-hole pressure. As it would be expected, the higher the injection rate is, the faster the pressure builds up and the sooner the caprock fracture would open. For low injection rates (e.g. 50,000 m^3/day or ca. 34,000 t/y in this study), the fracture does not open throughout the injection phase (Figure 5.15).
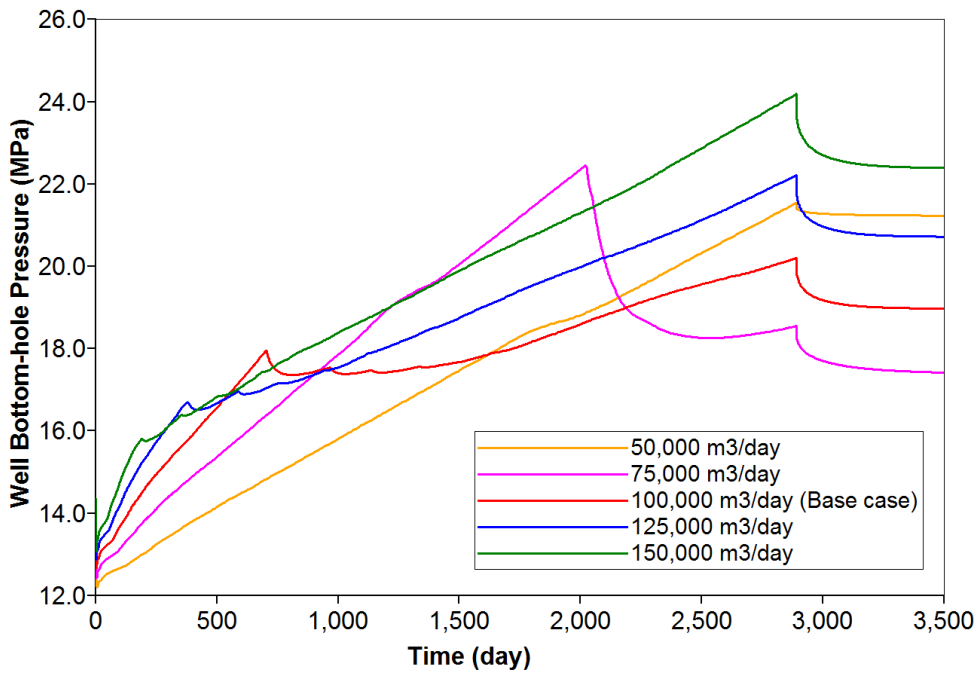
Figure 5.14: Effect of injection rate in the well bottom-hole pressure
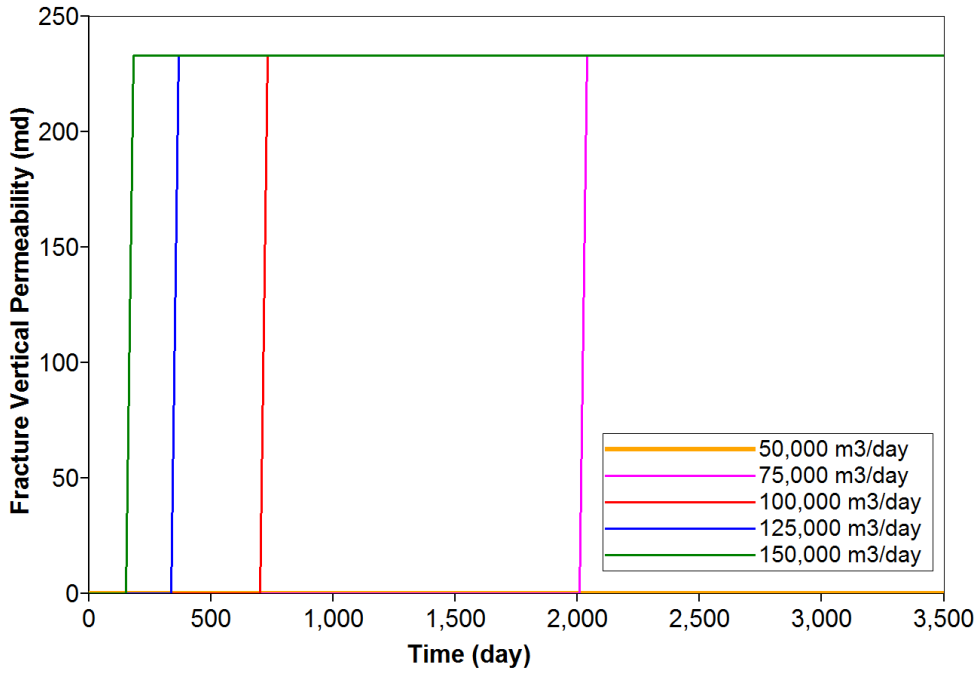
Figure 5.15: Effect of injection rate in the time of fracture opening

Similarly, displacement of the top of the reservoir is a function of the injection rate (Fig. 5.16), increasing as injection rate increases.

Horizontal wells

In a UCG–CCS scenario, the initial horizontal well drilled for connecting the injection and production boreholes will disappear as the cavity collapses. However, it can be the case that a hydraulically connected horizontal path exists when CO_2 injection takes place. This path could act to a certain extent as an open horizontal well during injection, so a case for comparison of the previous results obtained with a vertical well and horizontal well will be developed. Two horizontal wells will be studied: one approximately 400 m long, and another one extending up to 1000 m. In the case of the shorter horizontal well, the normal fracture effective stress in the caprock remains slightly higher than in the case of a vertical well, inducing a delay in caprock fracture opening of 62 days. As the length of the horizontal well increases, the pressure is

148
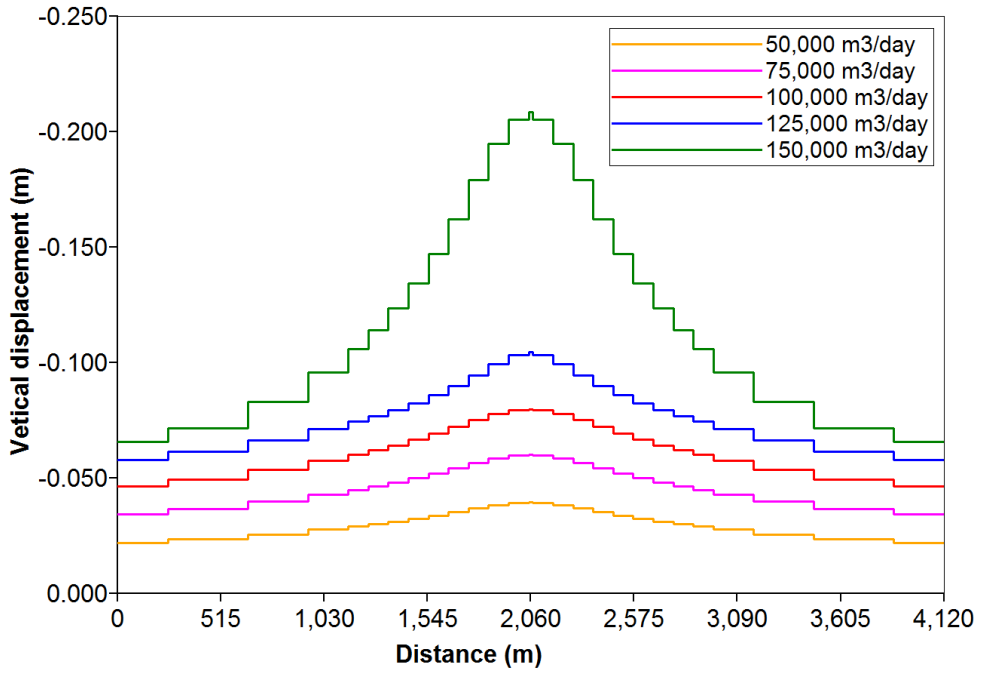
(a) After 366 days of injection
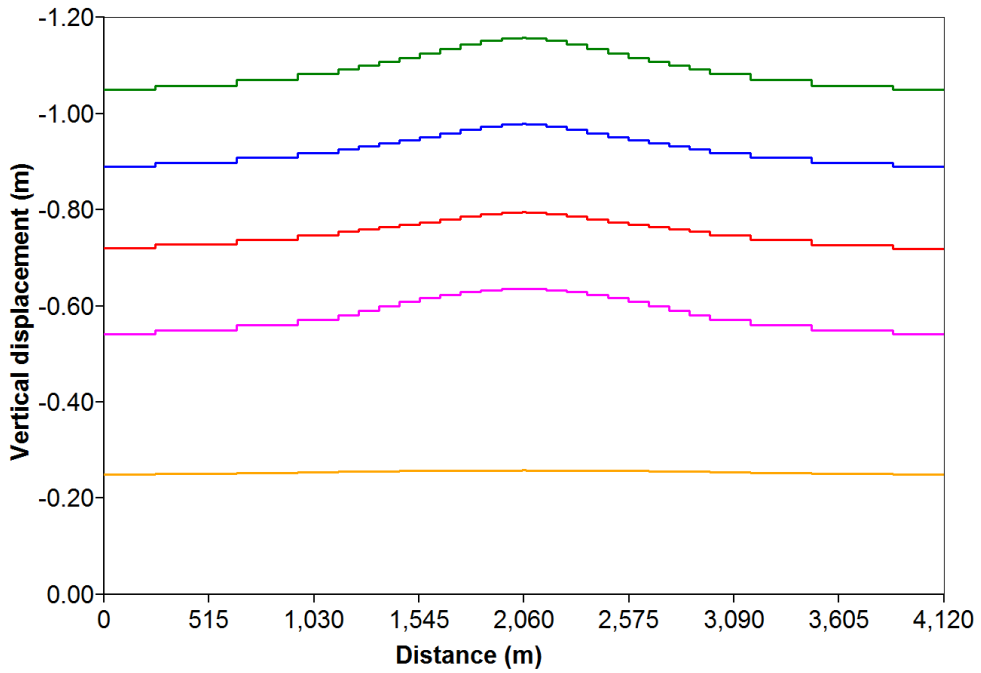
(b) After 2891 days of injection

Figure 5.16: Effect of injection rate in vertical displacement

149

dispersed more effectively, resulting in a delay in the caprock fracture opening of over 974 days compared to the vertical well set up (see Fig. 5.17).
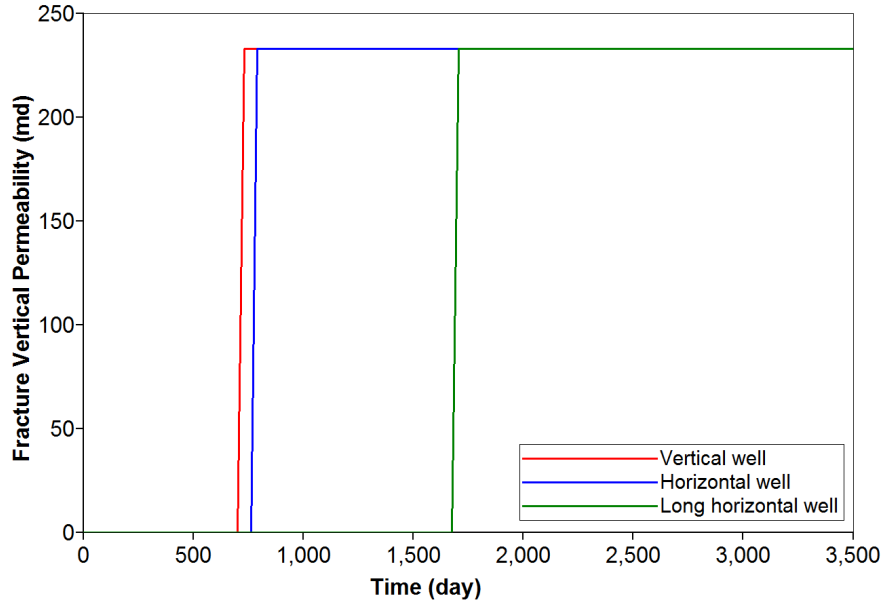
Figure 5.17: Comparison of the bottom caprock fracture permeability in the vertical direction for a vertical, horizontal and long horizontal well

It is also worth noting how a horizontal well affects CO_2 dissolution. Figure 5.18 shows that longer horizontal wells allow greater CO_2 dissolution, leading to increased storage security. The relationship between dissolved CO_2 and supercritical (free) CO_2 and the total mass of CO_2 injected can be observed in Figure 5.19. Dissolved CO_2 in the case of a long horizontal well reaches a 25.78% of the total injected.
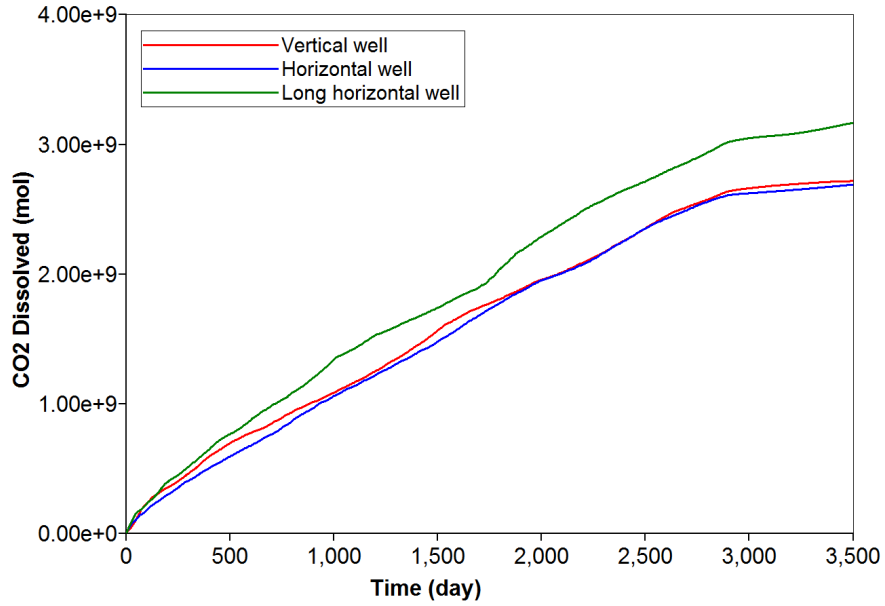
Figure 5.18: Comparison of the CO_2 dissolution for a vertical, horizontal and long horizontal well
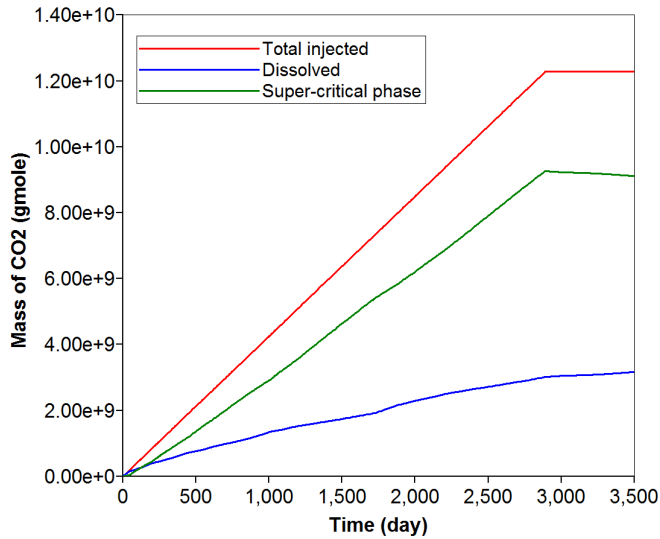
Figure 5.19: Cumulative mass of injected CO_2 and the amount of CO_2 present in its supercritical phase and dissolved in brine in the long horizontal well.

Figure 5.20 shows the spatial distribution of CO_2 in free gas or supercritical phase in the case of a vertical well, horizontal or long horizontal well.

151
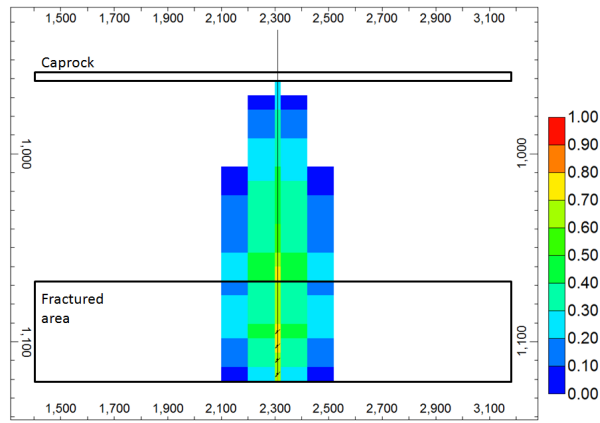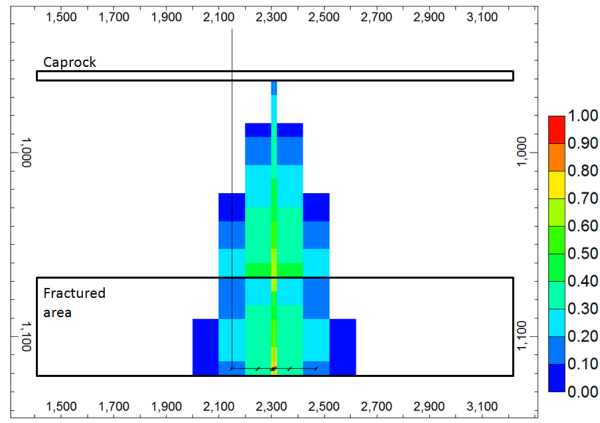
(a) Vertical well

(b) Horizontal well
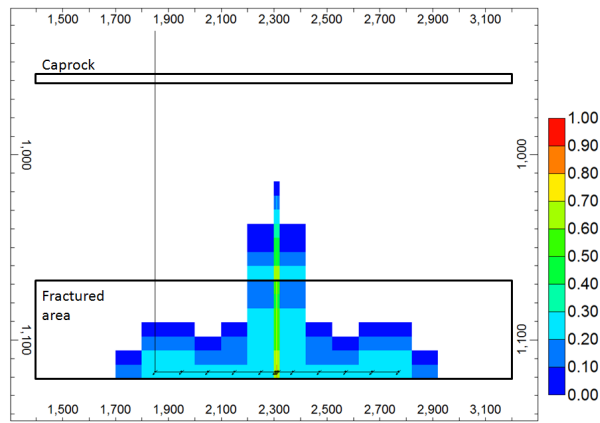
(c) Long horizontal well

Figure 5.20: Comparison of the free-phase CO_2 saturation distribution after 1461 days of injection for a vertical, horizontal and long horizontal well

Effect of reservoir and fluid temperature

It is known that injection of a cold fluid in a hot reservoir produces a thermal stress which can result in rock fracturing. This phenomenon has been studied in CO_2 injection and caprock failure by Gor et al. (2013) and Tran et al. (2009) applying non-isothermal coupled hydromechanical models. Both of them conclude that the cooler the fluid is in relation to the reservoir, the larger the increase in tensional stress is and therefore, the sooner the rock will fail. Here we test this effect in the case of the already heavily fractured zone. Gor et al. (2013) simulated injection of CO_2 at 40 ºC, 50 ºC, 60 ºC and 90ºC in a reservoir at 90ºC. They based their temperature assumption on measured data from Japan, where CO_2 temperature at the wellhead was 32 ºC and rose to 48 ºC at the bottom-hole.

A non-isothermal model has been applied to *Case 3* (a fractured zone around the injection point with fracture permeability stress dependence). Two initial thermal regimes are set :

- One represents the natural geothermal gradient. It has been assumed that temperature in the cavity and surroundings has reached its equilibrium after gasification. The temperature at 1000 m depth is set at 35 ºC. This corresponds to a geothermal gradient of 30 ºC/km and a surface temperature of 5 ºC, which is an average of the sea floor in the North Sea.

- The other one represents an area around the cavity which has not cooled down and remains at a temperature above the geothermal gradient. An arbitrary maximum temperature of 149 ºC (or 300 ºF) in this zone has been assumed.

The initial temperature profile is shown in (Figure 5.21).
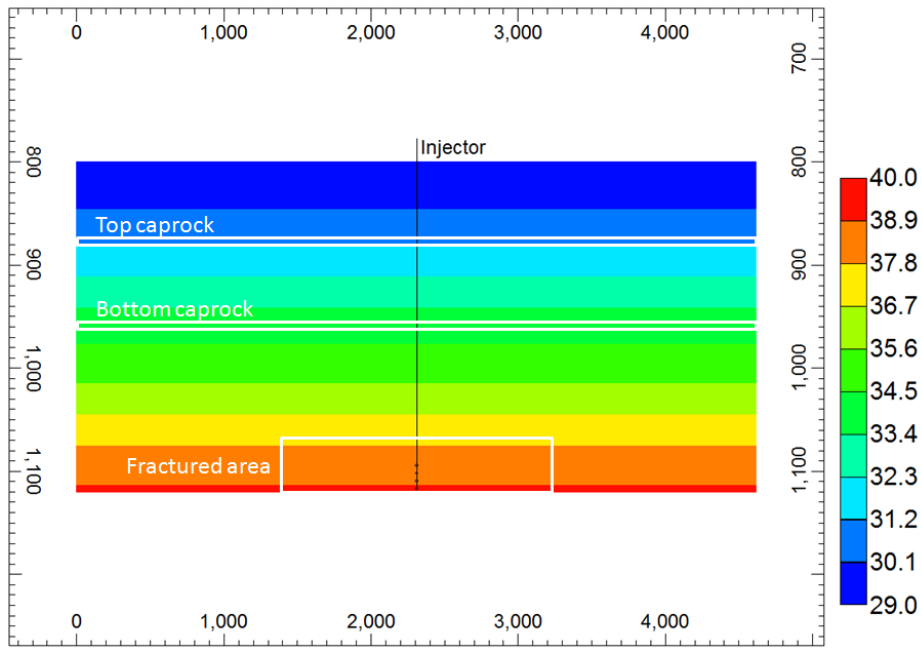
(a) With a geothermal gradient and maximum T=39 ^{o}C
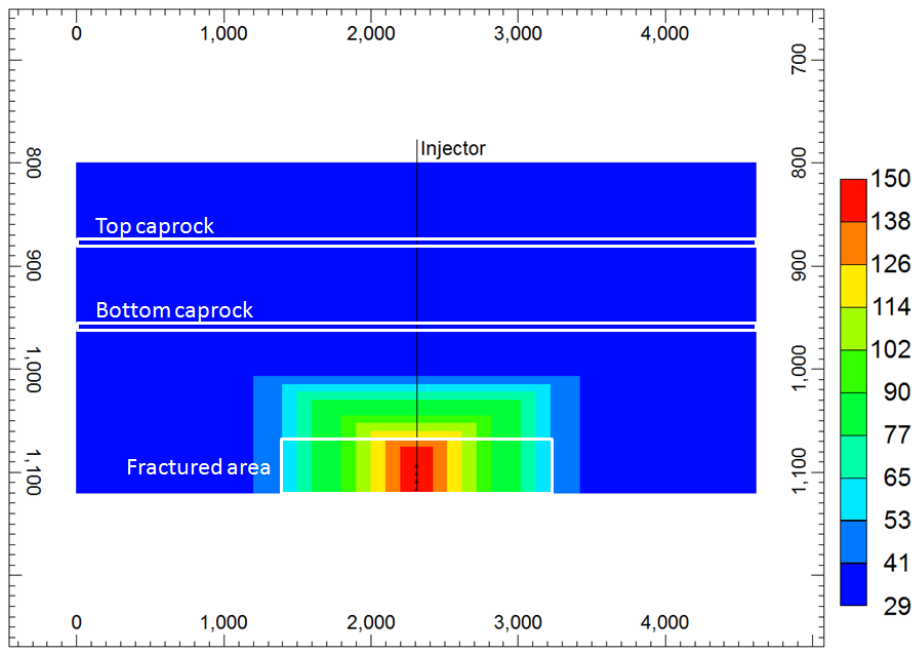
(b) With a maximum T=148.9 ^{o}C

Figure 5.21: Initial temperature spatial distribution in the non-isothermal models

The injected fluid temperature at bottom-hole is 38 ^{o}C in both cases. Figure 5.22 shows the difference in the bottom caprock opening time for the isothermal model and the two non-isothermal models. This outcome supports the presumption that cooling the gasification chamber before CO_2 injection starts is recommended for improved caprock integrity safety. The heat originated in surrounding gasification chambers in operation will also have to be considered in the assessment of the operation.
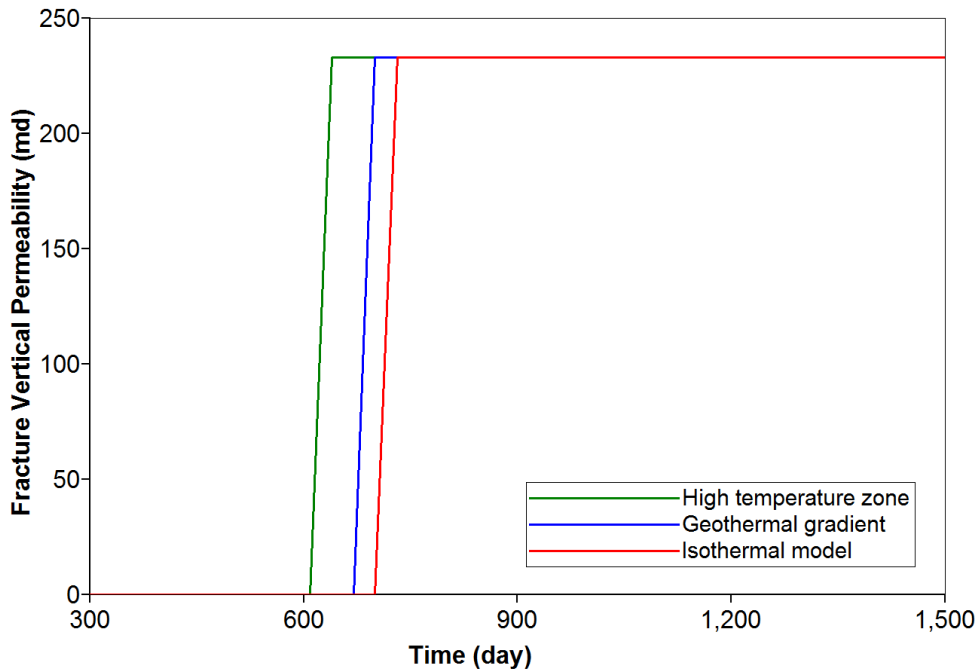
Figure 5.22: Time at which caprock bottom fracture opens in the case of the different thermal regimes assumed.

5.6.2 Fracture Barton–Bandis parameters

Fracture opening stress

One of the main uncertainties in the UCG–CCS scenario for CO_2 injection is the characterization of the fractures around the well. Some core analysis can be obtained during the drilling of injector and producer boreholes, with subsequent rock mechanics laboratory testing. This can shed some light on the behaviour of the

rock, but it provides no information on the actual fracture network parameters after gasification.

Figures 5.23 and 5.24 show respectively the effect of variation of the fracture opening stress in the well bottom- hole pressure and the fracture permeability at the bottom caprock. Fracture opening stress does not have an impact on initial injection pressure, but it determines the time at which the fractures around the well and in the caprock will open. Fractures with a higher fracture opening threshold will react earlier, since the pressure increment needed to achieve that trigger point is lower.
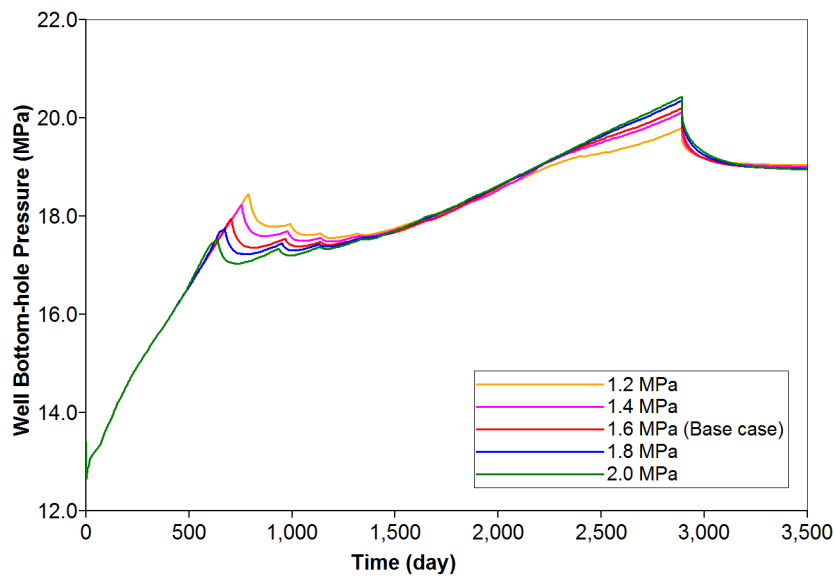
Figure 5.23: Fracture opening stress sensitivity analysis for the well bottom-hole pressure.
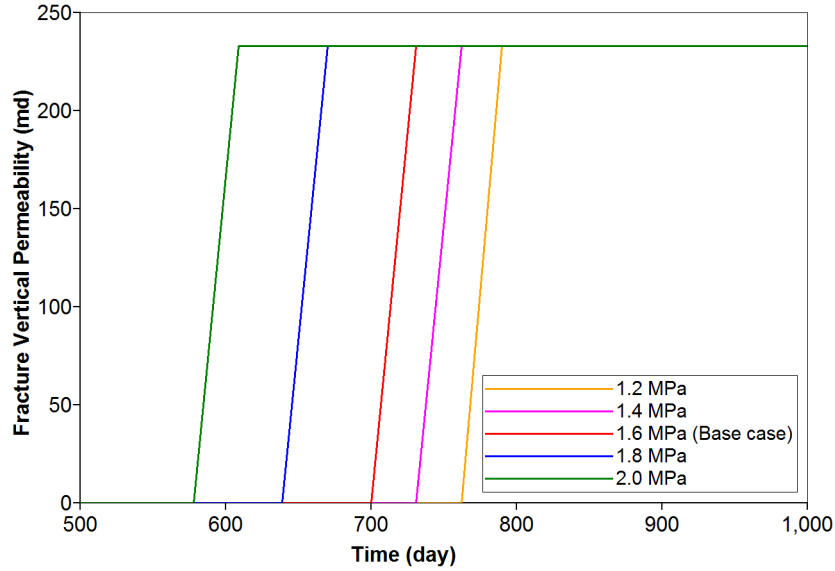
Figure 5.24: Fracture opening stress sensitivity analysis for the time when the caprock fracture opens

Maximum fracture permeability

Changes in the maximum fracture permeability once the fracture is open are not reflected in the initial injection pressure buildup (Fig. 5.25) and the caprock fracture opening time (Fig. 5.26). This could be expected since the fracture opening stress is independent from this parameter. However, a counterintuitive result is the observation that maximum fracture permeabilities after opening still do not significantly impact the evolution of the well bottom-hole pressure. The explanation is that fractures open firstly above the well perforations and in the proximity of the well in a reduced number. Then the caprock fails and pressure is relieved and fractures close again.

5.6.3 Effect of vaporization

Miscibility of CO_2 with water leads to partial dissolution of CO_2 in water and partial vaporization of water in the CO_2 gas phase (Spycher et al., 2003; Spycher and

157
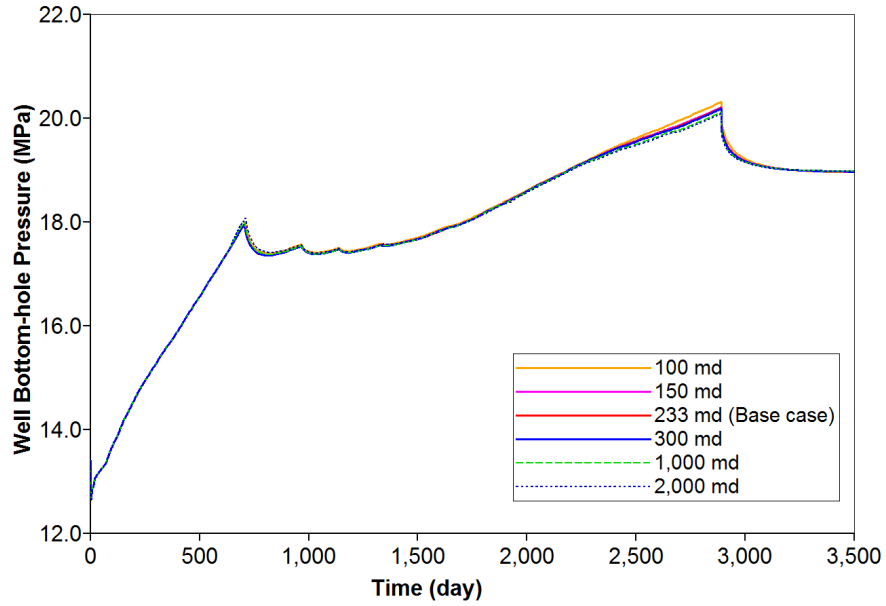
Figure 5.25: Maximum fracture permeability sensitivity analysis for the well bottom-hole pressure
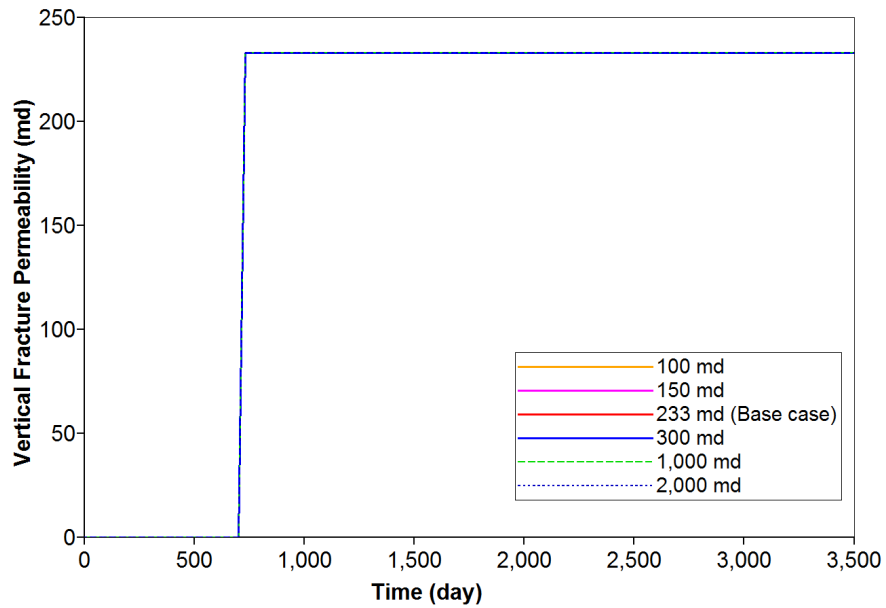
Figure 5.26: Maximum fracture permeability sensitivity analysis for the well bottom-hole pressure the well in the time when the fracture opens

Pruess, 2005). As seen in previous sections, GEM models the CO_2 dissolution in water with the Henry Law. In order to incorporate water vaporization, a third component (water) has to be added to the fluid in the Peng-Robinson equation of state model. Though salinity is not considered here, and therefore, no salt precipitation is accounted for during vaporization, the development of a dry-out zone results in a lower pressure increment compared to the case of immiscibility (Mathias et al., 2011a,b). The relevance of the vaporization effect with regards to pressure evolution and caprock failure in this scenario is not as significant as seen in Mathias et al. (2011b). However, it is interesting to observe that the absence of water vaporization in the model leads to overestimate the amount of dissolved CO_2 (see figures 5.27, 5.28 and 5.29).
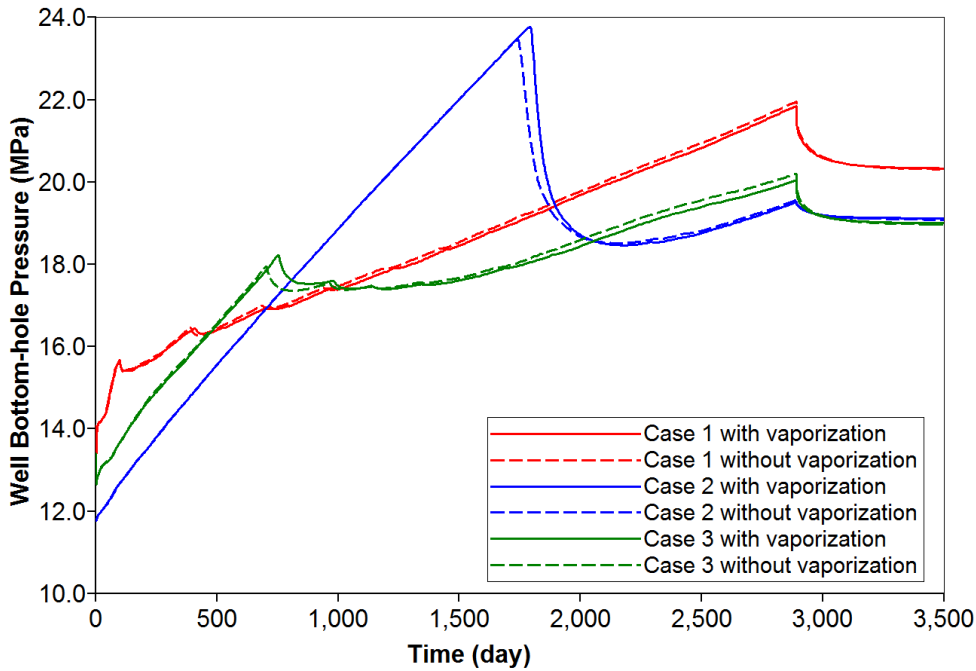
Figure 5.27: Effect of vaporization in the well bottom-hole pressure
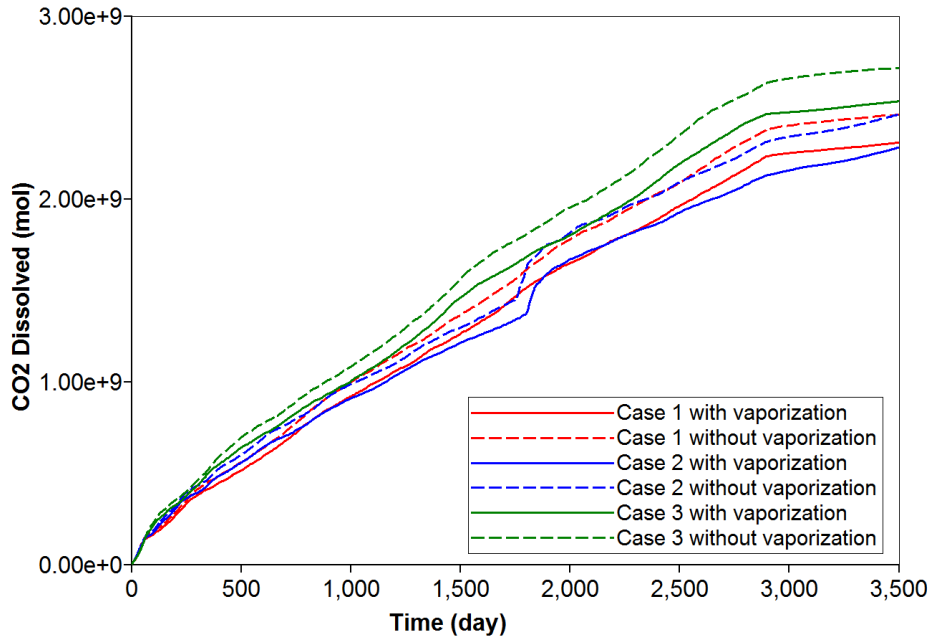
Figure 5.28: Effect of vaporization in the amount of dissolved CO_2
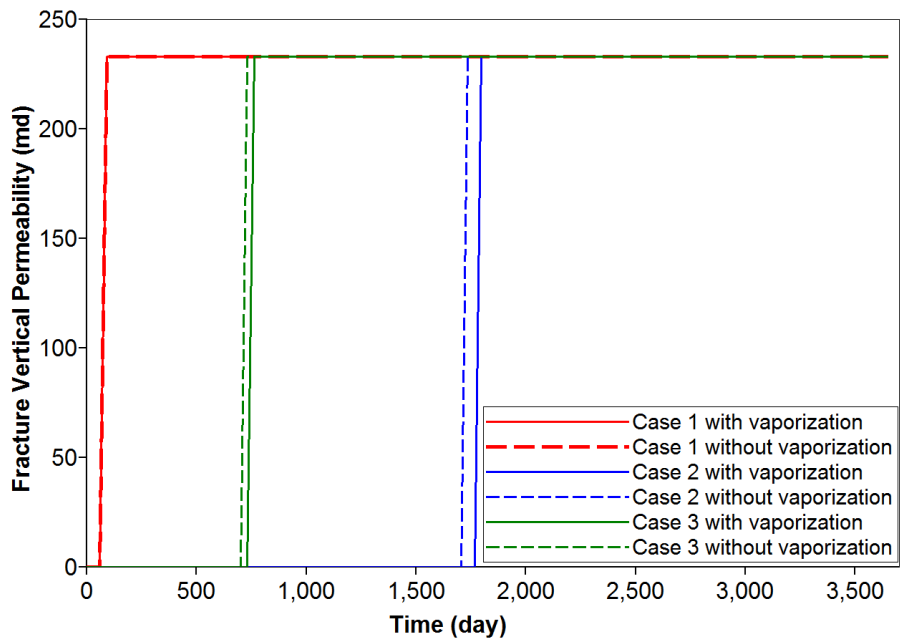
Figure 5.29: Effect of vaporization in the time when the fracture opens for *Case 1*, *Case 2* and *Case 3*.

160

5.6.4 Discussion of results

Injection rate is the easiest parameter to control in a CO_2 storage operation. It is obvious than higher injection rates require higher injection pressures and therefore pose a higher threat to the seal integrity. In the sensitivity analysis of the injection rate, it can be observed that the relationship between the injection rate and the moment of the caprock failure is not directly proportional. Further investigation showed that the injection rate and the maximum vertical displacement at the top of the model can be linked by means of a logarithmic function (Fig. 5.30). Similarly, an exponential function can be adjusted to the injection rate and time (Fig. 5.31) or injected CO_2 mass (Fig. 5.32). The implication is that, from a certain injection rate, a small decrease in that rate may yield a significant benefit in the storage capacity. However, it is important to note that too small rates may be uneconomic or technically not feasible if the produced CO_2 cannot be accommodated in a timely manner.
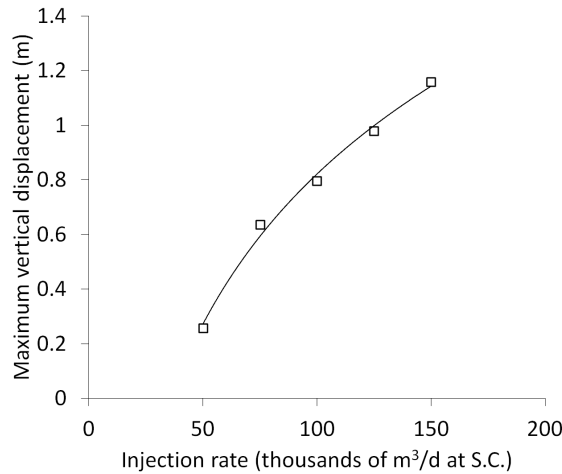
Figure 5.30: Injection rate and maximum displacement
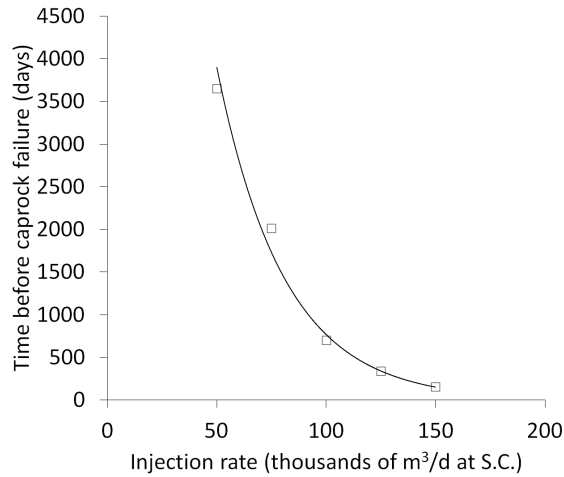
Figure 5.31: Injection rate and time before caprock failure
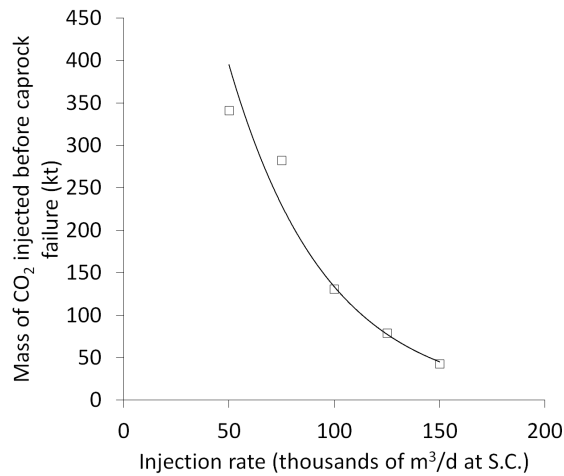
Figure 5.32: Injection rate and injected CO_2 mass before caprock failure

The results of the sensitivity analysis are presented in Figure 5.33. The reference criterion to evaluate the results is the mass of CO_2 injected before failure in the bottom caprock occurs, understanding this as a measurement of the storage capacity of the scenario.

Injected CO$_2$ mass until bottom caprock failure (ktonnes)

Parameter	Value (left)	Value (right)
Injection rate (100000 m3/d)	150000 m³/d	50000 m³/d
Fracture opening stress (1.6 MPa)	2 MPa	1.2 MPa
Maximum fracture permeability (233 md)	100 md	2000 md
Well horizontal length (Vertical well)		~1 km
Water vaporization (No)		Yes
Reservoir temperature (Isothermal at 38 °C)	149 °C (**)	39 °C (*)
Fracture spacing (10 m)	0.5 m	30 m
Young modulus (5 GPa) (***)		30 GPa
Poisson's coefficient (0.25)	0.35	
Rock compressibility (2.78E-061/kPa)		5.76E-06 1/kPa
kv/kh ratio (0.25)	0.1	
Matrix porosity (13%)	8 %	18 %
Fracture porosity (13%)	4 %	25 %
Matrix permeability (kh=15 md)	1 md	150 md
Initial fracture permeability (15 md)		2000 md

Figure 5.33: Tornado plot showing the deviation from the base case (*Case 3*) with changes in model parameters. Close to the color bars, the value of the modified parameter is shown, while the original parameter in the base case model appears in brackets at the right of the parameter name. (*) Geothermal gradient with T_{max}= 39 ^{o}C (**) High temperature zone with T_{max}= 149 ^{o}C (***) The base case intermediate overburden Young's modulus is 0.9 GPa; the variation has a constant Young's modulus of 30 GPa throughout the model.

There are four parameters which yield the highest difference in storage capacity before caprock failure. Two of them are controllable (injection rate and, to a lesser extent, horizontal length) and the other two are nature dependent (matrix perme-

ability and initial fracture permeability). All of them achieve a total injection over 0.3 Mtonnes in this scenario. Continuing with Nakaten et al. (2014) assumptions on coal gasification and CO_2 captured rates taken in Section 5.4, for a coal layer of 3.8 m thickness and a 40% recovery in the fractured area in the model, approximately 1 Mtonnes of CO_2 would need to be sequestered. This means that none of the foreseen scenarios could achieve a total reinjection of the produced CO_2. However, in the best case scenario, a reinjection of ca. 40% of the produced CO_2 would be possible. The drawback is that the million tonnes of CO_2 would be produced, according to Nakaten et al. (2014) in approximately 140 days, which means an injection rate of 2.7 MMt/y. The best case is only able to inject at 0.07 MMt/y.

The second group of parameters in order of importance comprises the Young's modulus, the Poisson's coefficient and the rock compressibility together with the fracture porosity, reiterating the necessity of adequate modelling and parameterization of rock mechanics and fracture development during cavity collapse.

The review of the performance of horizontal wells reveals that, as with the injection rate, the maximum storage capacity is not a linear function of the length of the well. A 400 m well does not provide a significant advantage over a vertical well in the tested scenario, and it is necessary to increase its length to 1 km to observe an improvement.

The isothermal models appears to be more conservative than non-isothermal ones. However, in the grand scheme, initial reservoir temperature, though it plays a role, is less significant than other contributors.

With regards to Barton–Bandis parameters, higher fracture opening stresses around the well affect negatively the caprock failure. This observation, together with the importance of a high initial fracture permeability, remarks the importance of having a high permeability fracture network prior to injection. The degree of re-compaction, role of surrounding coals and presence of tars and ashes in the fractures

164

will be fundamental in the potential for CO_2 storage in a UCG–CCS void.

Maximum fracture permeability after fracture opening does not have any effect in this case. However, this result has to be taken with caution, since it is dependent on the time at which fractures are open in relation to the caprock failure, which will be different in other scenarios.

5.7 Summary and conclusions

This Chapter aims to compare different approaches to the modelling of CO_2 injection in a fractured zone. For this purpose, the hydro-mechanically coupled model from Computer Modeling Group Ltd. (CMG), GEM, has been used. Three scenarios derived from the base case presented by Tran et al. (2009) have been produced, each of them accounting for *i)* no hydromechanical coupling, *ii)* hydromechanical coupling with no fracture permeability variation or *iii)* hydromechanical coupling with stress-dependent fracture permeability.

Observation of well bottom-hole pressures show that including a fractured area around the well decreases the initial value and slope of the injection pressure curve, facilitating injectivity and leading to a longer injection time before caprock failure. Storage capacity in the studied case can be increased by 10 to 35 fold from the non-fractured scenario to a fractured scenario. In addition, the approach taken to account for the fractured zone has relevant implications: if fractures are modelled with a constant permeability, the estimated maximum storage capacity before caprock failure can be over two times the case of stress-dependent fracture permeability model; if no hydro-mechanical coupling is modelled, and maximum capacity is estimated as the one resulting of pressure reaching a theoretical or calculated maximum rock stress, the storage capacity could be overestimated by a factor of more than 3. As a consequence, this study shows that the deviations in using one method or another are

not of a second order of magnitude, and it will be necessary to account for hydro-mechanical coupling and fracture permeability stress dependency.

The fracture network permeability will also have a significant impact on the CO_2 plume evolution. It was found that horizontal fracture permeabilities 4 times higher than matrix vertical permeability did not significantly increased the lateral spread of the CO_2 plume on top of the fractured area. However, when this ratio was increased to 40 (in *Case 2* with a constant fracture permeability), the CO_2 vertical migration is delayed in favour of lateral migration on top of the fractured zone, with the obvious incidence in storage security.

The sensitivity analysis on the fracture permeability stress dependent model showed that there are two main groups of parameters impacting the maximum storage capacity before caprock failure. The main group –which can triple the maximum CO_2 storage capacity compared to the base case– comprises the injection rate, horizontal length of the well, formation permeability and initial fracture permeability around the injection zone. A second group is formed by the rock mechanics properties (Young's modulus, Poisson's coefficient and rock compressibility) and the fracture porosity. This second group shows improvements of twice the maximum capacity compared to the base case. Finally, the rest of parameters studied have a low impact in final capacity in this study.

It has also been noticed that the parameters tested in the sensitivity analysis do not have a direct proportional relationship to the maximum mass of CO_2 injected before caprock failure. In particular, the injection rate against mass of CO_2 injected before caprock failure can be adjusted to an exponential curve. The implication is that small variations in injection rate from a certain threshold value can have significant impact on the final storage capacity.

Despite the sensitivity analysis promising potential increase of the storage capacity with the variation of some of the model parameters, and particularly the injection

rate, the results raise a concern on the feasibility of injection at commercial rates in such scenario. Assuming a coal gasification of 3100 t/d and CO_2 production of 7405 t/d as suggested by Nakaten et al. (2014) for an ICGG 308 MW plant, it was found that for a coal seam thickness of 3.8 m, the amount of CO_2 to store in the model of ca. 1 Mtonnes woud not be achievable in terms of total amount nor in injection rates. Total injected amount before caprock failure was found to be around a 40% of the total produced for a best case scenario, but injection rate in this case was 38 times slower than that expected at commercial rates.

However, it is important to remind at this stage the limitations of the model. Albeit this model accounts for hydro-mechanical coupling and fracture permeability stress dependency, which have been proved to have a non-negligible effect, there are still significant simplifications: the first and most important is that stress field redistribution after caprock failure has not been included. *In-situ* stress is decisive in the behaviour of the rock massif and tension and compression zones around and on top of the collapsed cavity will be formed, which ultimately will affect the stress transmitted to the caprock. Secondly, a higher spatial resolution in the parameterization on rock and formation properties around the gasification cavity should be incorporated.

Suggested further work therefore includes addressing the incorporation of *in-situ* stresses after cavity collapse and subsequent sensitivity analysis on variations on the initial stress field prior to gasification and to CO_2 injection. High spatial resolution which allows increased accuracy in parameterization of the model with increased number of cells it is also recommended. Finally, a further step in the development of the model would account for fracture propagation.

Chapter 6

Numerical Evaluation of Analytical and Semi-analytical Solutions for Pressure Buildup due to CO_2 Injection at a Constant Rate

6.1 Introduction

For closed geological formations, CO_2 injected into a porous formation is accommodated by reduction in the volume of the formation fluid and enlargement of the pore space, through compression of the formation fluids and rock material, respectively. For open formations, injected CO_2 is additionally accommodated by the displacement of native formation fluids from the host formation of concern. A critical concern is how the resulting pressure buildup will affect the mechanical integrity of the host formation and caprock. In assessing the storage capacity of a given formation, one should therefore verify that the estimated pressure buildup does not exceed the failure limit of the overlying cap-rock (Mathias et al., 2009c).

The calculation of pressure buildup requires simulating the injection of supercritical CO_2 into the porous formation. This can be achieved using a numerical multiphase reservoir simulator, as shown in the previous Chapters. However, such models can demand significant time for data input preparation and results analysis and, in

168

the case of large realistic geological models, they are computationally intensive to run. Therefore, there has been a parallel effort to develop simple semi-analytical methods which can allow a quick initial assessment.

Previously, Mathias et al. (2009c) derived a semi-analytical solution for predicting pressure buildup when the formation can be assumed to be of infinite radial extent. In Mathias et al. (2011a), the work of Mathias et al. (2009c) is extended to account for finite outer boundaries, by invoking a quasi-static condition. It also shows how to modify the solution presented in Mathias et al. (2009c), to account for residual brine saturation and the associated reduction in the effective relative permeability of the CO_2. The resulting equations remain simple to evaluate in spreadsheet software, and can be easily implemented in currently available storage capacity estimation frameworks (e.g. Mathias et al., 2009c)

6.2 Pressure Buildup During CO_2 Injection into a Closed Formation

The derivation of the approximate solution given by Eqs. (20) and (42) in Mathias et al. (2011a) involves the application of a number of simplifying assumptions, among which the most important are:

1. Vertical pressure equilibrium;

2. Negligible capillary pressure;

3. Constant fluid properties;

4. Homogenous, isotropic and cylindrical aquifer formation;

5. Constant mass injection rate through a centrally located fully completed vertical well;

6. Immiscible displacement;

To assess the impact of these assumptions, the approximate solution is compared to simulations conducted with the reservoir simulator TOUGH2 (Pruess, 1999) using the CO_2 and brine equations of state stored in the ECO2N module (Pruess, 2005). The scenarios simulated are loosely based on those previously described by Zhou et al. (2008).

The TOUGH2 simulations assume a fully penetrating well situated at the origin of a two-dimensional radially symmetric closed flow-field. The model assumes the Van Genuchten (1980) relationship between brine effective saturation, S_e [-], and capillary pressure, P_c [$ML^{-1}T^{-2}$]

$$ S_e = \frac{1 - S_g - S_{ar}}{1 - S_{gc} - S_{ar}} = \left(1 + \left| \frac{P_c}{P_{c0}} \right|^{n_v} \right)^{-m_v}, \quad n_v = \frac{1}{1 - m_v} \tag{6.1} $$

and that brine and CO_2 relative permeability are linearly related to S_e (effective brine saturation) and $(1-S_e)$, respectively, where — hereafter, referring to, for convenience, the aqueous and CO_2 rich phases, as the aqueous and gas phase, respectively —, S_g [-] is the gas phase volumetric saturation (i.e., the volumetric proportion of pore-space occupied by CO_2 rich phase), S_{ar} [-] is the residual aqueous phase saturation, S_{gc} [-] is the critical gas saturation, and P_{c0} [$ML^{-1}T^{-2}$] and m_v [-] are empirical parameters taken to be the same values as those used in the saline aquifer studies of Zhou et al. (2008).

The values of the model parameters used are given in Table 6.1. The effect of salt precipitation on permeability was ignored.

Vertically, the domain is divided into ten equally spaced layers, which corresponds to 5 m/layer in the case of a 50 m thickness aquifer and 20 m/layer in the case of a 200 m thickness aquifer. To invoke a mean initial pressure of 10 MPa, the initial pressure distribution is set to impose initially hydrostatic conditions with pressure

Table 6.1: Parameters used for the TOUGH2 simulations (Mathias et al., 2011a).

Parameter	Symbol	Value
Area,	A	1257 km^2
Injection rate,	M_0	100 kg/s
Well radius,	r_W	0.2 m
Radial extent,	r_E	20 km
Porosity,	ϕ	0.2
Rock compressibility,	c_r	4.5×10^{-10} Pa^{-1}
Initial pressure,	P_0	10 MPa
Temperature,	T	40 ^{o}C
Mass fraction of salt in brine,	ω_{sb}	0.15
Residual brine saturation,	S_{ar}	0.5
Critical gas saturation,	S_{gc}	0
End-point relative permeability for CO$_2$,	k_{rg0}	0.3
End-point relative permeability for brine,	k_{ra0}	1.0
Permeability reduction factor due to salt precipitation,	k_{rs}	1
van Genuchten parameter,	m_v	0.46
van Genuchten parameter,	P_{c0}	19600 Pa
Formation thickness,	H	50 or 200 m
Permeability,	k	10^{-13} or 10^{-12} m^2

along the central horizontal axis set at 10 MPa. Horizontally, the 20 km radial extent of the model is divided into four sub-domains with boundaries located at 0.2 m, 10 m, 500 m, 1000 m and 20,000 m from the origin. Each sub-domain is discretized in the radial direction by a set of logarithmically spaced nodes. The inner zone contains two-hundred nodes, the outer zone contains fifty nodes and the two intermediate zones contain one-hundred nodes each. The four zones are necessary to allow sufficiently high resolution around the well without requiring an excessive number of grid-points. Specifically, the four sub-domains allow the node spacing to grow from 5 mm at the well-face to 3280 m at the outer boundary using only 450 nodes in the radial direction. Such refinement was found to be necessary to ensure

adequate resolution for accurately evaluating well pressures. Figure 6.1 shows the model grid constructed in this way.
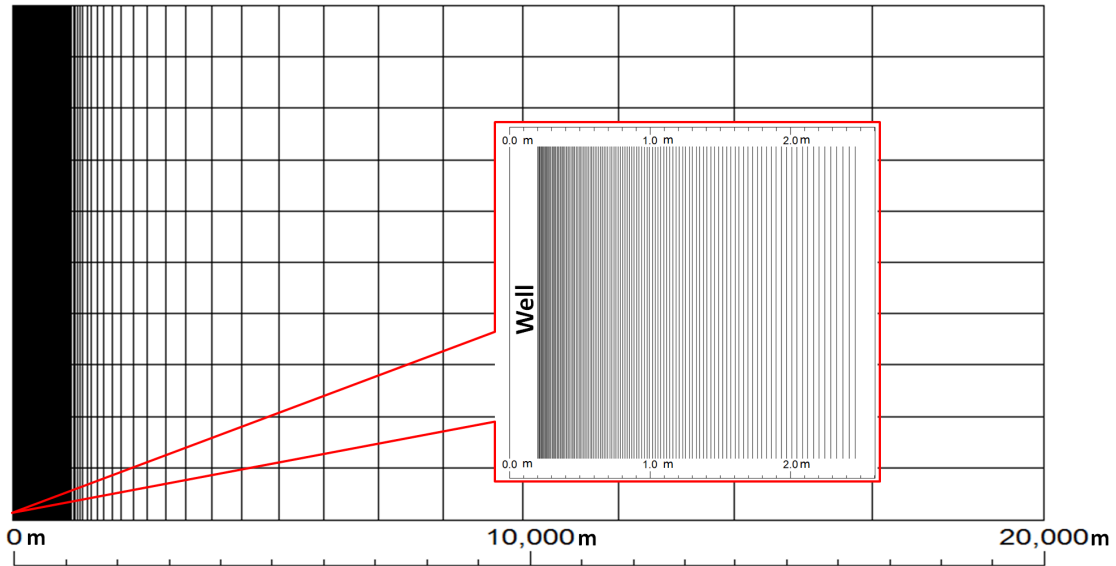
Figure 6.1: Mesh for the model. The well has a radius of 0.2 m and the first element at the well-face is 5 mm long. The layers are either 5 m or 20 m thick, depending on the case of a total aquifer thickness of 50 m or 200 m respectively.

To check for adequate grid resolution, five different grid patterns were employed, characterized by the number of points and the length of the first element (nearest the injection well). The details of the five grids are given in Table 6.2.

Table 6.2: Description of logarithmically spaced grids used.

Name	Number of points	First element length (m)
Grid 1	451	2.000
Grid 2	451	1.000
Grid 3	451	0.100
Grid 4	451	0.010
Grid 5	451	0.001

Figure 6.2a shows a plot of well pressures from TOUGH2 with $m = n = 3$ for the different grid resolutions as described by Table 6.2. The simulation using Grid

1 shows an early-time pressure spike followed by some minor pressure fluctuations and then another step decline in pressure shortly after one day, which corresponds to the establishment of a dry-out front. With increasing grid resolution around the well the magnitude of the pressure spike reduces. Specifically, for Grid 3 and finer, the well pressure becomes monotonically increasing with time. Interestingly, a visible difference between well pressures is seen between Grid 5 (first element length $= 0.001$ m) and Grid 4 (first element length $= 0.01$ m). Clearly, exceptional grid resolution is needed to properly resolve the early time pressure response in the well. Figure 6.2b is the same as Figure 6.2a but assuming linear permeability functions (i.e., $m = n = 1$). Here it can also be seen that low grid resolution around the injection well gives rise to a pressure spike at early times, albeit of lower magnitude. It is clear that the pressure spike presented in this study is nothing more than an artefact of numerical error caused by inadequate grid resolution. It was therefore found that a resolution of 5 mm was sufficient for this study.
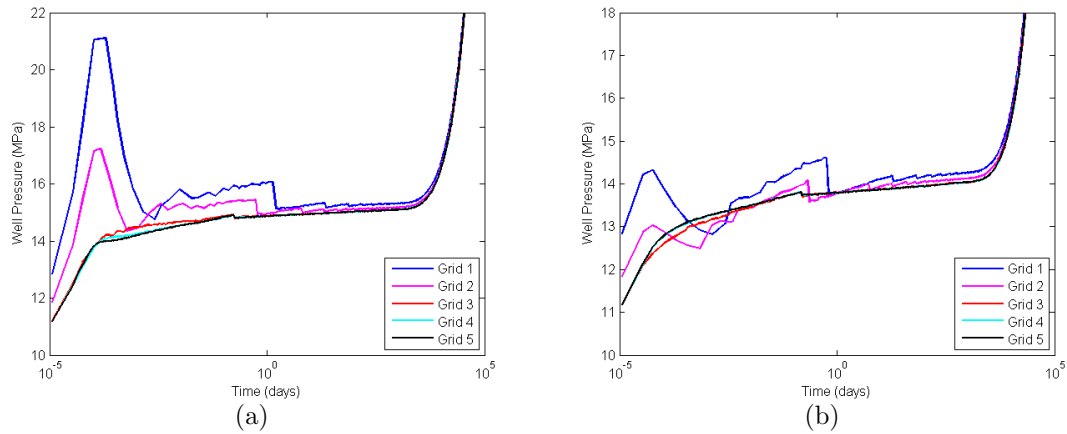
Figure 6.2: Comparison of simulated well pressures from TOUGH2 with $m = n = 3$ (a) and $m = n = 1$ (b) using the different levels of grid resolution, as described in Table 6.2. Grid 1 and Grid 5 have the lowest and highest resolution around the well, respectively.

173

Vertically averaged (by taking the mean in the vertical direction) well pressures from the TOUGH2 ECO2N two-dimensional miscible radial flow simulations are presented in Fig. 6.3 as green thick lines (2D Miscible). For the case presented in Fig. 6.3d ($k = 10^{-12}$ m^2 and $H = 200$ m), the TOUGH2 simulation was terminated after just less than a year due to model convergence difficulties. Nevertheless, all four scenarios exhibit a similar pressure response. Pressure increases monotonically with time. After 10^{-6} years, the pressure increase exhibits a constant linear-log slope until around 10^{-4} years beyond which pressure increases according to a new reduced linear-log slope. The latter effect is due to an increase in CO_2 relative permeability that develops once the residual brine is evaporated in the near-well region. Finally, after around 10 years, the pressure disturbance reaches the outer boundary of the reservoir and the well pressure increases asymptotically.

Plotted alongside, as black dashed lines (Approx. Sol. 1), are well pressures estimated using the approximate solution with fluid properties calculated for the initial pressure using equations previously presented by Mathias et al. (2009c,b). Approx. Sol. 1 shows the correct initial linear-log slope, but tends to overestimate the pressure buildup and does not predict the reduction in slope due to brine evaporation. Nevertheless, Approx. Sol. 1 predicts similar (to TOUGH2) pressure increases once the pressure wave reaches the outer boundary.

To explore the role of gravity in pressure evolution, the TOUGH2 simulations have been repeated but with just one layer for the entire formation thickness (as opposed to ten). Well pressures for these are plotted in Fig. 6.3 as thin black lines (1D Miscible). It is clear that there is very little difference between vertically averaged well pressures estimated by 2D Miscible and 1D Miscible, from which it is concluded that gravity has little impact on vertically averaged well pressures for these scenarios.
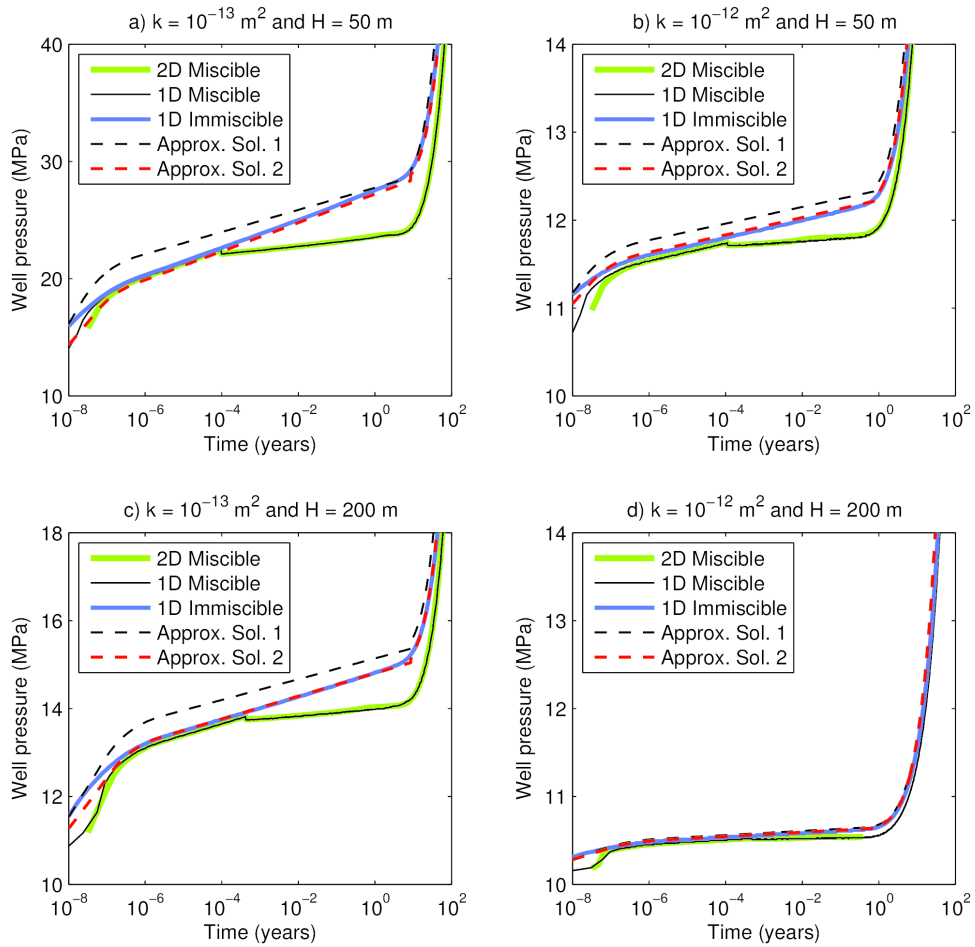
Figure 6.3: Comparison of well pressures from the approximate solution with output from TOUGH2 ECO2N (2D Miscible, 1D Miscible and 1D Immiscible). The output from 2D Miscible is vertically averaged by taking the mean in the vertical direction. Approx. Sol. 1 uses fluid properties based on the initial pressure. Approx. Sol. 2 uses fluid properties based on the pressure given by Approx. Sol. 1 at $t_D = t_{cD}$.

To explore the role of miscibility (evaporation of brine and dissolution of CO_2), the one dimensional TOUGH2 simulations have been repeated with the solubility limits of CO_2 in brine and water in CO_2 set to zero. Well pressures for these are plotted in Fig. 6.3 as thick blue lines (1D Immiscible). The pressure response for 1D Immiscible closely follows that for 2D Miscible except that 1D Immiscible maintains the initial linear-log slope until the pressure wave hits the reservoir boundary. This

is because brine is not evaporated and the presence of residual brine is maintained around the well-bore throughout the simulation. Approx. Sol. 1 (black dashed lines) closely mimics the 1D Immiscible results although it consistently overestimates pressure due to the assumption of a constant CO_2 fluid density based on the initial pressure.

Vilarrasa et al. (2010b) attempted to address this problem by iterating their analytical solution until the resulting mean pressure is equal to the pressure assumed for calculating the fluid properties. Mathias et al. (2011a) use a simpler method, which involves re-evaluating the approximate solution using a second set of fluid properties based on the well pressure (from the first iteration) that occurs when the pressure disturbance meets the outer boundary of the reservoir (i.e., $t_D = t_{cD}$). The basis for choosing this pressure is that one is unlikely to want to inject fluid far beyond this point, as the fracture pressure is quickly approached once the outer boundary is felt. The resulting set of curves are the thicker red dashed lines (Approx. Sol. 2) in Fig. 6.3. Once the pressure for calculating the fluid properties is corrected in this way, the approximate solution can be seen to accurately approximate 1D Immiscible for each of the four scenarios studied.

Recalling that there is negligible difference between vertically averaged well pressures estimated by 2D Miscible and 1D Miscible, the above discussion leads empirically to the conclusion that (1) vertical pressure equilibrium; (2) negligible capillary pressure; and (3) constant fluid properties; are useful assumptions for estimating vertically averaged well pressures. However, the assumption of immiscible displacement leads to an overestimate of pressure buildup during intermediate times due to the ignoring of brine evaporation around the well-bore.

Although well pressure is of primary interest in this context (Mathias et al., 2009c), it is interesting to study the spatial distributions of pressure and CO_2 predicted by the approximate solution as well.
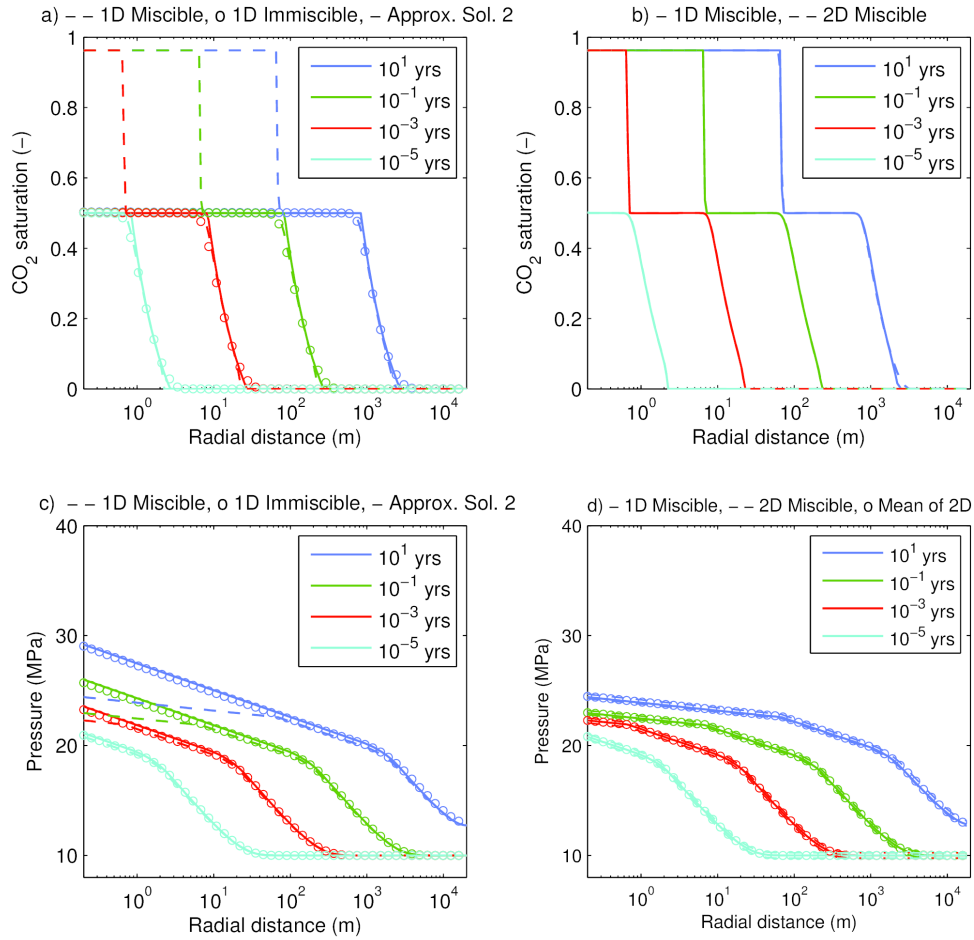
Figure 6.4: Profile plots for $k = 10^{-13}$ m^2 and $H = 50$ m (i.e., the scenario assumed for Fig. 1a). a) and c) show saturation and pressure profiles, respectively, obtained from Approx. Sol. 2 (solid lines) compared with corresponding output from 1D Miscible (dashed lines) and 1D Immiscible (circular markers) simulations from TOUGH2 ECO2N. b) and d) show saturation and pressure profiles, respectively, obtained from 1D Miscible TOUGH2 ECO2N simulations (solid lines) and 2D Miscible TOUGH2 ECO2N simulations (dashed lines). In d) there are two dashed lines for each 2D Miscible profile ; the lower and upper lines are for pressures at the top and bottom of the formation, respectively. The circular markers are vertically averaged pressures from 2D Miscible.

Fig 6.4a and c present pressure and saturation profiles at various times for the case presented in Fig. 6.3a ($k = 10^{-13}$ m^2 and $H = 50$ m) as predicted by 1D Miscible,

1D Immiscible and Approx. Sol. 2. The saturation and pressure profiles for 1D Immiscible and Approx. Sol. 2 are virtually identical. These are also very similar to those for 1D Miscible, outside the dry-out zone (where CO_2 saturation rises above $(1 - S_r)$ around the well-bore). Inside the dry-out zone, 1D Miscible predicts lower pressure gradients due to the increased availability of permeable pathways for CO_2 resulting from the evaporation of the residual brine.

Fig. 6.4b compares 1D Miscible with vertically averaged (by taking the mean in the vertical direction) CO_2 saturations from 2D Miscible. Fig. 6.4d compares 1D Miscible with bottom (upper dashed line), top (lower dashed line) and vertically averaged pressures (circular markers) from 2D Miscible. There is negligible difference between results from 1D Miscible and 2D Miscible again verifying that the vertical equilibrium assumption is highly appropriate for this scenario.

However, the $k = 10^{-13}$ m^2 and $H = 50$ m scenario is least likely to be effected by gravity segregation due it having the smallest permeability and smallest formation thickness. Fig. 6.5 shows the same data as Fig. 6.4 but for the case presented in Fig. 6.3c ($k = 10^{-13}$ m^2 and $H = 200$ m). Again, Figs. 6.5a and c demonstrate the ability of Approx. Sol. 2 to accurately approximate the internal states of 1D Immiscible. However, in Fig 6.5b it is seen that for times > 0.1 years, there is a significant difference between the vertically averaged CO_2 saturation from 2D Miscible and that of 1D Miscible. This is due to the effect of gravity segregation (Lu et al., 2009a; Yamamoto and Doughty, 2011). Fig 6.5d compares pressures estimated by 1D Miscible and 2D Miscible. Although there is a wide variation between the upper and lower pressures (the dashed lines), 1D Miscible again provides an accurate estimate of vertically averaged pressure (the circular markers). The variations between the upper and lower pressures are largely due to differences in elevation. Total hydrostatic pressure over the reservoir formation is ($\rho_w g H =$) 0.54 MPa when $H = 50$ m and 2.17 MPa when $H = 200$ m.

178
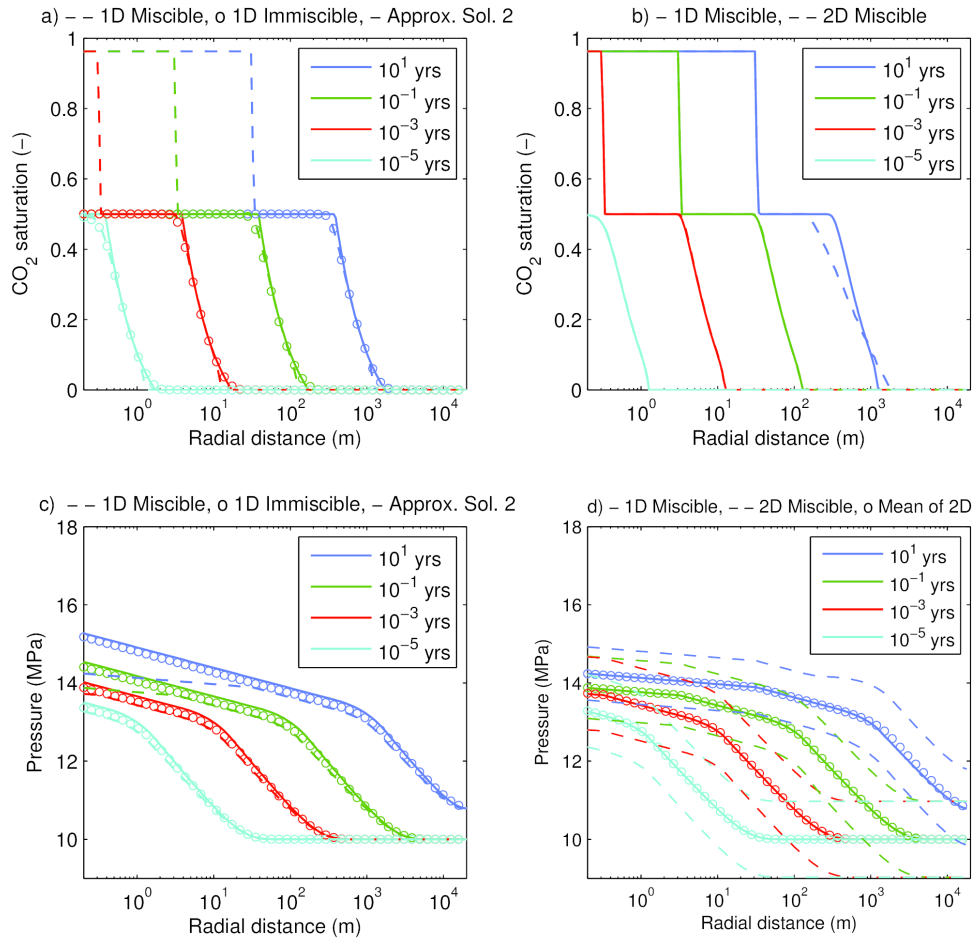
Figure 6.5: Profile plots for $k = 10^{-13}$ m^2 and $H = 200$ m (i.e., the scenario assumed for Fig. 1c). a) and c) show saturation and pressure profiles, respectively, obtained from Approx. Sol. 2 (solid lines) compared with corresponding output from 1D Miscible (dashed lines) and 1D Immiscible (circular markers) simulations from TOUGH2 ECO2N. b) and d) show saturation and pressure profiles, respectively, obtained from 1D Miscible TOUGH2 ECO2N simulations (solid lines) and 2D Miscible TOUGH2 ECO2N simulations (dashed lines). In d) there are two dashed lines for each 2D Miscible profile ; the lower and upper lines are for pressures at the top and bottom of the formation, respectively. The circular markers are vertically averaged pressures from 2D Miscible.

6.3   Effect of Partial Miscibility on Pressure Buildup

The assumptions of vertical pressure equilibrium and negligible capillary pressure in Mathias et al. (2011a) have been found not to significantly affect pressure buildup estimation. The assumption of constant fluid properties works well providing an estimate of final pressure is used to calculate CO_2 fluid properties. The assumption of immiscible flow has also been found to be appropriate providing enough time has passed for the pressure perturbation to reach the outer impermeable boundary of the reservoir. But prior to that, ignoring partial miscibility led to an overestimate of pressure.

The objective of Mathias et al. (2011b) was to extend the pressure buildup equations of Mathias et al. (2009a, 2011a) to account for effects associated with the partial miscibility of CO_2 and brine. These include evaporation of water into the CO_2 rich phase, dissolution of CO_2 into brine and salt precipitation. Note that permeability due to salt reduction is ignored.

The analytical solution was evaluated using CO_2 and brine properties from equations of state provided by Hassanzadeh et al. (2008). These incorporate work from a number of authors including Batzle and Wang (1992), Fenghour et al. (1998), Spycher et al. (2003) and Spycher and Pruess (2005). Following Mathias et al. (2011a), fluid properties were estimated using a preliminary estimate of well pressure (with fluid properties calculated using the initial pressure) that occurs when the pressure disturbance meets the outer boundary of the reservoir (i.e., $z_E = 0.5615/\alpha$). Consequently, a different set of fluid properties was applied to each of the four scenarios studied. These are detailed in Table 6.3.

Figs. 6.6a-d show time-series of well pressures. The markers are from TOUGH2 simulations and the lines from the analytical solution. The circles and solid lines are output from models that account for partial miscibility of CO_2 and brine. The

Table 6.3: Values of fluid properties calculated using Hassanzadeh et al. (2008) EOS for the four scenarios studied. Subscripts c, w and b refer to CO_2, water and brine respectively; gas (CO_2 rich), aqueous and solid phases are represented by subscripts g, a and s; subscript ca denotes CO_2 in aqueous phase and wg water in the gas phase; q_{D2} is the dimensionless flux between the leading and trailing shock and q_{D3} is the dimensionless flux in front of the leading shock (see Mathias et al. (2011b) for further details).

Parameter	Symbol	a)	b)	c)	d)
Thickness	H (m)	50	50	200	200
Permeability	k (m^2)	10^{-13}	10^{-12}	10^{-13}	10^{-12}
Pressure	P_{ref} (MPa)	25.13	12.01	14.53	10.58
Density	$\rho_c = \rho_g$ (kg/m^3)	869	692	746	647
	ρ_b (kg/m^3)	1100	1100	1100	1100
	ρ_a (kg/m^3)	1104	1104	1104	1104
	ρ_s (kg/m^3)	2160	2160	2160	2160
Viscosity	$\mu_c = \mu_g$ (cP)	0.0847	0.0558	0.0630	0.0507
	$\mu_b = \mu_a$ (cP)	0.963	0.963	0.963	0.963
Compressibility	c_b (Pa^{-1})	3.54×10^{-10}	3.54×10^{-10}	3.54×10^{-10}	3.54×10^{-10}
Mass fraction	ω_{ca} (-)	0.0318	0.0282	0.0289	0.0277
	ω_{wg} (-)	0.0021	0.0018	0.0019	0.0016
Flux	q_{D2} (-)	1.0003	1.0006	1.0005	1.0006
	q_{D3} (-)	0.9821	0.9479	0.9606	0.9355

dashed lines are output from the analytical solution previously presented by Mathias et al. (2011a), which assumes fully immiscible displacement. Recall that it is the extension of Mathias et al. (2011a) to account for partially miscible flow. Note that well pressures plotted from the two-dimensional radially symmetric TOUGH2 simulation have been vertically averaged.

As discussed in Mathias et al. (2011a), the distinctive feature between the partially miscible and immiscible simulations is the reduction in pressure rate increase that occurs after one hour (1.14×10^{-4} years). The new analytical solution for partially miscible flow is able to accurately predict this decline in pressure and closely
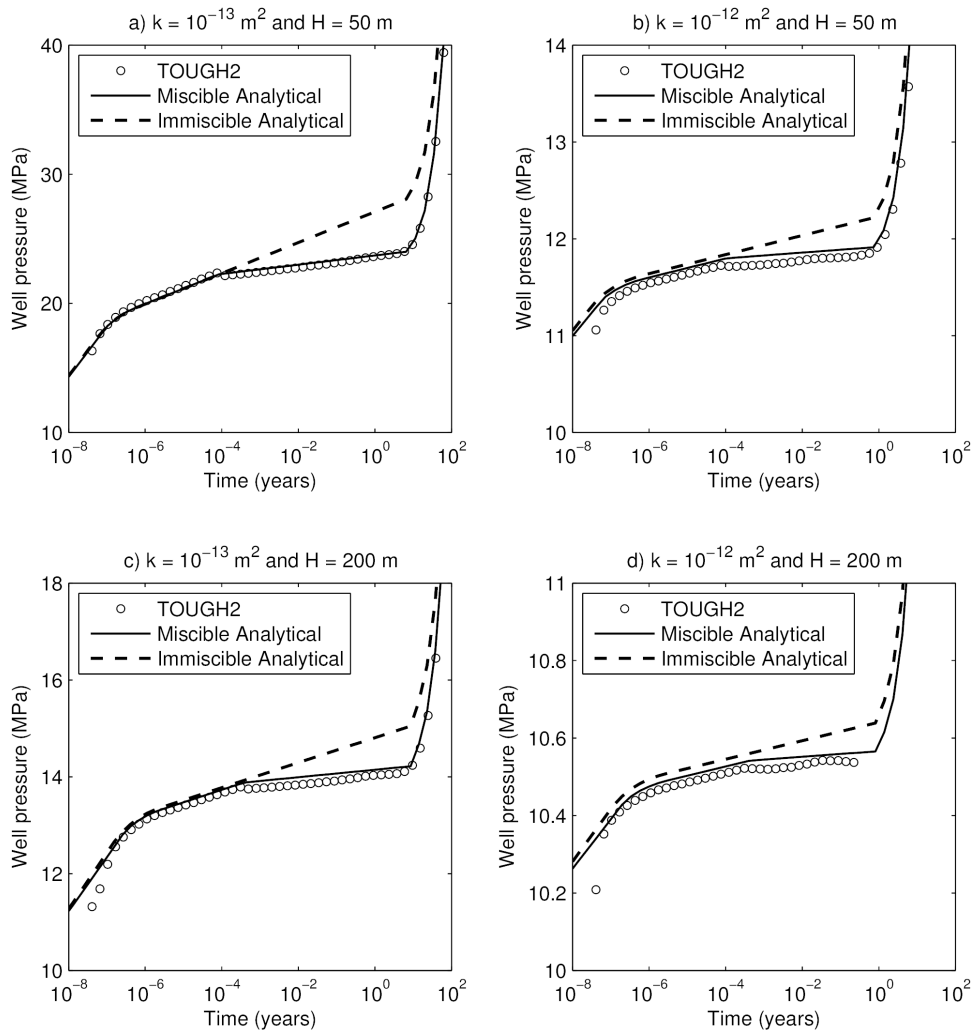
Figure 6.6: Comparison of well pressures for the four different scenarios. Results from TOUGH2 have been vertically averaged.

follows the model output from the TOUGH2 simulations.

The cause of the decline is due to the development of the dry-out zone leading to consumption of residual brine and a corresponding increase in CO_2 relative permeability around the well. This can be further understood by studying the saturation and pressure profile plots given in Fig. 6.7. Again, the results plotted from the TOUGH2 simulation have been vertically averaged. The analytical solution is seen

to accurately simulate both the extent of the dry-out zone and the saturation of precipitated salt. Similarly, the analytical solution accurately predicts the change in pressure gradient that occurs in the dry-out zone. Pressures from the immiscible analytical solution of Mathias et al. (2011a) are shown for comparison.
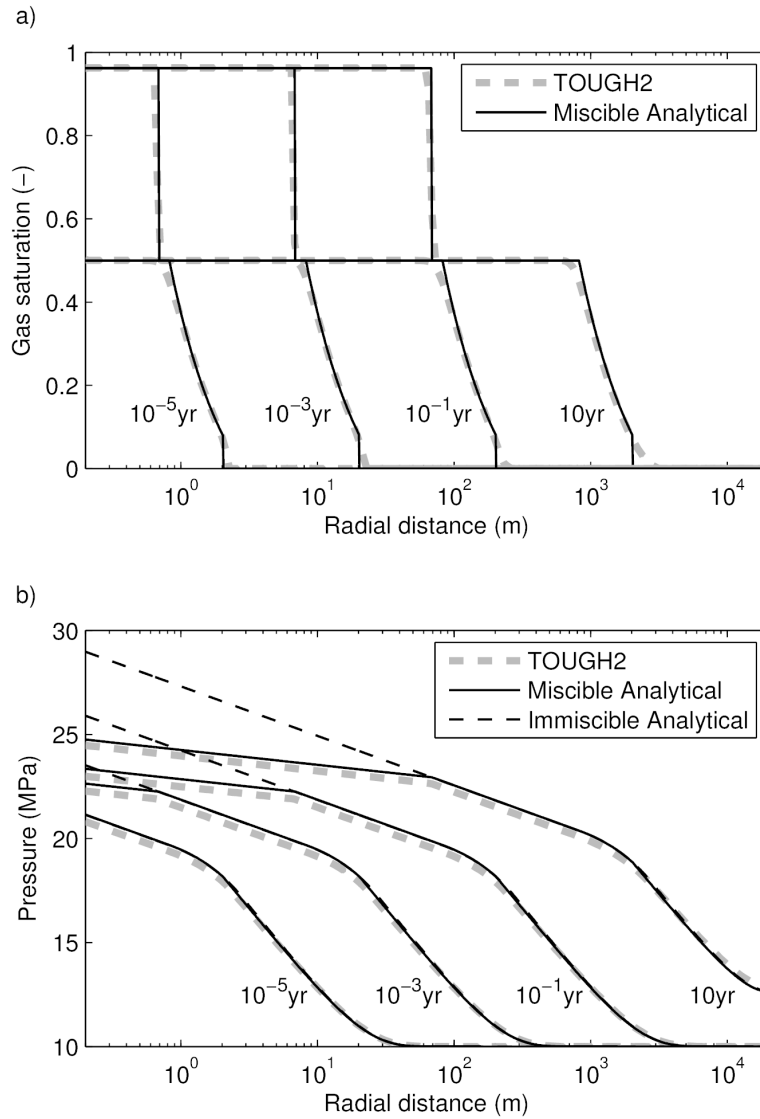
Figure 6.7: Comparison of gas saturation and pressure distributions for Scenario a). i.e., $k = 10^{-13}$ m^2 and $H = 50$ m. Results from TOUGH2 have been vertically averaged.

The effect of CO_2 dissolution into brine manifests itself in two respects. Firstly, in the presence of the leading shock fronts of the saturation profiles (see Figs. 6.7a). Secondly, in a slight reduction in pressure that occurs at early times (see Fig. 6.6d). The latter effect results from the corresponding reduction in volumetric flow rate, as shown by the q_{D3} values in Table 6.3. Note that q_{D2} is virtually one, indicating that brine evaporation has little effect on volumetric flow rate.

From a first glance at Fig. 6.6, there is a temptation to dismiss the difference between the partially miscible and miscible simulations, as both simulations converge with large time following the pressure disturbance meeting the outer boundary of the reservoir, which has been arbitrarily set at 20 km from the injection well. However, should the outer boundary be situated further away, Mathias et al. (2011b)'s Eq. (59) dictates that pressure will continue to increase along the same linear-log slope, and the miscible and immiscible simulations will continue to diverge. Nevertheless, considering Fig. 6.6c and applying a pressure constraint of 15 MPa, the immiscible model predicts that one can inject for just 8 years whereas the miscible model allows injection to continue for up to 22 years, almost three times as long.

As in the approximate solution given in Mathias et al. (2011a), the derivation of Mathias et al. (2011b) analytical solution involved a number of simplifying assumptions including: (1) vertical pressure equilibrium; (2) negligible capillary pressure; and (3) constant fluid properties. However, these three assumptions have been relaxed for the TOUGH2 simulations. As previously discussed in Section 6.2, the constant fluid properties assumption is reasonable providing an estimate of final pressure is used to calculate CO_2 fluid properties. From the comparison of the well pressures in Fig. 6.6, it is clear that both the vertical pressure equilibrium and negligible capillary pressure assumptions are also reasonable for estimating vertically averaged well pressures.
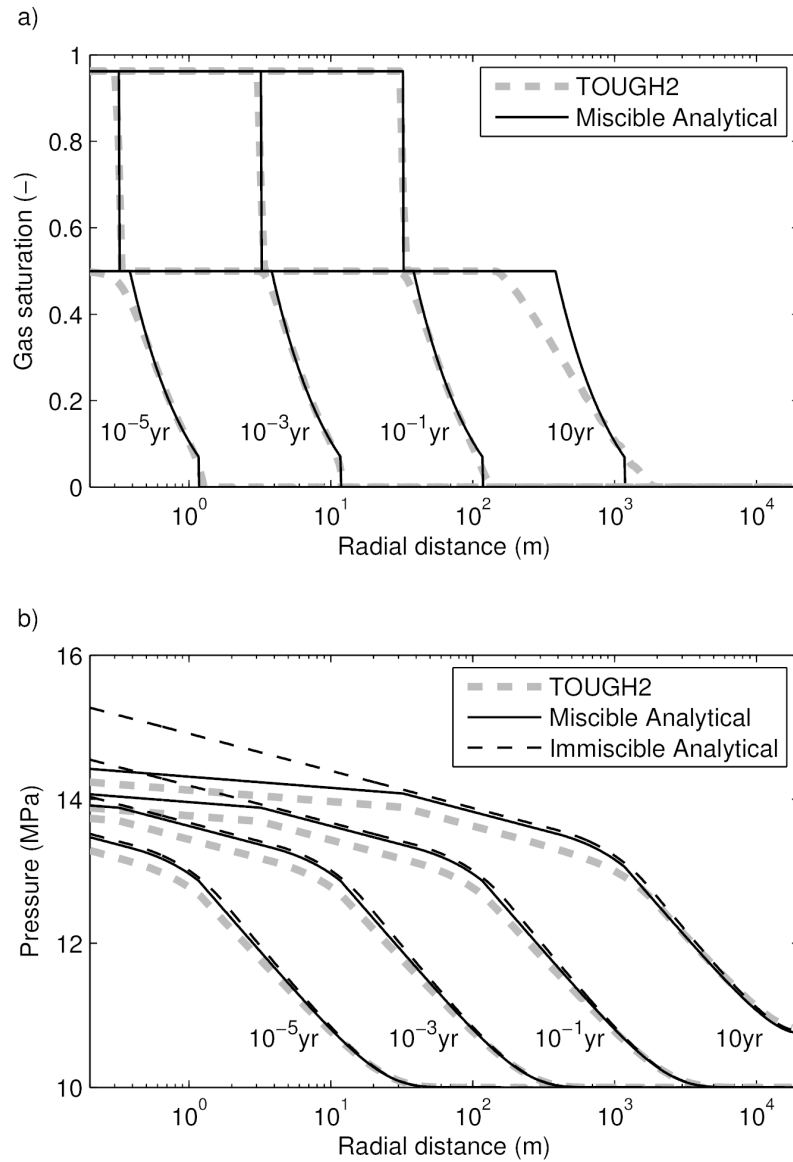
Figure 6.8: Comparison of gas saturation and pressure distributions for Scenario c). i.e., $k = 10^{-13}$ m^2 and $H = 200$ m. Results from TOUGH2 have been vertically averaged.

Fig. 6.8 shows profile plots for the case of $k = 10^{-13}$ m^2 and $H = 200$ m. The vertical pressure equilibrium assumption is less realistic for this case, as compared to that presented in Fig. 6.7, due to the larger formation thickness. Rigorous inclusion

185

of gravity in the vertically averaged formulation gives rise to an additional second-order (diffusive like) term in the saturation equation (Nordbotten and Celia, 2006; MacMinn and Juanes, 2009; Juanes et al., 2010). Accordingly, there is a notable discrepancy between the vertically averaged gas saturation at 10 years estimated by the analytical solution and the TOUGH2 simulation. Specifically, gravity segregation has caused the extent of the CO_2 plume to travel further in the TOUGH2 simulation. Nevertheless, as seen in Fig. 6.7, Fig. 6.8 shows that the analytical solution is able to accurately approximate the radial extent of the dry-out zone, the level of salt precipitation and the vertically averaged pressure distribution. The reason is that the dry-out zone and the pressures are controlled by the larger velocities situated close around the injection well, which are mostly horizontal due to the horizontal driving force provided by the injection well boundary.

With regards to capillary pressure, according to the simulations studied, there is no significant effect on vertically averaged well pressure (again compare results shown in Fig. 6.6). Recall from Mathias et al. (2011a), the capillary pressure parameters used are the same as previously adopted by Zhou et al. (2008). Of interest is that the dry-out zone can potentially lead to strong capillary forces where CO_2 will tend to re-imbibe towards the well, increasing the amount of salt precipitated in the dry-out zone. Accounting for counter-current imbibition is found to be particularly important when seeking to estimate the quantity of CO_2 that becomes residually trapped after injection has ceased (Javaheri and Jessen, 2011). But comparing results from models which ignored and included capillary pressure (and in turn, counter current imbibition) Pruess and Müller (2009) found that inclusion of capillary pressure effects is unlikely to increase salt precipitation by more than a factor of order 1.1. Furthermore, notable changes in the shape of the dry-out zone, as a result of counter current imbibition, were only observed for the exceptionally small injection rate of 0.25 kg/s (see their Fig. 7). Injection rates of practical interest for commercial scale

projects typically range from 3 to 120 kg/s (Oldenburg et al., 2004; Zhou et al., 2008). In the current study, an injection rate of 100 kg/s is assumed.

6.4 Effect of Non-linearity in Relative Permeability on Pressure Buildup

Relative permeability characteristics are often represented in numerical and mathematical reservoir simulators by power laws of the form (e.g. Orr Jr., 2007):

$$k_{ra} = k_{ra0} \left(\frac{1 - S_g - S_{ar}}{1 - S_{gc} - S_{ar}} \right)^m \tag{6.2}$$

$$k_{rg} = k_{rg0} \left(\frac{S_g - S_{gc}}{1 - S_{gc} - S_{ar}} \right)^n \tag{6.3}$$

where k_{ra} [-] and k_{rg} [-] are the relative permeabilities for the aqueous and CO_2 rich phases, respectively, S_g [-] is the gas phase volumetric saturation (i.e., the volumetric proportion of pore-space occupied by CO_2 rich phase), S_{ar} [-] is the residual aqueous phase saturation, S_{gc} [-] is the critical gas saturation, and k_{ra0} [-], k_{rg0} [-], m [-] and n [-] are the end-point relative permeabilities and power-law exponents for the aqueous and gas phases, respectively.

All the simulations studied in Sections 6.2 and 6.3 assumed linear relative permeability functions.

It is clear that a wide range of relative permeability characteristics can be expected from reservoir rocks and fluid composition. As stated earlier, to better understand the importance of this uncertainty on CO_2 injectivity, here we consider the semi-analytical pressure buildup equation recently presented by Mathias et al. (2011b).

Therefore, to further test the validity of the semi-analytical solution, additional

TOUGH2 (Pruess, 1999) simulations, with the equation of state module, ECO2N (Pruess, 2005; Pruess and Spycher, 2007), were performed with increasingly non-linear relative permeability.

The ECO2N module provides a number of different relative permeability functions that can be chosen. However, to be consistent with the CO_2 and brine relative permeability data sets given in Table 1 in Mathias et al. (2013), we implemented in TOUGH2 the equations Eqs. (1) and (2) given in Mathias et al. (2013).

To study the effect of non-linearity, a scenario similar to Scenario c) presented in 6.2 was simulated with different values of m with $m = n$ (recall that Mathias et al. (2011a) only studied the linear relative permeability case when $m = n = 1$). The full set of parameters used are listed in Table 6.4.

All the simulations assumed vertical pressure equilibrium and were setup as one-dimensional axially symmetric problems. See Mathias et al. (2011a,b) for further discussion concerning vertical pressure equilibrium in this context. Following Mathias et al. (2009a), the location of the discretized points in space were distributed logarithmically to ensure higher resolution at the injection well.

Fig. 6.9a compares well pressures from the semi-analytical solution (the solid lines) with those from TOUGH2 (the circular markers). The results from the semi-analytical solution were obtained by assuming a pressure of 18 MPa for the constant fluid properties. Fluid properties for CO_2 and brine mixtures were estimated using MATLAB implementations of equations presented by Batzle and Wang (1992), Spycher et al. (2003); Spycher and Pruess (2005) and Fenghour et al. (1998).

Both the semi-analytical solution and TOUGH2 predict pressure to rise monotonically with time. Increasing the non-linearity of the relative permeability functions (i.e., increasing m) leads to an almost constant increase in pressure. The plots confirm that the close correspondence between well pressures from the semi-analytical solution and TOUGH2 is not diminished with increasingly non-linear relative per-

Table 6.4: Parameters used for the TOUGH2 simulations study on the effect of non-linear relative permeability curves (Mathias et al., 2013).

Parameter	Symbol	Value
Injection rate,	M_0	15 kg/s
Well radius,	r_W	0.2 m
Radial extent,	r_E	20 km
Porosity,	ϕ	0.2
Rock compressibility,	c_r	4.5×10^{-10} Pa^{-1}
Initial pressure,	P_0	10 MPa
Temperature,	T	40 ^oC
Mass fraction of salt in brine,	ω_{sb}	0.15
Residual brine saturation,	S_{ar}	0.5
Critical gas saturation,	S_{gc}	0.0
End-point relative permeability for brine,	k_{ra0}	1.0
End-point relative permeability for CO_2,	k_{rg0}	0.3
Permeability reduction factor due to salt precipitation,	k_{rs}	1
van Genuchten parameter,	m_v	0.46
van Genuchten parameter,	P_{c0}	19600 Pa
Formation thickness,	H	30 m
Permeability,	k	100 mD

meability functions.

At this point it is also interesting to re-examine Burton et al. (2008)'s approximation. Burton et al. (2008, 2009) avoid numerical integration by assuming uniform relative permeabilities within the two-phase region based on the arithmetic mean of the CO_2 saturation at the trailing and leading shock fronts.

Results for well pressures using Burton's approximation are plotted as dashed lines in Fig. 6.9a alongside those from the TOUGH2 simulation and the semi-analytical solution. Well pressures predicted using Burton's approximation tend to overestimate those from the semi-analytical solution and TOUGH2. However, this error appears to decrease with increasingly non-linear relative permeability functions.
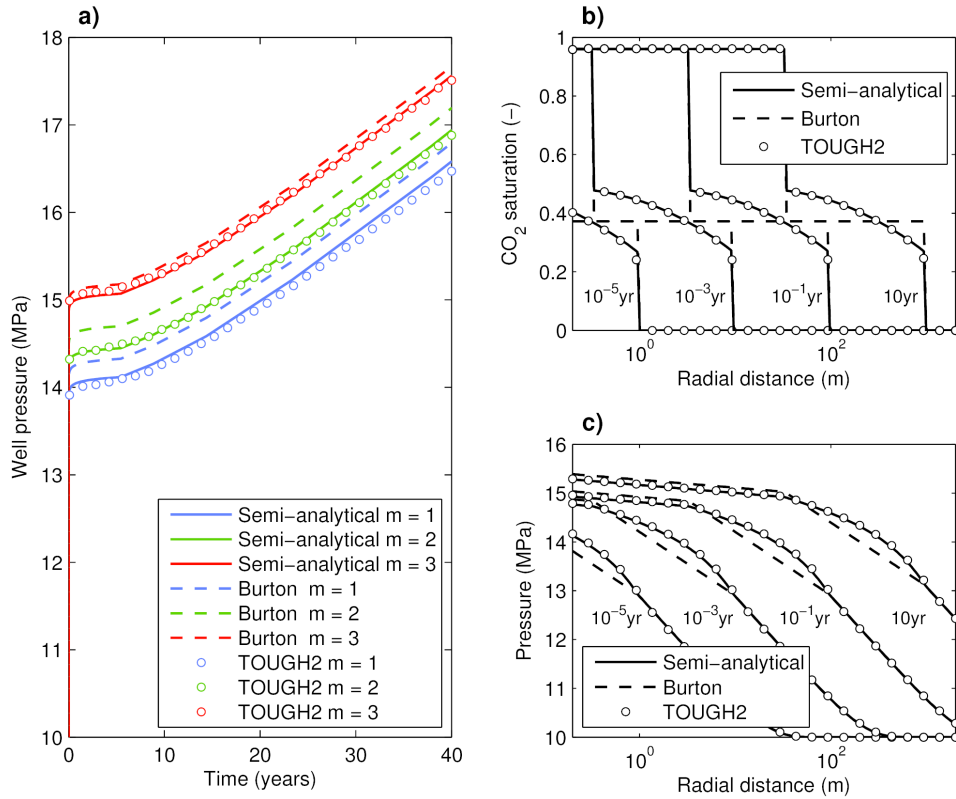
Figure 6.9: Comparison of the semi-analytical solution (solid lines), the semi-analytical solution with Burton et al. (2008)'s approximation (dashed lines) and TOUGH2 (circular markers). Note that all the simulations presented in this figure assumed n was equal to m. See Table 6.4 for other parameter values. a) Well pressures with m as indicated. b) CO_2 saturation with $m = 3$ and for times as indicated. c) Reservoir pressures with $m = 3$ and for times as indicated.

Profile plots of gas saturation and pressure against radial distance for various times, obtained using TOUGH2 (circular markers), the semi-analytical solution (solid lines) and Burton's approximation (dashed lines), are plotted for the $m = 3$ case in Figs. 6.9b and c, respectively. Again, the close correspondence between TOUGH2 and the semi-analytical solution is undiminished. Note that Burton's approximation gives rise to a linear-log pressure profile in the two-phase region, which closely follows that from TOUGH2 and the numerically integrated semi-analytical solution. Clearly Burton's method is a useful alternative to numerically evaluating the integral in

Mathias et al. (2013)'s Eq. (4). However, if one is in a position to iteratively solve Eq. (30) of Mathias et al. (2011b), accurate numerical integration of Eq. (58) of Mathias et al. (2011b) is quite a trivial extra step.

It is demonstrated here that the numerically integrated semi-analytical solution of Mathias et al. (2011b) is an accurate alternative to TOUGH2 ECO2N for the non-linear relative permeability simulation scenarios considered.

Recall that the well pressures plotted in Fig. 6.9a are all monotonically increasing with time. Numerically simulated constant rate CO_2 injections are often reported to lead to non-monotonic well pressure behavior in the form of an early-time pressure spike (e.g. Zhou et al., 2008; Chadwick et al., 2009a; Okwen et al., 2011). Indeed, the author has also observed a spike in pressure at early times from simulations undertaken using TOUGH2, ECLIPSE-100 and CMG-GEM. However, on increasing the grid resolution around well it is found that the pressure spike decreases in duration. Furthermore, once sufficient grid resolution is realized, the pressure spike ultimately vanishes, in accordance with the monotonic results predicted by the semi-analytical solution. Similar results are also reported by Pickup et al. (2012). The grid used to obtain the results given in Fig. 6.9 employed 451 logarithmically spaced points with the first element (next to the well) being of 1 mm length.

6.5   Summary and conclusions

When seeking to estimate storage capacity of geological reservoirs for CO_2 geo-sequestration, it is necessary to be able to estimate the pressure buildup resulting from the injection process. Mathias et al. (2011a) extension to closed systems of their previous (Mathias et al., 2009a) semi-analytical solution for predicting pressure buildup when the formation can be assumed to be of infinite radial extent was verified by comparison with vertically averaged results from TOUGH2 simulations of the

fully dynamic problem. Furthermore, Mathias et al. (2011b) solution accounting for effects associated with the partial miscibility of CO_2 and brine was found to prove an accurate match with TOUGH2 solution. The effects included evaporation of water into the CO_2 rich phase, dissolution of CO_2 into brine and salt precipitation. Mathias et al. (2011b)'s equations can be used to describe both closed and open systems.

Results from the analytical solution were obtained using fluid properties provided by equations of state documented in Hassanzadeh et al. (2008). The analytical solution was compared to results from TOUGH2 and found to accurately approximate the extent of the dry-out zone around the well, the resulting permeability enhancement due to residual brine evaporation, the volumetric saturation of precipitated salt, and the vertically averaged pressure distribution in both space and time for the four scenarios studied.

Whilst the effect of brine evaporation can be considerable, the effect of CO_2 dissolution is small. CO_2 dissolution into brine leads to a modest reduction in volumetric flow rate beyond the two-phase region, resulting in a reduction in pressure that occurs throughout injection. For the scenarios studied, volumetric flow rate reduction was found to be less than 7 % and the effect on pressure was barely noticeable.

The resulting equations from Mathias et al. (2011a) Mathias et al. (2011b) remain simple to evaluate in spreadsheet software, and can be easily implemented in currently available storage capacity estimation frameworks (e.g. Mathias et al., 2009c).

Since a wide range of relative permeability characteristics can be expected from reservoir rocks and fluid composition, to further test the validity of the semi-analytical solution, additional TOUGH2 (Pruess, 1999) simulations, with the equation of state module, ECO2N (Pruess, 2005; Pruess and Spycher, 2007), were performed with increasingly non-linear relative permeability. Again, the close correspondence between TOUGH2 and the semi-analytical solution is undiminished.

Chapter 7

Summary and conclusions

7.1 Summary of thesis

Environmental Risk Assessment Framework

An environmental risk assessment framework for UCG–CCS has to comply with fundamental criteria of transparency, clarity, consistency and reasonableness, in order to be able to take decisions at a risk management stage that can truly compare the risks of different alternatives for energy production. Ultimately, any CO_2 storage environmental assessment should quantify and compare the risks of undertaking the sequestration to the benefits that are expected to be obtained, notwithstanding that the storage is only one of the cumulative risks of capture, transport and sequestration.

Though hazards present in UCG and CCS are well known, important gaps exist in knowledge of exposure and effects quantification, and therefore in risk characterization. The combination of both technologies presents environmental advantages and disadvantages which need further research.

Some of the uncertainties arise from antagonistic effects that occur within UCG–CCS: regarding CO_2 storage capacity in a UCG–CCS operation, if the creation of a zone with higher porosity and permeability yields an initial higher capacity than e.g. in a deep saline aquifer or an intact coal seam, the presence of fractures and low permeability of the rock will compromise the maximum achievable injection pressure.

And storage capacity is ultimately based in overpressurization of the reservoir. In addition, time for dissipation of high temperatures will compromise the CO_2 storage capacity for obvious reasons of density and injection sequence.

For the same reason, injectivity is favoured by the creation of a high permeability zone around the injection point, and the elevated number of injection wells, but maximum pressures will be more limited due to the presence of fractures.

Containment is disfavoured by the disturbance of the rock and an increased number of wells, and also by the degree to which these are subjected to elevated thermal and mechanical stresses, chemical attack and corrosion. However, upper layers of coal can add sealing properties once cleats have closed due to the swelling of coal after contact with CO_2.

Major leakage pathways are likely to be wells, fractures, faults, dykes and other structural elements which give rise to discontinuities in the cap rock. Wells —the weakest link— will be especially stressed in UCG–CCS applications.

Therefore, an understanding of flow and transport processes in porous and fractured media, coupled with thermo-mechanical and chemical effects, is necessary to predict the behaviour of CO_2 and contaminants in UCG–CCS and ground movement. Other critical issues for exposure assessment, such as characterization of coal, gas and CO_2 streams, are essential to achieve quantitative estimates of exposure risk.

Effects of subsidence, organic contaminants, metals and CO_2 are well known in structures and individuals. However, effects of low releases extended in time on communities and their resilience is not so well understood. As in the case of the exposure assessment, more research is needed in order to be able to quantify the consequences.

It follows that, since risk characterization is the product of the probability of exposure and the severity of the consequence, current risk characterization can only be done in a qualitative or semi-quantitative form. However, the risk assessment of

UCG–CCS demands a quantitative assessment, so more research has to be done in both fields of climatology and CCS to be able to make a comparative analysis.

Due to the uniqueness of ecological systems, site-specific characterization is a key factor in problem formulation. On the other hand, it is advisable to clearly differentiate the steps and parts of the risk management process so a systematic approach can be applied without losing clarity, especially when different methods and techniques for hazard identification, exposure assessment or uncertainty treatment will have to be combined to obtain a satisfactory answer.

Modelling UCG-CCS

In the case of combined UCG–CCS, strongly coupled thermal-hydraulic-mechanical-chemical (THMC) processes are expected to occur in the various stages of operation and over the longer term after closure. However, at this point there is a lack of empirical UCG–CCS data and therefore, the use and comparison of different methods, models and scenarios seems the best way to narrow the uncertainty range. An analogue found in the coal mining industry can lay the basis for modelling stress field redistribution and its relation to hydrological parameters. General research on CO_2 and more recent laboratory research in sedimentary rock properties subjected to high temperature and coal gasification will help to populate the simulation models with adequate parameters and validate them.

Due to the complexity and time and spatial scales of processes, it cannot be foreseen that a single model will solve all the governing equations in a reasonable time and computational resources. When developing modelling tools, it will be necessary to achieve a minimum degree of coupling between the models, so the physics of the problem may be more accurately represented. In addition, upscaling of the problems from one model to another has to be possible.

When dealing with the thermo-hydro-mechanical modelling aspect of UCG–CCS,

195

the system can be conceptualized as a fractured porous rock (in the caved and fractured area) and a porous rock in the rest of the model. Thus, the former is treated as a multicontinuum and the latter as a single continuum. In the case of a typical sedimentary basin where a UCG–CCS operation would be carried out, the system consists of several horizontal or sub-horizontal layers of sandstone, shale, coal, mudstone and siltstone. Simplified models can group several of these layers and use average parameters to decrease the numerical calculation load.

Implementation of a hydro-mechanically coupled dual-porosity flow model in TOUGH2–FLAC3D

Once the necessity of hydro-mechanically coupled simulation models which can account for dual-porosity to represent the fractured area in UCG–CCS has been established, Chapter 4 implements this concept between two well-known models, TOUGH2 and FLAC3D. TOUGH2 is a multiphase, multi-component flow and transport model. FLAC3D is a numerical code for advanced geotechnical analysis in three dimensions. Rutqvist et al. (2002) developed a two-way iterative coupling module to link both codes. Here, this coupling module is extended to account for dual-porosity flow models.

One of the main advantages of using a research open source code such as TOUGH2 is the possibility to implement changes as required by the developer. FLAC3D also facilitates certain development potential by means of its built-in code FISH. However, ultimately, access to a commercial FLAC3D source code is not available. This may limit more drastic incursions and eventually an open source geomechanical code for TOUGH2 might be developed (Liu and Rutqvist, 2013).

Two cases have been setup and simulated: injection of CO_2 below the fractured area and migration along a vertical fault in the vicinity of that fractured zone and injection in the fracture area itself.

Results show that the simulator seems to adequately capture the flow and geomechanical processes. Benchmarking exercises to further test the implementation of the code are the next necessary step in the development of a code.

Two cases were simulated: a fractured area in the vicinity of a leaking fault and injection into a fractured zone. The presence of the fault dominates the behaviour of the system due to the significant difference in permeability and the reduced volume of fractures. Special attention has to be paid to effective stresses, which can induce surface heaving and development of shear stress in a large area distant from the injection point and therefore potentially less monitored. Though improvement in CO_2 dissolution and therefore storage security was observed when a fractured area is present, the flow rates along the leaking fault preferential path rendered it negligible.

A very significant outcome is the impact of avoiding the common simplification of using a Biot's coefficient of 1 and use a lower value for the fractured continuum. The subsequent calculation of pore pressure and its impact on effective stress, displacement and shear stress is paramount. It will be a key parameter to consider in hydromechanical simulation of UCG–CCS.

The second case, injection into a fractured zone, proved the advantage in terms of injectivity and dissolution of CO_2 as a trapping mechanism. However, it is also patent in this model that the buoyancy of CO_2 drives it to migrate vertically to the top of the fractured area. Horizontal fractures have a secondary role in CO_2 migration, to become important when vertical permeability differs greatly from permeability in the horizontal plane, as in the top of the fractured zone. Geomechanical response in this case yielded slightly harsher conditions in the case of injection in the fractured zone, but ultimately, this is dependent of the in-situ stress regime.

Though successfully tested in two scenarios, the current development of this dual-porosity, hydromechanically coupled TOUGH-FLAC3D model has a number of simplifications and limitations which may hinder its use:

197

One of the limitations is the temperature range (up to 110 ºC) of the ECO2N equation of state module. In UCG–CCS applications it will be desirable to investigate the effect of higher temperatures. Even if it is foreseen that sufficient cooling might take place in the gasification chamber before injection, a commercial operation with several gasification chambers operating simultaneously in the proximity may alter the temperature field over this value.

Mathematical convergence difficulties were found during the simulation and further attempts of a thorough sensitivity analysis and case variations. In particular, the injection rate in the *Case B* (injection into a fractured area) could not be increased to levels of commercial exploitation (e.g. the equivalent of 1–2 Mt/y for the model section considered). Linear equation failure to converge was repeatedly present despite the tuning of other parameters in TOUGH2. This can be due to the small fracture volume, especially in elements close to major flow paths, of fracture elements in comparison with the matrix block.

Simultaneously, several pre and post processing softwares were evaluated to integrate a dual-porosity model (e.g. *PetraSim, Paraview, T2B*). However, at the time of this research, none of them could provide the necessary capabilities, so pre and post processing tools have been developed during this work using FORTRAN and MATLAB. As a result of both the convergence difficulties and the laborious process of model preparation and analysis, only a limited number of simulations could be successfully run.

Modelling of CO_2 injection into a fractured zone with fracture stress-dependent permeability

The aim was to compare different approaches to the modelling of CO_2 injection in a fractured zone. For this purpose, the hydro-mechanically coupled model from Computer Modeling Group Ltd. (CMG), GEM has been used. Three scenarios

derived from the base case presented by Tran et al. (2009) have been produced, each of them accounting for *i)* no hydromechanical coupling, *ii)* hydromechanical coupling with no fracture permeability variation or *iii)* hydromechanical coupling with stress-dependent fracture permeability.

Observation of well bottom-hole pressures show that including a fractured area around the well decreases the initial value and slope of the injection pressure curve, facilitating injectivity and leading to a longer injection time before caprock failure. Storage capacity in the studied case can be increased by 10 to 35 fold from the non-fractured scenario to a fractured scenario. In addition, the approach taken to account for the fractured zone has relevant implications: if fractures are modelled with a constant permeability, the estimated maximum storage capacity before caprock failure can be over two times the case of stress-dependent fracture permeability model; if no hydro-mechanical coupling is modelled, and maximum capacity is estimated as the one resulting of pressure reaching a theoretical or calculated maximum rock stress, the storage capacity could be overestimated by a factor of more than 3. As a consequence, this study shows that the deviations in using one method or another are not of a second order of magnitude, and it will be necessary to account for hydro-mechanical coupling and fracture permeability stress dependency.

The fracture network permeability will also have a significant impact on the CO_2 plume evolution. It was found that horizontal fracture permeabilities 4 times higher than matrix vertical permeability did not significantly increased the lateral spread of the CO_2 plume on top of the fractured area. However, when this ratio was increased to 40 (in *Case 2* with a constant fracture permeability), the CO_2 vertical migration is delayed in favour of lateral migration on top of the fractured zone, with the obvious incidence in storage security.

The sensitivity analysis on the fracture permeability stress dependent model showed that there are two main groups of parameters impacting the maximum stor-

age capacity before caprock failure. The main group –which can triple the maximum CO_2 storage capacity compared to the base case– comprises the injection rate, horizontal length of the well, formation permeability and initial fracture permeability around the injection zone. A second group is formed by the rock mechanics properties (Young's modulus, Poisson's coefficient and rock compressibility) and the fracture porosity. This second group shows improvements of twice the maximum capacity compared to the base case. Finally, the rest of parameters studied have a low impact in final capacity in this study.

It has also been noticed that the parameters tested in the sensitivity analysis do not have a direct proportional relationship to the maximum mass of CO_2 injected before caprock failure. In particular, the injection rate against mass of CO_2 injected before caprock failure can be adjusted to an exponential curve. The implication is that small variations in injection rate from a certain threshold value can have significant impact on the final storage capacity.

Despite the sensitivity analysis promising potential increase of the storage capacity with the variation of some of the model parameters, and particularly the injection rate, the results raise a concern on the feasibility of injection at commercial rates in such scenario. Assuming a coal gasification of 3100 t/d and CO_2 production of 7405 t/d as suggested by Nakaten et al. (2014) for an ICGG 308 MW plant, it was found that for a coal seam thickness of 3.8 m, the amount of CO_2 to store in the model of ca. 1 Mtonnes woud not be achievable in terms of total amount nor in injection rates. Total injected amount before caprock failure was found to be around a 40% of the total produced for a best case scenario, but injection rate in this case was 38 times slower than that expected at commercial rates.

However, it is important to remind at this stage the limitations of the model. Albeit this model accounts for hydro-mechanical coupling and fracture permeability stress dependency, which have been proved to have a non-negligible effect, there

are still significant simplifications: the first and most important is that stress field redistribution after caprock failure has not been included. *In-situ* stress is decisive in the behaviour of the rock massif and tension and compression zones around and on top of the collapsed cavity will be formed, which ultimately will affect the stress transmitted to the caprock. Secondly, a higher spatial resolution in the parameterization on rock and formation properties around the gasification cavity should be incorporated.

Numerical evaluation of analytical and semi-analytical solutions for pressure buildup due to CO_2 injection at a constant rate

When seeking to estimate storage capacity of geological reservoirs for CO_2 geo-sequestration, it is necessary to be able to estimate the pressure buildup resulting from the injection process. Mathias et al. (2011a) extension to closed systems of their previous (Mathias et al., 2009a) semi-analytical solution for predicting pressure buildup when the formation can be assumed to be of infinite radial extent was verified by comparison with vertically averaged results from TOUGH2 simulations of the fully dynamic problem.

Furthermore, Mathias et al. (2011b) solution accounting for effects associated with the partial miscibility of CO_2 and brine was found to prove an accurate match with TOUGH2 solution. The effects included evaporation of water into the CO_2 rich phase, dissolution of CO_2 into brine and salt precipitation. Mathias et al. (2011b)'s equations can be used to describe both closed and open systems.

Results from the analytical solution were obtained using fluid properties provided by equations of state documented in Hassanzadeh et al. (2008). The analytical solution was compared to results from TOUGH2 and found to accurately approximate the extent of the dry-out zone around the well, the resulting permeability enhancement due to residual brine evaporation, the volumetric saturation of precipitated

salt, and the vertically averaged pressure distribution in both space and time for the four scenarios studied.

Whilst the effect of brine evaporation can be considerable, the effect of CO_2 dissolution is small. CO_2 dissolution into brine leads to a modest reduction in volumetric flow rate beyond the two-phase region, resulting in a reduction in pressure that occurs throughout injection. For the scenarios studied, volumetric flow rate reduction was found to be less than 7 % and the effect on pressure was barely noticeable.

The resulting equations from Mathias et al. (2011a) Mathias et al. (2011b) remain simple to evaluate in spreadsheet software, and can be easily implemented in currently available storage capacity estimation frameworks (e.g. Mathias et al., 2009c).

Since a wide range of relative permeability characteristics can be expected from reservoir rocks and fluid composition, to further test the validity of the semi-analytical solution, additional TOUGH2 (Pruess, 1999) simulations, with the equation of state module, ECO2N (Pruess, 2005; Pruess and Spycher, 2007), were performed with increasingly non-linear relative permeability. Again, the close correspondence between TOUGH2 and the semi-analytical solution is undiminished.

7.2   Conclusions

The initial objective of this research was to establish the interactions between the processes which take place at UCG and CCS and propose an Environmental Risk Assessment Framework which can guide the deployment of combined UCG–CCS operations in a responsible way. The exposure assessment –one of the steps in risk characterization— is of particular interest for this objective. Consequently, a further objective of the thesis was to determine the most appropriate modelling framework for the exposure assessment. A subset of objectives derived from this included the

analysis of analogue activities, the study of the effect of CO_2 injection in fractured formations and the evaluation of analytical solutions.

As a result of this research, we hold that a comprehensive framework for environmental risk assessment of UCG–CCS has to be approached in a holistic way that truly accounts for benefits and costs from both global and local perspectives. A conclusion which can never be over-stated is the necessity of a thorough site characterization to ensure success of the operation, as well as the proper design of the UCG layout. Some uncertainties arise from the antagonistic effects that occur with UCG–CCS. The preponderance of these effects needs to be established. The author believes that Chapter 2 exposes the Environmental Risk Assessment Framework that UCG–CCS should adhere to.

Furthermore, given the current state of development in modelling and computing, it is considered that coupled hydromechanical codes that account for fractures represented by dual-porosity models are best suited for the UCG–CCS exposure assessment. These models corroborate that some of the characteristics of a UCG scenario do actually favour CCS. Essentially, injectivity and CO_2 dissolution are clearly benefited. The repercussion in storage capacity and containment will have to be assessed case by case. However, an important concern is raised: the best case scenario modelled with CMG allowed injection of only the 40% of the produced and captured CO_2 but at an injection rate nearly 40 times lower than commercial rates, which would make the operation unfeasible. The other model, TOUGH2–FLAC did not manage to inject a commercial rate due to convergence issues. However, at minimum rates of 100 t/y, it already showed surface heaving when injecting at 1800 m of depth. Though a number of simplifications have been taken and further research is needed, the current study questions the feasibility of a total reinjection of the CO_2 into a UCG–CCS cavity.

7.3 Significance

The conclusions derived from this work question the feasibility of UCG–CCS implementation with CO_2 reinjection into the UCG cavity. Qualitatively and quantitatively the results indicate that technical (e.g. containment) and economical (e.g. injection rates) factors may prevent such operation. Though further research is needed before dismissing categorically the feasibility of UCG–CCS, the alternative of injection of the produced CO_2 in a different location might need to be considered.

7.4 Recommendations

Though hazards present in UCG and CCS are well known, important gaps exist in knowledge of exposure and effects quantification, and therefore in risk characterization. Some suggested further research includes:

- effects of low releases extended in time on communities and their resilience

- recovery time of background BTEX contamination levels in the presence of CO_2

- cement and well material long-term resistance to temperatures over 1,000 ^{o}C and presence of CO_2

- CO_2 plume monitoring techniques

With regards to necessary input parameters for improving models validity,

- coal gasification — by-products production, cavity size and geometry —

- effect of high temperatures in the mechanical properties of sedimentary rock

- fluid characterization of CO_2/CH_4/BTEX compounds/brine mixtures and

- fracture characterization — density of fractures, fracture aperture and conductivity, stress-permeability relationships, fractures propagation stress threshold, fractures travel distance —

- coal CO_2 adsorption — coal swelling, coal permeability —

Recommend further work on the TOUGH2–FLAC3D model should initially concentrate on:

- generalization of the model to account for dual-permeability systems — that is, with several nested blocks in the matrix which allow matrix-matrix flow —

- further development and generalization of pre and post processing tools which help in speeding up the model setup process and results analysis

- extensive model validation and comparison with other simulators and semi-analytical solutions

- implementation of additional capabilities in the ECO2N module to extend the temperature range

- research in Biot's coefficients expected in a UCG–CCS environment

Current capabilities of GEM could easily allow the study of:

- incorporate *in-situ* stresses after cavity collapse and subsequent sensitivity analysis on variations on the initial stress field

- increased number of UCG–CCS cases and sensitivity analysis

- 3D simulation with multiple gasification chambers

- multiseam UCG–CCS scenarios

- effect of temperature and CO_2 injection timing.

Appendix A

(Electronic format)

A.1 TOUGH2–FLAC3D simulations files for Chapter 4

A.1.1 Code implementation

A.1.2 Pre and post processing tools

A.1.3 Simulation files

A.2 GEM–CMG simulations files for Chapter 5

A.3 TOUGH2 simulations files for Chapter 6

References

ABC (2013), "Energy company to drop law suit against government," http://www.abc.net.au/news/2013-07-27/.

Akasofu, S. (2009), "Two natural components of the climate change: (1) The recovery from the Little Ice Age (A possible cause of global warming) and (2) The multi-decadal oscillation (The recent halting in the warming)," *International Arctic Research Center University of Alaska Fairbanks*.

Alam, M. M., Borre, M. K., Fabricius, I. L., Hedegaard, K., Rgen, B., Hossain, Z., and Krogsbll, A. S. (2010), "Biot's coefficient as an indicator of strength and porosity reduction: Calcareous sediments from Kerguelen Plateau," *Journal of Petroleum Science and Engineering*, 70, 282–297.

André, L., Audigane, P., Azaroual, M., and Menjoz, A. (2007), "Numerical modeling of fluid-rock chemical interactions at the supercritical CO_2-liquid interface during CO_2 injection into a carbonate reservoir, the Dogger aquifer (Paris Basin, France)," *Energy Conversion and Management*, 48, 1782–1797.

Andreani, M., Gouze, P., Luquot, L., and Jouanna, P. (2008), "Changes in seal capacity of fractured claystone caprocks induced by dissolved and gaseous CO_2 seepage," *Geophysical Research Letters*, 35.

Anheden, M., Andersson, A., Bernstone, C., Eriksson, S., Yan, J., Liljemark, S., Wall, C., Rubin, E. S., Keith, D. W., Gilboy, C. F., Wilson, M., Morris, T., Gale, J., and Thambimuthu, K. (2005), "CO_2 quality requirement for a system with CO_2 capture, transport and storage," in *Greenhouse Gas Control Technologies 7*, pp. 2559–2564, Elsevier Science Ltd, Oxford.

Bachu, S. (2008), "CO_2 storage in geological media: Role, means, status and barriers to deployment," *Progress in Energy and Combustion Science*, 34, 254–273.

Bachu, S. and Bennion, B. (2008), "Effects of in-situ conditions on relative permeability characteristics of CO_2-brine systems," *Environmental Geology*, 54, 1707–1722.

Bai, M. (1986), "Prediction of the fracture zone over mine workings and its effect on water inflow," Ph.D. thesis, Newcastle University, Mining Dept., Newcastle upon Tyne.

Barton, N. (1973), "Review of a new shear-strength criterion for rock joints," *Engineering Geology*, 7, 287 – 332.

Barton, N. and Bandis, S. (1982), "Effects Of Block Size On The Shear Behavior Of Jointed Rock," in *The 28th U.S. Symposium on Rock Mechanics (USRMS), June 29 - July 1, 1987 , Tucsan, AZ*, American Rock Mechanics Association.

Barton, N., Bandis, S., and Bakhtar, K. (1985), "Strength, deformation and conductivity coupling of rock joints," *International Journal of Rock Mechanics and Mining Sciences & Geomechanics Abstracts*, 22, 121 – 140.

Barton, N., Makurat, A., Christianson, M., and Bandis, S. (1987), "Modelling Rock Mass Conductivity Changes In Disturbed Zones," in *The 28th U.S. Symposium on Rock Mechanics (USRMS), June 29 - July 1, 1987 , Tucsan, AZ*, American Rock Mechanics Association.

Batzle, M. and Wang, Z. (1992), "Seismic properties of pore fluids," *Geophysics*, 57, 1396–1408.

Beaubien, S., Ciotoli, G., Coombs, P., Dictor, M., Krger, M., Lombardi, S., Pearce, J., and West, J. (2008), "The impact of a naturally occurring CO_2 gas vent on the shallow ecosystem and soil chemistry of a Mediterranean pasture (Latera, Italy)," *International Journal of Greenhouse Gas Control*, 2, 373 – 387.

Bellenfant, G., Guyonnet, D., Dubois, D., and Bouc, O. (2009), "Uncertainty theories applied to the analysis of CO_2 plume extension during geological storage," *Energy Procedia*, 1, 2447–2454.

Bicer, N. (1987), "The inflow of water into mine workings," Ph.D. thesis, Newcastle University, Department of Mining Engineering, Newcastle upon Tyne, PhD Thesis.

Bildstein, O., Jullien, M., Crédoz, A., and Garnier, J. (2009), "Integrated modeling and experimental approach for caprock integrity, risk analysis, and long term safety assessment," *Energy Procedia*, 1, 3237–3244.

Blackford, J., Jones, N., Proctor, R., Holt, J., Widdicombe, S., Lowe, D., and Rees, A. (2009), "An initial assessment of the potential environmental impact of CO_2 escape from marine carbon capture and storage systems," *Proceedings of the Institution of Mechanical Engineers, Part A: Journal of Power and Energy*, 223, 269–280.

Blinderman, M. J. (2002), "The Chinchilla IGCC Project to Date: Underground Coal Gasification and Environment," in *2002 Gasification Technologies Conference*, San Francisco, USA.

Bogen, K. T., Homann, S. G., Gouveia, F. J., and Neher, L. A. (2006), "Prototype Near-Field/GIS Model for Sequestered-CO_2 Risk Characterization and Management," in *International Symposium on Site Characterization for CO_2 Geological Storage.*

Bouc, O. and Fabriol, H. (2006), "Towards a methodology to define safety criteria for CO_2 geological storage," *NETL DOE.*

Bouc, O., Audigane, P., Bellenfant, G., Fabriol, H., Gastine, M., Rohmer, J., and Seyedi, D. (2009), "Determining safety criteria for CO_2 geological storage," *Energy Procedia*, 1, 2439–2446.

Bower, K. and Zyvoloski, G. (1997), "A numerical model for thermo-hydro-mechanical coupling in fractured rock," *International Journal of Rock Mechanics and Mining Sciences*, 34, 1201 – 1211.

Burton, E. and Ezzedine, S. (2010), "Impacts of increasing depth in underground coal gasification," in *5th UCG International Conference and Workshop*, London, UCG Partnership.

Burton, E., Friedmann, J., and Upadhye, R. (2006), "Best practices in Underground Coal Gasification," Lawrence Livermore National Laboratory.

Burton, M., Kumar, N., and Bryant, S. L. (2008), "Time-Dependent Injectivity During CO_2 Storage in Aquifers," SPE/DOE Symposium on Improved Oil Recovery, 20-23 April 2008, Tulsa, Oklahoma, USA, Society of Petroleum Engineers.

Burton, M., Kumar, N., and Bryant, S. L. (2009), "CO_2 injectivity into brine aquifers: Why relative permeability matters as much as absolute permeability," *Energy Procedia*, 1, 3091 – 3098.

Carey, J. W., Wigand, M., Chipera, S. J., WoldeGabriel, G., Pawar, R., Lichtner, P. C., Wehner, S. C., Raines, M. A., and Guthrie, J. G. D. (2007), "Analysis and performance of oil well cement with 30 years of CO_2 exposure from the SACROC Unit, West Texas, USA," *International Journal of Greenhouse Gas Control*, 1, 75–85.

Celia, M. A., Bachu, S., Nordbotten, J. M., Gasda, S. E., Dahle, H. K., Rubin, E. S., Keith, D. W., Gilboy, C. F., Wilson, M., Morris, T., Gale, J., and Thambimuthu, K. (2005), "Quantitative estimation of CO_2 leakage from geological storage: Analytical models, numerical models, and data needs," in *Greenhouse Gas Control Technologies 7*, pp. 663–671, Elsevier Science Ltd, Oxford.

Celia, M. A., Nordbotten, J. M., Bachu, S., Dobossy, M., and Court, B. (2009), "Risk of Leakage versus Depth of Injection in Geological Storage," *Energy Procedia*, 1, 2573–2580.

Chadwick, A., Arts, R., Bernstone, C., Mayer, B., Thibeau, S., and Zweigel, P. (2008), "Best practice for the storage of CO_2 in saline aquifes: Observations and guidelines from the SACS and CO_2STORE projects," Tech. rep., British Geological Survey.

Chadwick, R., Noy, D., and Holloway, S. (2009a), "Flow processes and pressure evolution in aquifers during injection of supercritical CO_2 as a greenhouse gas mitigation measure," *Pet. Geosci.*, 15, 59 – 73.

Chadwick, R. A., Arts, R., Bentham, M., Eiken, O., Holloway, S., Kirby, G. A., Pearce, J. M., Williamson, J. P., and Zweigel, P. (2009b), "Review of monitoring issues and technologies associated with the long-term underground storage of carbon dioxide," *Geological Society, London, Special Publications*, 313, 257–275.

Chen, P. (2008), "Forecasting of destroyed height of overlying rock with the top coal caving based on ANN," *Journal of Coal Science and Engineering (China)*, 14, 190–194.

Chiaramonte, L., Zoback, M., Friedmann, J., and Stamp, V. (2008), "Seal integrity and feasibility of CO_2 sequestration in the Teapot Dome EOR pilot: geomechanical site characterization," *Environmental Geology*, 54, 1667–1675.

Chiaramonte, L., White, J., and Johnson, S. (2011), "Preliminary Geomechanical Analysis of CO_2 Injection At Snhvit, Norway," in *45th U.S. Rock Mechanics / Geomechanics Symposium, June 26 - 29, 2011 , San Francisco, California*, American Rock Mechanics Association.

Class, H., Ebigbo, A., Helmig, R., Dahle, H., Nordbotten, J., Celia, M., Audigane, P., Darcis, M., Ennis-King, J., Fan, Y., Flemisch, B., Gasda, S., Jin, M., Krug, S., Labregere, D., Beni, A. N., Pawar, R., Sbai, A., Thomas, S., Trenty, L., and Wei, L. (2009), "A benchmark study on problems related to CO_2 storage in geologic formations," *Computational Geosciences*, 13, 409–434.

CMG Ltd. (2012), "GEM User's Guide, Version 2012," .

Covell, J. R. (1986), "Status and plans for environmental research for underground coal gasification-affected groundwater," p. 9.

Davies, R. J., Mathias, S. A., Moss, J., Hustoft, S., and Newport, L. (2012), "Hydraulic fractures: How far can they go?" *Marine and Petroleum Geology*, 37, 1 – 6.

Dean, R., Gai, X., Stone, C., and Minkoff, M. (2006), "A Comparison of Techniques for Coupling Porous Flow and Geomechanics," *SPE Journal*, 11, 132 – 140.

DECC (2013), "Energy Consumption in the UK (2013)," .

DEFRA (2008), "Guidelines for Environmental Risk Assessment and Management," http://www.defra.gov.uk/environment/quality/risk/eramguide/.

Dershowitz, B., LaPointe, P., Eiben, T., and Wei, L. (2000), "Integration of Discrete Feature Network Methods With Conventional Simulator Approaches," *SPE Reservoir Evaluation & Engineering*, 3, 165 – 170.

Detournay, C. and Hart, R. (1999), "FLAC and Numerical Modeling in Geomechanics," in *International FLAC Symposium on Numerical Modeling in Geomechanics*, Minneapolis, USA, Rotterdam A. A. Balkema.

Doughty, C., Freifeld, B., and Trautz, R. (2007), "Site characterization for CO_2 geologic storage and vice versa: the Frio brine pilot, Texas, USA as a case study," *Environmental Geology*.

Douglass, D. H. and Christy, J. R. (2009), "Limits on CO_2 climate forcing from recent temperature data of Earth," *Energy and Environment*, 20, 177–189.

Douglass, D. H., Christy, J. R., Pearson, B. D., and Singer, S. F. (2008), "A comparison of tropical temperature trends with model predictions," *International Journal of Climatology*, 28, 1693–1701.

DTI (2004), "Review of the feasibility of underground coal gasification in the UK, DTI/PUB URN 04/1643," Tech. Rep. DTI/PUB URN 04/1643.

Dumpleton, S. (2002), "Effects of longwall mining in the Selby Coalfield on the piezometry and aquifer properties of the overlying Sherwood Sandstone," *Geological Society, London, Special Publications*, 198, 75–88.

Duncan, I. J., Nicot, J., and Choi, J. (2009), "Risk Assessment for future CO_2 Sequestration Projects Based CO_2 Enhanced Oil Recovery in the U.S." *Energy Procedia*, 1, 2037–2042.

Dutta, P. and Zoback, M. D. (2012), "CO_2 sequestration into the Wyodak coal seam of Powder River Basin - Preliminary reservoir characterization and simulation," *International Journal of Greenhouse Gas Control*, 9, 103 – 116.

EPA, U. (2008), "Vulnerability Evaluation Framework for Geologic Sequestration of Carbon Dioxide," Tech. Rep. EPA430-R-08-009, U.S. EPA.

Esterhuizen, G. and Karacan, C. (2005), "Development of numerical models to investigate permeability changes and gas emissions around longwall mining panels," in *40th U.S. Rock Mechanics Symposium, June 25-29, 2005*, eds. G. Chen, S. Huang, W. Zhou, and J. Tinucci, Anchorage, AK, USA.

EU Parliament (2000), "Directive 2000/60/EC of the European Parliament and of the Council of 23 October 2000 establishing a framework for Community action in the field of water policy," .

EU Parliament (2009), "Directive 2009/31/EC of the European Parliament and of the Council of 23 April 2009 on the geological storage of carbon dioxide and amending Council Directive 85/337/EEC, European Parliament and Council Directives 2000/60/EC, 2001/80/EC, 2004/35/EC, 2006/12/EC, 2008/1/EC and Regulation (EC) No 1013/2006," .

European Environmental Agency (1998), "Environmental Risk Assessment - Approaches, Experiences and Information Sources," http://www.eea.europa.eu/publications/GH-07-97-595-EN-C2.

Fenghour, A., Wakeham, W., and Vesovic, V. (1998), "The Viscosity of Carbon Dioxide," *J. Phys. Chem. Ref. Data*, 27, 31 – 44.

Ferronato, M., Gambolati, G., Janna, C., and Teatini, P. (2010), "Geomechanical issues of anthropogenic CO_2 sequestration in exploited gas fields," *Energy Conversion and Management*, 51, 1918 – 1928.

Gale, W. (2006), "Water Inflow issues above longwall panels," in *Coal Operators' Conference, University of Wollongong & the Australasian Institute of Mining and Metallurgy*.

Galli, R. D., Jones, G. E., and Kiviat, F. E. (1983), "Simple field test model for underground coal gasification," *Ind. Eng. Chem. Proc. Des. Dev.*, 22, 538–544.

Ganow, H. C., Greenlaw, R. C., and Langland, R. T. (1978), "Geotechnical instrumentation applied to in situ coal gasification induced subsidence (Hoe Creek No.2)," pp. 327–340.

Garrity, P. (1980), "Effects of mining on surface and sub-surface water bodies," Ph.D. thesis, University of Newcastle, Newcastle Upon Tyne.

Gasda, S., Nordbotten, J., and Celia, M. (2009), "Vertical equilibrium with sub-scale analytical methods for geological CO_2 sequestration," *Computational Geosciences*, 13, 469–481.

Gibson-Poole, C., Svendsen, L., Underschultz, J., Watson, M., Ennis-King, J., van Ruth, P., Nelson, E., Daniel, R., and Cinar, Y. (2008), "Site characterisation of a basin-scale CO_2 geological storage system: Gippsland Basin, southeast Australia," *Environmental Geology*, 54, 1583–1606.

Goerke, U.-J., Park, C.-H., Wang, W., Singh, A. K., and Kolditz, O. (2011), "Numerical Simulation of Multiphase Hydromechanical Processes Induced by CO_2

Injection into Deep Saline Aquifers," *Oil Gas Sci. Technol. - Rev. IFP Energies nouvelles*, 66, 105–118.

Goodarzi, S., Settari, A., and Keith, D. (2011), "Geomechanical modeling for {CO$_2$} Storage in Wabamun Lake Area of Alberta, Canada," *Energy Procedia*, 4, 3399 – 3406.

Gor, G. Y., Elliot, T. R., and Prvost, J. H. (2013), "Effects of thermal stresses on caprock integrity during {CO$_2$} storage," *International Journal of Greenhouse Gas Control*, 12, 300 – 309.

Goulty, N. R. and Kragh, J. E. (1989), "Seismic delineation of fissures associated with mining subsidence at Houghton-le-Spring, Co. Durham," *Quarterly Journal of Engineering Geology and Hydrogeology*, 22, 185–193.

Gregg, D., Hill, R. W., and Olness, D. (1976), "An overview of the soviet effort in underground coal gasification," Tech. Rep. UCRL-52004, Lawrence Livermore National Laboratory.

Grimstad, A., Georgescu, S., Lindeberg, E., and Vuillaume, J. (2009), "Modelling and Simulation of Mechanisms for Leakage of CO$_2$ from Geological Storage," *Energy Procedia*, 1, 2511–2518.

Hassanzadeh, H., Pooladi-Darvish, M., Elsharkawy, A. M., Keith, D. W., and Leonenko, Y. (2008), "Predicting PVT data for CO$_2$–brine mixtures for black-oil simulation of CO$_2$ geological storage," *International Journal of Greenhouse Gas Control*, 2, 65 – 77.

Hawkes, C., McLellan, P., Zimmer, U., and Bachu, S. (2004), "Geomechanical Factors Affecting Geological Storage Of CO$_2$ In Depleted Oil And Gas Reservoirs: Risks And Mechanisms," Gulf Rocks 2004, the 6th North America Rock Mechanics Symposium (NARMS), Houston, TX, American Rock Mechanics Association.

Hawkes, C. D., Mclellan, P. J., and Bachu, S. (2005), "Geomechanical Factors Affecting Geological Storage of CO$_2$ in Depleted Oil and Gas Reservoirs," *Journal of Canadian Petroleum Technology*, 44.

Her-Yuan Chen, L. W. T. (2000), "Coupling Fluid-Flow and Geomechanics in Dual-Porosity Modeling of Naturally Fractured Reservoirs - Model Description and Comparison," in *SPE International Petroleum Conference and Exhibition in Mexico, 1-3 February 2000, Villahermosa, Mexico*, Society of Petroleum Engineers.

Hui Deng, Z. C. and Li, D. (2011), "Coupled Geomechanical Modeling of Underground Coal Gasification," in *Canadian Unconventional Resources Conference Proceedings, 15-17 November*, Canadian Unconventional Resources Conference., Alberta, Canada, Society of Petroleum Engineers.

Humenick, M. J. and Mattox, C. F. (1978), "Groundwater pollutants from underground coal gasification," *Water Research*, 12, 463–469.

Iding, M. and Ringrose, P. (2009), "Evaluating the impact of fractures on the long-term performance of the In Salah CO_2 storage site," *Energy Procedia*, 1, 2021 – 2028.

Iding, M. and Ringrose, P. (2010), "Evaluating the impact of fractures on the performance of the In Salah CO_2 storage site," *International Journal of Greenhouse Gas Control*, 4, 242 – 248.

IEA (2012), "2012 Key World Energy Statistics," http://www.iea.org/publications/freepublications/publication/kwes.pdf.

Iglesias, A. (2008), "Personal communication," .

ITASCA (2006), "FLAC3D Version 3.1 Manual, Theory and Background," .

Javaheri, M. and Jessen, K. (2011), "Integration of counter-current relative permeability in the simulation of CO_2 injection into saline aquifers," *International Journal of Greenhouse Gas Control*, 5, 1272 – 1283.

Jenkins, C., Gerstenberger, M., Buxton, R., Nicol, A., Christophersen, A., and Brackley, H. (2010), "Risk Assessment in CCS," in *China Australia Geological Storage of CO_2 Workshop*, Canberra, Australia, CO_2CRC.

Ji, L., Settari, A., and Sullivan, R. (2009), "A Novel Hydraulic Fracturing Model Fully Coupled with Geomechanics and Reservoir Simulator," in *SPE Annual Technical Conference and Exhibition, 11-14 November 2007, Anaheim, California, U.S.A.*, Society of Petroleum Engineers.

Jing, L. (2003), "A review of techniques, advances and outstanding issues in numerical modelling for rock mechanics and rock engineering," *International Journal of Rock Mechanics and Mining Sciences*, 40, 283–353.

Johnson, J. W. (2009), "Integrated modeling, monitoring, and site characterization to assess the isolation performance of geologic CO_2 storage: Requirements, challenges, and methodology," *Energy Procedia*, 1, 1855–1861.

Jordan, P. and Benson, S. (2009), "Well blowout rates and consequences in California Oil and Gas District 4 from 1991 to 2005: implications for geological storage of carbon dioxide," *Environmental Geology*, 57, 1103–1123.

Juanes, R., MacMinn, C., and Szulczewski, M. (2010), "The Footprint of the CO_2 Plume during Carbon Dioxide Storage in Saline Aquifers: Storage Efficiency for Capillary Trapping at the Basin Scale," *Transport in Porous Media*, 82, 19–30.

Judd, A. G. (2004), "Natural seabed gas seeps as sources of atmospheric methane," *Environmental Geology*, 46, 988–996.

Khadse, A., Qayyumi, M., Mahajani, S., and Aghalayam, P. (2007), "Underground coal gasification: A new clean coal utilization technique for India," *Energy*, 32, 2061–2071.

Kolluru, R. (1996), *Risk Assessment and Management Handbook For Environmental, Health and Safety Professionals*, McGraw-Hill.

Kvenvolden, K. A. and Cooper, C. K. (2003), "Natural seepage of crude oil into the marine environment," *Geo-Marine Letters*, 23, 140–146.

Laquer, F. C. and Manahan, S. E. (1987), "Solution factors affecting the adsorption of phenol onto a siltstone," *Chemosphere*, 16, 1431–1445.

Law, D. H. S. and Bachu, S. (1996), "Hydrogeological and numerical analysis of CO_2 disposal in deep aquifers in the Alberta sedimentary basin," *Energy Conversion and Management*, 37, 1167–1174.

LBNL (2004), "GEO-SEQ Best Practices Manual. Geologic Carboon Dioxide Sequestration: Site Evaluation to Implementation," .

Lewicki, J., Birkholzer, J., and Tsang, C. (2007), "Natural and industrial analogues for leakage of CO_2 from storage reservoirs: identification of features, events, and processes and lessons learned," *Environmental Geology*, 52, 457–467.

Li, H., Yan, J., Yan, J., and Anheden, M. (2009), "Impurity impacts on the purification process in oxy-fuel combustion based CO_2 capture and storage system," *Applied Energy*, 86, 202–213.

Li, Z., Zhang, X., Sugai, Y., Wang, J., and Sasaki, K. (2013), "Measurements of Gasification Characteristics of Coal and Char in CO_2-Rich Gas Flow by TG-DTA," *Journal of Combustion*, 2013, 15.

Liu, H.-H. and Rutqvist, J. (2013), "Coupled Hydro-mechanical Processes Associated with Multiphase Flow in a Dual-continuum System: Formulations and an Application," *Rock Mechanics and Rock Engineering*, 46, 1103–1112.

Liu, S., gang Li, J., Mei, M., and lin Dong, D. (2007), "Groundwater Pollution from Underground Coal Gasification," *Journal of China University of Mining and Technology*, 17, 467–472.

Liu, S., yuan Wang, Y., Zhao, K., and Yang, N. (2009), "Enhanced-hydrogen gas production through underground gasification of lignite," *Mining Science and Technology (China)*, 19, 389 – 394.

Lomborg, B. (2001), *The Skeptical Environmentalist. Measuring the Real State of the World*, Cambridge University Press, Edinburgh.

London Convention (2006), "Risk Assessment and Management Framework for CO_2 Sequestration in Sub-Seabed Geological Structures." .

Lu, C., Lee, S.-Y., Han, W., McPherson, B., and Lichtner, P. (2009a), "Comments on Abrupt-Interface Solution for Carbon dioxide Injection into Porous Media by M. Dentz and D. Tartakovsky," *Transport in Porous Media*, 79, 29–37.

Lu, C., Han, W. S., Lee, S., McPherson, B. J., and Lichtner, P. C. (2009b), "Effects of density and mutual solubility of a CO_2-brine system on CO_2 storage in geological formations: "Warm" vs. "cold" formations," *Advances in Water Resources*, 32, 1685 – 1702.

Lucier, A. and Zoback, M. (2008), "Assessing the economic feasibility of regional deep saline aquifer CO_2 injection and storage: A geomechanics-based workflow applied to the Rose Run sandstone in Eastern Ohio, USA," *International Journal of Greenhouse Gas Control*, 2, 230–247.

Luo, J. and Wang, L. (2011), "High-Temperature Mechanical Properties of Mudstone in the Process of Underground Coal Gasification," *Rock Mechanics and Rock Engineering*, 44, 749–754.

MacMinn, C. and Juanes, R. (2009), "Post-injection spreading and trapping of CO_2 in saline aquifers: impact of the plume shape at the end of injection," *Computational Geosciences*, 13, 483–491.

Malkowski, P., Niedbalski, Z., and Hydzik-Wisniewska, J. (2013), "The Change of Structural and Thermal Properties of Rocks Exposed to High Temperatures in the Vicinity of Designed Geo-Reactor / Zmiany wlasciwosci strukturalnych i cieplnych skal poddanych wysokim temperaturom w rejonie projektowanego georeaktora," *Archives of Mining Sciences*, 58, 465 – 480.

Mallet, C. and Davis, B. (2010), "From Trial to Power Station. Bloodwood Creek, Australia," in *5th International Conference and Workshop on Underground Coal Gasification*, ed. UCGP, London, UCG Partnership.

Mathias, S., Hardisty, P., Trudell, M., and Zimmerman, R. (2009a), "Approximate Solutions for Pressure Buildup During CO_2 Injection in Brine Aquifers," *Transport in Porous Media*, 79, 265–284.

Mathias, S., González Martínez de Miguel, G., Thatcher, K., and Zimmerman, R. (2011a), "Pressure Buildup During CO_2 Injection into a Closed Brine Aquifer," *Transport in Porous Media*, 89, 383–397.

Mathias, S. A., Hardisty, P. E., Trudell, M. R., and Zimmerman, R. W. (2009b), "Erratum to "Screening and selection of sites for CO_2 sequestration based on pressure buildup" [Int. J. Greenhouse Gas Control 3 (5) (2009) 577-585]," *International Journal of Greenhouse Gas Control*, 4, 108–109.

Mathias, S. A., Hardisty, P. E., Trudell, M. R., and Zimmerman, R. W. (2009c), "Screening and selection of sites for CO_2 sequestration based on pressure buildup," *International Journal of Greenhouse Gas Control*, 3, 577–585.

Mathias, S. A., Gluyas, J. G., Oldenburg, C. M., and Tsang, C.-F. (2010), "Analytical solution for Joule-Thomson cooling during CO_2 geo-sequestration in depleted oil and gas reservoirs," *International Journal of Greenhouse Gas Control*, 4, 806 – 810.

Mathias, S. A., Gluyas, J. G., González Martínez de Miguel, G. J., and Hosseini, S. A. (2011b), "Role of partial miscibility on pressure buildup due to constant rate injection of CO_2 into closed and open brine aquifers," *Water Resources Research*, 47, n/a–n/a.

Mathias, S. A., Gluyas, J. G., González Martínez de Miguel, G. J., Bryant, S. L., and Wilson, D. (2013), "On relative permeability data uncertainty and CO_2 injectivity estimation for brine aquifers," *International Journal of Greenhouse Gas Control*, 12, 200 – 212.

Maul, P. R., Metcalfe, R., Pearce, J., Savage, D., and West, J. M. (2007), "Performance assessments for the geological storage of carbon dioxide: Learning from the radioactive waste disposal experience," *International Journal of Greenhouse Gas Control*, 1, 444–455.

Metcalfe, R., Maul, P. R., Benbow, S. J., Watson, C. E., Hodgkinson, D. P., Paulley, A., Limer, L., Walke, R. C., and Savage, D. (2009), "A unified approach to Performance Assessment (PA) of geological CO_2 storage," *Energy Procedia*, 1, 2503–2510.

Metz, B., Davidson, O., de Coninck, H., Loos, M., and Meyer, L. (eds.) (2005), *IPCC Special Report on Carbon Dioxide, Capture and Storage.*, Cambridge University Press, London, UK.

Morris, J., Hao, Y., Foxall, W., and McNab, W. (2011a), "In Salah CO_2 storage JIP: hydromechanical simulations of surface uplift due to CO_2 injection at In Salah," *Energy Procedia*, 4, 3269 – 3275.

Morris, J. P., Detwiler, R. L., Friedmann, S. J., Vorobiev, O. Y., and Hao, Y. (2011b), "The large-scale geomechanical and hydrogeological effects of multiple CO_2 injection sites on formation stability," *International Journal of Greenhouse Gas Control*, 5, 69 – 74.

217

Nakaten, N., Schlter, R., Azzam, R., and Kempka, T. (2014), "Development of a techno-economic model for dynamic calculation of cost of electricity, energy demand and CO_2 emissions of an integrated UCG–CCS process," *Energy*, pp. –.

National Coal Board (1969), "Mining Department Instruction for working under the sea. PI1968/8," .

National Coal Board Mining Department (1975), *Subsidence Engineers' Handbook*.

National Coal Council (2008), "Underground Coal Gasification," .

Nordbotten, J. M. and Celia, M. A. (2006), "Similarity solutions for fluid injection into confined aquifers," *Journal of Fluid Mechanics*, 561, 307–327.

Oberkampf, W. L., Helton, J. C., Joslyn, C. A., Wojtkiewicz, S. F., and Ferson, S. (2004), "Challenge problems: uncertainty in system response given certain parameters," *Reliability Engineering & System Safety*, 85, 9.

Okwen, R. T., Stewart, M. T., and Cunningham, J. A. (2011), "Temporal variations in near-wellbore pressures during {CO_2} injection in saline aquifers," *International Journal of Greenhouse Gas Control*, 5, 1140 – 1148.

Oldenburg, C. (2008), "Screening and ranking framework for geologic CO_2 storage site selection on the basis of health, safety, and environmental risk," *Environmental Geology*, 54, 1687–1694.

Oldenburg, C., Stevens, S., and Benson, S. (2004), "Economic feasibility of carbon sequestration with enhanced gas recovery (CSEGR)," *Energy*, 29, 1413 – 1422.

Oldenburg, C. M. (2007), "Joule-Thomson cooling due to CO_2 injection into natural gas reservoirs," *Energy Conversion and Management*, 48, 1808 – 1815.

Oldenburg, C. M., Nicot, J., and Bryant, S. L. (2009), "Case studies of the application of the Certification Framework to two geologic carbon sequestration sites," *Energy Procedia*, 1, 63–70.

Olness, D. (1977), "The historical development of underground coal gasification," Tech. Rep. UCRL-52283, Lawrence Livermore National Laboratory.

Olson, J. E., Laubach, S. E., and Lander, R. H. (2009), "Natural fracture characterization in tight gas sandstones: integrating mechanics and diagenesis," *AAPG Bulletin*, 93, 1535 – 1549.

Orchard, R. J. (1969), "The control of ground movements in undersea working," *The Mining Engineer*, V. 128, 259–273.

Orr Jr., F. M. (2007), *Theory of Gas Injection Processes*, Tie-Line Publications, Copenhagen, Denmark.

OSPAR (2007), "OSPAR Guidelines for Risk Assessment and Management of Storage of CO_2 streams in Geological Formations," .

O'Sullivan, M. J., Bodvarsson, G. S., Pruess, K., and Blakeley, M. R. (1985), "Fluid and heat flow in gas-rich geothermal reservoirs," *Society of Petroleum Engineers journal*, 25, 215–226.

Ouellet, A., Brard, T., Desroches, J., Frykman, P., Welsh, P., Minton, J., Pamukcu, Y., Hurter, S., and Schmidt-Hattenberger, C. (2011), "Reservoir geomechanics for assessing containment in CO_2 storage: A case study at Ketzin, Germany," *Energy Procedia*, 4, 3298 – 3305.

Page, S. C., Williamson, A. G., and Mason, I. G. (2009), "Carbon capture and storage: Fundamental thermodynamics and current technology," *Energy Policy*, 37, 3314–3324.

Pan, L., Oldenburg, C. M., Wu, Y., and Pruess, K. (2009), "Wellbore flow model for carbon dioxide and brine," *Energy Procedia*, 1, 71–78.

Park, K. Y. and Edgar, T. F. (1987), "Modeling of early cavity growth for underground coal gasification," *Ind. Eng. Chem. Res.*, 26, 237–246.

Pearce, J., Chadwick, A., Bentham, M., Holloway, S., and Kirby, G. (2005), "Technology Status Review - Monitoring Technologies for the Geological Storage of CO_2," .

Perkins, G. and Sahajwalla, V. (2006), "A Numerical Study of the Effects of Operating Conditions and Coal Properties on Cavity Growth in Underground Coal Gasification," *Energy Fuels*, 20, 596–608.

Persoff, P. and Pruess, K. (1995), "Two-phase flow visualization and relative permeability measurement in natural rough-walled rock fractures," *Water Resources Research*, 31, 1175–1186.

Pickup, G., Jin, M., and Mackay, E. (2012), "Simulation of near-well pressure build-up in models of CO_2 injection," .

Pirard, J. P., Brasseur, A., Coeme, A., Mostade, M., and Pirlot, P. (2000), "Results of the tracer tests during the El Tremedal underground coal gasification at great depth," *Fuel*, 79, 471–478.

Pollard, S. J., Yearsley, R., Reynard, N., Meadowcroft, I. C., Duarte-Davidson, R., and Duerden, S. L. (2002), "Current Directions in the Practice of Environmental Risk Assessment in the United Kingdom," *Environ. Sci. Technol.*, 36, 530–538.

Pollard, S. J. T., Kemp, R. V., Crawford, M., Duarte-Davidson, R., Irwin, J. G., and Yearsley, R. (2004), "Characterizing Environmental Harm: Developments in an Approach to Strategic Risk Assessment and Risk Management," *Risk Analysis*, 24, 1551–1560.

Preisig, M. and Prvost, J. H. (2011), "Coupled multi-phase thermo-poromechanical effects. Case study: CO_2 injection at In Salah, Algeria," *International Journal of Greenhouse Gas Control*, 5, 1055 – 1064.

Pruess, K. (1999), "TOUGH2 User's Guide, Version 2.0," .

Pruess, K. (2005), "ECO_2N: A TOUGH2 Fluid Property Module for Mixtures of Water, NaCl and CO_2," Tech. rep.

Pruess, K. (2008), "On CO_2 fluid flow and heat transfer behavior in the subsurface, following leakage from a geologic storage reservoir," *Environmental Geology*, 54, 1677–1686.

Pruess, K. and Garcia, J. (2002), "Multiphase flow dynamics during CO_2 disposal into saline aquifers," *Environmental Geology*, 42, 282–295.

Pruess, K. and Müller, N. (2009), "Formation dry-out from CO_2 injection into saline aquifers: 1. Effects of solids precipitation and their mitigation," *Water Resources Research*, 45.

Pruess, K. and Narasimhan, T. N. (1985), "Practical method for modeling fluid and heat flow in fractured porous media," *Society of Petroleum Engineers journal*, 25, 14–26.

Pruess, K. and Spycher, N. (2007), "ECO_2N — A fluid property module for the TOUGH2 code for studies of CO_2 storage in saline aquifers," *Energy Conversion and Management*, 48, 1761 – 1767.

Pruess, K. and Tsang, Y. W. (1990), "On two-phase relative permeability and capillary pressure of rough- walled rock fractures," *Water Resources Research*, 26, 1915–1926.

Pruess, K. and Wang, J. S. Y. (1984), "TOUGH - A Numerical Model for Nonisothermal Unsaturated Flow to Study Waste Canister Heating Effects," in *Materials Research Society Symposia Proceedings*, vol. 26 of *Scientific Basis for Nuclear Waste Management 7. Symposium held as part of the Annual Meeting of the Materials Research Society.*, pp. 1031–1038, Boston, Mass, USA, North-Holland.

Pruess, K., García, J., Kovscek, T., Oldenburg, C., Rutqvist, J., Steefel, C., and Xu, T. (2002), "Intercomparison of numerical simulation codes for geologic disposal of CO_2," *Lawrence Berkeley National Laboratory*.

Ranjith, P., Viete, D. R., Chen, B. J., and Perera, M. S. A. (2012), "Transformation plasticity and the effect of temperature on the mechanical behaviour of Hawkesbury sandstone at atmospheric pressure," *Engineering Geology*, 151, 120 – 127.

Reguera, D. F., Riba, I., Forja, J., and DelValls, T. (2009), "An integrated approach to determine sediment quality in areas above CO_2 injection and storage in agreement with the requirements of the international conventions on the protection of the marine environment," *Ecotoxicology*, 18, 1123–1129.

Roddy, D. (2008), "Linking underground coal gasification to CCS and the downstream opportunities," Proceedings of the International Coal Conference, Pittsburgh, PA.

Roddy, D. J. and González, G. J. (2010), "Underground coal gasification (UCG) with Carbon Capture and Storage (CCS)," in *Carbon Capture: Sequestration and Storage*, eds. R. Hester and R. Harrison, Issues in Environmental Science and Technology, 29, Royal Society of Chemistry.

Rohmer, J. and Bouc, O. (2009), "Addressing uncertainties in cap rock integrity assessment through a response surface methodology," *Energy Procedia*, 1, 2879–2886.

Rohmer, J. and Bouc, O. (2010), "A response surface methodology to address uncertainties in cap rock failure assessment for CO_2 geological storage in deep aquifers," *International Journal of Greenhouse Gas Control*, 4, 198 – 208.

Rutqvist, J. (2009), "Personal communication," .

Rutqvist, J., Wu, Y.-S., Tsang, C.-F., and Bodvarsson, G. (2002), "A modeling approach for analysis of coupled multiphase fluid flow, heat transfer, and deformation in fractured porous rock," *International Journal of Rock Mechanics and Mining Sciences*, 39, 429 – 442.

Rutqvist, J., Birkholzer, J., Cappa, F., and Tsang, C. F. (2007), "Estimating maximum sustainable injection pressure during geological sequestration of CO_2 using coupled fluid flow and geomechanical fault-slip analysis," *Energy Conversion and Management*, 48, 1798–1807.

Rutqvist, J., Birkholzer, J. T., and Tsang, C. (2008), "Coupled reservoir-geomechanical analysis of the potential for tensile and shear failure associated with CO_2 injection in multilayered reservoir-caprock systems," *International Journal of Rock Mechanics and Mining Sciences*, 45, 132–143.

Saripalli, K. P., Mahasenan, N. M., Cook, E. M., Gale, J., and Kaya, Y. (2003), "Risk and Hazard Assessment for Projects Involving the Geological Sequestration of CO_2," in *Greenhouse Gas Control Technologies - 6th International Conference*, pp. 511–516, Pergamon, Oxford.

Schroot, B. M., Klaver, G. T., and Schuttenhelm, R. T. E. (2005), "Surface and subsurface expressions of gas seepage to the seabed–examples from the Southern North Sea," *Marine and Petroleum Geology*, 22, 499–515.

Seevam, P. N., Race, J. M., Downie, M. J., and Hopkins, P. (2008), "Transporting the Next Generation of CO_2 for Carbon, Capture and Storage: The Impact of Impurities on Supercritical CO_2 Pipelines," in *7th International Pipeline Conference*, p. 13, Calgary, Alberta, Canada, ASME.

Selvadurai, A. P. S. (2009), "Heave of a surficial rock layer due to pressures generated by injected fluids," *Geophysical Research Letters*, 36.

Settari, A. and Mourits, F. (1998), "A Coupled Reservoir and Geomechanical Simulation System," *SPE Journal*, 3, 219 – 226.

Siemaszko, A. (2010), "Preparations for CEEC Pilot in Poland," in *5th International Conference and Workshop on Underground Coal Gasification*, ed. UCGP, London, UCG Partnership.

Smith, J., Durucan, S., Korre, A., Shi, J.-Q., and Sinayuc, C. (2011), "Assessment of fracture connectivity and potential for CO_2 migration through the reservoir and lower caprock at the In Salah storage site," *Energy Procedia*, 4, 5299 – 5305.

Soltanzadeh, H. and Hawkes, C. D. (2009), "Assessing fault reactivation tendency within and surrounding porous reservoirs during fluid production or injection," *International Journal of Rock Mechanics and Mining Sciences*, 46, 1 – 7.

Spycher, N. and Pruess, K. (2005), "CO_2-H2O mixtures in the geological sequestration of CO_2. II. Partitioning in chloride brines at 12–100 C and up to 600 bar," *Geochimica et Cosmochimica Acta*, 69, 3309–3320.

Spycher, N., Pruess, K., and Ennis-King, J. (2003), "CO_2-H2O mixtures in the geological sequestration of CO_2. I. Assessment and calculation of mutual solubilities from 12 to 100 C and up to 600 bar," *Geochimica et Cosmochimica Acta*, 67, 3015 – 3031.

Stenhouse, M., Arthur, R., and Zhou, W. (2009a), "Assessing environmental impacts from geological CO_2 storage," *Energy Procedia*, 1, 1895–1902.

Stenhouse, M. J., Gale, J., and Zhou, W. (2009b), "Current status of risk assessment and regulatory frameworks for geological CO_2 storage," *Energy Procedia*, 1, 2455–2462.

Streit, J. E. and Hillis, R. R. (2004), "Estimating fault stability and sustainable fluid pressures for underground storage of CO_2 in porous rock," *Energy*, 29, 1445–1456.

Stuermer, D. H., Ng, D. J., and Morris, C. J. (1982), "Organic contaminants in groundwater near an underground coal gasification site in northeastern Wyoming," *Environ. Sci. Technol.*, 16, 582–587.

Sury, M., White, M., Kiron, J., Karr, P., and Woodbridge, R. (2004), "Review of Environmental Issues of Underground Coal Gasification– Best Practice Guide," Tech. Rep. DTI Report No. COAL R273 DTI/Pub URN 04/1881.

Talebian, M., Al-Khoury, R., and Sluys, L. (2013), "A computational model for coupled multiphysics processes of CO_2 sequestration in fractured porous media," *Advances in Water Resources*, 59, 238 – 255.

The National Archive (2013).

Thorsness, C. B. and Creighton, J. R. (1983), "Review of underground coal gasification field experiments at Hoe Creek," in *AIChE Symposium Series*, eds. B. K. William and D. G. Robert, Underground Coal Gasification: The State of the Art. Papers presented in 2 Special Technical Sessions at the AIChE 1982 Spring National Meeting., pp. 15–43, Anaheim, CA,USA, AIChE.

Tran, D., Settari, A., and Nghiem, L. (2004), "New Iterative Coupling Between a Reservoir Simulator and a Geomechanics Module," *SPE Journal*, 9, 362 – 369.

Tran, D., Nghiem, L., Buchanan, L., Geilikman, M., Leshchyshyn, T., Hannan, S., and Wong, S.-W. (2008), "Modelling Thermal Geomechanical Effects on Simulation Porosity," in *The 42nd U.S. Rock Mechanics Symposium (USRMS), June 29 - July 2, 2008 , San Francisco, CA*, American Rock Mechanics Association.

Tran, D., Shrivastava, V., Nghiem, L., and Kohse, B. (2009), "Geomechanical Risk Mitigation for CO_2 Sequestration in Saline Aquifers," in *SPE Annual Technical Conference and Exhibition, 4-7 October 2009, New Orleans, Louisiana.*

Tran, D., Nghiem, L., Shrivastava, V., and Kohse, B. (2010), "Study of Geomechanical Effects In Deep Aquifer CO_2 Storage," in *44th U.S. Rock Mechanics Symposium and 5th U.S.-Canada Rock Mechanics Symposium, June 27 - 30, 2010 , Salt Lake City, Utah (USA)*, American Rock Mechanics Association.

Trent, B. C. and Langland, R. T. (1981), "Computer models to support investigations of surface subsidence and associated ground motion induced by underground coal gasification (USA)," .

Trivedi, J. J. and Babadagli, T. (2009), "Oil Recovery and Sequestration Potential of Naturally Fractured Reservoirs During CO_2 Injection," *Energy & Fuels*, 23, 4025–4036.

Tsang, C., Birkholzer, J., and Rutqvist, J. (2008), "A comparative review of hydrologic issues involved in geologic storage of CO_2 and injection disposal of liquid waste," *Environmental Geology*, 54, 1723–1737.

Tsang, Y. W. and Pruess, K. (1987), "Study of thermally induced convection near a high-level nuclear waste repository in partially saturated fractured tuff," *Water Resources Research*, 23, 1958–1966.

Van Genuchten, M. T. (1980), "A closed form equation for predicting the hydraulic conductivity of unsaturated soils," *Soil Sci. Soc. Am. J.*, 44, 892 – 898.

Vilarrasa, V., Bolster, D., Olivella, S., and Carrera, J. (2010a), "Coupled hydromechanical modeling of CO_2 sequestration in deep saline aquifers," *International Journal of Greenhouse Gas Control*, 4, 910 – 919.

Vilarrasa, V., Bolster, D., Dentz, M., Olivella, S., and Carrera, J. (2010b), "Effects of CO_2 Compressibility on CO_2 Storage in Deep Saline Aquifers," *Transport in Porous Media*, 85, 619–639.

Vilarrasa, V., Olivella, S., and Carrera, J. (2011), "Geomechanical stability of the caprock during CO_2 sequestration in deep saline aquifers," *Energy Procedia*, 4, 5306 – 5313.

Vivalda, C., Loizzo, M., and Lefebvre, Y. (2009), "Building CO_2 Storage Risk Profiles With The Help Of Quantitative Simulations," *Energy Procedia*, 1, 2471–2477.

Walsh, J. B. (1981), "Effect of pore pressure and confining pressure on fracture permeability," *International Journal of Rock Mechanics and Mining Sciences & Geomechanics Abstracts*, 18, 429–435.

Wang, W. and Kolditz, O. (2007), "Object-oriented finite element analysis of thermo-hydro-mechanical (THM) problems in porous media," *International Journal for Numerical Methods in Engineering*, 69, 162–201.

Warren, J. E. and Root, P. (1963), "The behaviour of naturally fractured reservoirs," *Transactions of the Society of Petroleum Engineers*, 228, 245–255.

Webster, B. (2010), "Science chief John Beddington calls for honesty on climate change," *Times On Line*.

Whittles, D. N., Lowndes, I. S., Kingman, S. W., Yates, C., and Jobling, S. (2006), "Influence of geotechnical factors on gas flow experienced in a UK longwall coal mine panel," *International Journal of Rock Mechanics and Mining Sciences*, 43, 369–387.

Wildenborg, A. F. B., Leijnse, A. L., Kreft, E., Nepveu, M. N., Obdam, A. N. M., Orlic, B., Wipfler, E. L., van der Grift, B., van Kesteren, W., Gaus, I., Czernichowski-Lauriol, I., Torfs, P., and Wojcik, R. (2005), "Risk Assessment Methodology for CO_2 Storage: The Scenario Approach," in *Carbon Dioxide Capture for Storage in Deep Geologic Formations*, pp. 1293–1316, Elsevier Science, Amsterdam.

World Coal Association (2013), "Underground Coal Gasification," http://www.worldcoal.org/coal/uses-of-coal/underground-coal-gasification/.

Xu, T., Apps, J. A., and Pruess, K. (2004), "Numerical simulation of CO_2 disposal by mineral trapping in deep aquifers," *Applied Geochemistry*, 19, 917–936.

Yamamoto, H. and Doughty, C. (2011), "Investigation of gridding effects for numerical simulations of CO_2 geologic sequestration," *International Journal of Greenhouse Gas Control*, 5, 975 – 985.

Yang, L. (2008), "Coal Properties and System Operating Parameters for Underground Coal Gasification," *Energy Sources, Part A: Recovery, Utilization, and Environmental Effects*, 30, 516 – 528.

Yang, L., Liang, J., and Yu, L. (2003), "Clean coal technology - Study on the pilot project experiment of underground coal gasification," *Energy*, 28, 1445–1460.

Yang, L. H., Zhang, X., and Liu, S. (2010), "Characteristics of Temperature Field during the Oxygen-enriched Underground Coal Gasification in Steep Seams," *Energy Sources, Part A: Recovery, Utilization, and Environmental Effects*, 32, 384 – 393.

Younger, P. (2011), "Hydrogeological and Geomechanical Aspects of Underground Coal Gasification and its Direct Coupling to Carbon Capture and Storage," *Mine Water and the Environment*, 30, 127–140.

Younger, P. L., Banwart, S. A., and Hedin, R. S. (2002), *Mine Water: Hydrology, Pollution, REmediaton*, Kluwer Academic Publishers, Dordrecht.

Zhang, Y., Oldenburg, C. M., Finsterle, S., and Bodvarsson, G. S. (2007), "System-level modeling for economic evaluation of geological CO_2 storage in gas reservoirs," *Energy Conversion and Management*, 48, 1827–1833.

Zhou, Q., Birkholzer, J. T., Tsang, C., and Rutqvist, J. (2008), "A method for quick assessment of CO_2 storage capacity in closed and semi-closed saline formations," *International Journal of Greenhouse Gas Control*, 2, 626–639.